Quantitative MRI in obesity & reno-cardiovascular function

Dekkers, I.A.

Quantitative MRI in *Obesity* & Reno-cardiovascular Function

Ilona A. Dekkers

Quantitative MRI in Obesity & Reno-cardiovascular Function

Ilona A. Dekkers

Colophon

About the cover: the cover illustration is the native 5(3)3 MOLLI sequence of the left kidney of a healthy volunteer in sagittal plane at 3T. The front is the original T1-weighted source image in sagittal plane taken at 1723 ms after the inversion pulse at time t=0 for MOLLI 5(3)3. The color-encoded T1 map based on the eight different T1-weighted source images taken at different time points is visualized at the back, and represents the corresponding T1 relaxation times per voxel in ms. Copyright © Ilona A. Dekkers.

ISBN 978-94-6361-397-2

Cover design: Ilona A. Dekkers

Layout and printed by: Optima Grafische Communicatie, Rotterdam, the Netherlands

Financial support for printing this thesis was provided by: Hart Onderzoek Nederland, Nederlandse Hartstichting, and Universiteitsbibliotheek Leiden.

Quantitative MRI in Obesity & Reno-cardiovascular Function

PROEFSCHRIFT

Ter verkrijging van
de graad van Doctor aan de Universiteit Leiden,
op gezag van Rector Magnificus prof. dr. C.J.J.M. Stolker,
volgens besluit van het College voor Promoties
te verdedigen op donderdag 18 juni 2020
klokke 13:45 uur

door

Ilona Alexandra Dekkers
geboren te Rotterdam
in 1989

Promotor

Prof. dr. H. J. Lamb

Co-promotores

Dr. Ir. R. de Mutsert

Dr. A.P.J. de Vries

Leden promotiecommissie

Prof. dr. L.F. de Geus-Oei

Prof. dr. F.R. Rosendaal

Prof. dr. T. Leiner, Universitair Medisch Centrum Utrecht, Utrecht

dr. R.P.J. Budde, Erasmus Medisch Centrum, Rotterdam

Financial support

Financial support by the Dutch Heart Foundation for the publication of this thesis is gratefully acknowledged.

Para mis padres
Voor mijn ouders

TABLE OF CONTENTS

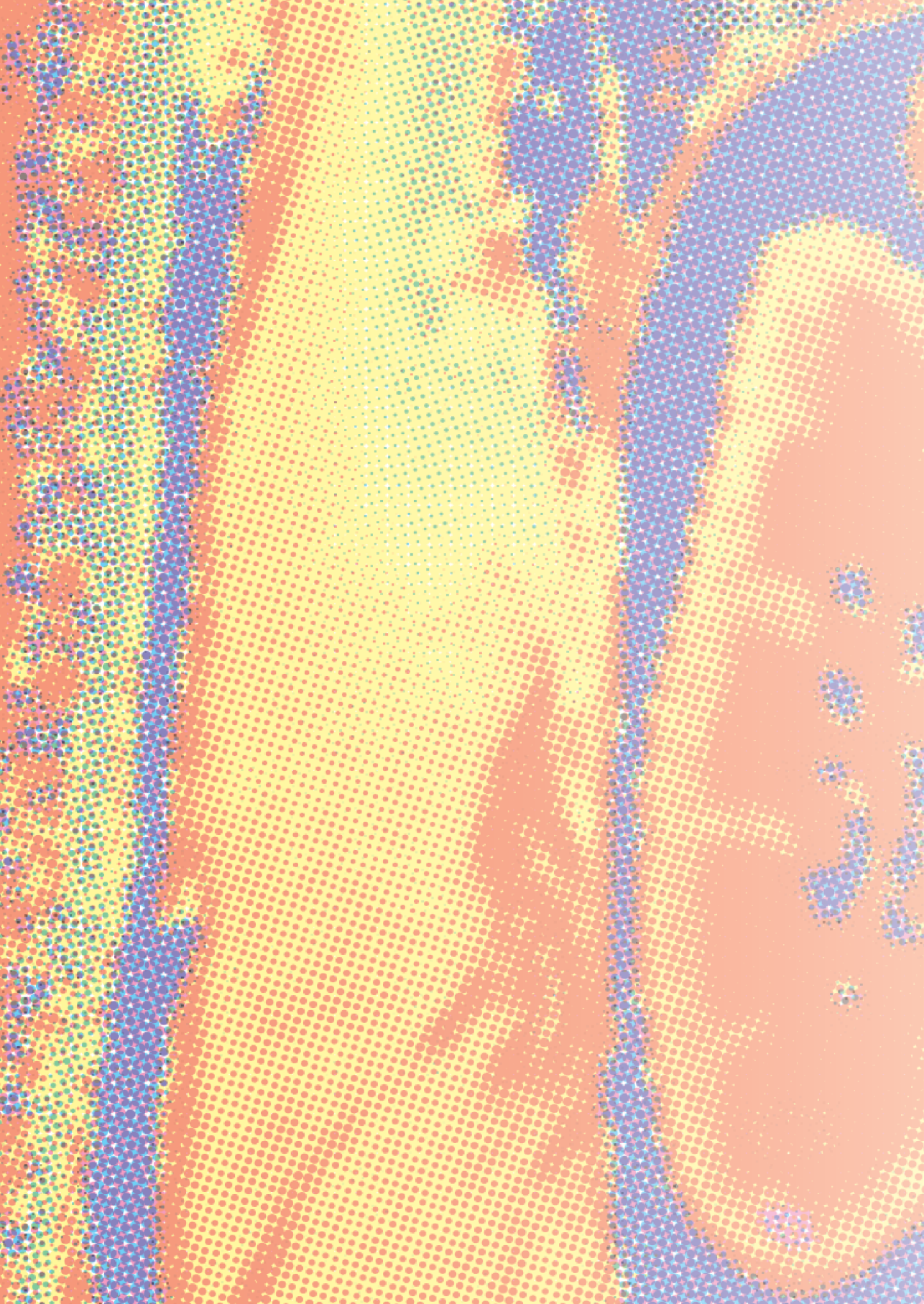

INTRODUCTION

1

General introduction and thesis outline

INTRODUCTION

In the past century, medical imaging has undergone several great transformations. First, from diagnosing pathologic conditions based on distinguishing abnormal opacities and lucencies on chest X-rays, to a discipline that is focused on defining and locating such conditions based on cross-sectional imaging by computer tomography (CT) and magnetic resonance imaging (MRI). The introduction of MRI has made it possible to diagnose diseases based on anatomical location of particular abnormalities, combined with contrast between "affected" and "normal" tissues due to differences in relaxation times of hydrogen atoms (e.g. longitudinal and transverse relaxation times) based on the underlying biophysical properties of the tissue of interest. The introduction of these techniques has radically changed the practice of medicine, making medical imaging essential in diagnostics as well as in the evaluation of therapeutic efficacy. In the 21st century, radiology is expected to evolve into a specialty that has integrated artificial intelligence with human interpretation to increase consistency and reduce errors in image analysis (1). This requires a new level of quantitative measurement metrics as conventional MRI is intrinsically insensitive to detect diffuse changes affecting the imaged tissue or organ of interest. The use of quantitative MRI based metrics allows for less biased and more reproducible measures compared to qualitative interpretations, and can be used for statistical modelling and longitudinal evaluation (2). The fields of neuroimaging and cardiovascular imaging were among the first to adopt quantitative imaging metrics, and in cardiovascular imaging the use of quantitative measures is considered part of standard clinical care. In body imaging however, the clinical application of quantitative MRI is less wide spread and in renal MRI only used in research settings, whilst these organs are particular vulnerable for diffuse disease to which conventional MRI is intrinsically insensitive. In addition, conditions that could potentially affect multiple organ systems, such as the metabolic syndrome, diabetes and obesity, could in particular be evaluated using multi-organ quantitative MRI metrics. The use of quantitative MRI allows for the comparison of individual measurements with normative values obtained from healthy populations. In the clinical setting, these quantitative MRI metrics could be utilized for monitoring treatment effect.

Aims of this thesis

The aims of this thesis are to evaluate quantitative MRI techniques in reno-cardiovascular health, and to study the links between obesity and reno-cardiovascular health using quantitative MRI metrics. Furthermore, we aim to address novel insights on the safety of contrast media with regard to the use of gadolinium.

Magnetic resonance imaging

MRI is based on the phenomenon of nuclear magnetic resonance, and MR images are constructed by measuring signals emitted from spinning anatomic nuclei (hydrogen in this thesis) in response to radiofrequency pulses with the same natural frequency as the nuclei themselves (3). The location of the excited protons (^{1}H atoms) is determined via predefined applied magnetic field gradients, and information on amplitude, frequency and phase of MR signals are mapped in K-space that result in the final MR image after the Fourier transform (3). Magnetization relaxation rates T1, T2, and proton density (PD) are important tissue-specific parameters that are characteristic for different body tissues, with T1 representing the rate of regrowth of longitudinal magnetization, T2 the rate of decay of transverse magnetization after the start of the MR experiment, and PD reflecting the actual density of protons (4). For qualitative interpretation of MRI, the images are obtained at a time when the relaxation curves are widely separated for different body tissues, producing an image that has high contrast between these tissues (e.g. T1-weighted images) with signal intensities on an arbitrary scale. Parametric maps however, are calculated matrices from two or more images of the same tissue of interest that have individual pixel values with numerical meaning (such as T1 in ms for T1 mapping) (2). Although MR images are conventionally displayed as gray-scale images for qualitative interpretation, the MR signals can also be reconstructed in a different basic "readout" compared to MR imaging, namely as a spectrum rather than an image (5). This is the basis of MR spectroscopy (MRS), in which the MR spectrum consists of resonances or peaks that represent signal intensities as a function of frequency (designated in parts per million) within a voxel of interest (6).

There are different ways in which MRI can be used for quantification of different image-derived phenotypes. This quantification of MR images, referred to as quantitative MRI, can be defined as the extraction of quantifiable features from medical images for the assessment of normal or the severity, degree of change, or status of a disease, injury, or chronic condition relative to normal (7). Quantification using MRI can broadly be done in four different approaches. First, quantification can be done on visual borders of anatomical structures using 'qualitative' MR images, such as in volumetric analysis. Second, quantification is possible via direct measurement of specific nuclear MR characteristics within a certain tissue-of-interest reflecting the tissue specific relaxation properties or tissue microstructure, as in parametric mapping and diffusion tensor imaging respectively. Third, specific organ function can be measured by changes in position of spins over time, as used in phase imaging and arterial spin labelling, or changes in magnetic susceptibility over time as in blood oxygen level-dependent imaging. Fourth, concentrations of different metabolites of a voxel of interest can be measured by MRS using the constructed MR spectrum.

Quantitative MRI in renal imaging

The global burden of kidney disease is considerable, as over 10 percent of the global adult population suffers from chronic kidney disease, and more than 2 million individuals annually endure acute kidney injury in developed countries (8,9). Currently, most kidney disorders are usually diagnosed by biochemical serum and urine analysis (e.g. serum creatinine). As biochemical analyses alone often provide insufficient information for classifying disease, renal biopsies commonly remain required for making a definitive diagnosis (10). Recent advances in new MRI techniques enable the measurement of biophysical tissue properties that have been linked to fibrosis, inflammation, tissue edema, perfusion, filtration and tissue oxygenation that can be used to study renal disease in patients non-invasively over time (11). As such, quantitative measurement of these renal biophysical tissue properties might contribute to earlier diagnosis, treatment-monitoring, and for evaluating the pathophysiology of potential risk factors of CKD and AKI. Quantification of tissue relaxation is a promising technique in renal imaging as it potentially enables the measurement of biophysical properties linked to fibrosis, analogous to imaging of myocardial scar in cardiac imaging or cirrhosis in liver imaging. In **Chapter 2**, we discuss the clinical application and technical considerations of multi-parametric of the kidney. Importantly, before the clinical application of novel quantitative MRI protocols can be further explored for the kidney, evaluation of the reproducibility of these new quantitative renal MRI protocols is needed first. As such, we explored the reproducibility of renal native T1 mapping and renal proton MR spectroscopy (^{1}H-MRS) in **Chapter 3**, and **Chapter 5** respectively. As renal quantitative MRI is a novel field, there is a need for a standardized approach to improve comparability of results by different research groups and to establish a common benchmark to evaluate future developments. To facilitate these aims, we developed an expert-based consensus imaging protocol for renal T1 mapping using the Delphi method, which is described in **Chapter 4**. Finally, we performed a clinical study evaluating the biomarker potential of renal triglyceride content measured by ^{1}H-MRS, which is described in **Chapter 6**.

MRI in epidemiological research

Epidemiology involves the study of the distribution and determinants of disease frequency (12). Prospective cohort studies are, as exposures can be assessed before they are affected by treatment or disease (thus avoiding recall bias and minimizing reverse causation), suited for identification and quantification of risk factors for disease (13). Prospective cohorts can be based on either a large amount of data on a small number of participants (e.g. the Framingham Heart Study, with extensive phenotyping of 5000 participants (14)), or a relatively small amount of data on a large number of participants (e.g. the Million Women Study, with questionnaire data on 1.3 million women (15)). In the recent decades, MRI has because of its non-invasive nature, increasingly been applied to population cohorts,

also referred to as population-based imaging studies. With the rapidly increasing sample sizes of population-based imaging studies, it can be considered as an emerging field with widespread applications and enabling multi-organ assessment (heart, liver, brain, vessel, kidney etc.) during one imaging session (16). Technical advances in image acquisition, optimized imaging sequences and automated post-processing of imaging data are among the major drivers of these rapid developments in population imaging (16). In the second part of this thesis, we present population-based imaging studies using quantitative MRI, in which **Chapter 7** to **Chapter 9** are based on the imaging data of the Netherlands Epidemiology of Obesity (NEO) study and **Chapter 10** is based on the UK Biobank. The NEO study (https://neostudie.nl) is a population-based cohort study in 6,671 men and women aged 45 to 65 years from the greater Leiden area, with an oversampling of individuals with a BMI of 27 kg/m^2 or higher (17). The NEO study is designed to investigate pathways that lead to common diseases and conditions, and the studies presented in thesis involve cross-sectional analyses of the baseline data of the NEO study. The UK Biobank Study (https://ukbiobank.ac.uk) is a large population-based cohort study in 503,325 men and women aged 45 to 69 years who were recruited across the United Kingdom (18). The study in this thesis based on UK Biobank data is a cross-sectional analysis of the imaging data of a consecutive subset of participants who underwent additional MRI scanning.

Quantitative MRI in cardiovascular imaging

Global cardiovascular mortality is increasing due to aging and population growth. Despite gains in cardiovascular health (19), it has been estimated that 40-55% of the decline in coronary heart disease in high-income countries can be attributed to the effects of medical and surgical treatments (20). The utilization of cardiovascular imaging tests including cardiac MRI is rapidly increasing in order to assist in clinical decision making (21). The possibility to quantify various aspects of the cardiovascular system (e.g. anatomy, function, flow, and perfusion) in different phases of the cardiac cycle under different conditions (rest and stress), makes cardiac MRI a promising tool for accurate and reliable assessment of cardiovascular risk. In **Chapter 2**, an overview is given on the similarities and differences of quantitative multiparametric imaging in cardiac, liver, and renal disease. **Chapter 7** and **Chapter 8** present the use of different quantitative metrics on left ventricular (LV) geometry, LV function and vascular function based on cardiac MRI in population-based studies evaluating the associations between renal and cardiovascular function.

Quantitative MRI in obesity

The disease burden related to obesity has increased significantly over the last decades, making excess body weight one of the most challenging public health problems of our time (22). Cardiovascular disease is globally the leading cause of death and disability

related to a high body mass index (BMI), followed by diabetes, and chronic kidney disease for BMI-related death and disability respectively (22). Increasing evidence indicates that global microvascular dysfunction is the underlying common pathway of obesity-related disease, leading to dysregulation of vascular tone, insulin resistance, and altered levels of paracrine and inflammatory factors (23). Subsequently, these changes could lead to impaired organ function and perfusion, predisposing obese individuals to the development of chronic kidney disease, microvascular dementia, and heart failure with preserved ejection fraction (23), see **Fig. 1**. BMI is currently used to classify overweight (25-30 kg/m^2) and obesity (>30 kg/m^2), however since BMI poorly differentiates between body fat, muscle mass, and water, this could lead to misclassification of cardiometabolic health risks (24,25). This limits the use of BMI as a clinical tool to identify overweight and obese individuals with excess visceral fat (who represent the subgroup of individuals at highest cardiometabolic risk), which has led to various strategies for the quantification of body fat distribution (26).

One of the unique capabilities of MRI is the detection of lipids based on its specific nuclear MR characteristics, making MRI ideal for the non-invasive visualization and quantification of fat. Lipids are stored in large vacuoles within adipocytes which consist for 99% of triglycerides and less than 1% of cholesterol, phospholipids, and free fatty acids (27). The MR signal obtained when exitating adipose tissue consists of signal based on protons from lipids (>80% of the signal), and signal based on protons from water molecules located within the loose connective tissue (<20% of the signal) of white fat (27). The ability of MRI to depict lipids against background water content stems from the intrinsic differences in the rate of nuclear spin relaxation (T1), with the T1 of fat being shorter than the T1 of water (27). These intrinsic differences in T1 are used in relaxometry based approaches, which are applied to quantify visceral and subcutaneous fat depots. Another difference between water and fat is that protons in water have a slightly different local magnetic field than protons in a lipid molecule, resulting in a "chemical shift" (difference in effective magnetic field induced by electron shielding) which leads to a slight difference in precessional frequency between water- and lipid-bound protons (6). Because of these differences in nuclear MR characteristics between water and fat, it is possible to accurately, precisely, and reliably quantify fat distributions throughout the body and inside organs (28). Chemical shift is widely used in different MR sequences such as frequency selective and water-fat MR imaging techniques, however also MR spectroscopy is based on the same principles of chemical shift imaging. Since ^{1}H-MRS enables the analysis and quantification of the chemical composition of a tissue volume of interest, this technique is very well suited for the quantification of low amounts of ectopic lipids.

MR imaging and spectroscopy can be used to accurately quantify different body fat distributions, i.e. visceral fat, subcutaneous fat, and intra-organ ectopic lipid accumulation, which is highly relevant in obesity studies since the distribution of fat accumulation

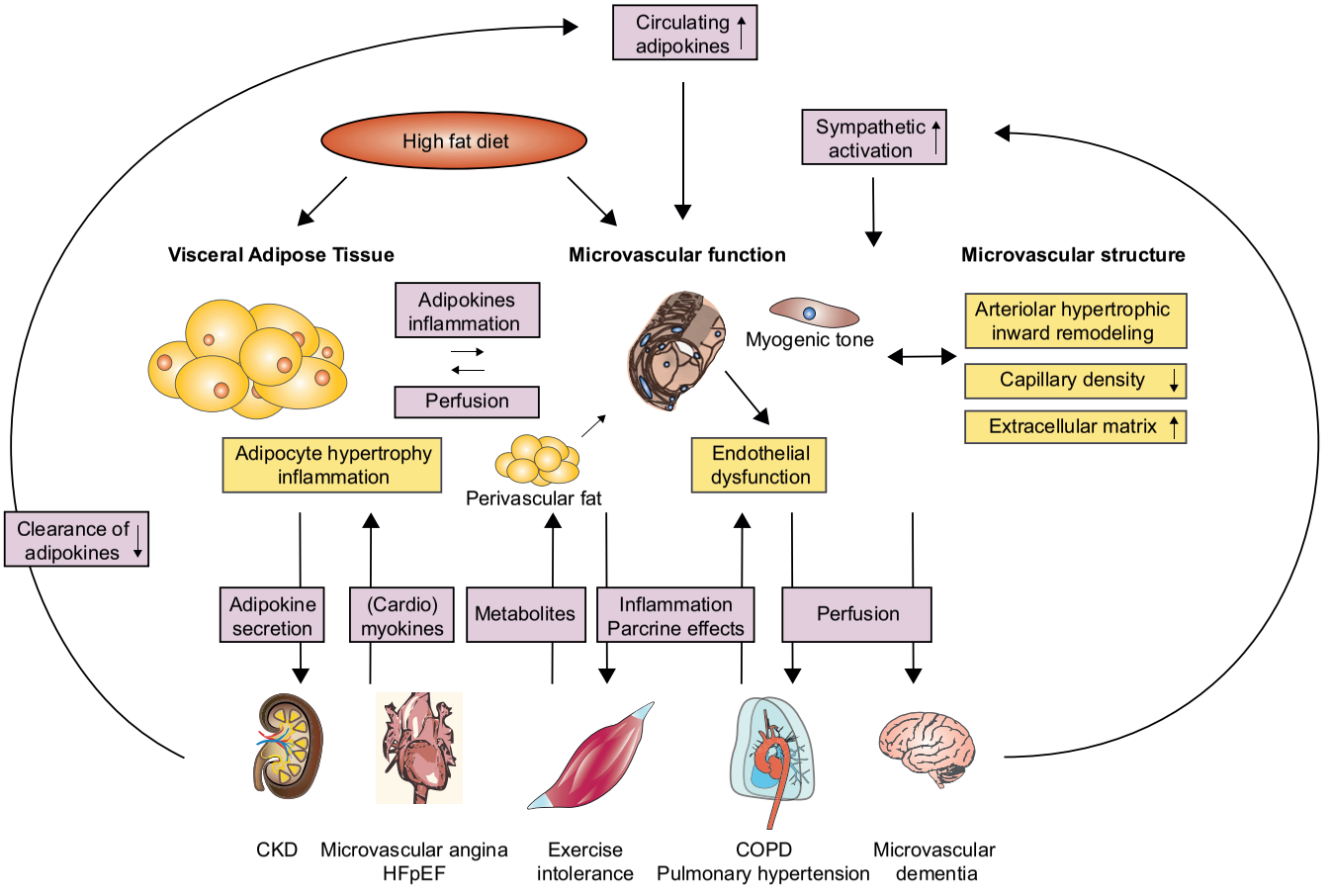

Figure 1. overview of proposed mechanisms of obesity-related global microvascular dysfunction predisposing to multi-organ disease, adapted from Sorop et al. (23).

is strongly related to metabolic risk (29,30). In addition, quantitative MRI can be used to study obesity in a holistic approach (e.g. to assess the inter-organ relation and multi-organ impact of obesity). In this thesis, we studied the negative health effects of obesity on a several organs using MRI. In **Chapter 5** and **6**, we explore the application of ^{1}H-MRS for the quantification of renal steatosis. In **Chapter 9**, we describe a population-based study that evaluates the associations between visceral adipose tissue, liver triglyceride content and renal function. In addition, considering obesity has been associated with an increased risk of dementia (31), we investigated whether measures of obesity were associated with brain morphology and microstructure in **Chapter 10**.

Contrast media safety

Gadolinium containing contrast agents (GCCAs) are used in MR imaging for improved lesion detection, and characterization for various indications such as in evaluation of malignancies, infections, inflammation, and vascular diseases. The safety profile of GCCAs is based on the strong binding properties of the chelate to the paramagnetic gadolinium ion (Gd^{3+}) to assure nearly complete renal excretion (33). GCCAs can be classified based on structure (linear or macrocyclic), and charge (ionic or nonionic), where macrocyclic chelates have demonstrated higher in vivo stability, and are thus considered safer than linear agents (33). The identification of nephrogenic systemic fibrosis (NSF) as a rare but serious adverse reaction to (mainly) linear GCCAs led to a new perception of the safety profile of GCCAs, and restricted the use of GCCAs in patients with an estimated renal filtration rate below 30 ml/min/1.73m^2 (34). Recent findings on accumulation of miniscule amounts of gadolinium in the human body have spurred further reassessments of the safety profile of GCCAs, which in July 2017 led to the recommendation of suspension of marketing authorization of linear chelates by the European Medicine Agency (EMA). In **Chapter 11**, we provide an overview of the safety profile of all GCCAs, and reflection of the EMA recommendations.

THESIS OUTLINE

This thesis is structured as follows. First, we evaluate the reproducibility and clinical validity of T1 mapping and ^{1}H-MRS in renal imaging, and provide consensus-based technical recommendations for renal T1 and T2 mapping (**part 1**). Second, we study the associations between obesity and reno-cardiovascular health, and multi-organ impact of obesity in population-based imaging studies using different quantitative MRI metrics (**part 2**). Finally, we contemplated contrast media safety with regard to the use of gadolinium (**appendix**).

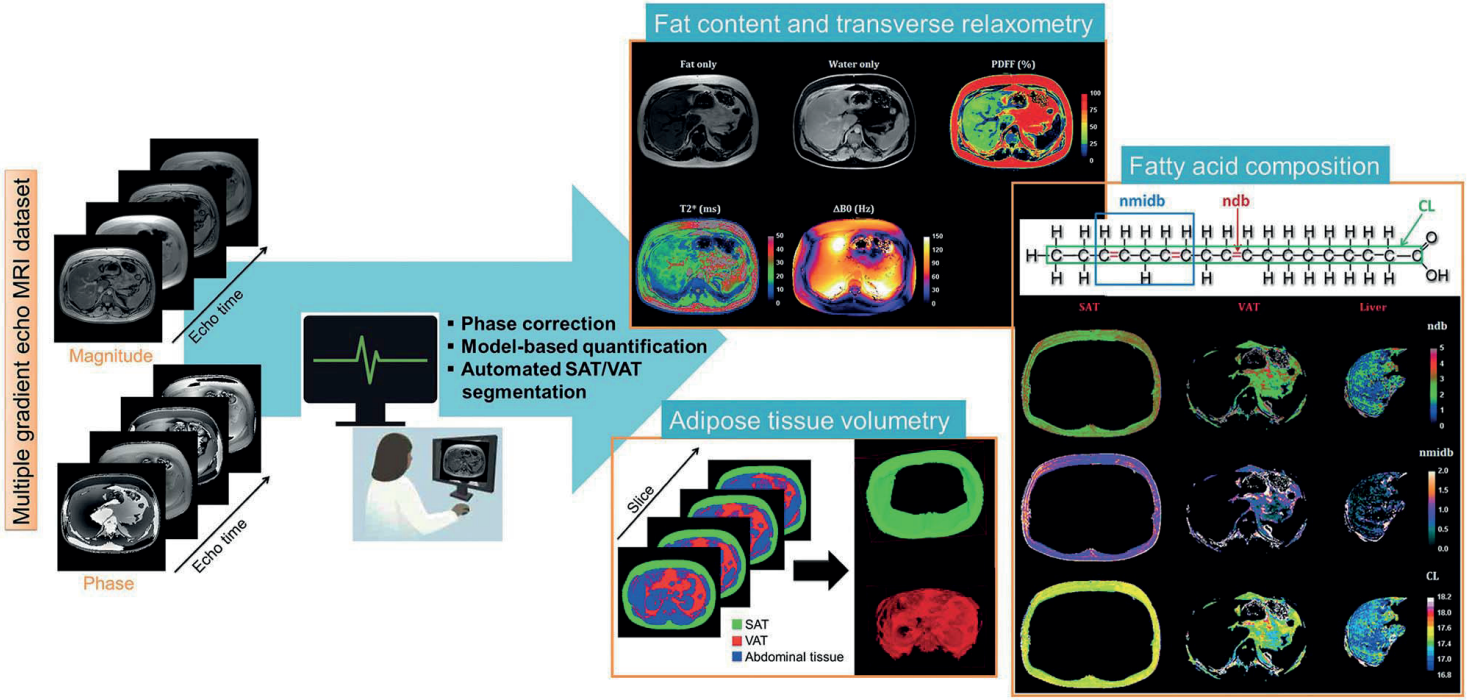

Figure 2. Different MRI approaches for the quantification of body fat distribution (32).

REFERENCES

1. Brink JA, Arenson RL, Grist TM, Lewin JS, Enzmann D. Bits and bytes: the future of radiology lies in informatics and information technology. Eur Radiol. 2017;27(9):3647–3651.
2. Cercignani M, Dowell N, Tofts P. Quantitative MRI of the brain: principles of physical measurement. CRC Press; 2018.
3. Mitchell D, Cohen M. MRI principles. Saunders; 1999.
4. Price RR. The AAPM/RSNA Physics Tutorial for Residents. RadioGraphics. Radiological Society of North America; 1999;19(6):1641–1651.
5. Oz G, Alger JR, Barker PB, et al. Clinical proton MR spectroscopy in central nervous system disorders. Radiology. 2014;270(3):658–679.
6. Pokharel SS, Macura KJ, Kamel IR, Zaheer A. Current MR Imaging Lipid Detection Techniques for Diagnosis of Lesions in the Abdomen and Pelvis. RadioGraphics. 2013;33(3):681–702.
7. Quantitative Imaging Biomarkers Alliance. https://www.rsna.org/en/research/quantitative-imaging-biomarkers-alliance. Accessed September 3, 2019.
8. Levin A, Tonelli M, Bonventre J, et al. Global kidney health 2017 and beyond: a roadmap for closing gaps in care, research, and policy. Lancet. 2017;390(10105):1888–1917.
9. Goldstein SL, Jaber BL, Faubel S, Chawla LS. AKI Transition of Care: A Potential Opportunity to Detect and Prevent CKD. Clin J Am Soc Nephrol. 2013;8(3):476–483.
10. Visconti L, Cernaro V, Ricciardi CA, et al. Renal biopsy: Still a landmark for the nephrologist. World J Nephrol. 2016;5(4):321–327.
11. Selby NM, Blankestijn PJ, Boor P, et al. Magnetic resonance imaging biomarkers for chronic kidney disease: a position paper from the European Cooperation in Science and Technology Action PARENCHIMA. Nephrol Dial Transplant. 2018;33(suppl_2):ii4–ii14.
12. MacMahon B, methods. TP. Epidemiology: principles and methods. 1970.
13. Allen N, Sudlow C, Downey P, et al. UK Biobank: Current status and what it means for epidemiology. Heal Policy Technol. 2012;1(3):123–126.
14. Higgins MW. The Framingham Heart Study: review of epidemiological design and data, limitations and prospects. Prog Clin Biol Res. 1984;147:51–64.
15. Million Women Study Collaborative Group TMWSC. The Million Women Study: design and characteristics of the study population. The Million Women Study Collaborative Group. Breast Cancer Res. BioMed Central; 1999;1(1):73–80.
16. Terwee C, Burdorf L, Dekker F. Inspiratie in de epidemiologie. Een bloemlezing van Nederlandse epidemiologische studies van het eerste uur. 2011.
17. de Mutsert R, den Heijer M, Rabelink TJ, et al. The Netherlands Epidemiology of Obesity (NEO) study: study design and data collection. Eur J Epidemiol. 2013;28(6):513–523.
18. Sudlow C, Gallacher J, Allen N, et al. UK Biobank: An Open Access Resource for Identifying the Causes of a Wide Range of Complex Diseases of Middle and Old Age. PLOS Med. 2015;12(3):e1001779.

19. Roth GA, Forouzanfar MH, Moran AE, et al. Demographic and Epidemiologic Drivers of Global Cardiovascular Mortality. N Engl J Med. 2015;372(14):1333–1341.

20. O'Flaherty M, Buchan I, Capewell S. Contributions of treatment and lifestyle to declining CVD mortality: why have CVD mortality rates declined so much since the 1960s? Heart. 2013;99(3):159–162.

21. Lucas FL, DeLorenzo MA, Siewers AE, Wennberg DE. Temporal Trends in the Utilization of Diagnostic Testing and Treatments for Cardiovascular Disease in the United States, 1993–2001. Circulation. 2006;113(3):374–379.

22. Collaborators, GBD 2015 Obesity, Afshin A, Forouzanfar MH et al. Health Effects of Overweight and Obesity in 195 Countries over 25Years. N Engl J Med. 2017;377(1):13–27.

23. Sorop O, Olver TD, van de Wouw J, et al. The microcirculation: a key player in obesity-associated cardiovascular disease. Cardiovasc Res. 2017;113(9):1035–1045.

24. Tomiyama AJ, Hunger JM, Nguyen-Cuu J, Wells C. Misclassification of cardiometabolic health when using body mass index categories in NHANES 2005–2012. Int J Obes. 2016;40(5):883–886.

25. Rothman KJ. BMI-related errors in the measurement of obesity. Int J Obes. 2008;32(S3):S56–S59.

26. Neeland IJ, Ross R, Després J-P, et al. Visceral and ectopic fat, atherosclerosis, and cardiometabolic disease: a position statement. Lancet Diabetes Endocrinol. 2019;7(9):715–725.

27. Bley TA, Wieben O, François CJ, Brittain JH, Reeder SB. Fat and water magnetic resonance imaging. J Magn Reson Imaging. 2010;31(1):4–18.

28. Hu HH, Kan HE. Quantitative proton MR techniques for measuring fat. NMR Biomed. 2013;26(12):1609–1629.

29. Lee JJ, Pedley A, Hoffmann U, Massaro JM, Fox CS. Association of Changes in Abdominal Fat Quantity and Quality With Incident Cardiovascular Disease Risk Factors. J Am Coll Cardiol. 2016;68(14):1509–1521.

30. Fox CS, Massaro JM, Hoffmann U, et al. Abdominal Visceral and Subcutaneous Adipose Tissue Compartments. Circulation. 2007;116(1):39–48.

31. Whitmer RA, Gunderson EP, Barrett-Connor E, Quesenberry CP, Yaffe K. Obesity in middle age and future risk of dementia: a 27 year longitudinal population based study. BMJ. 2005;330(7504):1360.

32. Viallon M, Leporq B, Drinda S, Wilhelmi de Toledo F, Galusca B, Ratiney H, Croisille P. Chemical-Shift-Encoded Magnetic Resonance Imaging and Spectroscopy to reveal immediate and long-term multi-organs composition changes of a 14-days periodic fasting intervention: a technological and case report. Frontiers in Nutrition. 2019 Mar 1;6:5.

33. Sherry AD, Caravan P, Lenkinski RE. Primer on gadolinium chemistry. J Magn Reson Imaging. 2009;30(6):1240–1248.

34. Runge VM. Critical Questions Regarding Gadolinium Deposition in the Brain and Body After Injections of the Gadolinium-Based Contrast Agents, Safety, and Clinical Recommendations in Consideration of the EMA' s Pharmacovigilance and Risk Assessment Committee Recommendation for Suspension of the Marketing Authorizations for 4 Linear Agents. Invest Radiol. 2017;52(6):317–323.

2

Clinical Application and Technical Considerations of T1 and T2(*) Mapping in Cardiac, Liver, and Renal Imaging

Dekkers IA, Lamb HJ.

Br J Radiol. 2018 Dec;91(1092):20170825

ABSTRACT

Pathological tissue alterations due to disease processes such as fibrosis, edema and infiltrative disease can be non-invasively visualized and quantified by magnetic resonance imaging using T1 and T2 relaxation properties. Pixel-wise mapping of T1 and T2 image sequences enable direct quantification of T1, T2(*), and extra-cellular volume (ECV) values of the target organ of interest. Tissue characterization based on T1 and T2(*) mapping is currently making the transition from a research tool to a clinical modality, as clinical usefulness has been established for several diseases such as myocarditis, amyloidosis, Anderson-Fabry and iron deposition. Other potential clinical applications besides the heart include, the quantification of steatosis, cirrhosis, hepatic siderosis and renal fibrosis. Here, we provide an overview of potential clinical applications of T1 and T2(*) mapping for imaging of cardiac, liver and renal disease. Furthermore, we give an overview of important technical considerations necessary for clinical implementation of quantitative parametric imaging, involving data acquisition, data analysis, quality assessment, and interpretation. In order to achieve clinical implementation of these techniques, standardization of T1 and T2(*) mapping methodology and validation of impact on clinical decision making is needed.

INTRODUCTION

Pathological alterations in tissue composition often have similar manifestations in different organ systems such as the heart, liver and kidney. To illustrate, fibrotic organs share similarities on both histopathology and imaging, including stiffness due to excessive extracellular matrix deposition, reduced vasculature, and an uneven surface due to fibroblast formation (1, 2). Also edema manifests in different organs as excessive fluid accumulation either within cells (cellular edema) or within the collagen matrix of the interstitial spaces (interstitial edema) (3). Infiltrative diseases (e.g. iron deposition, amyloidosis, and lipid accumulation) can lead to systemic alterations in tissue composition causing dysfunction of different organs, including heart, liver, and kidney. These pathological changes in tissue composition can be non-invasively visualized and quantified using novel multiparametic imaging techniques, whereas conventional MR imaging only enabled qualitative image interpretation and signal intensity based analysis using arbitrary units (4).

Direct quantification of the T1 and T2(*) via parametric imaging (i.e. imaging using quantitative sequences such as T1 and T2(*) mapping with milliseconds as the corresponding unit) addresses several of these limitations via the inherent quantitative results and elimination of user-dependent interpretation. Tissue characterization using late gadolinium enhancement (LGE) in cardiac MR is considered the gold standard non-invasive imaging technique for the assessment of myocardial scar, however several important limitations exist. Since LGE relies on differences in signal intensity between scar tissue and adjacent 'normal' tissue, it is not sensitive for the detection of diffuse fibrosis (5). Additionally, signal intensities in LGE are expressed on an arbitrary scale which challenges comparison over time, and the enhancing tissues are not only influenced by technical parameters during image acquisition but also to the arbitrarily set intensity threshold (6). T2 weighted imaging is commonly used to asses inflammation and edema, however these sequences are affected by various limitations including regional differences introduced by signal variation due to phased-array coil arrays, and difficulties in differentiating edema from sub-endocardial blood in cardiac MR (7). Quantification of T1 and T2 values based on a quantitative pixel-wise maps can reduce the variation in assessment and thus serve as an alternative for LGE and T2 weighted imaging (8). T1 and T2(*) mapping not only identifies and quantifies diseased tissue contents, but also allows for direct comparison over time with reduced analysis time (9). Initial efforts of multiparametric imaging using T1 and T2(*) mapping have mainly focused on cardiac imaging, however these techniques can also be applied in other organs, such as liver, and kidney. This ability of non-invasive tissue characterization could ultimately be used for better understanding of common disease pathways and monitoring of the effectiveness of different therapies. An overview of potential parametric imaging methods for the assessment of different heart, liver and kidney diseases is given in **Table 1**. In this review we provide an overview of the potential

clinical application of T1 and T2(*) mapping for the imaging of cardiac, liver and renal disease. Furthermore, we describe important technical considerations involving data acquisition, data analysis, quality assessment, and interpretation that are necessary for the clinical implementation of quantitative parametric imaging.

Table 1. Overview of potential parametric imaging methods for the assessment of different heart, liver and kidney diseases

Parametric imaging method	Organ of interest		
	Heart	Liver	Kidney
Native T1	edema (acute ischemia, acute inflammation), storage disease (amyloid, iron, lipid deposition)	Fibrosis, steatohepatitis, post-transplantation changes	Fibrosis, post-transplantation changes
ECV, Post-contrast T1	fibrosis (replacement: chronic infarction, primary cardiomyopathy; interstitial; primary cardiomyopathy, volume overload)	Functional liver parenchyma	
T2	edema (acute ischemia, acute inflammation)	edema (preclinical models only)	edema, renal cyst progression (preclinical models only)
T2*	iron deposition	iron deposition	

ECV, extracellular volume.

T1 mapping

T1 mapping is the geographical representation of true T1 of certain tissues within the field of view. In order to reconstruct the T1 map, proton spin-lattice relaxation times (T1) are calculated for every voxel within the field of view using multiple raw images with different degrees of recovery of magnetization along the longitudinal axis following inversion recovery (IR) or saturation recovery (SR) prepulses (10) (**Fig. 1a and 1b**). T1 maps are reconstructed in either colour or gray scale, where the intensity of a certain voxel represents the corresponding T1 value. This voxel-wise T1 mapping has led to numerous studies on the clinical utility of signal quantification for the detection of myocardial disease in cardiac MRI (11). Voxel-wise T1-mapping was first introduced by the inversion recovery based modified look-locker imaging (MOLLI) sequence (12), and has led to the development of shortened MOLLI (shMOLLI) (13), and variations. Saturation recovery based sequences are saturation-recovery single-shot Acquisition (SASHA) (14), and mixed IR-SR combinations such as saturation-pulse prepared heart-rate independent inversion-recovery (SAPPHIRE) (15).

T1 mapping can be used for tissue characterization by: a) native (non-contrast) T1 reflecting tissue disease involving both cellular components as interstitium, or b) extracellular volume fraction (ECV) after the administration of gadolinium based contrast agents. ECV

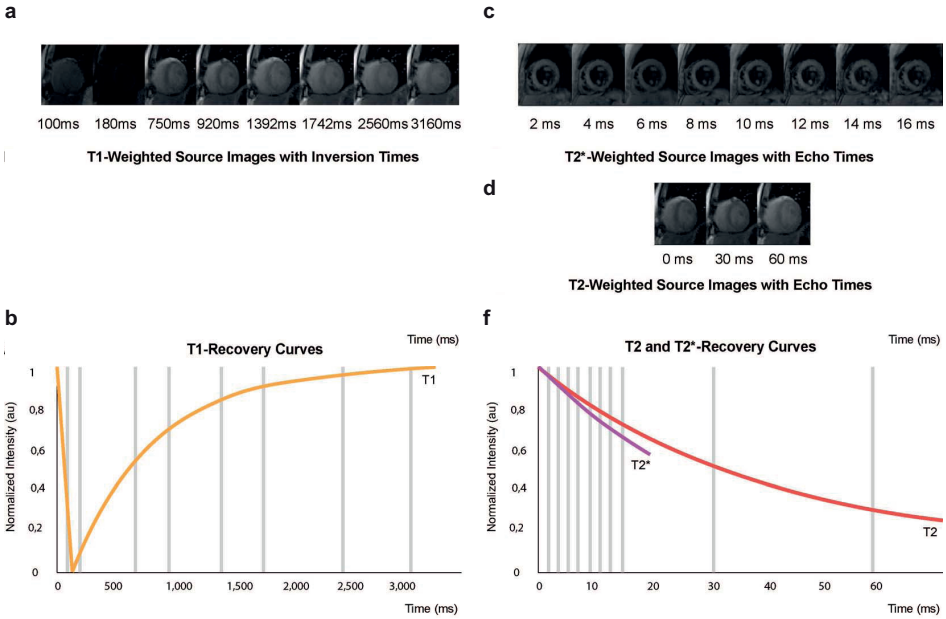

Figure 1. Magnetization Inversion Recovery for T1, T2*, T2 mapping. (**a**) Different images are obtained following an inversion pulse at multiple different inversion times for T1 mapping during the same phase of the cardiac cycle in subsequent heart beats. (**b**) As the inversion time increases the longitudinal magnetization increases due to T1 recovery, yellow curve. (**c**) Different gradient echo images are acquired at different echo times for T2* mapping, and (**d**) different spin-based preparation images are acquired at different echo times for T2 mapping. (**e**) As the TE increases, the myocardial signal intensity decreases due to T2 decay, red curve, and due to static field inhomogeneities for T2* decay, pink curve.

directly quantifies the size of the extracellular space as a percentage reflecting interstitial disease, and is independent of field strength (16). ECV is calculated as follows:

$$ECV\,(\% = (1 - hematocrit) \times \frac{\left(\frac{1}{T1\ post,\ tissue} - \frac{1}{T1\ native,\ tissue}\right)}{\left(\frac{1}{T1\ post,\ blood\ pool} - \frac{1}{T1\ native,\ blood\ pool}\right)}$$

where T1 post is the contrast-enhanced T1 of the tissue of interest or blood pool, T1 tissue native is the non-enhanced T1 of the tissue of interest or blood pool (**Fig. 2**).

T2 and T2* mapping

T2 mapping is the voxel-wise representation of the proton spin-spin relaxation time (T2) of the tissue of interest within the field of view. T2 values for each voxel are acquired via based T2 weighted images at various echo times with a long repetition time in order to minimize the effect of longitudinal relaxation (**Fig. 1c and Fig. 1d**). Acquired T2 values reflect the free water content present in the tissue of interest, which can be used for quantification of edema. The most frequently used sequence for T2 mapping is the balanced steady-state free precession (bSSFP) sequence (8), and other used sequences are

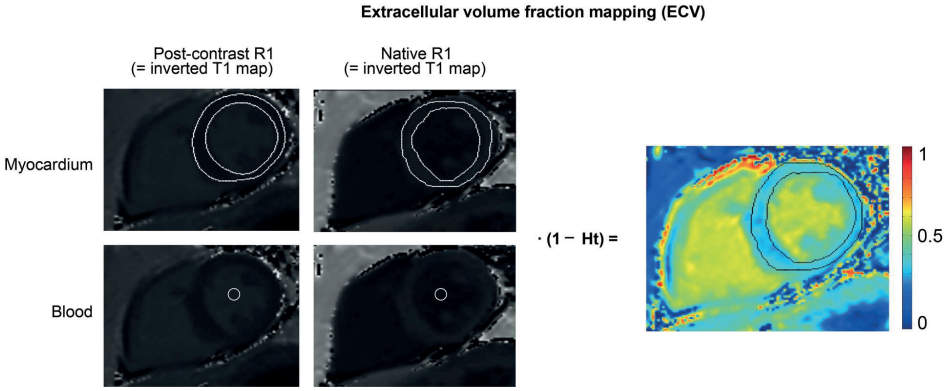

Figure 2. Calculation of ECV. Calculation of ECV using the inverse of the signal in each pixel (1/T1) is used to generate an R_1 map (F). The ΔR_1 map of the blood pool (ΔR_1blood) and myocardium (ΔR_1myocard) is generated by subtracting the corresponding precontrast R_1 map from the postcontrast R_1 map. ΔR_1 map pixel values are multiplied by one minus the hematocrit level, and then divided by the mean ΔR_1blood in order to calculate ECV. The final result is a colour encoded parametric map displaying the pixel-by-pixel ECV values.

gradient-recalled echo (17) and spiral imaging (18). These sequences are combined with several images with different T2 preparation module echo times.

T2 star (denoted as T2*) mapping uses the effective T2 value which decays faster than true T2 due to the dephasing effects of local field inhomogeneities from susceptibility differences present within the voxel (**Fig. 1c and Fig. 1e**). T2* mapping can be used for measurement of iron content in tissues. Used T2* mapping sequences are multi-echo gradient recalled echo (GRE) sequences (19).

CLINICAL APPLICATIONS

Heart

Diffuse fibrosis and infiltrative cardiac diseases

One of the major advantages of T1 mapping compared to LGE is the possibility to visualize infiltrative interstitial disease or extensive diffuse fibrosis (**Fig. 3 and Fig. 4**). Fibrosis which is a non-physiological scarring process leading to destruction of organ architecture and organ dysfunction via excessive deposition of extracellular matrix (2). Increased T1 on native, and post-contrast images due to diffuse fibrosis has extensively been described in several diseases, such as hypertrophic cardiomyopathy, aortic stenosis, sarcoidosis, systemic sclerosis, and myocarditis (20) (**Fig. 5**). Also, interstitial myocardial fibrosis after treatment with anthracycline chemotherapy has been associated with significantly increased ECV values compared with oncologic patients that had not yet initiated chemotherapy (21). These findings indicate that T1-mapping techniques may

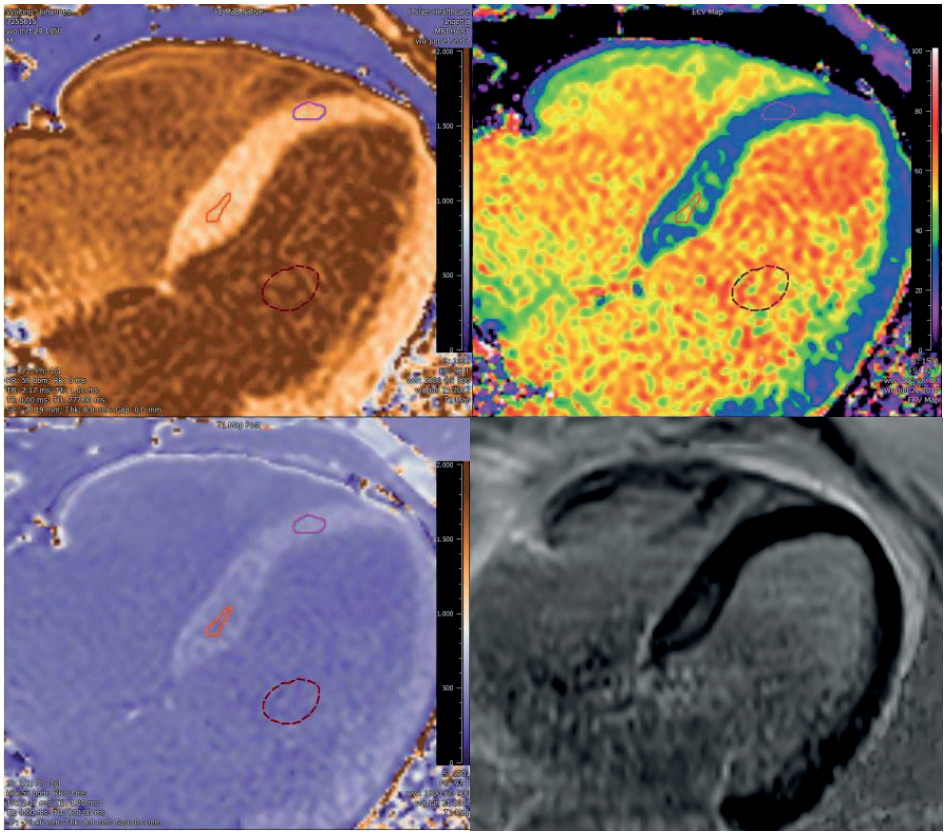

Figure 3. Example of added value ECV of the heart compared to LGE only in a patient with premature ventricular contractions (PVCs). LGE shows some enhancement basal septal, which is confirmed by the ECV map constructed using the pre- and post-contrast T1 maps. The ECV in the region of interest was 45% localized in focal septal hypertrophy, which is the likely origin of the PVC's. Quantitative T1 and ECV maps were automatically reconstructed on a voxel-by-voxel basis after data acquisition using the T1 map processing tool (Medis research, version 3.0, Leiden).

be useful as novel risk stratification biomarkers for cardiotoxicity prior to and during treatment with anthracycline agents. Increased interstitial space does not only result from fibrosis, but may also be due to the presence of infiltrates such as in amyloidosis (22, 23). In amyloidosis, T1 mapping and ECV have made great advance in diagnosing cardiac involvement and have shown to be predictive of mortality (23-25). As such, the necessity of cardiac biopsy for confirming cardiac involvement can be debated as native T1 and ECV can be used reliably for non-invasive diagnosis. Another exemplary disease with diffuse myocardial infiltration that can be well detected via parametric imaging is Anderson-Fabry disease. Anderson-Fabry is characterized by intracellular lysosomal lipid accumulation which results in decreased T1 values on native T1 mapping (26, 27). Other cardiomyopathies in which T1 mapping and ECV have been described to be potentially

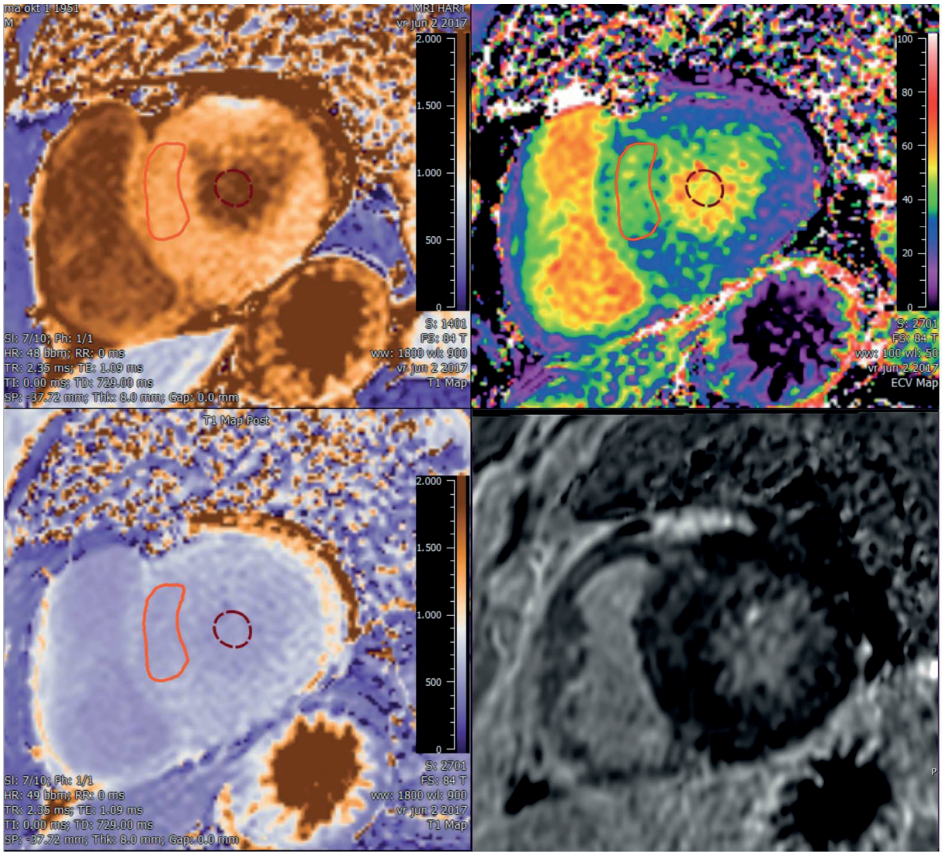

Figure 4. Example of added value of ECV compared to LGE in a patient with familial hypertrophic cardiomyopathy with diffuse fibrosis. Non-dilated left ventricle with septal hypertrophy with diffuse fibrosis (serum haematocrit of 45%, native T1 septum 1315 ms [N<1350 ms], and ECV 42 % [N<35%]). Quantitative T1 and ECV maps were automatically reconstructed on a voxel-by-voxel basis after data acquisition using the T1 map processing tool (Medis research, version 3.0, Leiden).

beneficial for diagnosis are hypertrophic (28) and dilating cardiomyopathy (29), however further research is still needed to validate diagnostic usefulness and prognostication. Another example of an interstitial disease in which T2* mapping can be of great value is cardiac siderosis. Previous research has showed that myocardial T2 values correlate well with tissue iron concentration (30), which has enabled visualization and quantification of iron accumulation in the heart using T2(*) mapping (**Fig. 6a**). Parametric imaging could be besides diagnosis also be used for treatment monitoring, such as plasma cell dyscrasia suppressive agents for light-chain Amyloidosis (31), enzyme replacement therapies for Anderson-Fabry (32), and modern chelation regimes for cardiac cardiac sidersosis (33). Early initiation of chelation therapy based on myocardial T2* has drastically influenced long-term prognosis in patients with thalassemia by decreasing the annual death rate

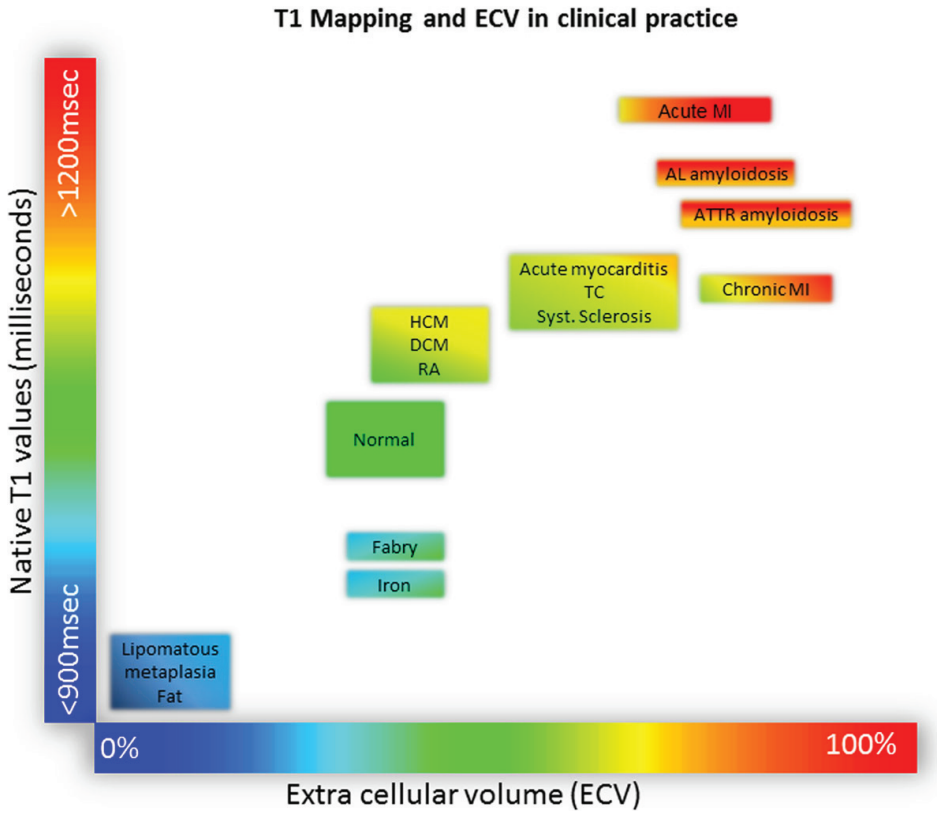

Figure 5. Tissue characterization using native T1 and extracellular volume fraction (ECV). Absolute values for native T1 depend greatly on field strength (1.5 T or 3 T), pulse sequence (MOLLI or ShMOLLI), scanner manufacturer and post-processing. For the purpose of comparability, only studies using 1.5 T scanners were considered in this figure. Reprinted from Haaf P et. al. (95), publisher BioMed Central under the terms of the Creative Commons License.

from cardiac iron overload (33). When available, T1 mapping and ECV could also be used for monitoring the effectiveness of antifibrotic treatments (34).

Cardiac dysfunction

Functional studies have showed that higher ECV values are correlated with reduced left ventricular ejection fraction, and lower myocardial blood flow in dilated cardiomyopathy and lower systolic strain in left ventricular hypertrophy (28, 35). Furthermore, interstitial fibrosis in diastolic dysfunction has also been linked to the development of heart failure with preserved ejection fraction (36). These findings suggest that the expansion of the extracellular matrix may be a key contributor to contractile dysfunction. Combining parametric imaging of the heart with functional cardiac MR imaging could be of great advantage for identifying focal areas of interstitial fibrosis that negatively influence car-

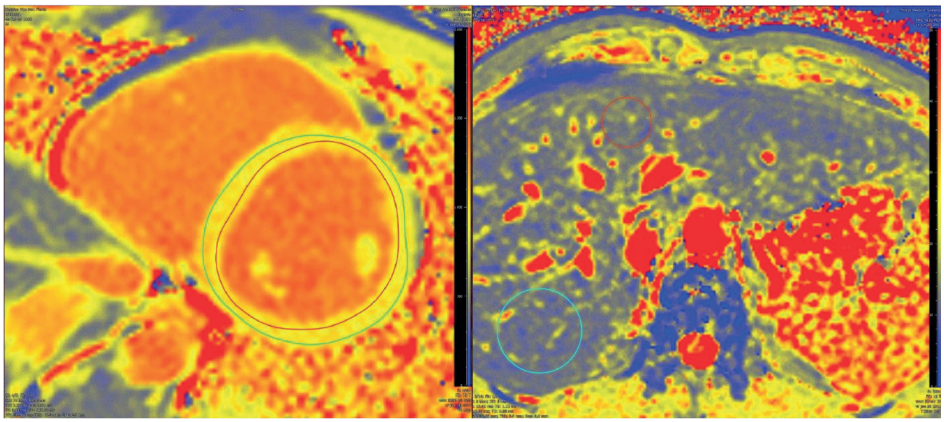

Figure 6. T2* mapping of heart (left) and liver (right) in a childhood cancer survivor at risk of secondary hemosiderosis after multiple blood transfusions and chemotherapy for acute lymphatic leukemia. Parametric imaging of heart and liver using StarQuant (Philips) heart and LiverMultiScan (Perspectum). The myocardial T2* value was 38 ms (normal reference >20 ms), and liver T2* value was 13.3 ms, indicating normal T2* values of the heart and minimal iron deposition in the liver. Quantitative T2 maps were automatically reconstructed on a voxel-by-voxel basis after data acquisition using the T2 map processing tool (Medis research, version 3.0, Leiden).

diac function. There is an growing body of evidence evaluating the prognostic value of T1 mapping and ECV in in patients with cardiac dysfunction (37). Several studies have been performed that evaluated the association between native T1 (38, 39), and ECV (11, 40-42) with incident heart failure and all-cause mortality. These studies have found that both native T1 and ECV are more sensitive for predicting adverse events that left ventricular ejection fraction which is the currently used for prognostication in heart failure (37). However, for T2 mapping thus far no prognostic evidence has been reported for patients with heart failure although the diagnostic role of T2 mapping for acute conditions such as acute myocardial infarction and acute myocarditis is promising.

Ischemic heart disease

Differentiation between acute and chronic myocardial infarction has important clinical implications. Late gadolinium enhancement (LGE), which is currently used for the detection of infarcted myocardium, is sensitive to motion-artefacts, and incomplete nulling of the myocardium, and does not differentiate well between acute and chronic myocardial infarction. Early studies using T1 mapping showed that acute and chronic myocardial infarction had different patterns of T1 changes after the administration of gadolinium (43). Besides contrast-enhanced techniques, also native T1 and T2 mapping have shown to be an accurate method for differentiating acute and chronic myocardial infarction via the detection of edema (44, 45). Expansion of current cardiac imaging protocols with T1 and

T2 mapping could thus potentially improve the sensitivity for the detection of myocardial infarction compared to LGE and T2 weighted black blood imaging alone.

Myocarditis

Acute myocarditis is associated with a high mortality if untreated, however clinical criteria alone are often of limited value for establishing the diagnosis. Both native T1 and T2 mapping have showed to be more sensitive for the detection of acute myocarditis with T2-weighted and LGE MR imaging techniques (46, 47), however native T1 mapping was found to have a superior diagnostic performance compared with T2 mapping (47). Moreover, recent studies have showed that both native T1 mapping and T2 mapping can reliably discriminate between healthy and diseased myocardial tissue (48, 49), and correspond to the clinical disease stage (50). The use of LGE and ECV seems to be beneficial for the detection of more chronic stages of myocarditis (50).

Liver

Estimated annual progression rates of compensated to decompensated liver cirrhosis range between 5 to 11% (51, 52), and prevention of decompensation is the primary treatment goal in compensated cirrhosis (53). However, currently available clinical scoring systems do not accurately identify patients at increased risk of decompensation (54). The observation that the extent of liver enhancement by hepatobiliary specific contrast agents, such as gadobenate dimeglumine and gadoxetate disodium, is liver function dependent has led to multiple studies on contrast-enhanced T1-mapping using these agents. Several of these studies have shown promising results indicating that hepatobiliary contrast enhanced T1-mapping and ECV correlates well with histological measurements of hepatic fibrosis (55), liver function tests (56-60), and Child-Pugh scores (61). Recent studies, however, have indicated that also native hepatic T1 corrected for iron content (cT1) can be used for estimating liver fibrosis (62, 63). cT1 was found to be independently associated with survival in a proof of principle study (64), and was not affected by the degree of adiposity or presence of ascites (62) in contrast to other acoustic-based techniques such as elastrography (62). Furthermore, higher liver inflammation and fibrosis scores based on hepatic T1 and T2* values were found to be associated with an increased risk of liver-related adverse outcomes such as encephalopathy, ascites and liver-related death (65).

Already in 2005, it has been described that relaxation rates 1/T2 and 1/T2* could be used as a non-invasive method for the quantification of hepatic iron concentration, as these measures were closely correlated by iron concentration measured via liver biopsy (66). When parametric mapping techniques became available, additional studies histologically validated the ability of T2* mapping for the quantification hepatic iron content (62, 67), and assessed reproducibility (62). A prospective study evaluating the predictive value of T2* on liver-related adverse outcomes found a protective effect with

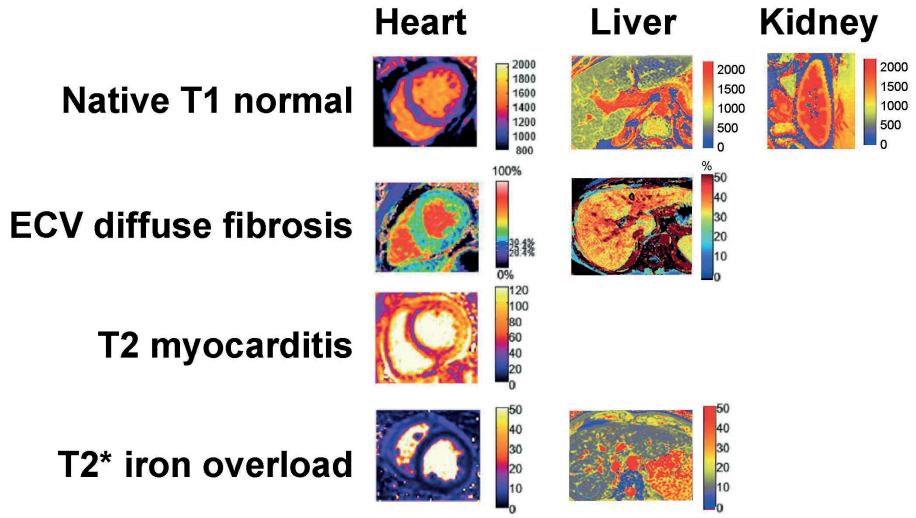

Figure 7. Typical appearance of T1, T2, T2*, and ECV maps in heart, liver, and kidney of healthy subjects and in patients with myocardial and liver disease. Adapted by permission from BioMed Central under the terms of the Creative Commons License (90), and adapted by permission from BMJ Publishing Group Limited (55).

increasing T2*, which is inversely related to iron load (65). These findings are in line with previous biopsy studies that observed hepatic iron content was predictive of death in alcohol-related liver cirrhosis (68), and more severe fibrosis in non-alcoholic fatty liver disease (69). Non-invasive parametric imaging of the liver could ultimately contribute to personalized medicine based approaches for treatment monitoring, such as evaluating the effects of hepatic iron lowering therapy (**Fig. 6b**) (70) or anti-fibrotic treatment strategies (1). However additional (multicenter) studies are needed in order to determine whether multiparametric MR imaging could indeed contribute to achieving this goal and ultimately replace liver biopsies.

Kidney

On conventional MR imaging of the kidney, anatomical differences between renal cortex and medulla can be clearly differentiated due to the shorter T1 relaxation times of the cortex. Loss of this so-called corticomedullary differentiation occurs in several renal diseases and has been primarily attributed to altered T1 relaxation times in the renal cortex (71). Recent studies suggest that characterization of renal tissue composition via true T1 values without contrast might be useful for differentiating specific renal disease states, such as renal fibrosis imaging. Preclinical studies have shown that T1-mapping could be used for the assessment of acute kidney injury and chronic kidney disease in mice (72-74). Recent clinical studies in renal transplant patients found that renal native T1 values

correlated well with renal fibrosis severity based on histology (75) and with glomerular filtration rate (GFR) after transplantation (76). Good intra- and inter-examination reproducibility has been reported for renal native T1 mapping using the MOLLI 5(3)3 scheme in both healthy human volunteers and diabetic nephropathy patients (77), supporting that native T1 could be used as a reliable and consistent measure of renal tissue composition. However, additional studies are needed to evaluate the reproducibility of renal T1 mapping at different imaging centers with various MRI scanner manufacturers. Since native T1 mapping is at least partially modulated by perfusion (which is also a major determinant of GFR), T1 relaxation times obtained in patients with impaired renal function could theoretically be confounded by lower renal perfusion rather reflecting true fibrosis only. More research is needed to determine to what extent native renal T1 values are affected by impaired perfusion, and whether renal native T1 mapping has added value for clinical decision-making compared to currently available renal function markers and other MR techniques such as diffusion weighted imaging, and blood-oxygen-level dependent imaging. Thus far no studies have evaluated renal extra-cellular (interstitial) volume using native and post-contrast T1-mapping. The administration of contrast in patients with severely impaired renal function is controversial due to the risk of nephrogenic systemic fibrosis (NSF) (78), however new insights suggest that modern macrocyclic GBCAs may not be associated with the development of NSF even when administered to high risk chronic kidney disease patients (79-82). Renal T2 mapping has thus far only been evaluated in mouse models, which showed that renal cortex T2 values increase after kidney transplantation (73) and that renal T2 is highly correlated with the histological cystic index in a polycystic kidney disease model (83). Further research is needed to assess whether T2 mapping could be useful for assessment of edema, or for the prediction of cyst progression in humans.

Technical considerations for clinical implementation

Data acquisition

The decision about the used pulse sequence and parameters starts with the clinical question that needs to be answered, and the disease and organ of interest (**table 2**). Roughly, it can be said that T1 mapping can be used for imaging of fibrosis, steatosis, edema, iron without the need for contrast agents. As native T1 is a measure of both intracellular and extracellular space it is less sensitive to increased extracellular space but more sensitive to other tissue characteristics, such as hemosiderosis, steatosis, and edema. The strength of ECV is; (a) the possibility to differentiate between intracellular versus extra-cellular (interstitial) compartments, and (b) its independence to field strength (84). T2 mapping and T2* mapping are very sensitive for edema and hemosiderosis respectively. Which field strength is optimal for a particular clinical application of T1 and T2(*) mapping is another important question. Most validation studies and references studies for cardiac parametric

imaging have been performed at 1.5T, however most parametric imaging studies of the liver have been performed at 3T. Advantages of higher field strengths are the increased signal to noise ratio, and disadvantages are the larger effects of field inhomogeneities. An overview of the advantages and disadvantages of inversion recovery versus saturation recovery based T1 mapping techniques are presented in **Table 2**.

Table 2. Inversion recovery versus saturation recovery T1-mapping techniques

Technique	Example	Advantages	Disadvantages
Inversion recovery (IR)	MOLLI (1), shMOLLI (2), modified MOLLI	Good precision and reproducibility, few image artefacts	Less absolute accuracy
Saturation recovery (SR)	SASHA (3)	Could potentially provide more accurate T1 measurements, less sensitive to magnetization transfer	More susceptible to noise and artefacts, reproducibility has less extensively been validated
Combined	SAPPHIRE (4)	Shares many of the advantages of IR and SR	Shares the disadvantages of IR

MOLLI, modified look-locker imaging; shMOLLI, shortened MOLLI; SASHA, saturation-recovery single-shot Acquisition; SAPPHIRE, saturation-pulse prepared heart-rate independent inversion-recovery (SAPPHIRE).

Planning

Tissues of interest should be orthogonal to the imaging plane in order to minimize through plane partial volume averaging, which is the two-chamber short axis for the heart, axial for the liver, and axial for the kidney. Furthermore, shimming and center frequency should be adjusted to minimize off resonance, which is especially important at higher field strengths since off-resonance variation may result in regional variations in apparent T1 (85). Adequate breath-holding is needed for correct registration of obtained images, since misregistration can introduce substantial errors in the calculated maps. For cardiac parametric imaging obtained images should be acquired at the same cardiac phase and respiratory position to eliminate tissue motion. Motion-correction could partly overcome the effects of suboptimal breath-holding, and minimize artefacts related to motion and misregistration. The use of fully automated motion correction and co-registration of breath-holds can significantly improve the quality of ECV maps, and increase clinical applicability (86). New developments are the application of 3D imaging and segmentation in order to achieve higher spatial resolution (87), and the use of automated ECV measurement (86) or volumetric ECV measurement for the determination of functional liver-volume (88).

Data analysis and reporting

Clinical imaging units currently provide MR T1 and T2(*) mapping software that can be used for visual evaluation and basic quantification. Post-processing software with dedi-

cated quantification packages are available, which contribute to appropriate scaling of the parametric maps in colour- or grayscale to maximize differentiation between diseased and normal tissues. Regions of interest should be placed with care in order to minimize partial volume effects and should have adequate margins from tissue interfaces, such as the intracardial blood pool, pericardial fat, renal sinus fat and perirenal fat, but also large vascular and biliary structures in the liver. Quantitative error estimates in post-processing software are useful for the assessment of the reliability of measured T1 and T2(*) values. The availability of such quantitative error estimates are an important requirement for the use of quantitative parametric imaging in clinical decision making, since these can help to identify unreliable regions in quantitative imaging and for interpretation and for comparison of imaging protocols (89). The importance of the quality of the pixel-wise T1 and T2(*) maps generated with the chosen pulse sequence, parameters, and field strength cannot be underestimated as for reliable clinical decision making high quality, artefact free pixel-wise maps are crucial (84). The detection of potential artefacts and handling still relies on human expertise, which hampers the easy application of these techniques in clinical practice. The Society for Cardiovascular Magnetic Resonance has recently recommended that local results in healthy volunteers for native T1, and T2 mapping should be primarily used and benchmarked against published reference values (90). For clinical use reference data based on a sufficiently large cohorts reflecting normal variations are needed. Since each T1 and T2(*) mapping technique has specific measurement errors, each technique should in principal be compared with normal reference values that were obtained using the same acquisition method, including same pulse sequence parameters and field strength (84). This requires verification on whether the scanner configurations are identical to the acquisition method used in the reference studies (91). Finally, implementation of T1 and T2(*) mapping results into picture archiving and communication systems could facilitate and enhance the use of parametric imaging data in the clinical work environment.

DISCUSSION

To make the transition from an investigational technique to a reliable clinical modality, T1 and T2(*) mapping studies need to prove that these techniques have the ability to make an early, non-invasive diagnosis or to increase confidence in a suspected diagnosis.

In order for an imaging technique to make a successful transition in clinical setting, the impact of the technique on health care needs to be assessed. Criteria that have been defined to assess the efficacy in diagnostic imaging are; technical feasibility, diagnostic accuracy, diagnostic impact, therapeutic impact, impact on outcome, and societal impact (92). Currently cardiac T1 mapping and hepatic T1 and T2* mapping fulfil the first two cri-

teria, and an increasing amount of studies on cardiac T1 mapping and ECV quantification have demonstrated impact on differential diagnosis, treatment strategies, and clinical outcome. Thus far, only few studies have evaluated societal impact, such as cost-benefit analysis. For multiparametric MR of the liver combined with transient elastography, it has been estimated to yield a cost saving over £500 for every patient needing diagnostic evaluation for non-alcoholic steatohepatitis (93). There is an increasing need for studies evaluating to what extent T1 and T2(*) mapping improve diagnosis and contribute to changes in treatment strategies resulting in improved patient outcomes. In cardiac imaging, T1 values overlap for the majority of cardiac pathologies so its value beyond conventional sequences for diagnostic purposes is remains to be proven. Since hepatic steatosis and siderosis can be easily and accurately quantified by parametric imaging and enable treatment response evaluation, it can expected that T1 and T2* mapping will be increasingly used clinically for liver imaging in the near future. Parametric imaging of the kidney however has just recently entered the research phase. Additional to the above mentioned criteria, more studies are needed to provide good reference data for T1 and T2(*) mapping in order to introduce these techniques into clinical practice.

Ultimately, the intra- and inter-examination reproducibility of measured T1 and T2(*) values determines the clinical utility of pixel-wise T1 and T2(*) mapping for disease assessment. To be of clinical value, assessed experimental and biologic variation in the quantified T1 and T2(*) values should be smaller than the changes caused by disease. In order to assess this, sufficiently large cohorts of subjects are needed to guaranty the robustness of a classifier (e.g. sensitivity and specificity) and ultimately findings should be validated in a multicenter trial. Two large on-going multicenter studies on this topic are currently registered on ClinicalTrials.gov. One will evaluate whether myocardial fibrosis based on LGE and T1 mapping can predict all cause and cardiovascular mortality, with an aimed sample size of 1,500 participants (94). The second study aims investigates whether it is cost-effective to use T1 and T2* imaging of the liver as a standardised diagnostic test for liver disease in 2,000 participants (64). The outcomes of these studies contribute to determining whether parametric imaging will truly find its way into clinical practice, or whether it will remain considered as an 'investigational technique' by medical professionals, and health care institutions.

In conclusion, T1 and T2(*) mapping can be considered promising techniques that can be used in addition to conventional MR imaging for the quantification of pathological changes in tissue composition. Disease entities for which T1 and T2(*) mapping could be used clinically are cardiomyopathies, and ischemic heart disease, and other possible applications are the quantification of liver cirrhosis, hemosiderosis and renal fibrosis. Availability of normative data together with standardization of data acquisition, and analysis is warranted. Multicenter trials with sufficient sample size are needed to establish the impact of T1 and T2(*) mapping on clinical outcome and economic benefit.

REFERENCES

1. Rockey DC, Bell PD, Hill JA. Fibrosis—a common pathway to organ injury and failure. N Engl J Med. 2015;372(12):1138-49.
2. Zeisberg M, Kalluri R. Cellular Mechanisms of Tissue Fibrosis. 1. Common and organ-specific mechanisms associated with tissue fibrosis. Am J Physiol. 2013;304:C216-C25.
3. Scallan J, Huxley V, Korthuis R. Capillary Fluid. Exchange: Regulation, Functions, and Pathology. Integrated Systems Physiology: from Molecule to Function to Disease. San Rafael, CA: Morgan & Claypool Life Sciences; 2010.
4. Abdel-Aty H, Schulz-Menger J. Cardiovascular magnetic resonance T2-weighted imaging of myocardial edema in acute myocardial infarction. Recent Pat Cardiovascular Drug Discov. 2007;2(1):63-8.
5. Pattanayak P, Bleumke DA. Tissue characterization of the myocardium: state of the art characterization by magnetic resonance and computed tomography imaging. Radiol Clin North Am. 2015;53(2):413-23.
6. Spiewak M, Malek LA, Misko J, Chojnowska L, Milosz B, Klopotowski M, et al. Comparison of different quantification methods of late gadolinium enhancement in patients with hypertrophic cardiomyopathy. Eur J Radiol. 2010;74(3):e149-53.
7. Abdel-Aty H, Simonetti O, Friedrich MG. T2-weighted cardiovascular magnetic resonance imaging. J Magn Reson Imaging. 2007;26(3):452-9.
8. Giri S, Chung Y-C, Merchant A, Mihai G, Rajagopalan S, Raman SV, et al. T2 quantification for improved detection of myocardial edema. J Cardiovasc Magn Reson. 2009;11(1):56.
9. Blume U, Lockie T, Stehning C, Sinclair S, Uribe S, Razavi R, et al. Interleaved T1 and T2 relaxation time mapping for cardiac applications. J Magn ResonImaging. 2009;29(2):480-7.
10. Taylor AJ, Salerno M, Dharmakumar R, Jerosch-Herold M. T1 Mapping: Basic Techniques and Clinical Applications. JACC Cardiovasc Imaging. 2016;9(1):67-81.
11. Schelbert EB, Messroghli DR. State of the art: clinical applications of cardiac T1 mapping. Radiology. 2016;278(3):658-76.
12. Messroghli DR, Radjenovic A, Kozerke S, Higgins DM, Sivananthan MU, Ridgway JP. Modified Look-Locker inversion recovery (MOLLI) for high-resolution T1 mapping of the heart. Magn Reson Med. 2004;52(1):141-6.
13. Piechnik SK, Ferreira VM, Dall'Armellina E, Cochlin LE, Greiser A, Neubauer S, et al. Shortened Modified Look-Locker Inversion recovery (ShMOLLI) for clinical myocardial T1-mapping at 1.5 and 3 T within a 9 heartbeat breathhold. J Cardiovasc Magn Reson. 2010;12(1):69.
14. Chow K, Flewitt JA, Green JD, Pagano JJ, Friedrich MG, Thompson RB. Saturation recovery single-shot acquisition (SASHA) for myocardial T1 mapping. Magn Reson Med. 2014;71(6):2082-95.
15. Weingärtner S, Akçakaya M, Basha T, Kissinger KV, Goddu B, Berg S, et al. Combined saturation/inversion recovery sequences for improved evaluation of scar and diffuse fibrosis in patients with arrhythmia or heart rate variability. Magn Reson Med. 2014;71(3):1024-34.

16. Moon JC, Messroghli DR, Kellman P, Piechnik SK, Robson MD, Ugander M, et al. Myocardial T1 mapping and extracellular volume quantification: a Society for Cardiovascular Magnetic Resonance (SCMR) and CMR Working Group of the European Society of Cardiology consensus statement. J Cardiovasc Magn Reson. 2013;15:92.

17. Van Heeswijk RB, Feliciano H, Bongard C, Bonanno G, Coppo S, Lauriers N, et al. Free-breathing 3 T magnetic resonance T 2-mapping of the heart. JACC: Cardiovasc Imaging. 2012;5(12):1231-9.

18. Foltz WD, Al-Kwifi O, Sussman MS, Stainsby JA, Wright GA. Optimized spiral imaging for measurement of myocardial T2 relaxation. Magn Reson Med. 2003;49(6):1089-97.

19. Shah S, Xue H, Greiser A, Weale P, He T, Firmin DN, et al. Inline myocardial t2* mapping with iterative robust fitting. J Cardiovasc Magn Reson. 2011;13(1):P308.

20. Puntmann VO, Peker E, Chandrashekhar Y, Nagel E. T1 Mapping in Characterizing Myocardial Disease: A Comprehensive Review. Circ Res. 2016;119(2):277-99.

21. Jordan JH, Vasu S, Morgan TM, D'Agostino RB, Jr., Melendez GC, Hamilton CA, et al. Anthracycline-Associated T1 Mapping Characteristics Are Elevated Independent of the Presence of Cardiovascular Comorbidities in Cancer Survivors. Circ Cardiovasc Imaging. 2016;9(8).

22. Fontana M, Banypersad SM, Treibel TA, Maestrini V, Sado DM, White SK, et al. Native T1 mapping in transthyretin amyloidosis. JACC Cardiovasc Imaging. 2014;7(2):157-65.

23. Banypersad SM, Fontana M, Maestrini V, Sado DM, Captur G, Petrie A, et al. T1 mapping and survival in systemic light-chain amyloidosis. Eur Heart J. 2014;36(4):244-51.

24. Fontana M, Banypersad SM, Treibel TA, Maestrini V, Sado DM, White SK, et al. Native T1 mapping in transthyretin amyloidosis. JACC Cardiovasc Imaging. 2014;7(2):157-65.

25. Martinez-Naharro A, Kotecha T, Norrington K, Boldrini M, Rezk T, Quarta C, et al. Native T1 and Extracellular Volume in Transthyretin Amyloidosis. JACC Cardiovasc Imaging. 2018 pii: S1936-878X(18)30198-0.

26. Sado DM, White SK, Piechnik SK, Banypersad SM, Treibel T, Captur G, et al. The identification and assessment of Anderson Fabry disease by cardiovascular magnetic resonance non-contrast myocardial T1 mapping. Circ Cardiovasc Imaging. 2013;6(3):392-8.

27. Sado DM, Maestrini V, Piechnik SK, Banypersad SM, White SK, Flett AS, et al. Noncontrast myocardial T1 mapping using cardiovascular magnetic resonance for iron overload. J Magn Reson Imaging. 2015;41(6):1505-11.

28. Kuruvilla S, Janardhanan R, Antkowiak P, Keeley EC, Adenaw N, Brooks J, et al. Increased extracellular volume and altered mechanics are associated with LVH in hypertensive heart disease, not hypertension alone. JACC Cardiovasc Imaging. 2015;8(2):172-80.

29. Nakamori S, Dohi K, Ishida M, Goto Y, Imanaka-Yoshida K, Omori T, et al. Native T1 Mapping and Extracellular Volume Mapping for the Assessment of Diffuse Myocardial Fibrosis in Dilated Cardiomyopathy. JACC Cardiovasc Imaging. 2018;11(1):48-59.

30. Carpenter J-P, He T, Kirk P, Roughton M, Anderson LJ, de Noronha SV, et al. On T2* Magnetic Resonance and Cardiac Iron. Circulation. 2011;123(14):1519-28.

31. Hur DJ, Dicks DL, Huber S, Mojibian HR, Meadows JL, Seropian SE, et al. Serial Native T1 Mapping to Monitor Cardiac Response to Treatment in Light-Chain Amyloidosis. Circ Cardiovasc Imaging. 2016;9(10).

32. Messalli G, Imbriaco M, Avitabile G, Russo R, Iodice D, Spinelli L, et al. Role of cardiac MRI in evaluating patients with Anderson-Fabry disease: assessing cardiac effects of long-term enzyme replacement therapy. Radiol Med. 2012;117(1):19-28.

33. Modell B, Khan M, Darlison M, Westwood MA, Ingram D, Pennell DJ. Improved survival of thalassaemia major in the UK and relation to T2* cardiovascular magnetic resonance. J Cardiovasc Magn Reson. 2008;10:42.

34. Stuckey DJ, McSweeney SJ, Thin MZ, Habib J, Price AN, Fiedler LR, et al. T(1) mapping detects pharmacological retardation of diffuse cardiac fibrosis in mouse pressure-overload hypertrophy. Circ Cardiovasc Imaging. 2014;7(2):240-9.

35. Jerosch-Herold M, Sheridan DC, Kushner JD, Nauman D, Burgess D, Dutton D, et al. Cardiac magnetic resonance imaging of myocardial contrast uptake and blood flow in patients affected with idiopathic or familial dilated cardiomyopathy. Am J Physiol Heart Circ Physiol. 2008;295(3):H1234-H42.

36. Su M-YM, Lin L-Y, Tseng Y-HE, Chang C-C, Wu C-K, Lin J-L, et al. CMR-verified diffuse myocardial fibrosis is associated with diastolic dysfunction in HFpEF. JACC Cardiovasc Imaging. 2014;7(10):991-7.

37. Adam RD, Shambrook J, Flett AS. The Prognostic Role of Tissue Characterisation using Cardiovascular Magnetic Resonance in Heart Failure. Cardiac Fail Rev. 2017;3(2):86-96.

38. Mascherbauer J, Marzluf BA, Tufaro C, Pfaffenberger S, Graf A, Wexberg P, et al. Cardiac magnetic resonance postcontrast T1 time is associated with outcome in patients with heart failure and preserved ejection fraction. Circ Cardiovasc Imaging. 2013;6(6):1056-65.

39. Puntmann VO, Carr-White G, Jabbour A, Yu CY, Gebker R, Kelle S, et al. T1-Mapping and Outcome in Nonischemic Cardiomyopathy: All-Cause Mortality and Heart Failure. JACC Cardiovasc imaging. 2016;9(1):40-50.

40. Youn JC, Hong YJ, Lee HJ, Han K, Shim CY, Hong GR, et al. Contrast-enhanced T1 mapping-based extracellular volume fraction independently predicts clinical outcome in patients with non-ischemic dilated cardiomyopathy: a prospective cohort study. Eur Radiol. 2017;27(9):3924-33.

41. Duca F, Kammerlander AA, Zotter-Tufaro C, Aschauer S, Schwaiger ML, Marzluf BA, et al. Interstitial Fibrosis, Functional Status, and Outcomes in Heart Failure With Preserved Ejection Fraction: Insights From a Prospective Cardiac Magnetic Resonance Imaging Study. Circ Cardiovasc Imaging. 2016;9(12).

42. Barison A, Del Torto A, Chiappino S, Aquaro GD, Todiere G, Vergaro G, et al. Prognostic significance of myocardial extracellular volume fraction in nonischaemic dilated cardiomyopathy. J Cardiovasc Med. 2015;16(10):681-7.

43. Messroghli DR, Walters K, Plein S, Sparrow P, Friedrich MG, Ridgway JP, et al. Myocardial T1 mapping: application to patients with acute and chronic myocardial infarction. Magn Reson Med. 2007;58(1):34-40.

44. Ugander M, Bagi PS, Oki AJ, Chen B, Hsu L-Y, Aletras AH, et al. Myocardial edema as detected by pre-contrast T1 and T2 CMR delineates area at risk associated with acute myocardial infarction. JACC: Cardiovasc Imaging. 2012;5(6):596-603.

45. Tahir E, Sinn M, Bohnen S, Avanesov M, Säring D, Stehning C, et al. Acute versus Chronic Myocardial Infarction: Diagnostic Accuracy of Quantitative Native T1 and T2 Mapping versus Assessment of Edema on Standard T2-weighted Cardiovascular MR Images for Differentiation. Radiology. 2017:162338.

46. Thavendiranathan P, Walls M, Giri S, Verhaert D, Rajagopalan S, Moore S, et al. Improved detection of myocardial involvement in acute inflammatory cardiomyopathies using T2 mapping. Circ Cardiovasc Imaging. 2012;5(1):102-10.

47. Ferreira VM, Piechnik SK, Dall'Armellina E, Karamitsos TD, Francis JM, Ntusi N, et al. T 1 Mapping for the Diagnosis of Acute Myocarditis Using CMR. JACC Cardiovasc Imaging. 2013;6(10):1048-58.

48. Hinojar R, Foote L, Ucar EA, Jackson T, Jabbour A, Yu C-Y, et al. Native T1 in discrimination of acute and convalescent stages in patients with clinical diagnosis of myocarditis: a proposed diagnostic algorithm using CMR. JACC Cardiovasc Imaging. 2015;8(1):37-46.

49. von Knobelsdorff-Brenkenhoff F, Schüler J, Dogangüzel S, Dieringer MA, Rudolph A, Greiser A, et al. Detection and Monitoring of Acute Myocarditis Applying Quantitative Cardiovascular Magnetic Resonance. Circ Cardiovasc Imaging. 2017;10(2).

50. Bohnen S, Radunski U, Lund G, Ojeda F, Looft Y, Senel M, et al. Tissue characterization by T1 and T2 mapping cardiovascular magnetic resonance imaging to monitor myocardial inflammation in healing myocarditis. Eur Heart J Cardiovasc Imaging. 2017;18(7):744-751.

51. D'Amico G, Garcia-Tsao G, Pagliaro L. Natural history and prognostic indicators of survival in cirrhosis: a systematic review of 118 studies. J Hepatol. 2006;44(1):217-31.

52. Fleming KM, Aithal G, Card T, West J. The rate of decompensation and clinical progression of disease in people with cirrhosis: a cohort study. Alimen Pharmacol Ther. 2010;32(11-12):1343-50.

53. Garcia-Tsao G, Lim J. Management and treatment of patients with cirrhosis and portal hypertension: recommendations from the Department of Veterans Affairs Hepatitis C Resource Center Program and the National Hepatitis C Program. Am J Gastroenterol. 2009;104(7):1802.

54. Garcia-Tsao G, Friedman S, Iredale J, Pinzani M. Now there are many (stages) where before there was one: In search of a pathophysiological classification of cirrhosis. Hepatology. 2010;51(4):1445-9.

55. Luetkens JA, Klein S, Traeber F, Schmeel FC, Sprinkart AM, Kuetting DLR, et al. Quantitative liver MRI including extracellular volume fraction for non-invasive quantification of liver fibrosis: a prospective proof-of-concept study. Gut. 2018;67(3):593-4.

56. Katsube T, Okada M, Kumano S, Hori M, Imaoka I, Ishii K, et al. Estimation of liver function using T1 mapping on Gd-EOB-DTPA-enhanced magnetic resonance imaging. Invest Radiol. 2011;46(4):277-83.

57. Haimerl M, Verloh N, Zeman F, Fellner C, Müller-Wille R, Schreyer AG, et al. Assessment of clinical signs of liver cirrhosis using T1 mapping on Gd-EOB-DTPA-enhanced 3T MRI. PloS One. 2013;8(12):e85658.

58. Ding Y, Rao S-X, Chen C, Li R, Zeng M-S. Assessing liver function in patients with HBV-related HCC: a comparison of T1 mapping on Gd-EOB-DTPA-enhanced MR imaging with DWI. Eur Radiol. 2015;25(5):1392-8.

59. Ding Y, Rao S-X, Zhu T, Chen C-Z, Li R-C, Zeng M-S. Liver fibrosis staging using T1 mapping on gadoxetic acid-enhanced MRI compared with DW imaging. Clin Radiol. 2015;70(10):1096-103.

60. Besa C, Bane O, Jajamovich G, Marchione J, Taouli B. 3D T1 relaxometry pre and post gadoxetic acid injection for the assessment of liver cirrhosis and liver function. Magn Reson Imaging. 2015;33(9):1075-82.

61. Yoon JH, Lee JM, Paek M, Han JK, Choi BI. Quantitative assessment of hepatic function: modified look-locker inversion recovery (MOLLI) sequence for T1 mapping on Gd-EOB-DTPA-enhanced liver MR imaging. Eur Radiol. 2016;26(6):1775-82.

62. Banerjee R, Pavlides M, Tunnicliffe EM, Piechnik SK, Sarania N, Philips R, et al. Multiparametric magnetic resonance for the non-invasive diagnosis of liver disease. J Hepatol. 2014;60(1):69-77.

63. Cassinotto C, Feldis M, Vergniol J, Mouries A, Cochet H, Lapuyade B, et al. MR relaxometry in chronic liver diseases: Comparison of T1 mapping, T2 mapping, and diffusion-weighted imaging for assessing cirrhosis diagnosis and severity. Eur J Radiol. 2015;84(8):1459-65.

64. Clinicaltrials.gov [homepage on the internet] Non-Invasive Rapid Assessment of Patients With Liver Transplants Using Magnetic Resonance Imaging With LiverMultiScan (RADIcAL2) [updated 2017 September 19; cited 2018 April 28]. Available from: https://clinicaltrials.gov/ct2/show/NCT03165201?term=LiverMultiScan&rank=1: ClinicalTrials.gov.

65. Pavlides M, Banerjee R, Sellwood J, Kelly CJ, Robson MD, Booth JC, et al. Multiparametric magnetic resonance imaging predicts clinical outcomes in patients with chronic liver disease. J Hepatol. 2016;64(2):308-15.

66. Wood JC, Enriquez C, Ghugre N, Tyzka JM, Carson S, Nelson MD, et al. MRI R2 and R2* mapping accurately estimates hepatic iron concentration in transfusion-dependent thalassemia and sickle cell disease patients. Blood. 2005;106(4):1460-5.

67. Henninger B, Kremser C, Rauch S, Eder R, Zoller H, Finkenstedt A, et al. Evaluation of MR imaging with T1 and T2* mapping for the determination of hepatic iron overload. Eur Radiol. 2012;22(11):2478-86.

68. Ganne-Carrié N, Christidis C, Chastang C, Ziol M, Chapel F, Imbert-Bismut F, et al. Liver iron is predictive of death in alcoholic cirrhosis: a multivariate study of 229 consecutive patients with alcoholic and/or hepatitis C virus cirrhosis: a prospective follow up study. Gut. 2000;46(2):277-82.

69. Valenti L, Fracanzani AL, Bugianesi E, Dongiovanni P, Galmozzi E, Vanni E, et al. HFE Genotype, Parenchymal Iron Accumulation, and Liver Fibrosis in Patients With Nonalcoholic Fatty Liver Disease. Gastroenterology. 2010;138(3):905-12.

70. Fischer R, Piga A, Harmatz P, Nielsen P. Monitoring long-term efficacy of iron chelation treatment with biomagnetic liver susceptometry. Ann N Y Acad Sci. 2005;1054:350-7.

71. Lee VS, Kaur M, Bokacheva L, Chen Q, Rusinek H, Thakur R, et al. What causes diminished corticomedullary differentiation in renal insufficiency? J Magn Reson Imaging. 2007;25(4):790-5.

72. Hueper K, Peperhove M, Rong S, Gerstenberg J, Mengel M, Meier M, et al. T1-mapping for assessment of ischemia-induced acute kidney injury and prediction of chronic kidney disease in mice. Eur Radiol. 2014;24(9):2252-60.

73. Hueper K, Hensen B, Gutberlet M, Chen R, Hartung D, Barrmeyer A, et al. Kidney Transplantation: Multiparametric Functional Magnetic Resonance Imaging for Assessment of Renal Allograft Pathophysiology in Mice. Invest Radiol. 2016;51(1):58-65.

74. Tewes S, Gueler F, Chen R, Gutberlet M, Jang M-S, Meier M, et al. Functional MRI for characterization of renal perfusion impairment and edema formation due to acute kidney injury in different mouse strains. PLOS One. 2017;12(3):e0173248.

75. Friedli I, Crowe LA, Berchtold L, Moll S, Hadaya K, de Perrot T, et al. New Magnetic Resonance Imaging Index for Renal Fibrosis Assessment: A Comparison between Diffusion-Weighted Imaging and T1 Mapping with Histological Validation. Sci Rep. 2016;6:30088.

76. Peperhove M, Vo Chieu VD, Jang MS, Gutberlet M, Hartung D, Tewes S, et al. Assessment of acute kidney injury with T1 mapping MRI following solid organ transplantation. Eur Radiol. 2017.

77. Reproducibility of Native T1 Mapping for Renal Tissue Characterization at 3T. Dekkers IA, Paiman EHM, de Vries APJ, Lamb HJ. J Magn Reson Imaging. 2019 Feb;49(2):588-96.78. Perazella MA. Gadolinium-contrast toxicity in patients with kidney disease: nephrotoxicity and nephrogenic systemic fibrosis. Curr Drug Saf. 2008;3(1):67-75.

79. Martin DR, Kalb B, Mittal A, Salman K, Vedantham S, Mittal PK. No Incidence of Nephrogenic Systemic Fibrosis after Gadobenate Dimeglumine Administration in Patients Undergoing Dialysis or Those with Severe Chronic Kidney Disease. Radiology. 2017;0(0):170102.

80. Soulez G, Bloomgarden DC, Rofsky NM, Smith MP, Abujudeh HH, Morgan DE, et al. Prospective cohort study of nephrogenic systemic fibrosis in patients with stage 3–5 chronic kidney disease undergoing MRI with injected gadobenate dimeglumine or gadoteridol. AJR Am J Roentgenol. 2015;205(3):469-78.

81. Bruce R, Wentland AL, Haemel AK, Garrett RW, Sadowski DR, Djamali A, et al. Incidence of nephrogenic systemic fibrosis using gadobenate dimeglumine in 1423 patients with renal insufficiency compared with gadodiamide. Invest Radiol. 2016;51(11):701-5.

82. Michaely HJ, Aschauer M, Deutschmann H, Bongartz G, Gutberlet M, Woitek R, et al. Gadobutrol in renally impaired patients: results of the GRIP Study. Invest Radiol. 2017;52(1):55.

83. Franke M, Baessler B, Vechtel J, Dafinger C, Hohne M, Borgal L, et al. Magnetic resonance T2 mapping and diffusion-weighted imaging for early detection of cystogenesis and response to therapy in a mouse model of polycystic kidney disease. Kidney Int. 2017.

84. Kellman P, Hansen MS. T1-mapping in the heart: accuracy and precision. J Cardiovasc Magn Reson. 2014;16:2.

85. Kellman P, Herzka DA, Arai AE, Hansen MS. Influence of Off-resonance in myocardial T1-mapping using SSFP based MOLLI method. J Cardiovasc Magn Reson. 2013;15(1):63.

86. Kellman P, Wilson JR, Xue H, Ugander M, Arai AE. Extracellular volume fraction mapping in the myocardium, part 1: evaluation of an automated method. J Cardiovasc Magn Reson. 2012;14(1):63.

87. Kvernby S, Warntjes MJB, Haraldsson H, Carlhäll C-J, Engvall J, Ebbers T. Simultaneous three-dimensional myocardial T1 and T2 mapping in one breath hold with 3D-QALAS. J Cardiovasc Magn Reson. 2014;16(1):102.

88. Yoon JH, Lee JM, Kim E, Okuaki T, Han JK. Quantitative Liver Function Analysis: Volumetric T1 Mapping with Fast Multisection B1 Inhomogeneity Correction in Hepatocyte-specific Contrast-enhanced Liver MR Imaging. Radiology. 2016;282(2):408-17.

89. Sandino CM, Kellman P, Arai AE, Hansen MS, Xue H. Myocardial T2* mapping: influence of noise on accuracy and precision. J Cardiovasc Magn Reson. 2015;17(1):7.

90. Messroghli DR, Moon JC, Ferreira VM, Grosse-Wortmann L, He T, Kellman P, et al. Clinical recommendations for cardiovascular magnetic resonance mapping of T1, T2, T2* and extracellular volume: A consensus statement by the Society for Cardiovascular Magnetic Resonance (SCMR) endorsed by the European Association for Cardiovascular Imaging (EACVI). J Cardiovasc Magn Reson. 2017;19(1):75.

91. Moon JC, Messroghli DR, Kellman P, Piechnik SK, Robson MD, Ugander M, et al. Myocardial T1 mapping and extracellular volume quantification: a Society for Cardiovascular Magnetic Resonance (SCMR) and CMR Working Group of the European Society of Cardiology consensus statement. J Cardiovasc Magn Reson. 2013;15(1):92.

92. Fryback DG, Thornbury JR. The efficacy of diagnostic imaging. Med Decis Making. 1991;11(2):88-94.

93. Blake L, Duarte RV, Cummins C. Decision analytic model of the diagnostic pathways for patients with suspected non-alcoholic fatty liver disease using non-invasive transient elastography and multiparametric magnetic resonance imaging. BMJ open. 2016;6(9):e010507.

94. Clinicaltrials.gov [homepage on the internet] International T1 Multicenter CMR Outcome Study in Patients With Nonischaemic Cardiomyopathies (T1-CMR). [updated 2015 April 2; cited 2018 April 28]. Available from: https://clinicaltrials.gov/ct2/show/NCT02407197

95. Haaf P, Garg P, Messroghli DR, Broadbent DA, Greenwood JP, Plein S. Cardiac T1 Mapping and Extracellular Volume (ECV) in clinical practice: a comprehensive review. J Cardiovasc Magn Reson. 2016;18(1):89.

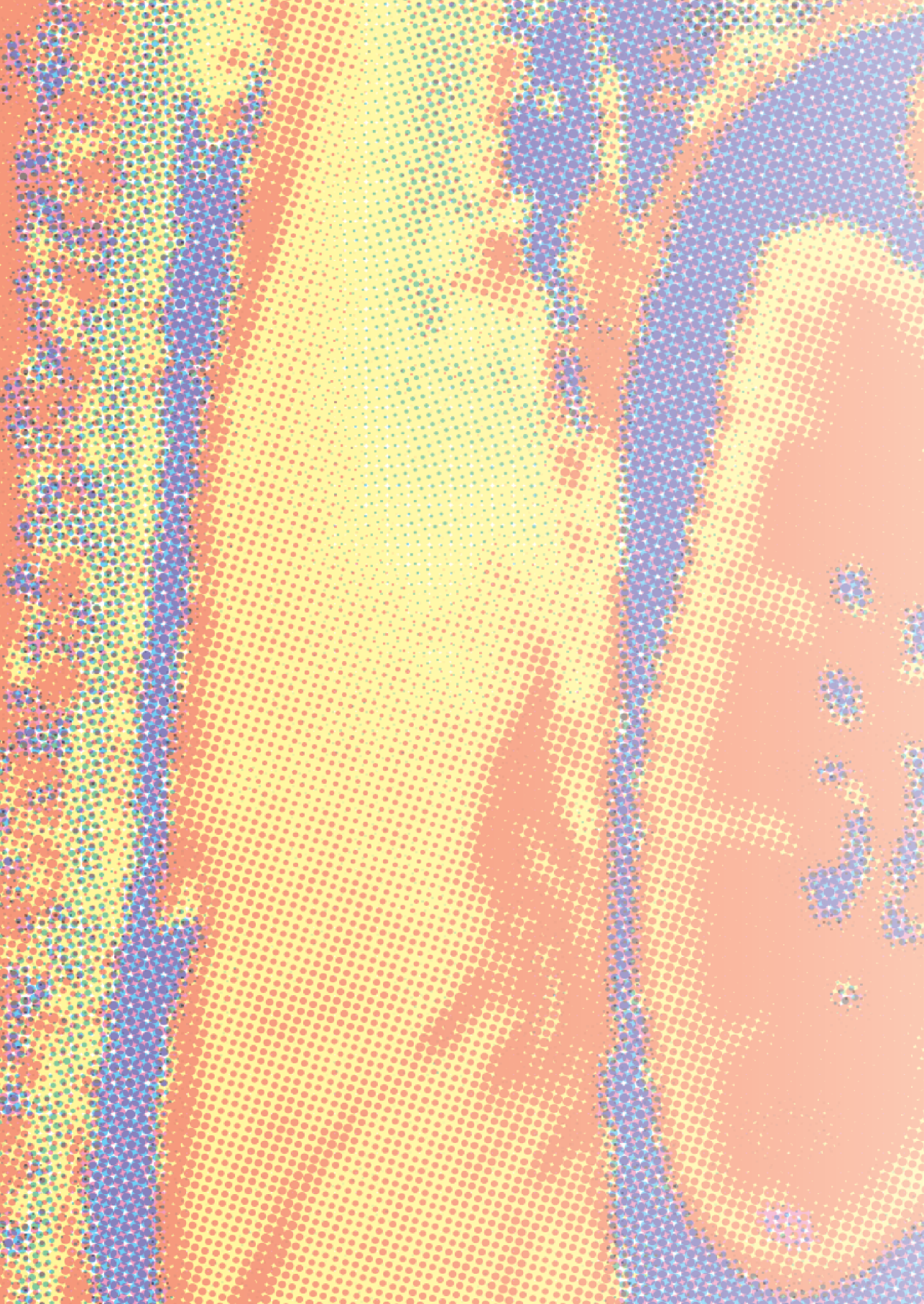

PART 1

Reproducibility and clinical validation studies

3

Reproducibility of Native T1-mapping for Renal Tissue Characterization using MOLLI at 3 Tesla

Dekkers IA, Paiman EHM, de Vries APJ, Lamb HJ.

J Magn Reson Imaging. 2019 Feb;49(2):588-96.

ABSTRACT

Background

Advanced renal disease is characterized by adverse changes in renal structure, however non-invasive techniques to diagnose and monitor these changes are currently lacking.

Objectives

Our aim was to assess the reproducibility of native T1 mapping for renal tissue characterization.

Methods

Fifteen healthy volunteers (mean age 31 ± 15 years, range 19–63 years), and 11 patients with diabetic nephropathy (mean age 57 ± 8 years, range 51–69 years) underwent renal T1 mapping using the Modified Look-Locker Imaging (MOLLI) 5(3)3 sequence at a 3T clinical MRI scanner. Intra- and inter-examination reproducibility of voxel based T1 relaxation times of renal cortex and medulla was assessed in healthy human volunteers and diabetic nephropathy patients. Reproducibility was evaluated using Bland-Altman and intra-class correlation coefficients (ICCs).

Results

Intra- and interexamination reproducibility of renal native T1 mapping showed good–strong ICCs (0.83–0.89) for renal cortex and medulla, and moderate–good ICCs (0.62–0.81) for cortex–medulla ratio in both healthy volunteers and diabetic nephropathy patients. Intra- and interexamination limits of agreement were respectively (–124 ms, +82 ms) and (–134 ms, +98 ms) for renal cortex and (–138 ms, +107 ms) and (–118 ms, +151 ms) for medulla. Overall T1 values for renal cortex ($P = 0.277$) and medulla ($P = 0.973$) were not significantly different between healthy volunteers and diabetic nephropathy patients, in contrast to the cortex–medulla ratio ($P = 0.003$).

Conclusion

Renal native T1 mapping is a technique with good–strong intra- and examination reproducibility in both healthy volunteers and diabetic nephropathy patients.

INTRODUCTION

Renal disease often progresses unnoticed as clinical parameters, such as glomerular filtration rate (GFR), tend to deteriorate only late in the disease course (1). There is an increasing need for the development of non-invasive imaging biomarkers that can help to predict clinical and functional outcomes in renal disease, and guide clinical decision making (2). Renal disease is characterized by adverse changes in both renal macrostructure (renal volume, and corticomedullary differentiation) and microstructure (renal inflammation, fibrosis, and lipid fat fraction) (3). These alterations in renal structure or renal tissue composition may be useful for differentiating specific renal disease states, and monitoring disease activity over time. Magnetic resonance imaging has the ability to discriminate tissue composition using T1 (spin-lattice) relaxation properties. Recent technical advances have enabled non-invasive tissue characterization via pixel-wise mapping of true T1 values of the target organ of interest, without the use of contrast agents. This so-called native T1 mapping, in which color-encoded pixel values represent the corresponding T1 relaxation times per voxel, has been used in cardiac MRI to visualize myocardial fibrosis, steatosis, edema, and hemosiderosis (4).

Previous clinical studies have shown that native T1 mapping could be helpful for identifying acute kidney injury and prediction of chronic kidney disease in mice (5–7). Additionally, recent clinical studies have showed promising results of renal native T1 mapping for the detection of fibrosis and prediction of graft functioning after kidney transplantation (8,9). Given the considerable influence of the imaging protocol, scanner, and patient related factors on measured T1 values, evaluation of reproducibility and robustness is critical (10).

The purpose of the present study was to evaluate the reproducibility of native T1 mapping for renal tissue characterization at 3T in healthy volunteers and diabetic nephropathy patients.

MATERIALS AND METHODS

Participants

The Institutional Review Board of our institution approved the study protocol for MR technique development, and written informed consent was obtained from all participants. Fifteen healthy volunteers (mean age 31 ± 15 years, range 19–63, 67% male) without known renal disease agreed to participate in the current study and were recruited from a database of healthy volunteers who regularly participate in technical MRI development studies. Eleven subjects with a known history of diabetic nephropathy (mean age 57 ± 8 years, range 51–69, 80% male, urinary albumin excretion ratio >2.5 mg/mmol for men or

>3.5 mg/mmol for women, and estimated GFR >60ml/min/1.73m²) agreed to participate in the present study and were recruited from a database of past clinical trial participants.

Data acquisition

MR examinations were performed at a 3T clinical MRI scanner (Ingenia, Philips, Best, The Netherlands). The standard cardiac/body coil was used for transmission with two arrays (anterior and posterior with respectively 16 and 12 elements) for reception. After a breath-hold survey was obtained, three orthogonal modified Dixon scans were acquired of the left kidney. T1 mapping was performed using the modified Look-Locker inversion-recovery (MOLLI) sequence at the center of the kidney in sagittal orientation (**Fig. 1a**). The sagittal orientation was chosen as this orientation is less prone to through-plane volume effects compared to the coronal orientation while maintaining an overview of the upper and lower poles of the kidney which is useful for assessing potential local differences. Breath-holds were used for respiratory motion compensation. A turbo field echo (TFE) prepulse with an inversion delay of 350 ms was the longest (and last) inversion delay in the MOLLI scheme. Other inversion times in the MOLLI scheme were equidistantly distributed between shortest and longest value, according to the 5(3)3 cardiac MR protocol. Since the cardiac 5(3)3 protocol is normally electrocardio-graphically gated, we used the physiology simulator (Philips) to ensure scan triggering by simulating cardiac triggering in order to apply the protocol for renal imaging. The shortest inversion time was used for the first part of the MOLLI scheme, and depended on the TFE shot duration which is around 100 ms. Finally, 8 images were acquired, and in-line motion correction and map generation were performed. Used readout parameters were: slice thickness 8 mm, spacing between slices 8 mm, field of view 300 x 300 mm; matrix 256 x 256 x 1 slice; pixel size 1.17 x 1.17 mm. Intra-examination reproducibility measurements were obtained by repeating the scan without repositioning of the subject or changing the position of the surface coil or measurement volumes. Inter-examination reproducibility was assessed on the same day after removal and repositioning of subject in the magnet, and repositioning of the surface coil and measurements volumes. Inter-examination scans were added later in the scan protocol and were therefore not assessed in all healthy volunteers. Total acquisition time including positioning of the subject, scanning preparatory sequences, planning and data acquisition was on average 4 minutes.

T1 mapping quantification

Eight T1-weighted source images were taken at different times (ms) after an inversion pulse at time t=0 for MOLLI 5(3)3 during a single breath-hold (**Fig. 1b**). Post-processing was done using QMap Research Edition (Medis, Leiden, the Netherlands) using received data in DICOM format. Inversion recovery curves were constructed for renal cortex (orange) and medulla (red) based on MOLLI images with varying effective inversion time

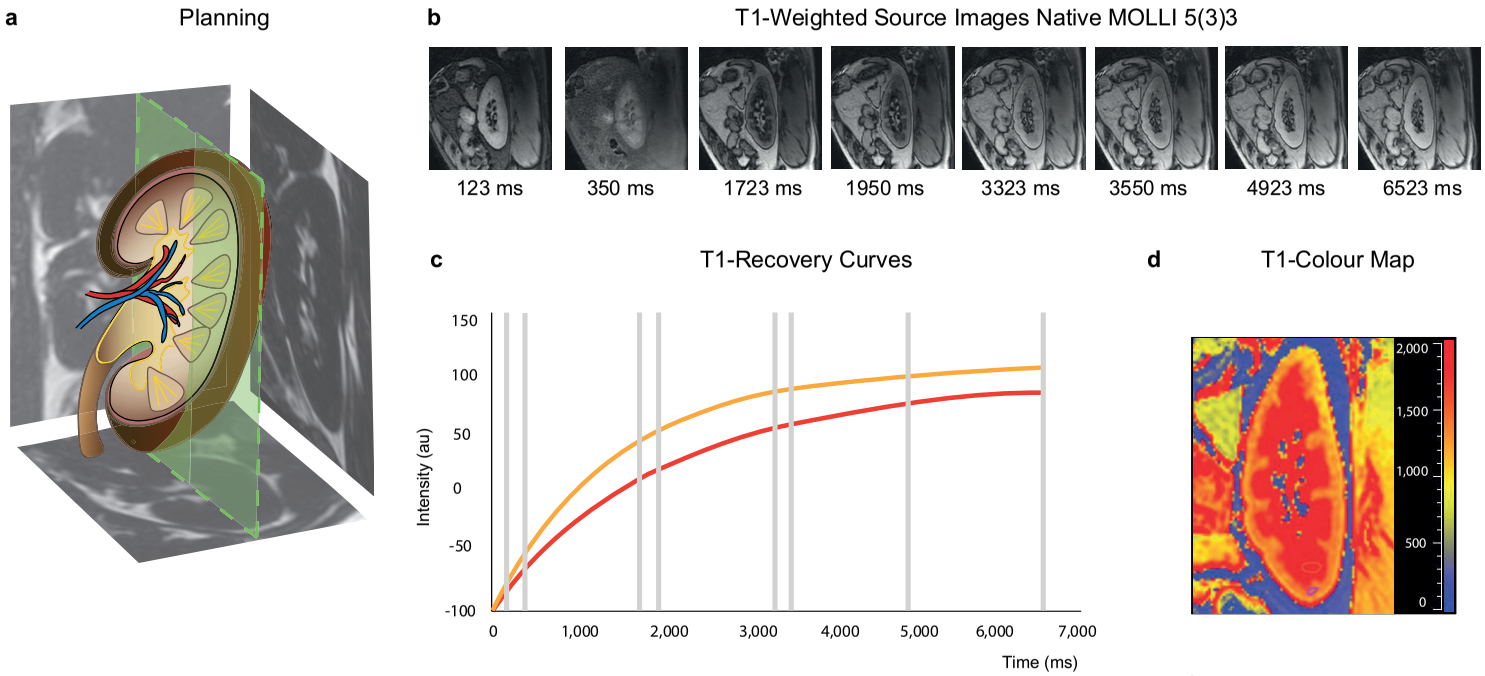

Figure 1. Planning and acquisition protocol of native MOLLI 5(3)3. (**a**) Planning of T1-mapping in the sagittal plane based on three orthogonal on mDixon images. (**b**) T1-weighted source images in sagittal plane taken at different times (ms) after an inversion pulse at time t=0 for MOLLI 5(3)3 all acquired during a single breath-hold. (**c**) Inversion recovery curves for renal cortex (orange) and medulla (red) generated from the source images. (**d**) Generated color-encoded T1 map in which pixel values represent corresponding T1 relaxation times per voxel.

(TI) with one series containing multiple images (**Fig. 1c**). The T1 mapping curve fitting to a three-parameter nonlinear cuve can be described as (y=A-B*exp(-TI/T1*) and correction (T1=T1*(B/A-1)) (11).

Offset, scaling, and T1 were calculated via fitting the algorithm at each pixel {x,y}, resulting in additional offset, scaling and T1 maps. The color-encoded pixel based T1 maps provide a quantitative visualization of the tissue T1 properties since the signal intensity of each pixel directly reflects the relaxation time calculated in milliseconds (**Fig. 1d**). The offset, scaling and T1 maps were used to calculate additional R2 and residual maps for quality control, where good quality is reflected by R2 values and low residual values. The R2 and residual error map are sensitive for poor fitting due to motion related artifacts, and spatial variation in off resonance due to B0-field inhomogeneity (**Fig. 2**) In case necessary manual motion correction was performed.

Freehand region of interest (ROI) based measurements were made for the mean T1 values by manually drawing small sample ROIs in the renal cortex and medulla of the lower pole of the left kidney (**Fig. 2**). Both renal cortex and medulla showed minimal regional differences and limited variance (SD) of the small sample ROI measurements. Outer borders of the kidney were not included in ROI measurements, since the outer border between renal parenchyma and perirenal fat or renal sinus fat are prone to gradual changes in T1 values due to partial volume averaging artifacts and possible residual registration error after motion correction. Regions with banding artifacts in the kidney due to off-resonance were also avoided for ROI measurement, since these artifacts can cause significant error at relatively small off-resonance frequencies (12). The cortex-medulla ratio was determined by dividing the (ROI-based) native T1 value of renal cortex by the native T1 value of the medulla.

Statistical analysis

T1 values and other descriptors are presented as mean (SD), range, and percentage. The Shapiro-Wilk test and assessment of histogram plots was applied to determine whether the data was normally distributed and to select appropriate parametric tests. Pearson's correlation, and intra-class correlation coefficients (ICC) were calculated for intra- and inter-examination measurements. The ICC can be interpreted as the ratio of the between subject variance compared to the total variance (sum of the between subject and within subject variances), and was computed using a two-way mixed effects model (13). Agreement was classified as follows: ICC >0.95; excellent, 0.95–0.85; strong, 0.85–0.70; good, 0.70–0.50; moderate, <0.5; poor. Bland-Altman plots were constructed for intra- and inter-examination measurements and were visualized through a scatterplot of the differences, with reference lines at the mean difference, and mean difference ± 2 × standard deviation of the differences (limits of agreement) (14).

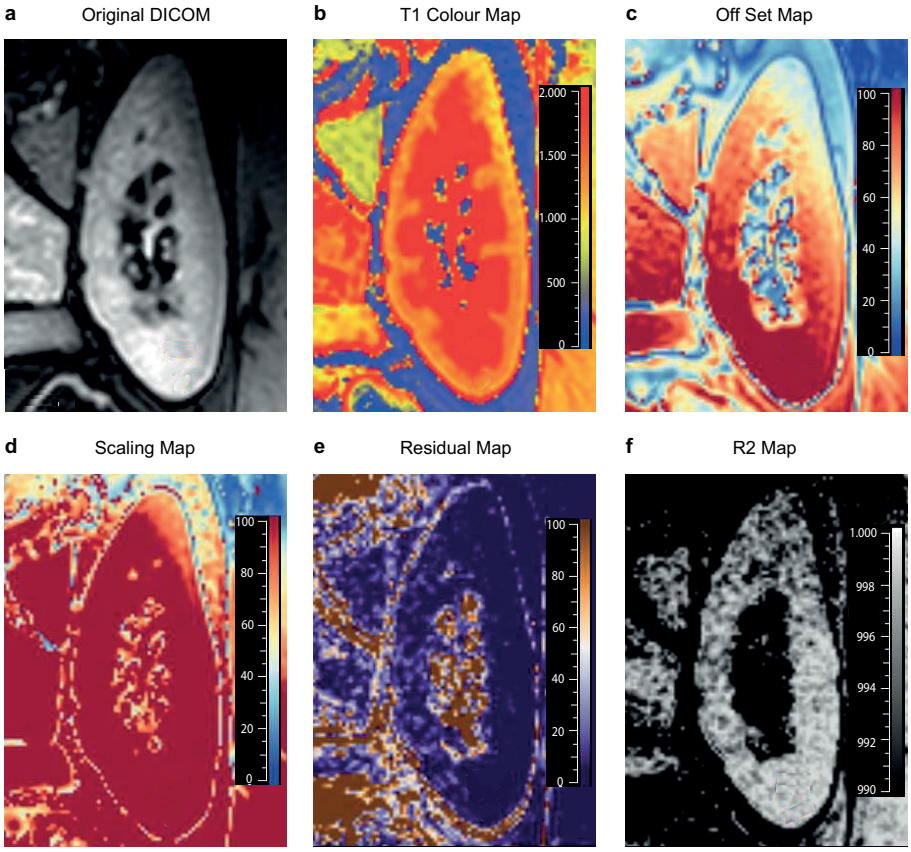

Figure 2. Region of interest measurements for renal cortex and medulla on original DICOM, T1 Colour Map, Offset Map, Scaling Map, Residual Map, R2 Map.(**a**) Original DICOM image of the MOLLI 5(3)3 sequence in sagittal plane of the left kidney, (**b**) Color-encoded pixel based T1 map (**c**) Offset map corresponds to the plateau value of the function which should be equal to the last time point of the MOLLI 5(3)3 sequence, (**d**) Scaling map which ideally should have be twice the value of the offset because than the T1 is equal to the apparent recovery time T1*, (**e**) residual map reflects the sum of squared differences between the fitted intensity value and the original image normalized for the number of image frames, (**d**) R2 map corresponds to the coefficients of determination, which lies between 0 and 1000 since the DICOM images store only integer values.

Two-tailed $P<0.05$ was considered to indicate a statistically significant difference. Statistical analyses were performed using STATA version 12.0 (Statacorp, College Station, Texas).

RESULTS

The overall results regarding the mean T1-values, Pearson correlation and ICCs for first, intra- and inter-examination scans are presented in **Table 1**. Overall mean T1 values

Table 1. Mean T1-values, Pearson correlation and ICCs for first, intra- and inter-examination scans.

	Healthy volunteers			Diabetic Nephropathy patients			Combined		
	Scan 1 n=15	Intra-examination scan n=15	Inter-examination scan n=9	Scan 1 n=11	Intra-examination scan n=11	Inter-examination scan n=11	Scan 1 n=26	Intra-examination scan n=26	Inter-examination scan n=20
T1 value (ms)									
Cortex	1408 ± 80	1437 ± 78	1427 ± 62	1433 ± 88	1445 ± 82	1449 ± 80	1419 ± 83	1440 ± 78	1861 ± 85
Medulla	1882 ± 108	1912 ± 83	1923 ± 63	1850 ± 89	1846 ± 100	1810 ± 65	1868 ± 100	1883 ± 95	1439 ± 72
CM ratio	0.75 ± 0.05	0.75 ± 0.03	0.74 ± 0.04	0.77 ± 0.03	0.78 ± 0.03	0.80 ± 0.04	0.76 ± 0.04	0.77 ± 0.03	0.77 ± 0.05
Pearson correlation (r)									
Cortex		0.65	0.49		0.96	0.79		0.80	0.71
Medulla		0.80	0.88		0.85	0.66		0.80	0.71
CM ratio		0.36	0.65		0.38	0.58		0.45	0.70
ICC (95% CI)									
Cortex	0.79 (0.37, 0.93)		0.66 (-0.51, 0.86)	0.98 (0.93, 0.99)		0.88 (0.55, 0.97)	0.89 (0.75, 0.95)		0.83 (0.56, 0.93)
Medulla	0.87 (0.62, 0.96)		0.91 (0.56, 0.98)	0.91 (0.70, 0.98)		0.77 (0.14, 0.94)	0.89 (0.76, 0.95)		0.83 (0.57, 0.93)
CM ratio	0.52 (-0.44, 0.84)		0.79 (0.06, 0.95)	0.55 (-0.57, 0.87)		0.70 (-0.14, 0.92)	0.62 (0.16, 0.83)		0.81 (0.52, 0.93)

T1 values are expressed as mean ± SD. CM ratio; cortex-medulla ratio. ICC; intra-class correlation coefficient.

of healthy volunteers were 1418 ± 73 ms (range 1270–1482 ms) for renal cortex and 1886 ± 86 ms (range 1695–2006 ms) for medulla. Overall mean T1 values of diabetic nephropathy patients were 1445 ± 81 ms (range 1392–1545 ms) for renal cortex and 1840 ± 79 ms (range 1751–2003 ms) for medulla. The overall mean cortex-medulla ratio was 0.75 ± 0.03 (range 0.70–0.80) for healthy volunteers and 0.79 ± 0.03 (range 0.74–0.82) for diabetic nephropathy patients. No significant differences were present when comparing T1 values for renal cortex (*P*=0.277) and medulla (*P*=0.73) of healthy volunteers with diabetic nephropathy patients. The cortex–medulla ratio was significantly different between healthy volunteers and diabetic nephropathy patients (*P*=0.003) (**Fig. 3**). Intra- and inter-examination measurements were highly correlated with first T1 value measurements of renal cortex and medulla.

Intra-examination ICCs of renal cortex and medulla for both healthy volunteers and diabetic nephropathy patients combined were respectively 0.89 (95% CI 0.75, 0.95) and 0.89 (95% CI 0.76, 0.95). Inter-examination ICCs for renal cortex and medulla were 0.83 (95% CI 0.56, 0.93) and 0.83 (95% CI 0.57, 0.93). The cortex-medulla ratio had an intra-examination ICC of 0.62 (95% CI 0.16, 0.83) and 0.81 (95% CI 0.52, 0.93).

The Bland-Altman lower and upper limits of agreement for intra-examination and inter-examination T1 measurements of renal cortex were respectively -124 ms (95% CI -159, -88) and 82 ms (95% CI 47, 118), and -134 (95% CI -181, -87) and 98 ms (95% CI -51, 145) (**Fig. 4a and Fig. 4b**). Intra- and inter examination Bland-Altman lower and upper limits of agreement for renal medulla were -138 ms (95% CI -180, -96), 107 ms (95% CI 65, 149) (**Fig. 4c and Fig. 4d**), and -118 ms (95% CI -172, -63), 151 ms (95% CI 96, 205). Cortex-medulla ratio measurements had lower and upper limits of agreement of -0.08 (95% CI -0.11, -0.06) and 0.07 (95% CI 0.05, 0.10) for intra-examination measurements, and -0.09 (95% CI -0.12, -0.06) and 0.06 (95% CI 0.03, 0.08) for inter-examination measurements (**Fig. 4e and Fig. 4f**).

To illustrate the potential application of renal T1 mapping, we have visualized coronal renal T1 maps of a healthy volunteer (left), and renal transplant recipient (right) in **Figure 5**. The renal T1 map the healthy volunteer has T1 values of 1468 ms in the renal cortex, and 1941 ms for medulla (cortex–medulla ratio of 0.76), compared to native T1 values of 1658 ms for renal cortex and 1951 ms for medulla (cortex–medulla ratio of 0.85) in the transplanted kidney.

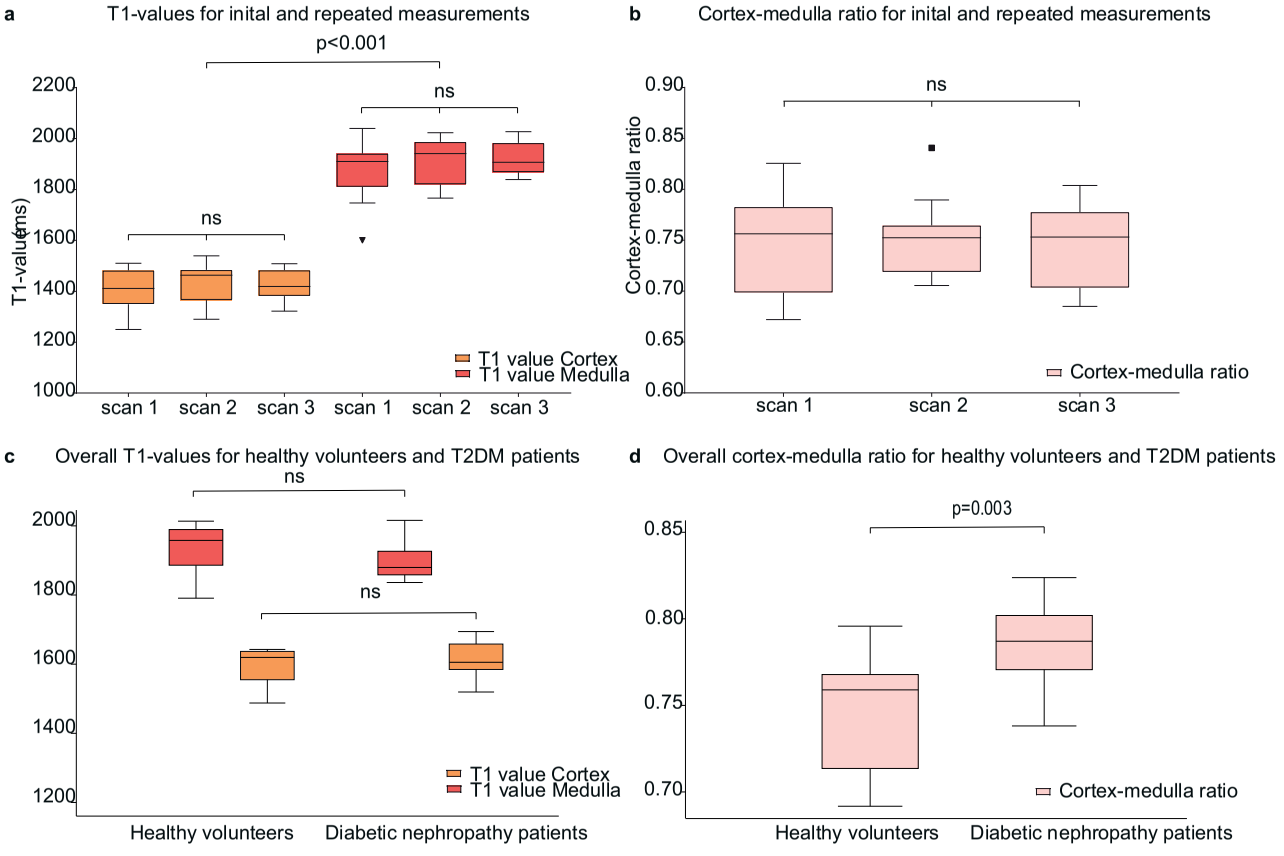

Figure 3. Distribution of MOLLI 5(3)3 ROI based T1 values of renal cortex, medulla and cortex-medulla ratio for first, intra- and inter-examination measurements. (**a**) Distribution of T1 values of renal cortex (orange) and medulla (red) for first scan and repeated intra- and inter-examination scans in healthy volunteers. (**b**) Distribution of cortex-medulla ratio based on first scan and repeated intra- and inter-examination scans in healthy volunteers.

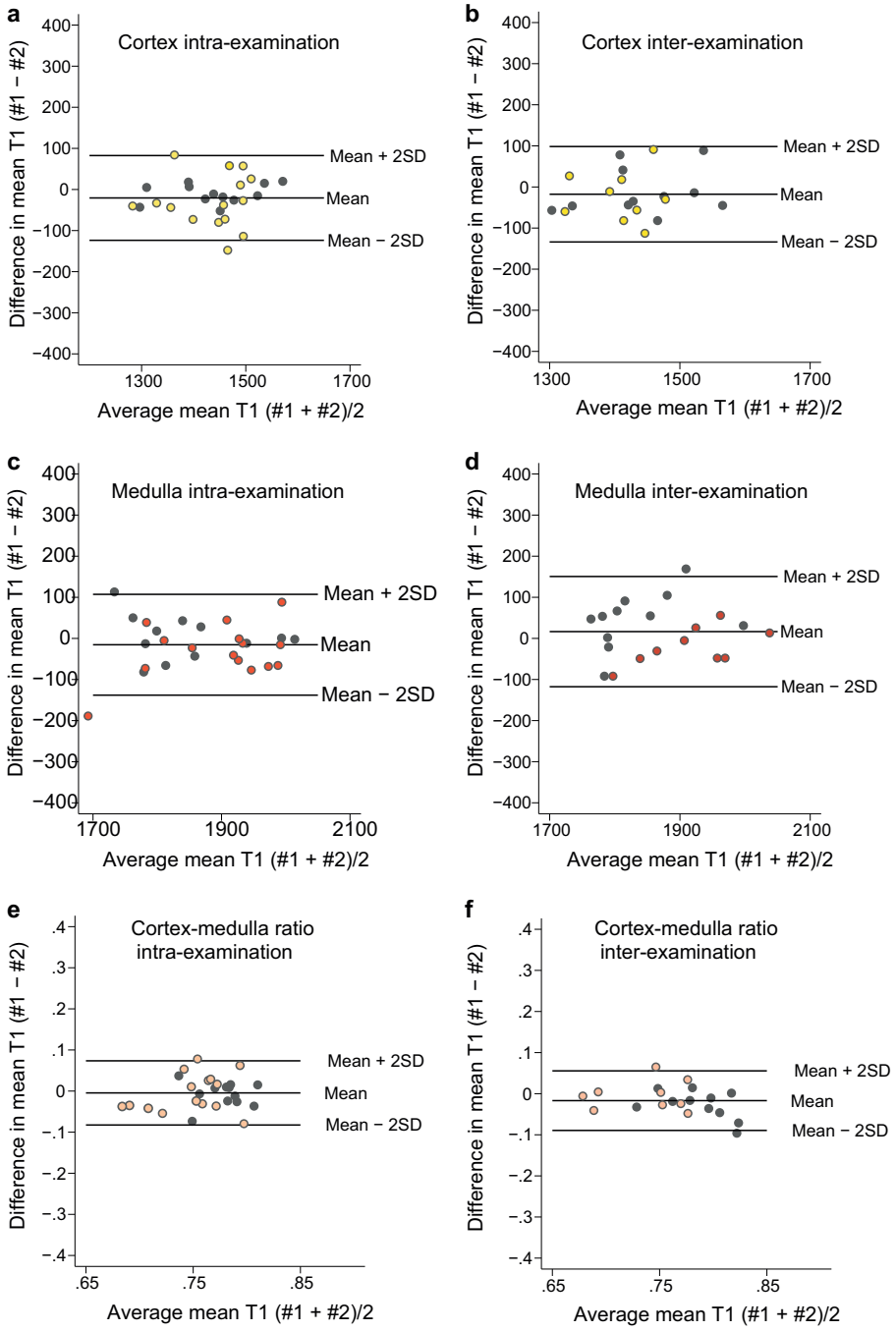

Figure. 4. Bland-Altman Plots of intra-examination and inter-examination T1-measurements of renal cortex, medulla and cortex-medulla ratio in healthy volunteers (in color) and diabetic nephropathy patients (in black).

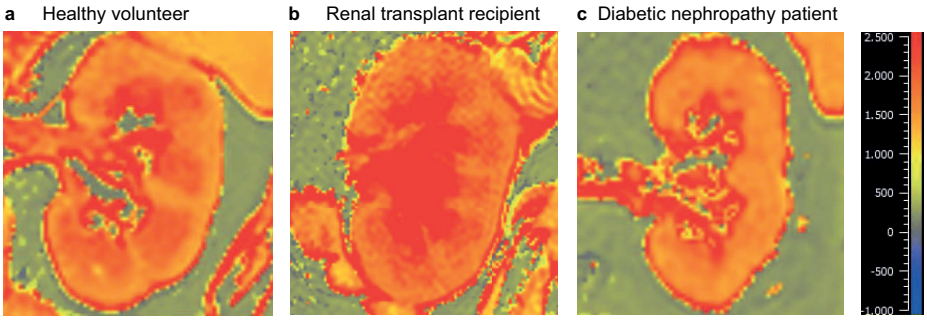

Figure 5. Coronal T1 map of a healthy volunteer (left), a renal transplant recipient (middle), and a patient with diabetic nephropathy (right). (**a**) T1 map of a kidney of a healthy volunteer in coronal view with values of 1468 ms for renal cortex, 1941ms for medulla, and a cortex-medulla ratio of 0.76. (**b**) T1 map of a renal transplant patient with an eGFR of 56 ml/min/1.73m² at time of scanning, native T1 values were of 1658 ms for renal cortex, 1951 ms for medulla, and a cortex-medulla ratio of 0.85. (**c**) T1 map of a patient with diabetic nephropathy showing a diminished cortico-medullary differentiation.

DISCUSSION

We demonstrated that renal native T1 mapping using the MOLLI 5(3)3 sequence is a reproducible technique that could be used for renal tissue characterization.

The intra- and inter-examination reproducibility of measured renal T1 values are an important determinant of the clinical utility of pixel-wise T1 mapping for disease assessment. We evaluated the reproducibility of T1 measurements in renal cortex, renal medulla and for the cortex-medulla ratio. Both intra- and inter-examination ICCs ranged between moderate–strong in healthy volunteers and diabetic nephropathy patients separately. Intra- and inter examination ICCs for both groups combined were respectively 0.89 and 0.83 for both renal cortex and renal medulla indicating strong intra-examination reproducibility. This is supported by the Bland-Altman plots showing good agreement. One outlier was present in the intra- and inter-examination Bland-Altman plots, which is likely the same healthy volunteer with residual motion artefacts due to non-compliance to breath-hold instructions during the data acquisition of scan 1. In general, ICC values were higher for renal medulla compared to cortex. The cortex is likely more sensitive for trough-plane partial volume effects than the medulla based on its anatomical borders and relatively limited thickness. This could potentially be improved via high resolution 3D T1 mapping or via the use of post-processing techniques such as automated motion correction of residual motion artefacts. The cortex-medulla ratio had ICCs ranging between moderate–good, indicating that this is a less reliable measure than T1 values directly measured in renal cortex and medulla.

Conventional MR imaging of the kidney clearly demonstrates anatomical differences between renal cortex and medulla due to the shorter T1 relaxation times of the cortex.

Loss of this so-called corticomedullary differentiation occurs in several renal diseases and has been primarily attributed to altered T1 relaxation times in the renal cortex (15). Determination the cortex-medulla ratio using true native T1 values of renal cortex and medulla enables quantification of the corticomedullary differentiation, which might be useful for differentiating specific renal disease states, such as renal fibrosis. In the present study T1 values of the cortex ranged between 1270–1482 ms, compared to 1695–2006 ms for medulla in healthy volunteers at 3T. Since native T1 values are considered to reflect both cellular components as interstitium, we postulate that the found differences between cortical and medullary T1 values convey anatomical differences in the renal (tubular) interstitium, which is defined as the extravascular, extraglomerular and (inter)tubular space of the kidney (16). Renal interstitial volume, in contrast to severity of glomerular disease, is highly correlated with kidney function, (17,18) and can occupy over 60% of kidney tissue in severe renal disease (19,20). Recently, it has been showed by Friedli et al. that renal native T1 values correlate well with renal fibrosis stage based on histology, suggesting that native renal T1 might be a useful parameter to detect (subclinical) renal fibrosis (8). Another very recent study in renal transplant recipients found prolonged T1 values after transplantation and increased cortical T1 values in higher stages of renal functional impairment (9), indicating the potential use for prediction of graft survival/functioning. However, to what extent native T1 mapping could be used as a safe non-invasive alternative for diagnosis and follow-up of renal disease, remains to be further investigated.

Several limitations are present in this study that need to be considered. Since native T1 mapping is at least partially modulated by perfusion (which is also a major determinant of GFR), T1 relaxation times obtained in patients with impaired renal function could potentially be confounded by lower renal perfusion rather reflecting true fibrosis only. This could also have important implications when other T1-mapping based techniques are used such as arterial spin labelling, which could potentially limit the application of these techniques in the kidney. More research is needed to determine to what extent native renal T1 values are affected by altered perfusion, however we expect that current reproducibility measurements are minimally influenced by differences in renal perfusion since the study population consists of healthy volunteers and diabetic nephropathy patients with an eGFR >60ml/min/1.73m^2. In the present study the aim was to evaluate the reproducibility of renal T1 mapping rather than evaluating the differences between healthy volunteers and renal disease patients, as this would have required a much larger sample size encompassing a wide variety with renal disease patients as chronic kidney disease is a highly heterogeneous disease group with different underlying pathologies and stages (21). We hypothesize that certain specific renal diseases (e.g. focal and diffuse fibrosis, and renal infiltrative diseases such as renal involvement in Fabry disease) might potentially benefit form renal T1 mapping while others may not, based on the underlying

disease-specific changes in renal tissue composition. Native renal T1 mapping could be of added value to the renal diagnostic arsenal considering it facilitates direct quantification of renal tissue and enables assessment of regional variances. To what extent renal T1 mapping could truly influence clinical decision-making compared to currently available renal function markers and other new MR techniques such as diffusion weighted imaging, and blood-oxygen-level dependent imaging remains to be investigated, and further histological validation of renal T1 mapping for tissue characterization is warranted. In the present study we used the same 5(3)3 MOLLI scheme as in cardiac MR imaging because of practical advantages for clinical implementation. However other T1 mapping acquisition protocols might provide more accurate renal T1 measurements since MOLLI measurements are known to be influenced by T2-dependence, magnetization transfer effect, and inversion efficiency (22). Although automated parametric mapping using dedicated software minimizes user-dependent influences, we cannot completely exclude possible intra- and inter-observer variation in the current measurements. Further research is needed to correlate renal native T1-values with disease severity based on histopathology, and whether renal native T1 mapping has added value for clinical decision making. In addition, more studies are needed to assess the reproducibility of renal native T1 mapping at different imaging centers with various MRI scanner manufacturers, in order to compare current measurements to other centers and to establish normal reference values.

In conclusion, renal native T1-mapping is a promising technique for renal tissue characterization with good–strong intra- and inter-examination reproducibility. Further research is needed to correlate renal native T1-values with histologic disease severity, and to determine the impact on clinical decision making.

REFRENCES

1. Porrini E, Ruggenenti P, Mogensen CE, et al. ERA-EDTA diabesity working group. Non-proteinuric pathways in loss of renal function in patients with type 2 diabetes. Lancet Diabetes Endocrinol 2015;3: 382–391
2. O'neill WC. Structure, not just function. Kidney Int 2014;85:503–505.
3. Grenier N, Merville P, Combe C. Radiologic imaging of the renal parenchyma structure and function. Nat Rev Nephrol 2016;12:348–359.
4. Taylor AJ, Salerno M, Dharmakumar R, Jerosch-Herold M. T1 mapping: Basic techniques and clinical applications. JACC Cardiovasc Imaging 2016;9:67–81.
5. Hueper K, Peperhove M, Rong S, et al. T1-mapping for assessment of ischemia-induced acute kidney injury and prediction of chronic kidney disease in mice. Eur Radiol 2014;24:2252–2260.
6. Hueper K, Hensen B, Gutberlet M, et al. Kidney transplantation: Multiparametric functional magnetic resonance imaging for assessment of renal allograft pathophysiology in mice. Invest Radiol 2016;51:58–65.
7. Tewes S, Gueler F, Chen R, et al. Functional MRI for characterization of renal perfusion impairment and edema formation due to acute kidney injury in different mouse strains. PLoS One 2017;12:e0173248.
8. Friedli I, Crowe LA, Berchtold L, et al. New magnetic resonance imaging index for renal fibrosis assessment: A comparison between diffusion-weighted imaging and T1 mapping with histological validation. Sci Rep 2016;6:30088.
9. Peperhove M, Vo Chieu VD, Jang MS, et al. Assessment of acute kidney injury with T1 mapping MRI following solid organ transplantation. Eur Radiol 2018;28:44–50.
10. Kellman P, Hansen MS. T1-mapping in the heart: accuracy and precision. J Cardiovasc Magn Reson 2014;16:2.
11. Messroghli DR, Radjenovic A, Kozerke S, Higgins DM, Sivananthan MU, Ridgway JP. Modified Look-Locker inversion recovery (MOLLI) forhigh-resolution T1 mapping of the heart. Magn Reson Med 2004;52:141–146.
12. Kellman P, Herzka DA, Arai AE, Hansen MS. Influence of Offresonance in myocardial T1-mapping using SSFP based MOLLI method. J Cardiovasc Magn Reson 2013;15:63.
13. McGraw KO, Wong SP. Forming inferences about some intraclass correlation coefficients. Psychol Methods 1996;1:30.
14. Bland JM, Altman DG. Statistical methods for assessing agreement between two methods of clinical measurement. Lancet 1986;1:307–310.
15. Lee VS, Kaur M, Bokacheva L, et al. What causes diminished corticomedullary differentiation in renal insufficiency? J Magn Reson Imaging 2007;25:790–795.
16. Lemley KV, KRIz W. Anatomy of the renal interstitium. Kidney Int 1991;39:370–381.

17. Bohle A, Grund KE, Mackensen S, Tolon M. Correlations between renal interstitium and level of serum creatinine. Morphometric investigations of biopsies in perimembranous glomerulonephritis. Virch Arch A Pathol Anat Histol 1977;373:15–22.

18. Bohle A, von Gise H, Mackensen-Haen S, Stark-Jakob B. The obliteration of the postglomerular capillaries and its influence upon the function of both glomeruli and tubuli. Functional interpretation of morphologic findings. Klin Wochenschr 1981;59:1043–1051.

19. Zeisberg M, Kalluri R. Physiology of the renal interstitium. Clin J Am Soc Nephrol 2015;10:1831–1840.

20. Nath KA. Tubulointerstitial changes as a major determinant in the progression of renal damage. Am J Kidney Dis 1992;20:1–17.

21. Levey AS, Coresh J. Chronic kidney disease. Lancet 2012;379:165–180.

22. Roujol S, Weingartner S, Foppa M, et al. Accuracy, precision, andreproducibility of four T1 mapping sequences: A head-to-head comparison of MOLLI, ShMOLLI, SASHA, and SAPPHIRE. Radiology 2014;272:683–689.

4

Consensus-based technical recommendations for clinical translation of renal T1 and T2 mapping MRI

Dekkers IA, de Boer A, MD, Sharma K, Cox EF, Lamb HJ, Buckley DL, Bane O, Morris DM, Prasad P, Semple SIK, Gillis KA, Hockings P, Buchanan C, Wolf M, Laustsen C, Leiner T, Haddock B, Hoogduin JM, Pullens P, Sourbron S, Francis S.

MAGMA. 2020 Feb;33(1):163-176.

ABSTRACT

Objectives

To develop technical recommendations on the acquisition and post-processing of renal longitudinal (T1) and transverse (T2) relaxation time mapping.

Methods

A multidisciplinary panel consisting of 18 experts in the field of renal T1 and T2 mapping participated in a consensus project, which was initiated by the European Cooperation in Science and Technology Action PARENCHIMA CA16103. Consensus recommendations were formulated using a two-step modified Delphi method.

Results

The first survey consisted of 56 items on T1 mapping, of which 4 reached the predefined consensus threshold of 75% or higher. The second survey was expanded to include both T1 and T2 mapping, and consisted of 54 items of which 32 reached consensus. Recommendations based were formulated on hardware, patient preparation, acquisition, analysis and reporting.

Discussion

Consensus-based technical recommendations for renal T1 and T2 mapping were formulated. However, there was considerable lack of consensus for renal T1 and particularly renal T2 mapping, to some extent surprising considering the long history of relaxometry in MRI, highlighting key knowledge gaps that require further work. This paper should be regarded as a first step in a long-term evidence-based iterative process towards ever increasing harmonization of scan protocols across sites, to ultimately facilitate clinical implementation.

INTRODUCTION

There is an increasing need for the development of non-invasive imaging biomarkers to assess the influence of fibrosis and inflammation in the kidney. Renal disease often progresses unnoticed and clinical measurements such as estimated glomerular filtration rate (eGFR) and albuminuria tend to deteriorate late in the disease course. The application of MRI for non-invasive tissue characterization by voxel-wise mapping of longitudinal (T1) and transverse (T2) relaxation time of the kidney without contrast media, referred to as native T1 and T2 mapping, is a promising tool for predicting clinical outcomes in parenchymal renal disease and providing guidance in clinical decision-making. T1 and T2 relaxation times can be indicative of alterations in tissue composition such as fibrosis, edema or cyst progression (1–3). The ability of non-invasive tissue characterization could ultimately be used for better understanding of parenchymal renal disease and for the monitoring of novel drug effectiveness. However, one of the main challenges of research on new MRI biomarkers such as T1 and T2 mapping is the variability in measurement due to lack of standardization in patient preparation, hardware, data acquisition and post-processing.

The European Cooperation in Science and Technology (COST) Action Magnetic Resonance Imaging Biomarkers for Chronic Kidney Disease (PARENCHIMA, CA16103, https://renalmri.org) was established to share best practice and realize the full potential of renal MRI biomarkers. As part of the COST Action PARENCHIMA initiative a systematic review on T1 and T2 mapping was performed which indicated the lack of agreement in patient preparation, acquisition protocols and adequate patient selection, as well as widely accepted reference values (4). Thus, there is a need for optimization and standardization of (multi-parametric) MRI protocols to increase the specificity of renal T1 and T2 mapping. In line with these aims, the COST Action PARENCHIMA has initiated a consensus project to define expert-based technical recommendations to harmonize imaging protocols and image analysis. This PARENCHIMA consensus project aimed to develop and apply a process for generating technical recommendations on renal MRI using Arterial Spin Labelling (ASL), Diffusion Weighted Imaging (DWI), Blood Oxygenation Level Dependent (BOLD), and T1 & T2 mapping, with a common 7-stage process was defined for attaining consensus across each, as outlined in a covering paper (5). The technical recommendations outlined in this paper are intended to provide guidance on the current consensus of set-up of imaging protocols for researchers who are new to the field of renal T1 and T2 mapping or researchers who are interested in combining T1 and T2 mapping within a multi-parametric renal MRI protocol. However, these recommendations should not be interpreted as absolute, as specific research questions might require deviations from current proposed recommendations, and novel state-of-the art developments could bring new insights into scan acquisition protocols or image analysis. In addition, these recom-

mendations focus on the application of T1 and T2 mapping for visualization, quantification and monitoring of parenchymal renal disease rather than for the characterization of focal renal lesions. Moreover, it is outside the scope of the current consensus project to define recommendations on phantoms and/or reference standards to use. But it must be highlighted that any systematic comparison of T1 and T2 mapping schemes should include phantom validation across a range of T1/T2 values. A number of commercially available phantoms with a number of test vials across reference in-vivo T1 and T2 ranges are available (for example, the ISMRM/NIST phantom (6) or Eurospin test object TO5 (Diagnostic Sonar, Livingston, UK). These phantoms can be used to define reference T1 values from an inversion-recovery spin-echo series and T2 values using a Carr-Purcell-Meiboom-Gill (CPMG)-sequence with which to assess the accuracy and precision of other T1 and T2 mapping schemes. Such phantoms have been used in harmonization studies for example in the brain and heart, but to date limited studies have reported inter-vendor or site measures associated with renal T1 and T2 mapping protocols. In this paper we first provide a background overview of technical parameters related to renal T1 and T2 mapping at clinical field strengths (1.5 and 3 Tesla), in the methods section we describe how the consensus project was performed, in the results section the achieved consensus recommendations are discussed in detail, and in the discussion we elaborate on the issues not achieving consensus, and identify areas for future research.

Overview of technical parameters

T1 mapping schemes

Three different approaches for T1 mapping have generally been implemented.

a) Classical inversion recovery (IR): In this scheme, each repetition time (TR) contains a single 180° inversion pulse which, after a delay termed the inversion time (TI), is followed by a single readout. After waiting for full magnetization recovery, this is repeated for a number of TIs to accurately sample the IR curve. A single slice classic IR scheme can be implemented across all MR vendors. However, the disadvantage of this technique is that it is slow, with a single slice acquisition being dependent on the number of inversion recovery times used and the longest recovery time which is also field dependent. The total time can be reduced by using partial post-readout recovery, but if data is collected respiratory triggered then a full respiratory cycle must be allowed between inversion recovery times. A multislice version of the classic IR approach extends the scan time by a factor of the desired number of slices. Therefore, a number of alternative modifications have been proposed to accelerate this for multislice measurements. The simplest option is to follow the 180° inversion pulse by a multislice readout, as illustrated in **Figure 1a**, but this can limit the dynamic range of the TI values across slices, especially for non-EPI based readouts. An elegant solution to this problem is to use *slice cycling* (7,8). Here, instead of repeatedly sampling

the same initial slice after the inversion pulse, one can iterate to sample a different slice. Thus, in the next TR, the order of slices is shifted (the first slice is now measured last) and so on until all slices have been measured at each timepoint. Consequently, the number of slices equals the number of timepoints. To extend the dynamic range of the TI, a delay can be inserted between the slice readouts. However, this approach is not generally available on commercial MR systems. A simplified version of *slice cycling* in which the slice ordering is changed from ascending to descending between TR periods can be a practical solution to implement on commercial systems (9).

b) Look-Locker (LL) sequence and variants such as Modified Look-Locker Inversion Recovery (MOLLI): This is an attractive approach in which a given slice is repeatedly sampled after a single 180° inversion pulse (10,11). The original LL sequence consisted of repeated low flip-angle readouts of a given slice after the inversion pulse. In this way, a single-slice T1 measurement can be performed in a given TR, usually within one breath hold. An important consideration of this approach compared to classical inversion recovery is that the readouts influence the T1 recovery. Therefore, an 'apparent T1' is measured which has to be corrected to compute the 'true T1'.

Variants on the Look-Locker sequence, like MOLLI, were developed for cardiac T1 mapping, where the image readout must be aligned with the cardiac phase (12). Since MOLLI is widely available on commercial scanners within the cardiac package, it is now also being routinely used for renal T1 mapping (4). In the original MOLLI implementation a 3(3)3(3)5 scheme was proposed: 3 images acquired following an inversion pulse, a 3-heartbeat recovery period, an inversion pulse followed by a further 3 images and 3-heartbeat recovery period, and a third inversion pulse followed by 5 images (13). However, there is some dependency of the measured T1 on the heart rate. More recently a 5(3)3 scheme (**Fig. 1b**), which reduces the influence of heart-rate because the recovery time following the first inversion is increased, has been implemented and is available on all MR vendors. A fixed spacing between acquisitions can be used instead of using cardiac triggering which is more appropriate for renal T1 mapping applications. This can be achieved on all commercial systems, either as an option or by turning on physiological simulation on the scanner when in research mode.

c) The Variable Flip Angle (VFA) approach: This has been used for T1 mapping due to its ease of implementation on all commercial systems. This method does not use an inversion pulse, but instead collects spoiled gradient echo images at a number of different flip angles in separate acquisitions (**Fig. 1c**) from which a T1 map can be calculated (14). However, in abdominal imaging and especially at higher field strength, the actual flip angle (B1+) delivered to the abdomen will vary, altering the

fitted T1. For the VFA scheme, a separate B1 map is thus required to correct for any B1+ inhomogeneity which can result in poor precision for the absolute assessment of native T1 (15), although acceptable when using the VFA scheme to measure a change in T1 to a challenge (such as inhalation of oxygen).

T2 mapping schemes

For T2 mapping, the preparation consists at least of a combination of generally a 90º followed by 180º refocusing RF pulse. The most straightforward approach is a conventional *multi-echo spin echo (MESE)* sequence which acquires multiple T2 weightings of a given k-space line in turn (**Fig. 2a**). The MESE sequence can be accelerated using *turbo spin echo (TSE) or fast spin echo (FSE)* (**Fig. 2a**) In TSE/FSE, as the turbo-factor increases, the T2 weighting of the source image is slightly less defined, so high turbo-factors are not suitable for

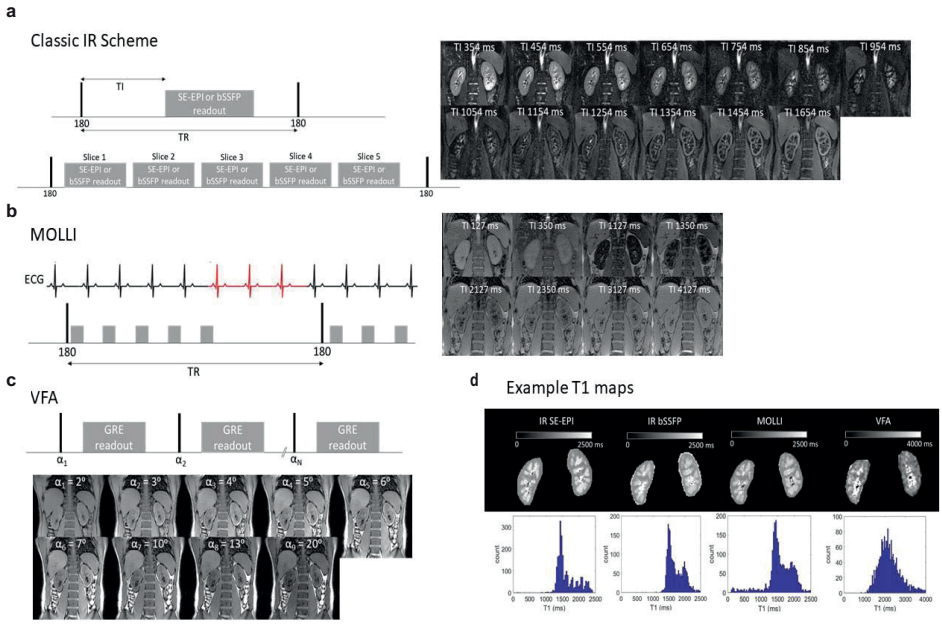

Figure 1. Renal T1 mapping acquisition schemes and example images and T1 maps. (a) Classic IR scheme illustrated here with a spin-echo EPI (SE-EPI) or balanced Fast Field Echo (bFFE) readout. Traditionally, after an inversion pulse a single image readout is acquired after an inversion time (TI), this scheme is available across all vendors. In the slice cycling approach, the empty space is filled with readouts of different slices, as shown here. In the next TR, the slice ordering is shifted to acquire a different initial slice in a given TR. To increase the dynamic range of the TIs, a delay can be added between slice acquisitions. (b) MOLLI with a 5(3)3 scheme: after the first 180o inversion pulse 5 image readouts are acquired in 5 consecutive heart-beats followed by a 3 beat recovery period. After the second 180o inversion pulse, three image readouts are acquired. Note, for renal T1 mapping, rather than ECG gating (which is required for cardiac T1 mapping), a fixed spacing of 1s between image readouts is recommended. (c)VFA, a spoiled gradient echo (GRE) image is collected at a number of flip angles in separate acquisitions from which a T1 map can be calculated.

T2 mapping. Variants of the MESE scheme can be implemented on MR scanners of all vendors. Alternatively, a *gradient and spin-echo (GRASE)* sequence (**Fig. 2b and 2d**) can be used which contains both spin and gradient echo characteristics (16). GRASE is much faster as compared to TSE/FSE and has a lower specific absorption rate (SAR), however T2* effects are introduced, especially at higher acceleration factors.

MESE-based sequences have limitations in that they are sensitive to imperfect slice profiles, diffusion, flow and field inhomogeneities. To minimize such sensitivities, *T2 preparation modules (T2 prep)* can be used (as shown in **Fig. 2c**). Similar to the application of an inversion pulse prior to the readout in T1 mapping, here '*T2 prep*' modules are placed before a fast single-shot readout. Typical *T2 prep* modules include Carr-Purcell-Meiboom-

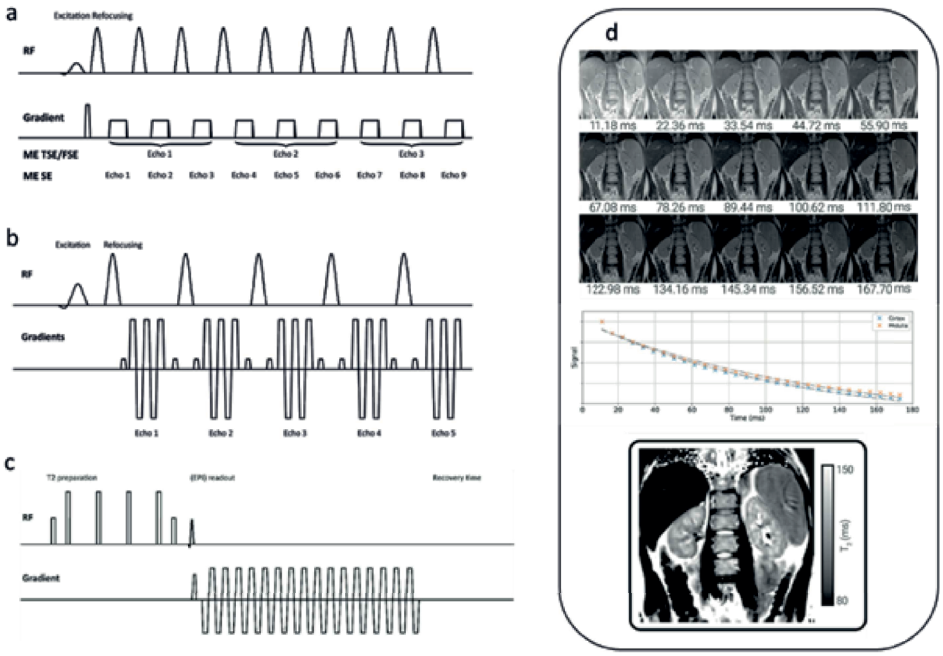

Figure 2. Acquisition schemes (**a**) MESE, **b**) GRASE, **c**) T2 prep) for renal T2 mapping, and example T2 maps using the GRASE scheme. a) MESE: After a 90° excitation pulse, the transverse magnetization is repeatedly refocused by a train of 180° pulses, with a single k-line acquired after each refocusing pulse (here illustrated for 9 echoes). Multiple TRs are then needed to fill the entire of k-space. For MESE, the number of refocusing pulses equals the number of images, each with a different T2 weighting, so every k-line acquired in a single TR is assigned to a different image. For TSE/FSE, a number of k-lines (here illustrated for 3 k-lines) are assigned to the same image, which consequently results in a slightly mixed T2 weighting. The more subsequent k-lines assigned to the same image (higher turbo-factor), the less defined is the T2 weighting of the resulting image. **b**) GRASE: Contrary to MESE, multiple k-lines are acquired after every refocusing pulse using an EPI-like acquisition. **c**) T2 prep: A T2 preparation is immediately followed by a single-shot readout (in the image an EPI readout). Note that it is important to add some time after the readout to allow the longitudinal magnetization to recover before repeating the acquisition at the next effective echo time. **d**) Example images for a GRASE T2 mapping scheme, with associated signal in the cortex and medulla and T2 map.

Gill (CPMG) or four equally spaced composite refocusing pulses with Malcolm-Levitt phase cycling (MLEV4, **Fig. 2c** (17)), but this scheme is sensitive to B0 and B1 inhomogeneities (18–20). Alternatively, a modified B1-insensitive rotation (mBIR-4) scheme (21) can be used, or schemes which use a pair (Silver-Hoult–pair) (22) or multiple adiabatic full passage (AFP) pulses (23).The performance of these schemes have been compared for cardiac imaging (23), (24), but to our knowledge a detailed comparison of different T2 mapping methods has yet to be performed for imaging the kidney. A sufficient recovery time between preparations must be allowed for full T1 recovery, else incomplete T1 recovery results in T1 weighting and errors in the T2 relaxation time measurements (25). The main disadvantage of a 'T2 prep' scheme is the long acquisition time (TR x number of T2 weightings x number of slices). T2 mapping with T2 prep is not generally implemented across all commercial MR systems and may have a limited choice and number of different effective echo times.

Readout strategy

In general, the image readout for a mapping scheme should be a stable 2D single-shot sequence with high SNR, which enables fast imaging, making the readout less sensitive to motion. In renal imaging, gradient or spin echo echo planar imaging (EPI), fast gradient-echo or balanced gradient echo / balanced steady state free precession readouts, and single shot fast spin echo (FSE) are used (4), spin echo schemes can be preferable at higher field strength by limiting distortion. For multi-parametric examinations, it is advantageous to match the readout across the acquisitions in a multi-parametric protocol. This is especially relevant when combining T1 mapping with ASL, where T1 maps in the same data space may be used for the perfusion quantification in ASL (26), important in renal disease where T1 significantly changes with the degree of fibrosis/inflammation. For matched readouts a SE-EPI scheme provides the advantage that it can be for T1, ASL and DWI mapping. Usually, a transversal or coronal (oblique) readout is used (4) to capture both kidneys in one field of view, with a coronal orientation limiting through plane motion.

Respiratory compensation

Adequate compensation for respiratory motion is of relevance since misalignment between acquisitions can introduce substantial errors in the calculated maps. Different strategies exist. For short acquisitions, breath-holding may suffice. However, especially in multiparametric acquisitions, the use of multiple breath-holds might be too challenging for patients. Alternatively, acquisitions can be aligned with respiration (respiratory triggering or gating) or paced breathing used preferably with post-hoc motion correction. When fast single-shot 2D readouts are used, free-breathing acquisitions can be considered, enhancing patient comfort and decreasing scan time, but post-hoc motion correc-

tion (image registration) is then mandatory. Underlying respiratory motion can induce signal fluctuations in the kidneys due to field (both B0 and B1) inhomogeneities in the abdomen, introducing additional noise. Furthermore, it can induce through-plane motion making motion correction more difficult. For T1 mapping, the inversion of contrast between source images makes image registration especially challenging, so some form of respiratory compensation during acquisition is advisable.

B_0 and B_1 mapping

Another aspect to consider when performing T1 and T2 mapping is the collection of separate B0 and B1 maps to improve interpretation of data or to correct underlying inhomogeneities. B0 maps, computed from the phase difference between dual-echo gradient echo images, allow the assessment of off-resonance effects on image quality. B1 mapping allows the quantification of the local RF transmit (B1+) field. In the abdomen, variations in image intensity can be notable due to B0 and B1 inhomogeneity, which can lead to significant differences between left and right kidneys. Non-ideal flip angles (in inversion pulse and readouts) can be included as a fitting parameter in the T1 fit or a separately acquired B1 map can be used in the fitting of the T1 data (as is required for the VFA method). Several B1 mapping methods have been developed, including the dual-TR or actual-flip angle (AFI) method (27), saturated double angle method (SDAM) (28), dual refocusing echo acquisition mode (DREAM) (29), phase sensitive method (30), Bloch-Siegert method (31) and use of a preconditioning RF pulse with turboFLASH readout (32). Despite this, the commercial availability of B1 mapping schemes is limited, and there is no commonality in the natively availability of B1 mapping schemes across vendors, as highlighted in a recent paper to establish inter-vendor reproducibility of T1 relaxation times for brain imaging (33).

Data analysis and reporting

Several data analysis and reporting steps are of relevance in renal T1 and T2 mapping.

a) *Image Registration.* Prior to segmentation and ROI selection, it may be important to perform image registration across different TI times/VFA (T1 mapping) or echo times/preparation times (T2 mapping) to account for misalignment of slices due to abdominal motion. Motion-correction can be performed using an affine registration or a deformable registration for severely motion affected slices.

b) *Outlier detection and rejection.* Outlier detection and rejection is crucial in order to avoid anomalous contributions from acquisition artifacts or motion-induced artifacts (seen as signal intensity errors across imaging slices) during data analysis. Outliers must be excluded from the dataset prior to ROI selection for correct estimation of T1/T2 values. Image registration techniques may help reduce outliers. In case of outliers due

to imaging artifacts, care must be taken by excluding such slices from the analysis or data reporting.

c) *Quantification.* For each T1 mapping scheme, a different curve fitting function is used to obtain a T1 value. The Levenberg-Marquardt algorithm is the standard way to solve this nonlinear curve fitting problem. It should be noted that different estimation biases result depending on the fitting model such as number of parameters in the fit. T2 mapping sequences can be quantified by fitting a mono-exponential decay to the data. An overview of the T1 and T2 fitting functions and fitted parameters is presented in **Table 1**. Thermal and physiological noise, for example motion varies across subjects, will alter the model fitting, so it is important to determine the quality of the data. Robust estimation can be used to fit T1/T2 and estimate its standard deviation. This uses iterative re-weighting to improve the fit in the presence of outliers, at each iteration the weighting of outliers is reduced based on the value of their residuals.

d) *Reporting.* The classical method of choice for reporting T1 and T2 mapping in the kidney involves manual ROI selection in the renal cortex and medulla on single/multiple slices, and/or different regions of the kidney (upper pole, interpolar and lower pole), with the combination of these yielding a single T1 or T2 value each for the cortex and the medulla, respectively. The main challenge of this method includes difficulty in drawing ROIs of an appropriate size and location avoiding partial volume effects when placed close to tissue interfaces, such as renal sinus fat and perirenal fat. Additionally, in the case of advanced renal disease such as chronic kidney disease (CKD), the cortico-medullary difference may become less apparent, due to alterations in the cortical and medullary T1 values, resulting in a decrease in cortico-medullary differentiation (CMD) (4). Unclear boundaries due to reduced CMD may further introduce intra- and inter-rater bias when selecting ROIs. Alternative methods have been proposed in the literature for extracting the cortex and medulla using semi-automated or automated segmentation to reduce measurement variability and time. Semi-automated methods include histogram analysis (34) of the T1 map of the kidney, whereby the renal cortex and medulla is segmented by creating a histogram of T1 values across the kidney from which the two peaks can be used to separate cortex from medulla. Automated segmentation of the kidneys and its compartments (cortex, medulla, renal pelvis) based on registered T1- and T2-weighted images has been proposed by Will et al. (35), and machine learning methods are now being explored. However, such a technique will likely require co-registration of the T1- and T2-weighted images to either the T1/T2 mapping data.

Table 1. Overview of functions used for quantification of T1 and T2 relaxation times.

T1 mapping	
(48)	**Classical Inversion Recovery (IR) T1 mapping** Fitting of the classical inversion recovery(IR) mapping scheme for M_0 and T_1: $$S_k = M_0\left(1 - 2e^{-\frac{TI_k}{T_1}}\right)$$ Eq. [1a] Assuming an ideal (100 %) inversion
(13, 48)	**Look Locker T1 mapping and variants such as Modified Look Locker T1 mapping (MOLLI)** Data fit to a three-parameter nonlinear curve for A, B and T_1^* $$S_k = A - Be^{-\frac{TI_k}{T_1^*}}$$ Eq. [1b] with 'true T_1' computed from: $T_1 = T_1^*\left(\frac{B}{A} - 1\right)$
(14)	**Variable Flip Angle T1 Mapping** Using multiple flip-angles, the T_1 can be estimated by fitting for M_0 and T_1: $$S_k = M_0 \sin\alpha_k \frac{\left(1-e^{-\frac{TR}{T_1}}\right)}{1-\cos\alpha_k e^{\left(-\frac{TR}{T_1}\right)}}$$ Eq. [1c] By collecting the signal at different flip angles, T_1 can be determined by first transforming Eq. [1c] into the linear form $\frac{S_k}{\sin\alpha_k} = E_1\frac{S_k}{\tan\alpha_k} + M_0(1-E_1)$ where $E_1 = e^{-\frac{TR}{T_1}}$, and extracting T_1 from the slope $m = E_1$ as $T_1 = -\frac{TR}{\ln(m)}$.
T2 mapping	
(49)	**Multi-echo spin echo sequence or T_2 preparation modules** The signal is defined using a mono-exponential decay fitting for M_0 and T_2 $$S_k = M_0 e^{\left(-\frac{TE_k}{T_2}\right)}$$ Eq. [2]

α, flip angle; α_k, flip angle at k^{th} pulse; M_0, equilibrium magnetization; M_k, magnetization at k^{th} sampling pulse; T_1, fitted pixel-by-pixel T_1 values; T_1^*, apparent T_1 (or modified T_1 in the LL experiment); T_2, fitted pixel-by-pixel T_2 values; T_2^*, 'observed' T_2 reflecting both true T_2 as field inhomogeneities; TE_k, multiple echo times/preparation times at k^{th} TE scan time; T_D, delay between flip angle and readout; TI, inversion recovery time; TI_k, inversion recovery time at k^{th} IR scan time; S_k, the signal value at k^{th} pulse.

MATERIALS AND METHODS

Description of survey process

The consensus project consisted of an approximation of a two-step modified Delphi method (36), which is a recommended approach to determine a reliable consensus in practice guidelines on health-care related issues. this is outlined in more detail in the covering paper (5). The Delphi method is an iterative process using repeated survey rounds to define consensus on proposed items and effective for determining expert group consensus on topics where there is little or no definitive evidence and where opinion is important (37). Members of the PARENCHIMA Working Group 1.2 (Renal T1 and T2 mapping) and experts on renal MRI biomarkers based on recent literature were invited to participate in the Delphi panel. The survey process was conducted as described below,

Comparison of scan protocols

A systematic literature search string for 'renal T1 mapping' and 'renal T2 mapping' was previously performed by the COST action PARENCHIMA and has been published elsewhere (4). This systematic review aimed to provide an overview on potential clinical applications of the measurement of the independent quantitative magnetic resonance relaxation times T1 and T2 at both 1.5T and 3T. Information on scan protocols of published renal T1 and T2 mapping studies in the literature were used to identify key differences (e.g. field strength, and sequences) between scan protocols that might limit pooling of data and future multicenter studies as a preparation for our electronic survey. In addition, members of the PARENCHIMA Working Group 1.2 (Renal T1 and T2 mapping) were asked to share detailed technical specifications of their local research T1 and T2 mapping protocols that were used in previous studies and/or unpublished work. In total four T1 mapping protocols (Aarhus, Leiden, Leeds, Utrecht), and two T2 mapping protocols (Aarhus, Utrecht) were collected. Obtained T1 and T2 mapping protocols were tabulated to identify key differences and similarities between different research groups, different vendors, and different models of MR scanners and software versions. Results of the comparison of these T1 and T2 mapping scan protocols by the PARENCHIMA Working Group 1.2 members and the results of the systematic review on T1 and T2 mapping, served as a basis for the development of our electronic surveys.

Consensus formation

The Delphi method consisted of online surveys covering (a) hardware options and positioning, (b) in-plane spatial encoding, (c) spatial parameters, (d) RF and contrast, (e) customization and image analysis. Results of the first electronic survey round were discussed face-to-face in Aarhus, Denmark on March 18-19, 2019. Based on these discussions follow-up survey questions were constructed for the second round, as well as to include questions on T2 mapping. In the follow-up electronic survey, Delphi panelists were presented consensus statements based on the results of earlier versions of the electronic survey, which could be commented on by the panelists. Consensus was pre-defined as at least 75% consensus on the proposed question by the Delphi panel (excluding panelists who reported to have insufficient experience to make a recommendation with regard to the proposed question or statement). Survey questions in which over 40% of the Delphi panel noted to have insufficient experience to make a recommendation were excluded. Items that achieved consensus are discussed in the Results sections in the following order: patient preparation, hardware considerations, T1 mapping scheme, T2 mapping scheme, readout strategy, quantification, data analysis and reporting T1 and T2 values. An overview of the items asked in survey 1 and 2 are available online, as electronic supplementary material.

RESULTS AND FINAL RECOMMENDATIONS

In total 18 experts participated in the Delphi panel of which 9 responded in the first round and 17 in the second round, which meets the considered adequate number of experts for content validation (38). Fourteen experts of the Delphi panel have a background in physics, three in clinical radiology, and one in nephrology. The first survey consisted of 56 items on renal T1 mapping of which four reached the pre-defined consensus threshold of 75% or higher. The second survey was expanded to include both renal T1 and T2 mapping, and consisted of 54 items of which 32 reached consensus. In the second round, 5 survey questions were excluded due to high number of experts reporting insufficient experience to make a recommendation. These five questions comprised survey statements on minimization of off-resonance, B1 maps, realignment and transformation of data acquired using breath hold scans, and whether outlier detection and rejection should be used. Nine experts noted that they collect both T1 mapping and ASL data routinely in their scan protocols. An overview of the items that reached consensus is provided in **Table 2**, and the recommendations arising from this process are discussed in the subsections below, indicated as "R" followed by a number (with an additional letter after this number if a recommendation belongs to the same category). In **Table 3** a summary is provided of the most important recommendations.

Patient preparation

In the literature, different strategies for patient preparation have been described for renal T1 and T2 mapping, varying from no specific approach to several hours (2 - 6 hours) of fasting. The expert panel recommended that subjects should be scanned in a normal hydration status when clinically appropriate **[R 1].** Little is known about the influence of hydration state on T1 or T2 values of the kidney, however cardiac T1 mapping has shown that fluid overload significantly prolongs native T1 (39). As fluid overload is also common in patients with renal disease, this can be an important confounder for the interpretation of native T1. No consensus was reached on whether diet needs to be controlled before scanning or whether subjects should follow a controlled or standardized salt intake. Factors for disagreement with the need for a diet control or standardized salt intake were practical limitations leading to difficulties in controlling diet or salt intake, particularly since data demonstrating a significant influence of diet on renal T1 or T2 is lacking.

Table 2. T1 and T2 mapping consensus based recommendations

No.	*Consensus based recommendation*	*Consensus n (%)*	*Excluded n (%)*
	Patient preparation		
1	Subjects should be scanned in a normal hydration status when clinically appropriate	13 (87)	2 (12)
	Hardware		
2a	T1 and T2 mapping can be performed at both 1.5T and 3T	T1 mapping: 6 (67) T2 mapping: 16 (94)	T1 mapping: 0 T2 mapping: 0
2b	A body coil transmitter and multi-channel receiver coil are hardware requirements for both T1 and T2 mapping	T1 mapping: 8 (100) T2 mapping: 16 (94)	T1 mapping: 1 (11) T2 mapping: 0
	Acquisition - General		
3a	A look-locker variant is recommended as the T1 mapping scheme	16 (94)	0
3b	A minimum in-plane resolution of 3 mm is recommended for both Classic IR, MOLLI variant, and T2 mapping	Classic IR: 12 (92) MOLLI: 15 (100) T2 mapping: 15 (100)	Classic IR: 4 (24) MOLLI: 2 (12) T2 mapping: 2 (12)
3c	A parallel imaging factor of 2 is recommended for both Classic IR and MOLLI variant	Classic IR: 11 (85) MOLLI: 12 (80)	Classic IR: 4 (24) MOLLI: 3 (18)
3d	Collection of separate B0 and B1 maps when T1 or T2 maps are acquired is suggested	B0: 11 (92) B1: 12 (79)	B0: 5 (29) B1: 3 (18)
3f	A coronal or coronal oblique orientation are recommended for obtaining T1 and T2 maps of both kidneys during the same acquisition	5 (83)	3 (33)
	Acquisition - Classic IR		
4a	Classic IR collected using an EPI readout with a minimum of 5 slices of 5 mm slice thickness are suggested scan parameters	5 (83)	3 (33)
4b	Considering renal T1 relaxation times, a minimum of 10 inversion times is suggested	11 (85)	4 (24)
4c	Classic IR data collected using respiratory triggering or paced breathing is suggested	14 (93)	2 (12)
4d	Classic IR data collected with right-left foldover is suggested	10 (83)	5 (29)
	Acquisition - MOLLI variant		
5a	A shortened MOLLI scheme with a bFFE readout with 35° flip angle with a minimum slice thickness of 5 mm are suggested scan parameters.	5 (83)	3 (33)
5b	A 5(3)3 MOLLI scheme is an acceptable sequence for renal T1 mapping	13 (100)	4 (24)
5c	MOLLI data should be collected with fixed spacing, i.e. ECG gating should not be used	11 (85)	4 (24)
5d	A fixed spacing of 1s between RF pulses is suggested	13 (100)	4 (24)
5e	A minimum of one slice is sufficient for renal T1 mapping using MOLLI variant	11 (85)	4 (24)
5f	For clinical populations, collecting each slice in a single breath hold (BH) is suggested, a BH of less than 15 s is recommended	14 (93)	2 (12)

Table 2. T1 and T2 mapping consensus based recommendations (continued)

No.	*Consensus based recommendation*	*Consensus n (%)*	*Excluded n (%)*
	Acquisition - T2 mapping		
6a	A minimum of 5 echo times is suggested for data collection	13 (100)	4 (24)
6b	The recommended maximum echo time/T2 preparation time is at least the T2 relaxation time of the kidney (e.g. 120 ms at 3T)	14 (100)	3 (18)
	T1 quantification		
7a	An inversion factor correction is not required in T1 quantification	10 (83)	5 (29)
7b	A B1 map can be of help to confirm good field inhomogeneity	11 (85)	4 (24)
7c	MOLLI T1 is quantified using a 3-parameter curve fit (y=A-B*exp(-TI/T1*) and correction (T1=T1*(B/A-1)) to yield T1	13 (100)	4 (24)
	Analysis of T1 and T2 values		
8a	A manual ROI selection of the medulla and cortex is an acceptable analysis method	14 (88)	1 (6)
8b	When collecting multiple slices, combining all ROIs across all slices is suggested	12 (79)	3 (18)
8c	Automated ROI is preferred over manual ROIs	12 (79)	3 (18)
	Reporting of T1 and T2 mapping		
9a	T1 and T2 values should be reported for cortex and medulla separately when possible and preferably contain either mean (standard deviation) or median (interquartile range)	Mean: 12 (79) Median: 14 (93)	Mean: 3 (18) Median: 3 (18)
9b	Reporting of the T1 cortex medulla difference (T1 medulla - T1 cortex) is suggested	15 (100)	2 (12)
9c	Reporting of the corticomedullary ratio (T1 cortex / T1 medulla) is suggested	13 (100)	4 (24)
9d	Reporting of number of cases without visible corticomedullary differentiation with regard to corresponding T1 and T2 values is recommended	15 (100)	2 (12)

Hardware considerations

Validation studies on renal T1/T2 mapping have been performed both at 1.5 and 3T, with recent multi-parametric studies being performed more frequently at 3T (4). T1 and T2 mapping are acceptable be performed at both 1.5T and 3T **[R 2a]**. Higher field strength provides increased signal-to-noise ratio and greater dynamic range of T1 values, but conversely there are greater field inhomogeneities and a shortened T2 dynamic range. The system-integrated body coil should be used for RF transmission and multichannel receivers are recommended when performing T1 and T2 mapping of the kidney **[R 2b]**, as implemented in cardiac and liver imaging.

Table 3. Final consensus recommendations on renal T1 and T2 mapping for patient preparation, acquisition, analysis and reporting.

	T1 mapping	T2 mapping
Preparation	Normal hydration	Normal hydration
Field strength and hardware	1.5T or 3T, body coil transmitter and multi-channel receiver coil	1.5T or 3T, body coil transmitter and multi-channel receiver coil
Consensus Sequence	MOLLI	MESE, GRASE, T2 prep†
Orientation	Coronal or coronal oblique	Coronal or coronal oblique
Acquisition MOLLI	≥1 slice, 3 mm in-plane resolution, slice thickness ≥5 mm, FA 35°, parallel imaging factor 2, 1s fixed spacing, breath hold <15 s	
Acquisition Classic IR	EPI readout, ≥5 slices, ≥10 inversion times, respiratory triggering or paced breathing, right-left foldover, parallel imaging factor 2	
Acquisition T2 mapping		≥ 5 echo times, max. TE/T2 prep time of 120 ms at 3T
Image quality control	Collection of B0 and B1 maps	Collection of B0 and B1 maps
ROI	Automated > manual, cortex and medulla, combining all ROIs across all slices	Automated > manual, cortex and medulla, combining all ROIs across all slices
Fitting	3-parameter curve fit (y=A-B*exp(-TI/T1*) and correction (T1=T1*(B/A-1))	
Reporting	Cortex and medulla, T1 medulla - T1 cortex, T1 cortex / T1 medulla, number of cases without visible corticomedullary differentiation	Cortex and medulla, number of cases without visible corticomedullary differentiation
Reported metric statistics	Mean, median, standard deviation, interquartile range	Mean, median, standard deviation, interquartile range

†consensus yet to be defined

T1 mapping scheme

For T1 mapping, a consensus was reached to recommend a Look-Locker variant (for example MOLLI) **[R 3a]**. This decision was reached as this is currently the only scheme that is widely available across MR vendors, with a 5(3)3 MOLLI scheme being an acceptable scheme **[R 5b]**. When a MOLLI scheme is chosen, a fixed spacing of 1s is recommended as opposed to ECG triggering **[R 5c-d]**, as ECG triggering is not applicable to the kidney in contrast to cardiac imaging. Despite the MOLLI scheme being only a single slice method, this was agreed to be sufficient [**R 5e**] and should be collected in a breath hold of less than 15 s in order to be useful in patients that might be compromised in their ability to hold their breath for longer durations [**R 5f**]. 10 of the 17 experts (59%, no consensus) also recommended a classic inversion recovery based scheme comprising at least 10 different TIs **[R 4b]**. A VFA method is not recommended, only 20% of the panel felt this scheme is suitable for native T1 mapping.

The ultimate choice of T1 mapping scheme depends on the goal of the study. At the current time, MOLLI will provide an appropriate choice for a large multicenter study comprising a multiparametric protocol, since it is widely available and fast. However, for a single-center study aimed to detect subtle changes in tissue microstructure, one might choose the classical inversion recovery sequence (with or without slice cycling) which has been shown to be more precise over a wide range of T1 values (34).

T2 mapping scheme

For T2 mapping, no consensus was reached on a preferential scheme to use. MESE or GRASE based schemes are the preferred choice for large-scale studies due to being widely available but are slow. However, a *T2 prep* scheme, though not widely available, yields highly reproducible T2 measurements independent of scanner type and manufacturer, as shown for myocardial T2 mapping (40) and has the advantage that the same readout can be shared over multiple sequences (e.g. T1, T2 and ASL) within a multiparametric protocol (41) [R1.4].

A consensus was reached that at least five T2 weightings should be acquired for accurate T2 estimation **[R 6a]** and that the maximum echo time should be at least equal to the T2 of the kidney (e.g. approximately 120 ms at 3T) **[R 6b]**.

Readout strategy

In general, for a multiparametric scan protocol it might be necessary, or at least convenient for data analysis and interrogation, to use the same readout for all acquisitions. In particular for T1 mapping and ASL we recommend using the same readout, since the T1 maps can be used in the perfusion quantification (26).

For MOLLI, a single-shot balanced gradient echo / balanced steady state free precession (bSSFP) readout with a flip angle of 35° is recommended **[R 5a]**, as this flip angle results in the highest signal-to-noise ratio. For classical inversion recovery, an EPI readout is recommended **[R 4a]**. No consensus was reached for T2 mapping.

Regarding spatial resolution, a minimal in-plane resolution of 3 mm is recommended **[R 3b]** to assess differences between cortex and medulla while maintaining signal-to-noise ratio. For T1 mapping, a maximum slice thickness of 5 mm is recommended **[R 4a, 5a],** but for T2 mapping no consensus was reached. Regarding field of view and matrix size, no consensus was reached. For classical inversion recovery with an EPI readout, left-right phase encoding direction, as is typical for abdominal imaging, is recommended. A parallel imaging factor of 2 is recommended for T1 mapping readout schemes to yield high SNR, artefact free maps.

A coronal or axial plane can be used to image both kidneys in the same field-of-view during one acquisition. However, a coronal or coronal oblique orientation (parallel to the long axis of the kidneys) is preferred **[R 3f]** as this orientation provides information about

the distribution of T1 or T2 values in different anatomical areas of the kidney; upper pole, interpolar region, and lower pole. Furthermore, in this orientation respiratory motion is in-plane and through plane motion is limited, enabling effective respiratory correction through registration. In contrast, for an axial acquisition, a given slice may be located at different levels in the kidney due to respiratory motion in free breathing acquisitions or inconsistent breath holds between multislice images.

Quantification

With regard to T1 quantification, a consensus was reached that inversion factor correction is not required **[R 7a]**. A B1 map can be beneficial for confirming good field homogeneity **[R 7b]**, though the need for a B1 map to correct for the readout flip angle (e.g. to ensure the exact flip angle is used in MOLLI scheme) is still debatable. Limitations of additional B0/B1 mapping increasing the technical complexity to the scan protocol were raised. For the MOLLI scheme, a consensus was reached that T1 values should be quantified using a 3-parameter curve fit (Eq. [1d]) **[R 7c]**.

Data analysis and reporting T1 and T2 values

For image analysis the expert panel considered manual ROI selection of the medulla and cortex to be an acceptable analysis method at this moment **[R 8a]**. However, the expert panel considered automated ROIs to be preferred over manual ROIs **[R 8c]**. For protocols that acquire multiple slices of the kidney in the same orientation, it is recommended to combine all ROIs across all slices **[R 8b]**, in order to reach a more balanced estimate of the ROI measurement. No consensus was reached on whether single or multiple ROIs in the cortex or medulla be used, or on the need for taking ROI size into account when using multiple ROIs.

Several recommendations were made by the expert panel with regard to the reporting of T1 and T2 mapping results. In subjects with visible corticomedullary differentiation, relaxation times should be provided for cortex and medulla separately **[R 9a]**. In addition, T1 and T2 values should be reported as either mean with corresponding standard deviation or median with interquartile range (depending on the distribution of the data). Suggested measures to reflect corticomedullary differentiation are both the T1 cortex medulla difference (T1 medulla - T1 cortex) **[R 9b]** and the corticomedullary ratio (T1 cortex/T1 medulla) **[R 9c]**. It is recommended to report the number of cases with no visible corticomedullary differentiation, as this limits the determination of separate relaxation times for renal cortex and medulla **[R 9d]**.

DISCUSSION

Issues not reaching consensus

No T2 mapping sequence (MESE, GRASE, T2 preparation module) reached consensus. In addition, no consensus was reached with regard to a minimum matrix size for renal T1 and T2 mapping schemes. Noting that for an EPI acquisition, the minimum achievable echo time is dependent on the matrix size and acceleration factor used, it is suggested that a minimum field of view of 320 mm x 320 mm be considered to ensure a reasonable echo time for classic IR T1 mapping. With regard to adopting methods to minimize off-resonance effects to avoid banding artefacts in MOLLI variants of T1 mapping, 53% of the panel had insufficient experience to make a recommendation so no consensus was reached. To provide some guidelines, B0 shimming and center frequency can be adjusted to minimize off-resonance. This is especially important at higher field strengths where off-resonance effects can result in regional variations in apparent T1 (12). If available, B1 shimming also improves both T1 and T2 estimation. Although consensus was reached that manual ROI analysis of the renal cortex and medulla is acceptable, no specific strategy was decided upon from the following strategies: one large ROI parallel to the outer edge of the cortex; at least three ROIs of >0.1cm^2 in representative areas of both cortex and medulla; ROIs in upper pole, interpolar, lower pole region of both kidneys; and one ROI including respectively the cortex or medulla as a whole. In addition, it was highlighted that studies on the reproducibility of manual ROI measurement of renal T1 and T2 mapping are needed. For automated ROI analysis no specific strategy resulted from the questionnaire. Automated ROI analysis strategies mentioned by the expert panel included a visual distribution approach (e.g. k-means clustering), and histogram analysis to differentiate between cortex and medulla. Further it was highlighted that heterogeneity in the distribution of T1/T2 values across the kidney may be useful for assessing the presence and progression of CKD.

Limitations and remaining challenges for future research

The panel of experts that participated in this consensus formation process was of limited size (n=18), which can be considered a shortcoming of this work. However, it included scientists from groups that have all developed or applied renal T1 mapping applications. The proportion of technically oriented panel members was high, justified by the current state of development of the technique. Other limitations include differences in the level of detail in the provided recommendations as these are inherent to the maturity of the research field. As such, provided recommendation on data analysis and reporting include semi-automated approaches, and the influence of fitting routines, defining of outliers, handling of missing slice data, and the associated penitential bias for estimated T1 and T2 have not been addressed. Several knowledge gaps are highlighted based on the results

of this survey. More research is needed on possible factors influencing renal T1 and T2 measurements such as hydration state, fasting state, salt intake or medication use, with hydration state being of great interest as volume regulation can be affected in renal patient populations. Despite reaching consensus on the 5(3)3 MOLLI scheme for renal T1 mapping, this scheme has been optimized for cardiac T1 mapping and its use is in part driven by its availability across all major MR vendors, rather than its optimization for measurement of renal T1 values, leaving room for further improvement. Further the use of a 5(3)3 MOLLI scheme can be limited with respect to spatial resolution, since each of the 5,3,3 single-shot images must occur within a 1s interval. High spatial resolution MOLLI data can be achieved through the use of segmented multi-shot data acquisitions, assuming each breath-hold is consistent. Likewise, it should be noted that a classic IR with single-shot EPI acquisition is also limited in achievable spatial resolution due to the increased echo time at higher spatial resolution.

Although T1 values of renal cortex, medulla, and corticomedullary ratio have proven to be highly reproducible for both classic IR and MOLLI 5(3)3 schemes (9,42,43), no studies thus far have evaluated intra- and inter-observer reproducibility of manual and (semi) automated analysis strategies for the assessment of T1 values in the kidney. In addition, reproducibility studies on renal T2 mapping are lacking. Moreover, the survey responses underline the need for dedicated renal post-processing software to facilitate automated image analysis of T1 and T2 values in cortex and medulla and provide quantitative error estimates for reliability assessment, key for use in clinical decision making (44). Besides uniformity in scan protocols, high quality healthy volunteer reference data is needed to define a reference range, as has been recently published for cardiac T1 mapping (45), and which requires sufficiently large cohorts to reflect normal variations. Since T1 and T2 mapping sequences have specific precision and measurement errors, data collected in patient populations should be compared with normal reference values obtained using the same mapping scheme (pulse sequence parameters and field strength) (46). Multicenter studies require verification on whether the scanner configurations are identical (47) and phantom validation is essential component of intra- and inter-vendor validation prior to performing a multicenter study.

Conclusion

Technical recommendations were constructed to incorporate the opinions and advice of a multidisciplinary group on renal T1 and T2 mapping. These highlight the current lack of consensus in both renal T1 and T2 mapping, to some extent surprising considering the long history of relaxometry in MRI, highlighting key knowledge gaps that require further work. Given the dynamic nature of physiological imaging methods in terms of data acquisition and analysis, we expect and encourage detailed studies to systematically compare renal T1 and T2 mapping methods, and validate methods against reference stan-

dards for inter-site studies, and harmonize approaches across vendors. This paper should be regarded as a first step in a long-term evidence-based iterative process towards ever increasing harmonization of scan protocols across sites. These outcomes should inform periodic updates of these recommendations on renal T1 and T2 mapping. The panel will stay in existence and recommendations will be revisited and updated as and when new evidence becomes available.

Acknowledgements

The article is based upon work from COST Action Magnetic Resonance Imaging Biomarkers for Chronic Kidney Disease (PARENCHIMA, COST Action CA 16103, www.renalmri.org), supported by COST (European Cooperation in Science and Technology), www.cost.eu. K.S. & S.S. received funding from the Innovative Medicines Initiative 2 Joint Undertaking under grant agreement No 115974. O.B. was supported by the Grant support (2016-2018) from NIH NIDDK individual fellowship 1F32DK109591. S.F, C.B, and S.S receive funding from the Medical Research Council [grant number MR/R02264X/1]. A.B. was supported by an Alexandre Suerman stipend granted to MD-PhD students by the University Medical Center Utrecht, the Netherlands. P.P. has grant support: NIDDK R01 DK093793 and R01 DK106557. M.W. is supported by the Austrian Science Fund (FWF; project KLI 736-B30). I.D. is supported by the cardiovascular imaging group (CVIG), Leiden, the Netherlands.

REFERENCES

1. Friedli I, Crowe LA, Berchtold L, et al. New Magnetic Resonance Imaging Index for Renal Fibrosis Assessment: A Comparison between Diffusion-Weighted Imaging and T1 Mapping with Histological Validation. Sci Rep. 2016;6:30088
2. Hueper K, Hensen B, Gutberlet M, et al. Kidney Transplantation. Invest Radiol. 2016;51(1):58–65
3. Franke M, Baeßler B, Vechtel J, et al. Magnetic resonance T2 mapping and diffusion-weighted imaging for early detection of cystogenesis and response to therapy in a mouse model of polycystic kidney disease. Kidney Int. 2017;92(6):1544–1554
4. Wolf M, de Boer A, Sharma K, et al. Magnetic resonance imaging T1- and T2-mapping to assess renal structure and function: a systematic review and statement paper. Nephrol Dial Transplant. 2018;33(suppl_2):ii41–ii50
5. Mendichovszky I; Pullens P; Dekkers IA; Nery F. Technical recommendations for clinical translation of renal MRI: a consensus project of the Cooperation in Science and Technology Action PARENCHIMA. MAGMA. 2020 Feb;33(1):131-140.
6. Keenan KE, Ainslie M, Barker AJ, et al. Quantitative magnetic resonance imaging phantoms: A review and the need for a system phantom. Magn Reson Med. 2018;79(1):48–61
7. Ordidge RJ, Gibbs P, Chapman B, Stehling MK, Mansfield P. High-speed multislice T1 mapping using inversion-recovery echo-planar imaging. Magn Reson Med. 1990;16(2):238–245
8. Clare S, Jezzard P. RapidT1 mapping using multislice echo planar imaging. Magn Reson Med. 2001;45(4):630–634
9. Cox EF, Buchanan CE, Bradley CR, et al. Multiparametric Renal Magnetic Resonance Imaging: Validation, Interventions, and Alterations in Chronic Kidney Disease. Front Physiol. Frontiers Media SA; 2017;8:696
10. Look DC, Locker DR. Time Saving in Measurement of NMR and EPR Relaxation Times. Rev Sci Instrum. American Institute of Physics; 1970;41(2):250–251
11. Crawley AP, Henkelman RM. A comparison of one-shot and recovery methods in T1 imaging. Magn Reson Med. 1988;7(1):23–34
12. Kellman P, Herzka DA, Arai AE, Hansen MS. Influence of Off-resonance in myocardial T1-mapping using SSFP based MOLLI method. J Cardiovasc Magn Reson. BioMed Central; 2013;15(1):63
13. Messroghli DR, Radjenovic A, Kozerke S, Higgins DM, Sivananthan MU, Ridgway JP. Modified Look-Locker inversion recovery (MOLLI) for high-resolutionT1 mapping of the heart. Magn Reson Med. 2004;52(1):141–146
14. Fram EK, Herfkens RJ, Johnson GA, et al. Rapid calculation of T1 using variable flip angle gradient refocused imaging. Magn Reson Imaging. 1987;5(3):201–208
15. Liberman G, Louzoun Y, Ben Bashat D. T 1 Mapping using variable flip angle SPGR data with flip angle correction. J Magn Reson Imaging. 2014;40(1):171–180
16. Oshio K, Feinberg DA. GRASE (Gradient- and spin-echo) imaging: a novel fast MRI technique. Magn Reson Med. 1991;20(2):344–349

17. Brittain JH, Hu BS, Wright GA, Meyer CH, Macovski A, Nishimura DG. Coronary Angiography with Magnetization-PreparedT2 Contrast. Magn Reson Med. 1995;33(5):689–696

18. Carr HY, Purcell EM. Effects of Diffusion on Free Precession in Nuclear Magnetic Resonance Experiments. Phys Rev. American Physical Society; 1954;94(3):630–638

19. Meiboom S, Gill D. Modified Spin-Echo Method for Measuring Nuclear Relaxation Times. Rev Sci Instrum. American Institute of Physics; 1958;29(8):688–691

20. Levitt MH, Freeman R, Frenkiel T. Broadband heteronuclear decoupling. J Magn Reson. Academic Press; 1982;47(2):328–330

21. Garwood M, Ke Y. Symmetric pulses to induce arbitrary flip angles with compensation for rf inhomogeneity and resonance offsets. J Magn Reson. Academic Press; 1991;94(3):511–525

22. Nezafat R, Stuber M, Ouwerkerk R, Gharib AM, Desai MY, Pettigrew RI. B1-insensitiveT2 preparation for improved coronary magnetic resonance angiography at 3 T. Magn Reson Med. 2006;55(4):858–864

23. Jenista ER, Rehwald WG, Chen E-L, et al. Motion and flow insensitive adiabatic T 2 -preparation module for cardiac MR imaging at 3 tesla. Magn Reson Med. 2013;70(5):1360–1368

24. Baeßler B, Schaarschmidt F, Stehning C, Schnackenburg B, Maintz D, Bunck AC. Cardiac T2-mapping using a fast gradient echo spin echo sequence - first in vitro and in vivo experience. J Cardiovasc Magn Reson. BioMed Central; 2015;17(1):67

25. Ferreira VM, Piechnik SK, Robson MD, Neubauer S, Karamitsos TD. Myocardial Tissue Characterization by Magnetic Resonance Imaging. J Thorac Imaging. 2014;29(3):147–154

26. Nery F, De Vita E, Clark CA, Gordon I, Thomas DL. Robust kidney perfusion mapping in pediatric chronic kidney disease using single-shot 3D-GRASE ASL with optimized retrospective motion correction. Magn Reson Med. 2018;81(5):mrm.27614

27. Yarnykh VL. Actual flip-angle imaging in the pulsed steady state: A method for rapid three-dimensional mapping of the transmitted radiofrequency field. Magn Reson Med. 2007;57(1):192–200

28. Cunningham CH, Pauly JM, Nayak KS. Saturated double-angle method for rapidB1+ mapping. Magn Reson Med. 2006;55(6):1326–1333

29. Nehrke K, Börnert P. DREAM-a novel approach for robust, ultrafast, multislice B 1 mapping. Magn Reson Med. 2012;68(5):1517–1526

30. Morrell GR. A phase-sensitive method of flip angle mapping. Magn Reson Med. 2008;60(4):889–894

31. Sacolick LI, Wiesinger F, Hancu I, Vogel MW. B1 mapping by Bloch-Siegert shift. Magn Reson Med. 2010;63(5):1315–1322

32. Chung S, Kim D, Breton E, Axel L. Rapid B1+ mapping using a preconditioning RF pulse with TurboFLASH readout. Magn Reson Med. 2010;64(2):n/a.

33. Lee Y, Callaghan MF, Acosta-Cabronero J, Lutti A, Nagy Z. Establishing intra- and inter-vendor reproducibility of T 1 relaxation time measurements with 3T MRI. Magn Reson Med. 2019;81(1):454–465

34. Charlotte E Buchanan, Susan T Francis EFC. Accuracy of renal T1 mapping schemes: a comparison of four T1 mapping methods. Proc Intl Soc Mag Reson Med. 2019;27;1913.

35. Will S, Martirosian P, Würslin C, Schick F. Automated segmentation and volumetric analysis of renal cortex, medulla, and pelvis based on non-contrast-enhanced T1- and T2-weighted MR images. Magn Reson Mater Physics, Biol Med. 2014;27(5):445–454

36. Dalkey NC, Helmer-Hirschberg O. An Experimental Application of the Delphi Method to the Use of Experts. RAND Corporation; 1962.

37. Meshkat B, Cowman S, Gethin G, et al. Using an e-Delphi technique in achieving consensus across disciplines for developing best practice in day surgery in Ireland. J Hosp Adm. 2014;3(4):1

38. Lynn MR. Determination and quantification of content validity. Nurs Res. 35(6):382–385

39. Antlanger M, Aschauer S, Kammerlander AA, et al. Impact of Systemic Volume Status on Cardiac Magnetic Resonance T1 Mapping. Sci Rep. 2018;8(1):5572

40. Baeßler B, Schaarschmidt F, Stehning C, et al. Reproducibility of three different cardiac T 2 -mapping sequences at 1.5T. J Magn Reson Imaging. 2016;44(5):1168–117 8

41. Baeßler B, Schaarschmidt F, Stehning C, Schnackenburg B, Maintz D, Bunck AC. A systematic evaluation of three different cardiac T2-mapping sequences at 1.5 and 3T in healthy volunteers. Eur J Radiol. Elsevier; 2015;84(11):2161–2170

42. Eckerbom P, Hansell P, Cox E, et al. Multiparametric assessment of renal physiology in healthy volunteers using noninvasive magnetic resonance imaging. Am J Physiol Physiol. 2019;316(4):F693–F702

43. Dekkers IA, Paiman EHM, de Vries APJ, Lamb HJ. Reproducibility of native T 1 mapping for renal tissue characterization at 3T. J Magn Reson Imaging. 2019;49(2):588–596

44. Sandino CM, Kellman P, Arai AE, Hansen MS, Xue H. Myocardial T2* mapping: influence of noise on accuracy and precision. J Cardiovasc Magn Reson. BioMed Central; 2015;17(1):7

45. Higgins DM, Keeble C, Juli C, Dawson DK, Waterton JC. Reference range determination for imaging biomarkers: Myocardial T 1. J Magn Reson Imaging. 2019;

46. Kellman P, Hansen MS. T1-mapping in the heart: accuracy and precision. J Cardiovasc Magn Reson. 2014;16(1):2

47. Moon JC, Messroghli DR, Kellman P, et al. Myocardial T1 mapping and extracellular volume quantification: a Society for Cardiovascular Magnetic Resonance (SCMR) and CMR Working Group of the European Society of Cardiology consensus statement. J Cardiovasc Magn Reson. BioMed Central; 2013;15(1):92

48. Stikov N, Boudreau M, Levesque IR, Tardif CL, Barral JK, Pike GB. On the accuracy of T1 mapping: searching for common ground. Magn Reson Med. 2015 Feb;73(2):514-22.

49. de Bazelaire CM, Duhamel GD, Rofsky NM, Alsop DC. MR imaging relaxation times of abdominal and pelvic tissues measured in vivo at 3.0 T: preliminary results. Radiology. 2004 Mar;230(3):652-9.

5

^{1}H-MRS for the assessment of renal triglyceride content in humans at 3T: a primer and reproducibility study

IA Dekkers, P de Heer, MB Bizino, APJ de Vries, HJ Lamb.

J Magn Reson Imaging. 2018 Aug;48(2):507-513.

ABSTRACT

Background

Renal steatosis (fatty kidney) is a potential biomarker for obesity-related renal disease, however non-invasive assessment of renal fat content remains a technical challenge.

Objectives

To evaluate reproducibility and explore clinical application of renal metabolic imaging for the quantification of renal triglyceride content (TG) using proton magnetic resonance spectroscopy (^{1}H-MRS).

Methods

Twenty-three healthy volunteers (mean age 30.1 ± 13.4 years), and 15 patients with type 2 diabetes mellitus (T2DM) (mean age 59.3 ± 7.0 years) underwent ^{1}H-MRS using the Single-voxel Point Resolved Spectroscopy (PRESS) sequence at a clinical MRI scanner. Intra- and inter-examination reproducibility of renal TG was assessed in healthy volunteers, and compared to T2DM patients. Intra-examination differences were obtained by repeating the ^{1}H-MRS measurement directly after the first ^{1}H-MRS without repositioning of the subject or changing surface coil and measurement volumes. Inter-examination variability was studied by repeating the scan protocol after removal and replacement of the subject in the magnet, and subsequent repositioning of body coil and measurement volumes. Reproducibility was determined using Pearson's correlation and Bland-Altman-analyses. Differences in TG% between healthy volunteers and T2DM patients were assessed using the Mann-Whitney U test.

Results

After logarithmic (log) transformation both intra-examination (r=0.91, n=19) and inter-examination (r=0.73, n=9) measurements of renal TG content were highly correlated with first renal TG measurements. Intra-examination and inter-examination limits of agreement of renal log TG% were respectively [-1.36%, +0.84%] and [-0.77%, +0.62%]. Back-transformed limits of agreement were [-0.89%,+0.57%] and [-0.55%, +0.43%] multiplied by mean TG for intra- and inter-examination measurements. Overall median renal TG content was 0.12% [0.08, 0.22; 25th percentile, 75th percentile] in healthy volunteers and 0.20% [0.13, 0.22] in T2DM patients (P=0.08).

Conclusion

Renal metabolic imaging using 3T ^{1}H-MRS is a reproducible technique for the assessment of renal triglyceride content.

INTRODUCTION

The strong increase in the prevalence of obesity has coincided with an increase in chronic kidney disease (1). Lipid nephrotoxicity due to the accumulation of lipids in tubular or glomerular cells of the kidney, also known as renal steatosis or 'fatty kidney' (2), has been proposed as an important pathophysiological pathway of obesity-related renal disease (3). Furthermore, renal steatosis has been linked to renal hyperfiltration (4) and type 2 diabetic nephropathy (5). Studies evaluating possible biological mechanisms have remained confined to animal models (6–8), as it is unethical to perform kidney biopsies without clear evidence of (advanced) renal disease, indicating the need for non-invasive biomarkers of fatty kidney.

The ability of proton magnetic resonance spectroscopy (^{1}H-MRS) to non-invasively quantify triglycerides based on tissue specific metabolite spectra makes this technique a unique imaging modality to study obesity-related renal disease. ^{1}H-MRS has evolved over past years as a valid non-invasive technique to study lipid content in tissue such as liver (9), muscle (10), and heart (11). Technical advances of spectroscopy have created the opportunity to also explore metabolic and physiologic processes in the kidney. Renal triglyceride (TG) content measured using ^{1}H-MRS has previously been described at 1.5T (12) and was recently validated against gold-standard enzymatic assay in ex-vivo porcine kidneys (similar sized to human kidneys) (13).

As higher field strengths result in a better resolution and spectral peak quantification, we aimed to improve the ^{1}H-MRS protocol for renal TG measurements at 3T. We examined intra- and inter-examination reproducibility and explored the application of renal metabolic imaging in type 2 diabetes patients.

MATERIAL AND METHODS

Participants

The Institutional Review Board of our institution approved the study protocol and study design. Written informed consent was obtained from all participants in the present study.

This study consisted of healthy volunteers who participated in the reproducibility analyses, and type 2 diabetes (T2DM) patients. The healthy volunteers were recruited via a local database of people who participate regularly in technical MRI development studies (≥18 years and without known renal disease). The type 2 diabetes patients were the first 15 consecutive patients who were recruited via the endocrinology outpatient clinic to undergo renal metabolic imaging. Inclusion criteria were: age between 18 to 70 years, overweight or obesity (Body mass index, BMI >25 kg/m^{2}), type 2 diabetes with HbA1c levels between 7 to 10%, moderately impaired to normal renal function (estimated glo-

merular filtration rate >60 ml/min/1.73m²), and normal blood pressure (<150/85 mmHg). All renal TG content and serum measurements were performed after overnight fasting, or at least 4 hours fasting to exclude potential dietary effects.

Data acquisition

MR examinations were performed on a 3T Ingenia whole-body MRI scanner (Philips Healthcare, Best, The Netherlands). Spectra were obtained from the parenchyma of the left kidney. The standard posterior (12 channels) and anterior (16 channels) torso/cardiac surface receiver coils were used with the participants placed in supine position. After a standard survey, breath-hold Dixon water/fat scans were acquired of the kidney in three directions at end-expiration. Planning of the single ^{1}H-MRS voxel (40 x 10 x 10 mm^3) within the renal parenchyma was performed on the Dixon fat-only images to avoid contamination with renal sinus or peri-renal fat (**Fig. 1a**). The static magnetic field was homogenized at the voxel location using a first order pencil beam (nine projections) volume static field (B0) shimming algorithm. This method measures nine beams through the voxel of interest and reconstructs the B0 distribution in that voxel. The main advantage of this method is that it is performed in the preparation of the spectroscopy measurement and does not require user input. The location of the shim volumes (50 x 20 x 20 mm^3) was centered around the ^{1}H-MRS voxel. Single voxel Point Resolved Spectroscopy (PRESS) spectra were acquired with an echo time of 40ms, repetition time of 3s for the water-suppressed acquisition (64 signal averages) and 8s for the unsuppressed acquisition (8 averages), ensuring full relaxation of the water and lipid signals (14,15). Spectral bandwidth was 1700 Hz, and 1024 samples were acquired resulting in a spectral resolution of 1.66 Hz/sample. The water-suppressed spectra were acquired using a Multiply Optimized Insensitive Suppression Train (MOIST) suppression method with a bandwidth of 150 Hz. Previous research in cardiac ^{1}H-MRS showed that MOIST performed best at suppression of the water signal, and excitation pulse water suppression should be avoided since this introduces bias in the baseline of the spectra (16). Local power optimization was performed by monitoring the intensity of the water peak and incrementing the tip angles of the excitation pulse and the two refocusing pulses in the PRESS sequence in steps of 5% (range, 90%–150% of the global power optimization result), and selecting the power setting that produced the highest signal intensity. The spectroscopy acquisition was triggered using a pencil beam respiratory navigator technique (17). The navigator volume was placed at the right diaphragm liver-lung interface (**Fig. 1b**), and the spectroscopy measurement was triggered when the diaphragm was in the automatically defined acceptance window of 5mm diaphragm displacement in end-expiration. To further minimize the respiratory motion effects, residual motion was compensated with motion tracking (**Fig. 1c**). To improve navigator stability and performance, the size of the navigator preparation voxel was increased to the same size of the regular navigator voxel. Furthermore, the navigator

signal was improved by using the surface coil rather than the build-in body coil for signal reception. Use of the surface coil resulted in better approximation of the navigator voxel location due to its direct position on top of the body, thereby increasing the respiratory navigator signal.

Intra-examination differences were obtained by repeating the ^{1}H-MRS measurement directly after the first ^{1}H-MRS without repositioning of the subject or changing the position of the surface coil or measurement volumes. Inter-examination variability was studied by repeating the scan protocol after removal and replacement of the subject in the magnet, and subsequent repositioning of the surface coil and measurement volumes. Inter-examination scans were added later in the protocol because of limited research scan time and were therefore not assessed in all participants.

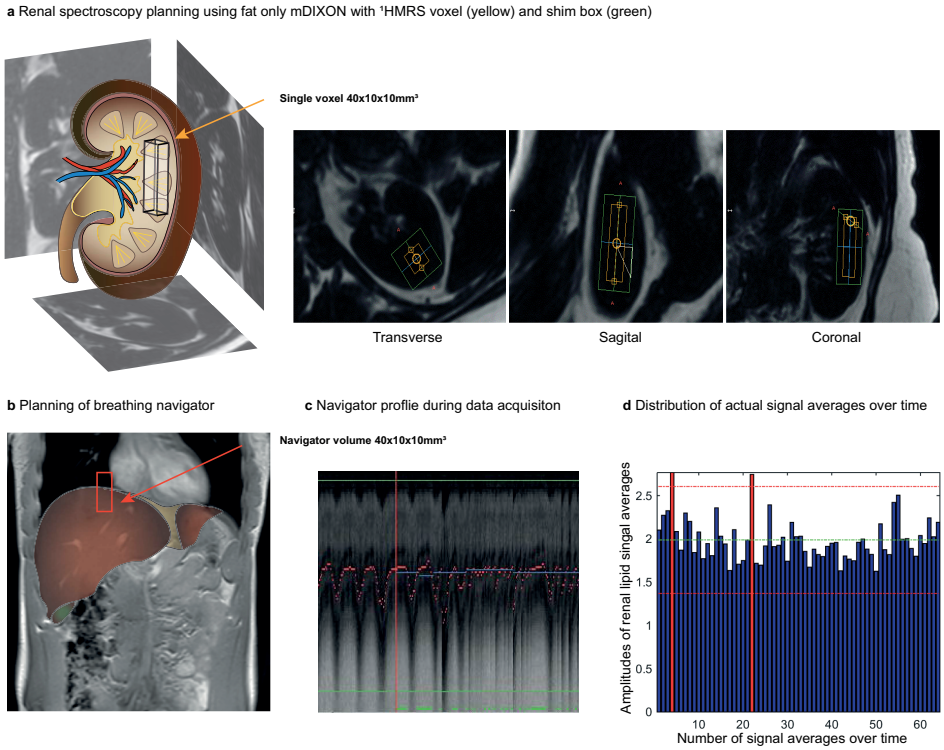

Figure 1. Planning and post-processing analysis of renal ^{1}H-MRS. (a) Planning of single voxel ^{1}H-MRS (yellow) and shim box (green) in renal parenchyma on orthogonal transverse, coronal and sagittal Dixon fat only sequences, (b) planning of breathing navigator at liver-lung interface (c) Navigator profile during acquisition, with bottom white signal form the liver, and dark signal from the lungs. (d) Distribution of amplitudes of renal lipid resonances over time for all water suppressed signal averages. Dotted lines indicate mean amplitude (green) and ± 2.5 SDs (red). Signal averages outside this range were considered outliers and were excluded (marked in red).

Spectral quantification

Acquired spectral raw data output files were reconstructed using an in-house created MATLAB version 8.4 (MathWorks, Natick, Massachusetts, USA) reconstruction script. The raw data was phase corrected after which a weighted sum of the channel signals was calculated for every average. By calculating the phase variation over time, of the unsuppressed spectra, both the unsuppressed and the suppressed spectra were eddy current corrected. Variation in lipid signal amplitude between the signal averages is visualized in **Figure 1d**. Averages outside the 95% confidence interval (CI) were considered outliers and were excluded if present. In the final reconstruction step the included averages were summed. Reconstructed data were fitted in the time domain using Java-based MR User Interface software (jMRUI version 5.0; Katholieke Universiteit Leuven, Leuven, Belgium) (18,19). Residual water signal was removed using the Hankel-Lanczos filter (singular-value decomposition method) (**Fig. 2a**). The Advanced Method for Accurate, Robust and Efficient Spectral fitting (AMARES) algorithm was used to fit the spectra (20). The water suppressed spectra were analyzed using starting values based on known frequency (ppm) and line width (Hz) estimates for renal lipids: triglyceride methyl (CH_3) 0.9 ppm, 10.0 Hz; triglyceride methylene (CH_2)n 1.3 ppm, 13.6 Hz; COO-CH_2 2.1 ppm, 10.0 Hz; trimethylamines (TMA) 3.25 ppm, 8.0 Hz (**Fig. 2b**). As prior knowledge the relative TG resonance frequencies and resonance amplitudes were kept unconstrained, while soft constrains were applied on the linewidth of the resonances: CH_3 0–30 Hz; (CH_2)n 0–30 Hz; COO-CH_2

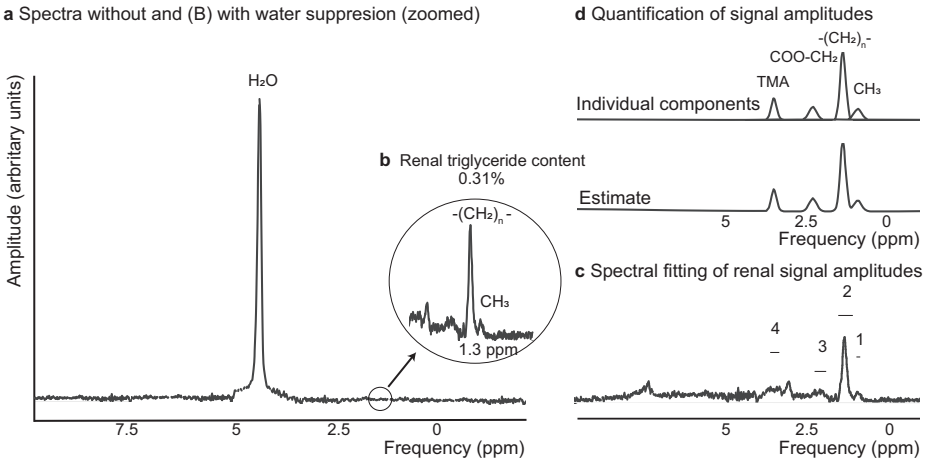

Figure 2. Spectral post-processing of renal ^{1}H-MRS. (a) Single voxel renal ^{1}H-MRS spectra without and with (b) water suppression, resonances from protons of water (peak at 4.7 ppm, H2O), methylene (peak at 1.3 ppm, [CH2]n) and methyl (peak at 0.9 ppm, CH3) are highlighted, (c) Spectral fitting of renal signal amplitudes using estimates for resonances from protons of renal lipids (prior knowledge). Peak number, peak name, frequency, line width: 1. CH3, 0.9 ppm, 10.0 Hz, 2. (CH2)n 1.3 ppm, 13.6 Hz; 3. COO-CH2, 2.1 ppm, 10.0 Hz, 4. TMA 3.25 ppm, 8.0 Hz, (d) AMARES result of individual components of renal lipid signal amplitudes based on original signal and estimated signal using prior knowledge.

0–30 Hz; TMA 0–21 Hz. (**Fig. 2c**). The unsuppressed spectra were analyzed using a starting value of 4.7 ppm for the water signal. All resonances in the suppressed and the unsuppressed spectra were fitted to a Gaussian line shape. Renal TG content was calculated as a percentage of the (unsuppressed) water peak using the following equation:

$$Renal\ TG\% = \frac{triglyceride\ methyl\ (CH_3) + triglyceride\ methylene\ (CH_2)n}{water + triglyceride\ methyl\ (CH_3) + triglyceride\ methylene\ (CH_2)n} \times 100\%$$

Statistical analysis

Renal TG percentages are presented as median (25^{th}, 75^{th} percentile), and other descriptors such as mean (standard deviation SD, range) are also presented. TG percentages were tested for normality using the Shapiro-Wilk test. Logarithmic (log) base 2 transformation of original TG data was performed since renal TG content is not normally distributed (21). Pearson correlations were calculated for first and second measurement of renal log TG% for both intra- and inter-examination measurements. Bland-Altman plots were visualized through a scatterplot of the differences, with reference lines at the mean difference, and mean difference ±2 × SD of the differences (limits of agreement) (22, 23). Back transformed limits of agreement were calculated for intra- and inter-examination measurements by applying $\pm 2\ \overline{X} \times (2^a - 1)/(2^a + 1)$, where $a = \overline{d} \pm 2 \times SD$, $\overline{X}$ is mean TG, and $\overline{d}$ is the mean difference. Group differences in renal TG content between healthy volunteers and T2DM patients were assessed using the Mann-Whitney U test. Two-tailed significance levels of $P<0.05$ were considered to indicate a statistically significant difference. Statistical analyses were performed using STATA version 12.0 (Statacorp, College Station, Texas, USA).

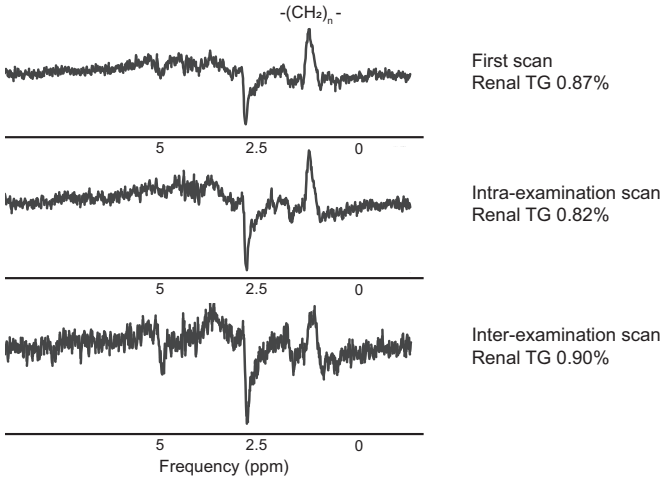

Figure 3. Example of renal ^{1}H-MRS spectra of a healthy volunteer from the three reproducibility acquisitions with corresponding renal TG values.

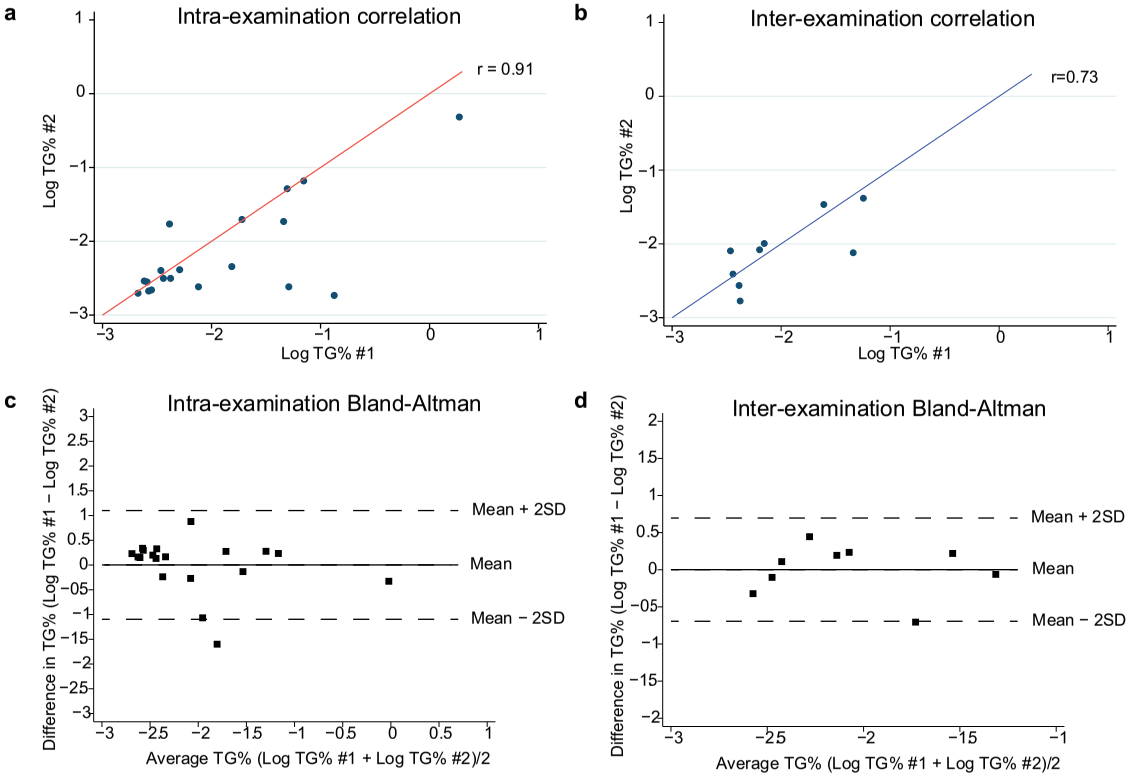

Figure 4. Scatterplots of log-transformed TG with linear fit and Bland-Altman analyses of intra- and inter-examination measurements. (**a**) Scatterplots of within-subject intra-examinations (n=19) with Pearson correlation of 0.91, (**b**) Scatterplots of within-subject inter-examinations (n=9) with Pearson correlation of 0.73. (**c**) Bland-Altman plot of the intra-examination differences (n=19) between measurement #1 and #2 versus the mean of measurement #1 and #2 (mean difference -0.26, lower limit -1.36, upper limit 0.84), (**d**) Bland-Altman plot of the inter-examination differences (n=9) between measurement #1 and #2 versus the mean of measurement #1 and #2 (mean difference -0.07, lower limit -0.77, upper limit 0.62).

RESULTS

Healthy volunteers

Twenty-three healthy participants (mean age 30.1 ± 13.4 years, mean BMI 22.8 ± 5.2 kg/m², 43% men) underwent ^{1}H-MRS for reproducibility assessment (intra-examination n=19, inter-examination n=9). Overall median renal triglyceride content was 0.12% [0.08, 0.22] (range 0.07-1.02%). Both intra-examination (r=0.91) and inter-examination (r=0.73) measurements were highly correlated with first renal TG measurements after log transformation to correct for normality (**Fig. 4 a, b**). Bland-Altman analysis for the intra-examination measurements showed a mean difference of -0.26 log TG% with a lower limit of -1.36 log TG% (95% CI -1.81, -0.90), and a upper limit of agreement of 0.84 log TG% (95% CI 0.38, 1.30) (**Fig. 4c**). For inter-examination measurements, the Bland-Altman analysis showed a mean difference of -0.07 log TG% with a lower limit of -0.77 log TG% (95% CI -1.23, -0.31) and a upper limit of agreement of 0.62 log TG% (95% CI 0.16, 1.08) (**Fig. 4 d**). Corresponding back transformed limits of agreement for intra-examination measurements were -0.89 (95% CI -1.82, -0.90) and 0.57 (95% CI 0.38, 1.30) multiplied by mean TG. For inter-examination measurements back transformed limits of agreement were -0.55 (95% CI -1.31, -0.32) and 0.43 (95% CI 0.13 to 1.11) multiplied by mean TG.

Type 2 diabetes mellitus patients

Fifteen T2DM patients (mean age 59.3 ± 7.0 years, mean BMI 32.9 ± 2.9 kg/m², 47% male) underwent ^{1}H-MRS. Included T2DM patients had a mean creatinine of 73.5 ± 16 umol/L, and mean HbA1c levels of 6.5 ± 1.0%. Median renal TG content in T2DM patients was 0.20% [0.13, 0.22] (range 0.09-0.45). Median renal triglyceride content in T2DM patients was higher compared to healthy volunteers, but observed differences did not reach statistical significance in this small sample size (P=0.08) (**Fig. 5**).

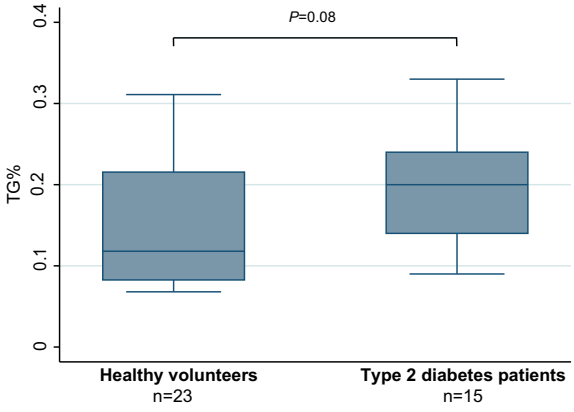

Figure 5. Distribution of renal triglycerides in healthy volunteers and type 2 diabetes patients. Boxplot of renal TG content in 23 healthy volunteers with median TG of 0.12% [0.08, 0.22] (left) and in 15 type 2 diabetes patients with a median TG of 0.20% [0.13, 0.22] (right).

DISCUSSION

We demonstrated that renal metabolic imaging using 3T proton spectroscopy is a reproducible technique that could be used for evaluating the biomarker potential of renal triglyceride in obesity-related renal disease.

We found an overall median renal triglyceride content of 0.12% [0.08, 0.22] in healthy volunteers and 0.20% [0.14, 0.24] in patients with type 2 diabetes. Previously described mean renal triglyceride or fat percentages based on non-invasive human imaging studies range from 0.43 ± 0.10% to 2.18 ± 2.52% (12, 24), however these results are difficult to compare considering technical differences (field strength, acquisition method), and differences in study populations (healthy volunteers, obese participants and type 2 diabetes patients). It has been estimated that the normal human kidney consists of 79.5% water, and overall lipid content in cortex and medulla has been estimated to comprise 0.6% and 1.64% of mean wet kidney weight (25). Obtained renal spectra showed a large peak visible between 1.2 to 1.4 ppm, which predominantly originates from proton resonances of methylene (CH_2) groups of TG. Cholesterol contains methylene groups as well, but these are not visible with current resolution of clinical ^{1}H-MRS since cholesterol is more restricted in its movement (i.e. less magnetic susceptibility or anisotropy due to a greater association with its membranes) resulting in spectral broadening and resonance loss in the background. Based on pathology studies, the estimated overall lipid content in the normal human kidney is composed of approximately one-fifth triglycerides, one-tenth of free fatty acids (non-esterified fatty acids), and the intracellular cholesterol concentration is estimated at one-twentieth or less (25, 26).

Higher levels of renal TG content were observed in type 2 diabetes patients compared to healthy volunteers, but did not reach statistical significance likely due to small sample size. These results need to be validated in a larger cohort with age- and sex-matched controls to draw inferences on whether renal steatosis is truly associated with type 2 diabetes. The underlying mechanisms of fatty kidney have only been investigated in animal models and clinical translation has been hampered by lack of noninvasive tests. A recent pathology study based on nephrectomy specimens found that renal TG content was positively associated with BMI and mainly involved proximal tubule cells, suggesting that renal steatosis is a possible marker of renal fatty acid oversupply (27). These findings have been supported by preclinical studies that showed an increased tubular uptake of free fatty acids (FFAs) in the presence of high FFA plasma concentrations and glomerular albuminuria, which can lead to renal TG storage (6, 28). Low TG storage will most likely not interfere with organ function (e.g. heart, muscle), however excessive renal TG accumulation may lead to tubulointerstitial injury (29, 30) and has been associated with overt albuminuria in obese patients (4). Another potential pathway of renal lipid accumulation and inflammation is increased glucose absorption in hyperglycemia via the

sodium/glucose cotransporter 2 (SGLT2) transporter in proximal tubule cells (31, 32). Improved understanding of renal lipid metabolism in vivo could lead to the identification of potential therapeutic targets for the prevention of obesity-related renal disease, and renal diabetic nephropathy (e.g. fibrates or SGLT-inhibitors) (31). Although the present study shows that ^{1}H-MRS is a reproducible technique for the assessment of renal TG content, several technical limitations exist. The intrinsically low renal TG concentration and voxel size remain important limiting factors of the signal-to-noise ratio even though the field strength in the present study was improved to 3T compared to previous studies at 1.5T. Unintentional locational variation of acquired spectra may be introduced by technical differences in voxel planning and subject repositioning during the examination, which could introduce spectral contamination of non-renal parenchyma tissue such as renal sinus fat and peri-renal fat. Other general technical factors that may affect spectral quality are suboptimal static field shimming, incomplete water suppression, phasing errors, and chemical shift displacement. Since renal ^{1}H-MRS involves metabolites with extremely low concentrations, adequate water suppression and shimming are especially of great importance for sufficient spectral quality. These above-mentioned factors contribute to the inter-subject, intra-examination and inter-examination variability of measured renal TG% by ^{1}H-MRS. Our inter-subject difference (inter-quartile range, IQR) in renal TG% was 0.14% in healthy volunteers, which indicates that the scatter among healthy subjects in their renal fat and renal TG percentages limits the statistical sensitivity to detect significant differences when a single patient or a small group of patients is compared to healthy controls. Inter-subject differences (SDs or IQRs) may reflect technical factors (spectral noise, partial volume effects), and biological variability (low intrinsic renal TG percentages, renal size and cortical thickness).

Intra-examination differences, representing the unchanged position of the ^{1}H-MRS volume and the receive coils, mainly reflect physiologic motion rather than signal-to-noise related variance. One outlier was present in the intra-examination Bland-Altman plot, and was likely due to subject motion in the left-right position that cannot be controlled for by the respiratory navigator. Practical aspects of ^{1}H-MRS measurements, such as the positioning of the surface coil and planning of sensitive volumes are reflected in inter-examination differences. Although calibrations, data acquisition parameters and data post-processing were identical for both measurements, some differences between inter-examination renal TG percentages were present, reflecting measurement variation.

There are several limitations that need to be considered regarding the design of the study. The small sample size of the clinical cohort limits the evaluation of associations between clinical parameters (e.g. BMI, renal function, albuminuria etc.) and renal TG content, as these require adequate adjustment for age, sex, and other possible confounders. Prospective studies are needed to assess to what extent renal TG is associated with renal parameters (glomerular filtration rate, albuminuria, etc.), and to assess potential effects

of medical interventions (glucoregulation, fibrates, statins, stringent weight reduction) on renal triglyceride accumulation (33). Furthermore, we cannot exclude residual effects of fasting on current renal TG measurements (participants were scanned after overnight or ≥4 hours fasting), as this has been described to influence renal TG accumulation in mice (6). Other limitations are the possible influence of intra- and inter-observer variation in the spectral quantification process.

In conclusion, renal metabolic imaging using 3T ^{1}H-MRS is a promising reproducible technique for the assessment of renal triglyceride content that could improve our understanding of obesity-associated renal disease. Further research is needed to assess the potential of renal triglyceride content as a biomarker for obesity-related renal disease.

REFERENCES

1. Ruan XZ, Varghese Z, Moorhead JF. An update on the lipid nephrotoxicity hypothesis. Nat Rev Nephrol. 2009;5(12):713-21.
2. de Vries AP, Ruggenenti P, Ruan XZ, et al. Fatty kidney: emerging role of ectopic lipid in obesity-related renal disease. Lancet Diabetes Endocrinol. 2014;2(5):417-26.
3. D'Agati VD, Chagnac A, de Vries AP, et al. Obesity-related glomerulopathy: clinical and pathologic characteristics and pathogenesis. Nat Rev Nephrol. 2016;12(8):453-71.
4. Li Z, Woollard JR, Wang S, et al. Increased glomerular filtration rate in early metabolic syndrome is associated with renal adiposity and microvascular proliferation. Am J Physiol Renal Physiol. 2011;301(5):F1078-87.
5. Rutledge JC, Ng KF, Aung HH, Wilson DW. Role of triglyceride-rich lipoproteins in diabetic nephropathy. Nat Rev Nephrol. 2010;6(6):361-70.
6. Scerbo D, Son N-H, Sirwi A, et al. Kidney triglyceride accumulation in the fasted mouse is dependent upon serum free fatty acids. J Lipid Res. 2017;58(6):1132-42.
7. Zhou Y, Lin S, Zhang L, Li Y. Resveratrol prevents renal lipotoxicity in high-fat diet-treated mouse model through regulating PPAR-α pathway. Mol Cell Biochem. 2016;411(1-2):143-50.
8. Li L, Zhao Z, Xia J, et al. A long-term high-fat/high-sucrose diet promotes kidney lipid deposition and causes apoptosis and glomerular hypertrophy in bama minipigs. PloS One. 2015;10(11):e0142884.
9. Thomas EL, Hamilton G, Patel N, et al. Hepatic triglyceride content and its relation to body adiposity: a magnetic resonance imaging and proton magnetic resonance spectroscopy study. Gut. 2005;54(1):122-7.
10. Boesch C, Machann J, Vermathen P, Schick F. Role of proton MR for the study of muscle lipid metabolism. NMR Biomed. 2006;19(7):968-88.
11. Rijzewijk LJ, van der Meer RW, Smit JW, et al. Myocardial steatosis is an independent predictor of diastolic dysfunction in type 2 diabetes mellitus. J American Coll Cardiol. 2008;52(22):1793-9.
12. Hammer S, de Vries AP, de Heer P, et al. Metabolic imaging of human kidney triglyceride content: reproducibility of proton magnetic resonance spectroscopy. PLoS One. 2013;8(4):e62209.
13. Jonker JT, de Heer P, Engelse MA, et al. Metabolic imaging of fatty kidney in diabesity: validation and dietary intervention. Nephrol Dial Transplant. 2018 Feb 1;33(2):224-230.

6

The effect of glycemic control on renal triglyceride content assessed by proton-spectroscopy in patients with type 2 diabetes mellitus: a single-center parallel-group trial

Dekkers IA, Bizino MB, Paiman EHM, Smit JW, Jazet IM, de Vries APJ, Lamb HJ.

Submitted

ABSTRACT

Objective

Since renal steatosis is a potential driver of diabetic kidney disease, and tight glycemic control can reduce risk of diabetic nephropathy, we assessed whether glycemic control influences renal triglyceride content (RTGC). Furthermore, we compared GLP-1 receptor agonist liraglutide versus standard glucose-lowering therapy.

Methods

In this single-center parallel-group trial T2DM patients were randomized to liraglutide or placebo added to standard care (metformin/sulfonylurea-derivative/insulin). Change in RTGC after 26 weeks of glycemic control measured by proton-spectroscopy and difference in RTGC between treatment groups was analyzed.

Results

Fifty T2DM patients were included in the baseline analysis (mean age of 56.5 ± 9.1 years; range 33–73 years; 46% males). Seventeen patients had baseline and follow-up measurements. Mean HbA1c was 61.6 ± 8.4 mmol/mol, which changed to 56.3 ± 9.5 mmol/mol after 26 weeks of glycemic control irrespective of treatment group (P=0.046). Log-transformed RTGC was -0.68 ± 0.30%, and changed to -0.83 ± 0.32% after 26 weeks of glycemic control irrespective of treatment group (P=0.049). 26-weeks ' to ' baseline RTGC ratio (95% CI) was significantly different between liraglutide (-0.30 [-0.50,-0.09]) and placebo added to standard care (-0.003 [-0.34,0.34]) (P=0.04).

Conclusions

In this exploratory study we found that twenty-six weeks of glycemic control resulted in lower RTGC, in particular for liraglutide, however larger clinical studies are needed to assess whether these changes reflect a true effect of glycemic control on renal steatosis.

INTRODUCTION

Roughly a third of patients with type 2 diabetes mellitus (T2DM) will develop diabetic kidney disease (DKD) depending on age, ethnicity, diabetes duration and/or extent of hyperglycemia exposure (1). DKD is one of the leading causes of end-stage renal disease (ESRD) worldwide, and the UKPDS (2) and ADVANCE (3) studies showed that improved glycemic control reduces microvascular disease and ESRD. Additionally, the RENAAL (4) and IDNT (5) trials showed that treatment of hypertension and proteinuria in particular when using renin-angiotensin-aldosterone system inhibitors, conveyed a 30% risk reduction for ESRD. In spite of these cornerstone therapies, the incidence of ESRD by DKD continues to rise (6), indicating possible involvement of other (non-proteinuric) pathways related to e.g. hyperfiltration and metabolic regulation (7).

In particular, the combination of T2DM and obesity has been linked to ectopic lipid accumulation in non-adipose tissues such as liver, heart, and kidney, which can interfere with the cellular function of the respective organ (8,9). With regard to the kidney, ectopic lipid accumulation has been linked to structural changes including glomerular hypertrophy (10), and maladaptive functional responses such as hyperfiltration and albuminuria (9). Renal steatosis has been associated with renal gluconeogenesis in experimental models (9), however it is unknown whether glycemic control is conversely linked to ectopic lipid accumulation in kidney. The LEADER trial (11) showed that the glucagon-like peptide-1 receptor agonists (GLP1-RA) liraglutide was renoprotective in DKD compared to current standard glycemic care, which could possibly be related to improved glycemia, amended blood pressure regulation and reduction of weight and/or ectopic fat depots such liver fat and visceral fat. Alternatively, direct actions of GLP1-RA on the kidney have been proposed (12). Currently, it is unknown to which extent improved glycemic control, either by standard glycemic care or via additional direct effects of GLP1-RA, relates to renal steatosis in vivo. Experimental studies have shown that liraglutide might have a renoprotective effect via restoring renal metabolism by inhibiting renal lipid accumulation (13,14).

Clinical studies on renal lipid metabolism have been hampered by the absence of a non-invasive technique to measure renal lipid content. Magnetic resonance spectroscopy (^{1}H-MRS) is considered the gold standard technique to measure hepatic lipid content in vivo (15), however the application of ^{1}H-MRS to the kidney is technically challenging due to respiratory motion and low signal-to-noise ratio related to the low quantities of renal lipids and limited voxel size (16). Recently, we validated and assessed the reproducibility of renal triglyceride content (RTGC) measured using ^{1}H-MRS (16,17). Assessment of RTGC using ^{1}H-MRS offers the possibility to study the potential influence of glucose control on renal lipid metabolism, including novel drugs such as GLP1-RA, in a clinical trial. Here, we aimed to study whether glycemic control influenced RTGC as a secondary outcome of

a 26 week clinical trial of liraglutide versus placebo, added to standard glucose-lowering therapy using metformin, sulphonylurea derivatives (SUD) and/or insulin. A secondary aim was to investigate whether these two treatment groups differed in reduction of renal steatosis.

MATERIALS AND METHODS

Study design

This study is a single-center parallel-group trial containing the baseline and follow-up data of the MAGNA VICTORIA studies in Western European (ClinicalTrials.gov NCT01761318), and South Asian (NCT02660047) T2DM patients. The present study involved RTGC as a prespecified secondary endpoint, previously published primary and secondary endpoints were e.g. left ventricular function, HbA1c, body weight and measures of body fat distribution (visceral fat, hepatic triglyceride content) (18–20). Study protocols have been described elsewhere in more detail (18–20). In short, patients were randomized (1:1 stratification for sex and insulin use in both studies separately, block size 4) to receive either liraglutide (Victoza, Novo Nordisk A/S, Bagsvaerd, Denmark) or placebo (provided by Novo Nordisk A/S, Bagsvaerd, Denmark) for 26 weeks, added to standard glucose-lowering therapy using metformin, SUD and/or insulin (18–20). Study participants, researchers, and other staff involved in the study were blinded to treatment allocation until completion of the study and analysis. Written informed consent was obtained prior to inclusion. The present study was performed according to the revised Declaration of Helsinki and was approved by the institutional review board (Leiden University Medical Center, Leiden, the Netherlands).

Participants

At start of the study, the inclusion criteria for T2DM patients were defined irrespective of ethnicity (self-identified and self-reported origin of both biological parents and their ancestors), however due to the scarcity of eligible patients of South Asian descent the inclusion criteria for this group were adjusted. Final inclusion criteria for the European and South Asian T2DM patients were, respectively: age 18-70 and 18-75 years, glycated hemoglobin (HbA1c) between ≥53.0 and <86.5 mmol/mol (≥7.0 and ≤10.0%) and ≥47.5 and <96.5 mmol/mol (≥6.5 and ≤11.0%), systolic and diastolic blood pressure between <150/85 mmHg and <180/110 mmHg, estimated glomerular filtration rate (eGFR) above >60 ml/min/1.73m^2 and >30 ml/min/1.73m^2, no history of heart failure (New York Heart Association class III-IV), no history of coronary artery disease for the European T2DM patients, and no acute coronary accident in the preceding 30 days for the South Asian T2DM patients (19,21).

Data collection

Potential participants were evaluated at a screening visit to verify eligibility for inclusion. Clinical examinations and MR scanning (including ^{1}H-MRS) were scheduled either in the morning after an overnight fast or evening (≥6 hours fasting) (for T2DM patients, the insulin dose was adjusted and study drug and other glucose-lowering medication were discontinued for maximum of 24 hours). At start and at the end of the study fasting blood samples were taken, and weight and blood pressure measurements were performed. Blood pressure was measured in seated position on the right arm after rest, using a validated automatic oscillometric device (SureSigns VS3 Vital signs monitor, Philips, Best, the Netherlands) and was the mean of two consecutive measurements. Due to logistical reasons, HbA1c was measured with boronate affinity high-performance liquid chromatography (Primus Ultra, Siemens HealthcareDiagnostics, Breda, the Netherlands) and with ion-exchange high-performance liquid chromatography (HPLC; Tosoh G8, Sysmex Nederland B.V., Etten-Leur, the Netherlands), therefore HbA1c measurements were corrected based on the correlation coefficient of a validation sample measured on both analyzers (18). Serum creatinine (SCr), triglyceride, total cholesterol, HDL-cholesterol, LDL-cholesterol (Friedewald formula) were measured on a Modular P800 analyzer (Roche Diagnostics, Mannheim, Germany), and urine samples for the measurement of urinary creatinine albumin ratio (UACR) were collected and analyzed on a Modular P800 analyzer (Roche Diagnostics, Mannheim, Germany) (18). Bioelectrical impedance analysis was used to estimate total body fat percentage (BIA; Bodystat 1500, Bodystart Ltd., Douglas, United Kingdom). Serum creatinine (mg/dl) was used to calculate the estimated GFR according to the Chronic Kidney Disease Epidemiology Collaboration (CKD-EPI) formula (22).

MRI protocol

All participants underwent baseline and follow-up MRI and ^{1}H-MRS using a clinical 3 Tesla Ingenia whole-body MR system (Philips Medical Systems, Best, the Netherlands). All images and proton spectra were blinded for study participant and occasion.

Renal single voxel spectroscopy was performed for the quantification of RTGC using a 40 x 10 x 10 mm voxel placed in the parenchyma of the left kidney (16), and baseline voxel position served as a guide for voxel placement at follow-up. Single voxel Point Resolved Spectroscopy (PRESS) unsuppressed spectra (echo time 40ms; unsuppressed repetition time 8s; averages 8) and suppressed spectra using Multiply Optimized Insensitive Suppression Train (MOIST) (echo time 40 ms; repetition time 3s; averages 64) were acquired. Spectra were acquired during free-breathing at end-expiration with pencil beam navigator-based respiratory triggering. Reconstructed spectra were fitted to a Gaussian line shape in the time domain using Java-based MR User Interface software (jMRUI version 5.0; Katholieke Universiteit Leuven, Leuven, Belgium) (23,24).

RTGC was calculated as a percentage of the (unsuppressed) water peak using the following formula: (renal signal amplitude of methylene + methyl) / (renal signal amplitude of water) × 100%. Since renal ^{1}H-MRS is a novel method for quantification of ectopic lipid and involves triglyceride concentrations that are substantially lower than in the liver resulting in a low signal-to-noise-ratio (SNR), the following spectral quality criteria were applied: (a) variation in lipid signal amplitudes between the signal averages were analyzed to exclude potential contamination of the RTGC signal with triglyceride signal originating from renal sinus fat or perirenal fat), (b) spectra were included if Cramér–Rao lower bound (CRLB) divided by the triglyceride amplitude of <20% (to discriminate well-fitted metabolites from more poorly fitted metabolites), (c) spectra were included if linewidth of triglyceride peaks were <100 Hz, (d) exclusion of spectra and residuals with artifacts or strongly asymmetric line shapes after eddy correction (25). Technical details and validation of renal ^{1}H-MRS have been described elsewhere in more detail (16,17). An example of voxel planning and resulting ^{1}H-MRS voxel is given in **Figure 1**. Hepatic triglyceride content was assessed via single voxel spectroscopy using the PRESS unsuppressed (echo time 35 ms; repetition time 9 s; averages 4) and MOIST-suppressed spectra (echo time 35 ms; repetition time 3.5s; 32 signal averages) (19, 26). Visceral fat was calculated based on three segmented transverse slices (mDIXON sequence, repetition time 3.5 ms; first echo time 1.19 ms; second echo time 2.3 ms; flip angle 10°; spatial resolution 1.6 x 1.7 mm; slice thickness 4 mm; slice gap 2 mm) at level L4-L5 (MASS software, LUMC, Leiden, the Netherlands) (19) .

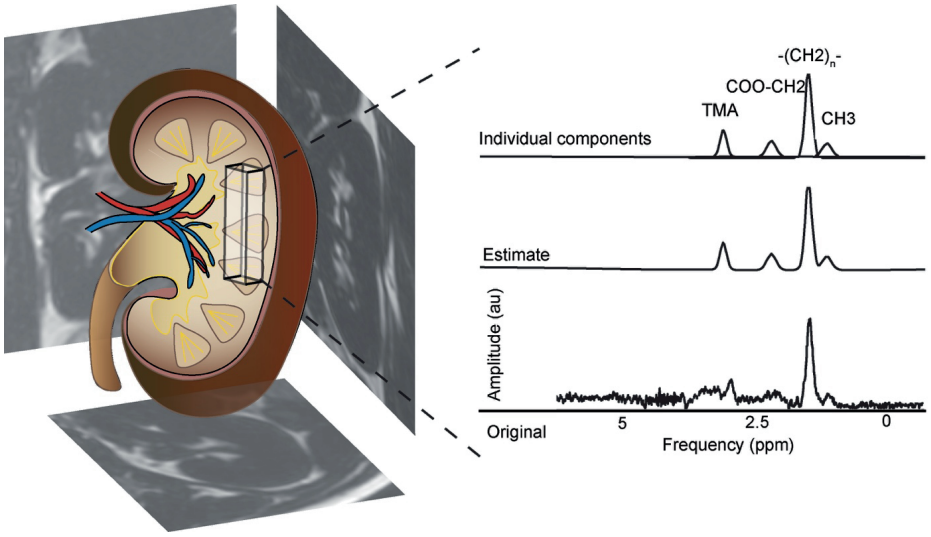

Figure 1. Planning of single voxel ^{1}H-MRS in the kidney (left), and corresponding spectra with methylene –(CH2)n– and methyl CH3 peak (right).

Statistical analysis

Data are shown as mean ± SD, or as median (25^{th}, 75^{th} percentile) when not normally distributed, and range. RTGC, UACR, SCr and eGFR were analyzed as renal outcomes. RTGC and UACR were log-transformed for normalization of their distributions. The difference (Δ) between log-transformed baseline from 26-weeks follow-up levels of RTGC and UACR respectively, are presented as 26-weeks ' to ' baseline ratio's. Correlations between RTGC and clinical determinants were assessed using Spearman correlation. Between-group differences at baseline and follow-up were analyzed using the independent samples t-test, and the paired-samples t-test was used for the within-group differences. Outcome measures were studied according to intention-to-treat analysis. Two-tailed significance levels of $P<0.05$ were considered to indicate a statistically significant difference.

RESULTS

Baseline characteristics

The parallel groups randomized to receive liraglutide or placebo consisted of 46 and 51 T2DM patients, of which 45 and 51 respectively underwent baseline MRI scanning. Due to limited scan time ^{1}H-MRS was not performed as part of the MRI scan protocol in 11 patients. Of these, 28 patients in the liraglutide group and 22 patients in the placebo group had ^{1}H-MRS spectra that met the quality criteria (excluded based on quality criteria n=35; poor fitting due to low SNR n=15, too broad linewidths n=10, likely contamination with triglyceride signal originating from extra-renal fat n=6, and artifacts n=4. In total 50 patients had baseline RTGC measurements available (mean age of 56.5 ± 9.1 years; range 33–73 years; 46% males). Baseline RTGC was not correlated with age (rs=0.08, P=0.58), BMI (rs=-0.10, P=0.47), total body fat percentage (rs=0.13, P=0.37), visceral fat (rs=0.07, P=0.63), liver fat (rs=-0.01, P=0.94), HbA1c (rs=-0.15, P=0.30), creatinine (rs=-0.14, P=0.32), eGFR (rs=-0.028, P=0.81), serum triglyceride (rs=-0.041, P=0.73) and UACR (rs=-0.10, P=0.50). Median RTGC in patients of Western European descent was 0.19% [25^{th}, 75^{th} percentile; 0.13, 0.31], and 0.21% [0.11, 0.38] in patients of South Asian descent.

At 26-weeks, 44 out of 50 patients underwent follow-up ^{1}H-MRS (25 patients in the liraglutide group and 19 patients in the placebo group). After exclusion of participants with ^{1}H-MRS that did not meet the quality criteria (n=27; poor fitting due to low SNR n=10, too broad linewidths n=8, likely contamination with triglyceride signal originating from extra-renal fat n=4, artifacts n=4, corrupted reference file n=1), nine patients of the liraglutide group and eight patients of the placebo group with both baseline and 26-weeks follow-up RTGC data were included for the intention-to-treat analysis. The trial profile is shown in **Figure 2**, and baseline characteristics in **Table 1**.

Table 1: Baseline characteristics of included patients with at least one RTGC measurement.

Demographics	**T2DM patients (n=50)**	
Treatment arm	**Liraglutide (n=22)**	**Placebo (n=28)**
Age (years)	55.6 (10.7)	57.2 (7.8)
Sex (male)	11 (50%)	12 (43%)
Ethnicity		
Western European	9 (41%)	15 (54%)
South Asian	13 (59%)	13 (46%)
Diabetes duration (years)	17.1 (10.0)	14.6 (9.9)
Diabetes complications		
Retinopathy	10 (46%)	7 (25%)
Nephropathy*	5 (24%)	7 (25%)
Neuropathy	10 (46%)	8 (29%)
Macrovascular†	5 (23%)	5 (18%)
Clinical parameters		
Body-mass index (kg/m^2)	31.1 (4.4)	31.3 (4.0)
Total body fat (%)	35.2 (9.3)	39.1 (9.3)
Hepatic triglyceride content (%)	11.9 (11.9)	17.5 (13.2)
Visceral fat (cm^2)	198.2 (61.6)	177.7 (64.0)
Systolic blood pressure (mmHg)	140.9 (21.1)	139.7 (16)
Diastolic blood pressure (mmHg)	83.2 (6.3)	85.1 (9.3)
HbA1c (mmol/mol)	67.0 (10.9)	67.1 (12.4)
HbA1c % (SD)	8.3 (1.0)	8.3 (1.1)
Triglycerides (mmol/L)	2.0 (1.6)	2.2 (1.3)
Total cholesterol (mmol/L)	4.3 (1.2)	4.8 (1.0)
HDL-c (mmol/L)	1.1 (0.3)	1.3 (0.4)
LDL-c (mmol/L) ‡	2.3 (1.0)	2.5 (1.0)
Smoking history		
Never smoked, n (%)	12 (55%)	18 (64%)
Current smoker, n (%)	4 (18%)	3 (11%)
Ex-smoker, n (%)	6 (27%)	7 (25%)
Concomitant drug use		
Metformin, (yes)	22 (100%)	27 (96%)
Metformin dose g/day	1.9 (0.6)	1.8 (0.4)
Sulfonylurea (yes)	4 (18%)	8 (29%)
Sulfonylurea dose mg/day	150 (107)	177 (338)
Insulin (yes)	15 (68%)	19 (68%)
Insulin (IU/day, average over last 2 weeks)	88 (58)	59 (30)
Statins (yes)	16 (73%)	20 (71%)
Anti-hypertensives (yes)	18 (82%)	21 (75%)
Angiontensin II recepter antagonists (yes)	7 (32%)	19 (32%)
ACE-inhibitors (yes)	9 (41%)	9 (32%)

Table 1: Baseline characteristics of included patients with at least one RTGC measurement. (continued)

Demographics	**T2DM patients (n=50)**	
Participants with baseline and follow-up ^{1}H-MRS		
Treatment artm	**Liraglutide (n=9)**	**Placebo (n=8)**
Baseline		
Log-transformed RTGC (%)	-0.67 (0.32)	-0.68 (0.30)
Log-transformed UACR (ug/umol)	14.2 (24.8)	2.1 (1.6)
SCr (umol/L)	69.6 (21.3)	64.8 (13.5)
eGFR (ml/min/1.72m²)	92.7 (23.1)	99.8 (10.6)
HbA1c (mmol/mol)	61.8 (9.4)	61.5 (7.8)
Week 26		
Log-transformed RTGC (%)	-0.97 (0.16)	-0.68 (0.40)
Log-transformed UACR (ug/umol)	16.7 (24.8)	4.1 (3.8)
SCr (umol/L)	66.9 (21.3)	64.3 (13.3)
eGFR (ml/min/1.72m²)	94.9 (23.9)	99.2 (13.5)
HbA1c (mmol/mol)	55.9 (10.4)	56.8 (9.0)

Data presented are n (%), and mean (SD). *nephropathy was defined as urinary albumin creatinine ratio ≥ 2.5 ug/umol in men and ≥ 3.5 ug/umol in women. †macrovascular complications were cerebrovascular or peripheral artery disease and not cardiovascular. ‡LDL-c was calculated using the Friedewald formula. ACE, angiotensin-converting-enzyme inhibitor; HbA1c, Glycated haemoglobin A1c; HDL-c, high-density lipoprotein-cholesterol; LDL-c, low-density lipoprotein-cholesterol; UACR, urinary-creatinine ratio; RTGC, renal triglyceride content;SCr, serum creatinine.

Results of 26 weeks of glycemic control on RTGC

An overview of renal outcomes and HbA1c at baseline and after 26 weeks of glycemic control irrespective of randomized treatment group is provided in **Table 2** and **Figure 3**. Seventeen patients had baseline and follow-up RTGC measurements available irrespective of treatment group allocation. Baseline HbA1c was 61.6 ± 8.4 mmol/mol, which changed to 56.3 ± 9.5 umol/L at follow-up (*P*=0.046). Median RTGC at baseline was 0.23% (0.13, 0.34), and 0.14% (0.10, 0.21) at follow-up. Log-transformed RTGC was significantly lower after 26-weeks of glycemic control compared to baseline (*P*=0.049). Baseline median UACR was 1.8 ug/umol (0.6, 4.1), and 1.8 ug/umol (0.7, 9.8) at follow-up. Log-transformed UACR at 26-weeks follow-up was not significantly different from baseline (*P*=0.77). Mean SCr was 67.3 ± 17.7 umol/L, which was 65.6 ± 17.5 umol/L at follow-up (*P*=0.26). Mean eGFR at baseline was 96.1 ± 18.4 ml/min/1.73m², and 96.9 ± 19.2 ml/min/1.73m² at follow-up (*P*=0.49).

Results of liraglutide versus standard glycemic control on RTGC

Nine T2DM patients randomized to liraglutide, and eight T2DM patients randomized to placebo, added to usual glycemic care had both baseline and follow-up ^{1}H-MRS data available that met the quality criteria. An overview of the outcomes at baseline and after

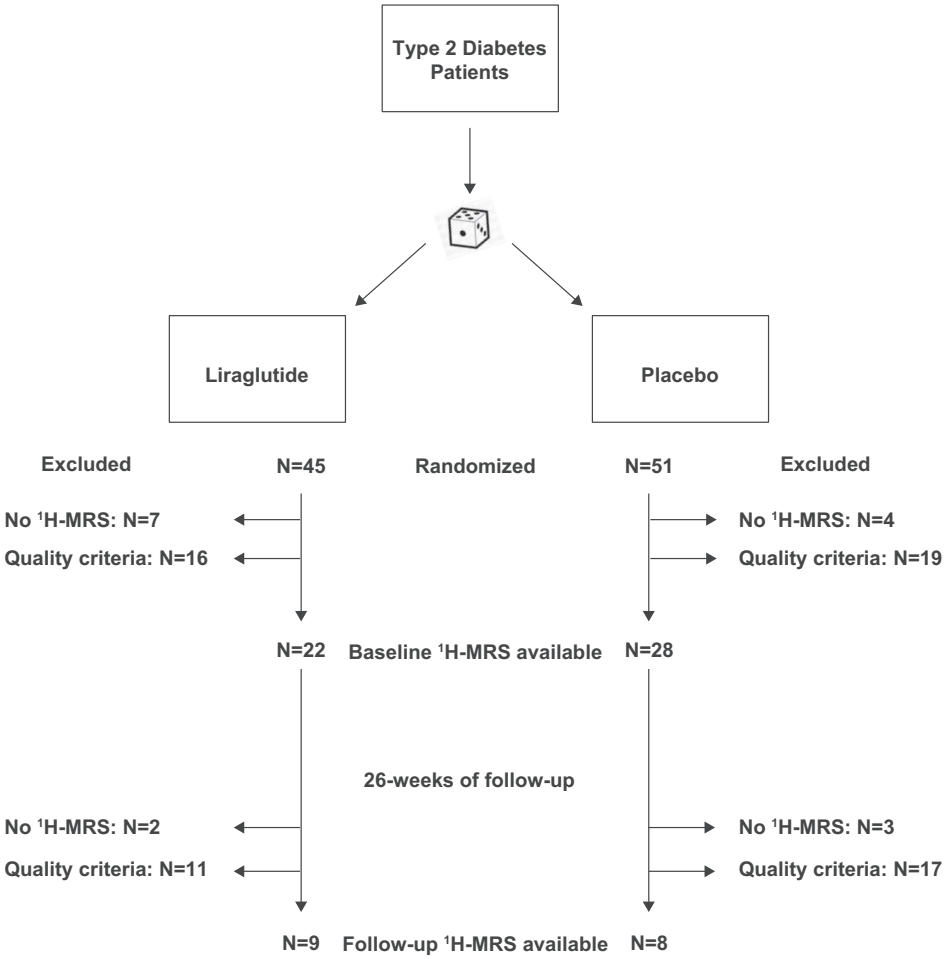

Figure 2. Flow chart. Patients were randomized to either liraglutide or placebo with stratification according to sex and insulin use.

Table 2. Outcomes at baseline and after 26-weeks of glycemic control irrespective of randomized treatment group

Outcome	Baseline, mean (SD) (n=17)	Week 26, mean (SD) (n=17)	*P*-value
Log-transformed RTGC (%)	-0.68 (0.30)	-0.83 (0.32)	0.049
Log-transformed UACR (ug/umol)	8.5 (18.7)	10.8 (26.0)	0.77
SCr (umol/L)	67.3 (17.7)	65.6 (17.5)	0.26
eGFR (ml/min/1.73m²)	96.1 (18.4)	96.9 (19.2)	0.49
HbA1c (mmol/mol)	61.6 (8.4)	56.3 (9.5)	0.046

Table includes outcome comparisons for study participants with RTGC values at both baseline and follow-up (n=17). HbA1c, Glycated haemoglobin A1c; SCr, serum creatinine; UACR, urinary-creatinine ratio; RTGC, renal triglyceride content.

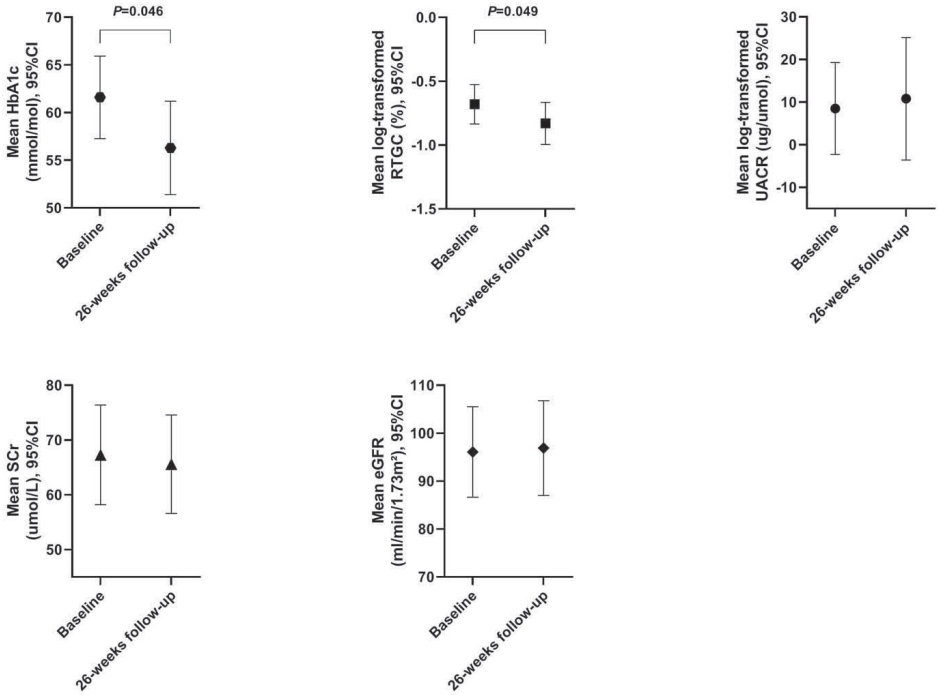

Figure 3. Treatment effect of glycemic control on Glycated haemoglobin A1c (HbA1c), renal triglyceride content (RTGC), urine-albumin-creatinine ratio (UACR), serum creatinine (SCr), and estimated glomerular filtration rate (eGFR) irrespective of randomized treatment group (n=17).

Table 3. Outcomes at baseline and after 26-weeks of liraglutide or placebo, added to usual glycemic care

Mean change in outcomes between baseline and follow up (95% CI)	Liraglutide (n=9)	Placebo (n=8)	*P*-value
26-weeks - to - baseline RTGC ratio†	-0.30 (-0.50, -0.09)	-0.003 (-0.34, 0.34)	0.04
26-weeks - to - baseline UACR ratio†	-0.38 (-0.67,-0.08)	0.22 (0.03, 0.40)	<0.01
Mean change SCr (umol/L)	-2.7 (-7.1, 6.1)	-0.5 (-8.0, 6.1)	0.46
Mean change eGFR (ml/min/1.72m²))	-2.3 (-6.5, -5.3)	-0.6 (-4.4, 5.6)	0.27
Mean change HbA1c (mmol/mol)	-5.9 (-17.8, 6.0)	-4.7 (-13.2, -2.3)	0.82

Table includes outcome comparisons for study participants with RTGC values at both baseline and follow-up (n=17). †26-weeks - to - baseline ratio derived from the difference between the log-transformed baseline and 26-weeks levels of RTGC and UACR respectively. eGFR, estimated glomerular filtration rate; SCr, serum creatinine; UACR, urinary-creatinine ratio; RTGC, renal triglyceride content.

26-weeks of liraglutide or placebo is provided in **Table 1, Table 3** and **Figure 4**. Baseline HbA1c in the liraglutide group was 61.8 ± 9.4 mmol/mol and 61.5 ± 7.8 mmol/mol. At follow-up this changed to 55.9 ± mmol/mol and 61.5 ± 7.8 mmol/mol for the liraglutide and placebo group respectively. No significant differences were found in HbA1c between the liraglutide group and placebo group (*P*=0.82). Median RTGC at baseline was 0.23% (0.11,

0.34), and 0.19% (0.13, 0.33) in the placebo group. At 26-weeks RTGC was 0.11% (0.08, 0.14) in the liraglutide group and 0.23% (0.16, 0.39) in the placebo group. 26-weeks- to - baseline RTGC ratio (95% CI) was significantly different between liraglutide (-0.30 [-0.50, -0.09]) and placebo added to standard care (-0.003 [-0.34, 0.34]) (*P*=0.04) (**Table 3, Fig. 4**). Median UACR in the liraglutide group at baseline was 1.8 [0.7, 6.6] ug/umol, and 2.0 [0.8, 3.3] ug/umol in the placebo group. At follow-up median UACR was 1.7 [0.3, 11.5] ug/umol in the liraglutide group, and 2.5 [1.3, 6.1] ug/umol in the placebo group. 26-weeks- to - baseline UACR ratio (95% CI) was significantly different between liraglutide (0.22 [0.0.3, 0.40]) and placebo added to standard care (-0.38 [-0.67, 0.08]) (*P*=0.04). Mean change in SCr and eGFR were not statistically different between the liraglutide and placebo group (SCr: *P*=0.46; eGFR: *P*=0.27).

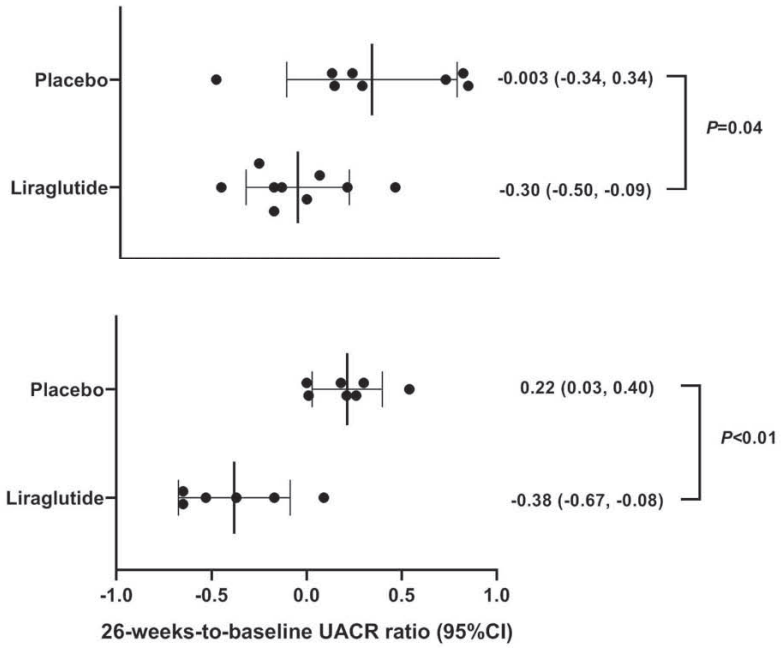

Figure 4. Treatment effect of liraglutide (n=9) versus placebo (n=8) on renal triglyceride content (RTGC) and urinary albumin-creatinine ratio (UACR).

DISCUSSION

The aim of this exploratory study was to assess whether glycemic control influences renal triglyceride content, including comparing the GLP-1RA liraglutide versus placebo, added to standard glucose-lowering therapy. In this study we found a significant reduction in RTGC after 26-weeks of glycemic control (irrespective of randomized treatment group).

From DKD literature, it is known that intensive glycemic control improves renal outcomes as evidenced by reduction of proteinuria progression and reduced risk of ESRD [3]. In our secondary analysis of the MAGNA VICTORIA studies we showed that RTGC reduced significantly more with liraglutide than placebo, while the HbA1c reduction was not different between these groups. Although this subgroup analysis should be considered cautiously with regard to the size and exploratory character of our study, our findings suggest that glycemic control, via GLP-1RA or standard glucose lowering therapy, might potentially beneficially influence renal steatosis. However, it should be noted that considering the lack of a control group (participants with no treatment at all) with baseline and follow-up measurements of RTGC, the phenomenon of 'regression to the mean' as a possible explanation for the found reduction in RTGC over time cannot be excluded. Taking this into account, and considering the small sample size of the current study as well as the limited prevalence/severity of DKD in our sample (since eGFR below 60 ml/min/1.73m^2 was an exclusion criterium), further research in larger clinical trials is warranted to better delineate the association between glycemic control and renal steatosis.

Based on the findings of the LEADER trial, glycemic control via liraglutide seems to have an additional independent effect on renal outcomes when added to usual glycemic care (11). We have previously shown in the MAGNA VICTORIA study that T2DM patients treated with liraglutide, compared to placebo, lost significantly more body weight, but liraglutide did not significantly change other ectopic fat depots such as visceral fat and hepatic triglyceride content (19,20). It remains area of further research whether GLP1-RA affects renal steatosis by direct effect of GLP1-RA on the kidney considering the existence of renal GLP1 receptors (12), or alternatively whether current findings stem from the composite effects of GLP1-RA on body weight and/or HbA1c.

There are several limitations that need to be considered. First, because of the exploratory nature of this study, and considering that this study is the first clinical trial using renal ^{1}H-MRS, we applied several quality criteria for the obtained renal spectra to assure the quality of the measurements. Because of these, we excluded a substantial amount of renal spectra from the analysis. Although renal outcomes were pre-specified in the MAGNA VICTORIA studies, these studies were powered for primary endpoints involving left ventricular diastolic and systolic function and not for RTGC. We have previously assessed the reproducibility of ^{1}H-MRS for the measurement of renal triglycerides in humans (16), and performed a porcine histologic validation and dietary intervention study, which showed that ^{1}H-MRS closely predicts triglyceride content as measured enzymatically in biopsies (17). However, considering the substantial number of obtained renal spectra that did not meet the quality criteria, renal ^{1}H-MRS remains a technically challenging technique, limiting the use of RTGC as a biomarker for the evaluation of treatment effects on renal lipid metabolism. Furthermore, although we have previously found much lower levels of RTGC in healthy volunteers (median RTGC of 0.12% [0.08,

0.22]) (16), additional studies are needed to determine reference values and to assess differences in RTGC between T2DM patients and healthy volunteers while taking age and sex into account. Another limitation is that we cannot exclude the potential influence of ethnicity on RTGC reduction, albeit baseline RTGC levels were comparable for T2DM patients of Western European and South Asian descent, as well as the proportion of T2DM patients of South Asian descent in the liraglutide and placebo arm. Future studies are needed to better understand how renal lipid metabolism and DKD are interrelated. Moreover, better understanding of the interplay of other ectopic fat compartments (e.g. renal sinus fat, hepatic fat and visceral fat) with renal lipid metabolism may contribute to the development of new therapeutic strategies.

In conclusion, in this exploratory study we found that twenty-six weeks of glycemic control resulted in lower RTGC, in particular for liraglutide, however larger clinical studies are needed to assess whether these changes reflect a true effect of glycemic control on renal steatosis.

Acknowledgements

We would like to thank P. de Heer and H.J. van Eyk for their help with data acquisition. We express our gratitude to all individuals who participated in the MAGNA VICTORIA. We are grateful to all participating general practitioners and nurses (M.A. Diez Canseco Quintana, C. Overman, I. Minken, H. Laurier, E. Pleij, M. de Winde, T.N. Bonten and L. van Duijn) and the physicians and nurses of the Haaglanden Medical Center (P.H.L.M. Geelhoed, A.H. Bootsma and A.V. Kharagjitsingh, The Hague, The Netherlands) for inviting eligible participants.

Funding

Novo Nordisk (Denmark) funded this investigator-initiated study. Novo Nordisk had no role in the design of the study, data collection, data analysis, data interpretation, or writing of the report. All authors had access to all the data and final responsibility for the decision to submit for publication. Dutch Kidney Foundation (innovation grant IP11.56).

REFERENCES

1. Anders H-J, Huber TB, Isermann B, Schiffer M. CKD in diabetes: diabetic kidney disease versus non-diabetic kidney disease. Nat Rev Nephrol 2018;14:361–77.
2. Holman RR, Paul SK, Bethel MA, Matthews DR, Neil HAW. 10-Year Follow-up of Intensive Glucose Control in Type 2 Diabetes. N Engl J Med 2008;359:1577–89.
3. Perkovic V, Heerspink HL, Chalmers J, Woodward M, Jun M, Li Q, et al. Intensive glucose control improves kidney outcomes in patients with type 2 diabetes. Kidney Int 2013;83:517–23.
4. Brenner BM, Cooper ME, de Zeeuw D, Keane WF, Mitch WE, Parving H-H, et al. Effects of Losartan on Renal and Cardiovascular Outcomes in Patients with Type 2 Diabetes and Nephropathy. N Engl J Med 2001;345:861–9.
5. Lewis EJ, Hunsicker LG, Clarke WR, Berl T, Pohl MA, Lewis JB, et al. Renoprotective Effect of the Angiotensin-Receptor Antagonist Irbesartan in Patients with Nephropathy Due to Type 2 Diabetes. N Engl J Med 2001;345:851–60.
6. Hoekstra T, Van Ittersum FJ, Hemmelder MH. RENINE Annual Report 2017. Nederlandse Federatie voor Nefrologie.
7. Porrini E, Ruggenenti P, Mogensen CE, Barlovic DP, Praga M, Cruzado JM, et al. Non-proteinuric pathways in loss of renal function in patients with type 2 diabetes. Lancet Diabetes Endocrinol 2015;3:382–91.
8. Shulman GI. Ectopic Fat in Insulin Resistance, Dyslipidemia, and Cardiometabolic Disease. N Engl J Med 2014;371:1131–41.
9. de Vries APJ, Ruggenenti P, Ruan XZ, Praga M, Cruzado JM, Bajema IM, et al. Fatty kidney: emerging role of ectopic lipid in obesity-related renal disease. Lancet Diabetes Endocrinol 2014;2:417–26.
10. Li L, Zhao Z, Xia J, Xin L, Chen Y, Yang S, et al. A Long-Term High-Fat/High-Sucrose Diet Promotes Kidney Lipid Deposition and Causes Apoptosis and Glomerular Hypertrophy in Bama Minipigs. PLoS One 2015 Nov 16;10(11):e0142884. 2015.
11. Mann JFE, Ørsted DD, Brown-Frandsen K, Marso SP, Poulter NR, Rasmussen S, et al. Liraglutide and Renal Outcomes in Type 2 Diabetes. N Engl J Med 2017;377:839–48.
12. Muskiet MHA, Tonneijck L, Smits MM, van Baar MJB, Kramer MHH, Hoorn EJ, et al. GLP-1 and the kidney: from physiology to pharmacology and outcomes in diabetes. Nat Rev Nephrol 2017;13:605–28.
13. Wang C, Li L, Liu S, Liao G, Li L, Chen Y, et al. GLP-1 receptor agonist ameliorates obesity-induced chronic kidney injury via restoring renal metabolism homeostasis. PLoS One 2018;13:e0193473.
14. Guo H, Wang B, Li H, Ling L, Niu J, Gu Y. Glucagon-like peptide-1 analog prevents obesity-related glomerulopathy by inhibiting excessive autophagy in podocytes. Am J Physiol Physiol 2018;314:F181–9.
15. Szczepaniak LS, Nurenberg P, Leonard D, Browning JD, Reingold JS, Grundy S, et al. Magnetic resonance spectroscopy to measure hepatic triglyceride content: prevalence of hepatic steatosis in the general population. Am J Physiol Metab 2005;288:E462–8.

16. Dekkers IA, de Heer P, Bizino MB, de Vries APJ, Lamb HJ. 1 H-MRS for the assessment of renal triglyceride content in humans at 3T: A primer and reproducibility study. J Magn Reson Imaging 2018;48:507–13.

17. Jonker JT, de Heer P, Engelse MA, van Rossenberg EH, Klessens CQF, Baelde HJ, et al. Metabolic imaging of fatty kidney in diabesity: validation and dietary intervention. Nephrol Dial Transplant 2018;33:224–30.

18. Bizino MB, Jazet IM, Westenberg JJM, van Eyk HJ, Paiman EHM, Smit JWA, et al. Effect of liraglutide on cardiac function in patients with type 2 diabetes mellitus: randomized placebo-controlled trial. Cardiovasc Diabetol 2019;18:55.

19. van Eyk HJ, M Paiman EH, Bizino MB, de Heer P, Geelhoed-Duijvestijn PH, Kharagjitsingh A V, et al. A double-blind, placebo-controlled, randomised trial to assess the effect of liraglutide on ectopic fat accumulation in South Asian type 2 diabetes patients. Cardiovasc Diabetol 2019;18:87.

20. Bizino MB, Jazet IM, de Heer P, van Eyk HJ, Dekkers IA, Rensen PCN, et al. Placebo-controlled randomised trial with liraglutide on magnetic resonance endpoints in individuals with type 2 diabetes: a pre-specified secondary study on ectopic fat accumulation. Diabetologia 2019.

21. Paiman EHM, van Eyk HJ, Bizino MB, Dekkers IA, de Heer P, Smit JWA, et al. Phenotyping diabetic cardiomyopathy in Europeans and South Asians. Cardiovasc Diabetol 2019;18:133.

22. Levey AS, Stevens LA, Schmid CH, Zhang Y, Castro AF, Feldman HI, et al. A new equation to estimate glomerular filtration rate. Ann Intern Med 2009;150:604–12.

23. Naressi A, Couturier C, Devos JM, Janssen M, Mangeat C, Beer R de, et al. Java-based graphical user interface for the MRUI quantitation package. MAGMA 2001;12:141–52.

24. Stefan D, Cesare F Di, Andrasescu A, Popa E, Lazariev A, Vescovo E, et al. Quantitation of magnetic resonance spectroscopy signals: The jMRUI software package. Meas Sci Technol 2009;20.

25. Kreis R. Issues of spectral quality in clinical 1 H-magnetic resonance spectroscopy and a gallery of artifacts. NMR Biomed NMR Biomed 2004;17:361–81.

26. Van Eyk HJ, Blauw LL, Bizino MB, et al. Hepatic triglyceride content does not affect circulating CETP: lessons from a liraglutide intervention trial and a population-based cohort. Sci Rep. 2019;9(1)9996.

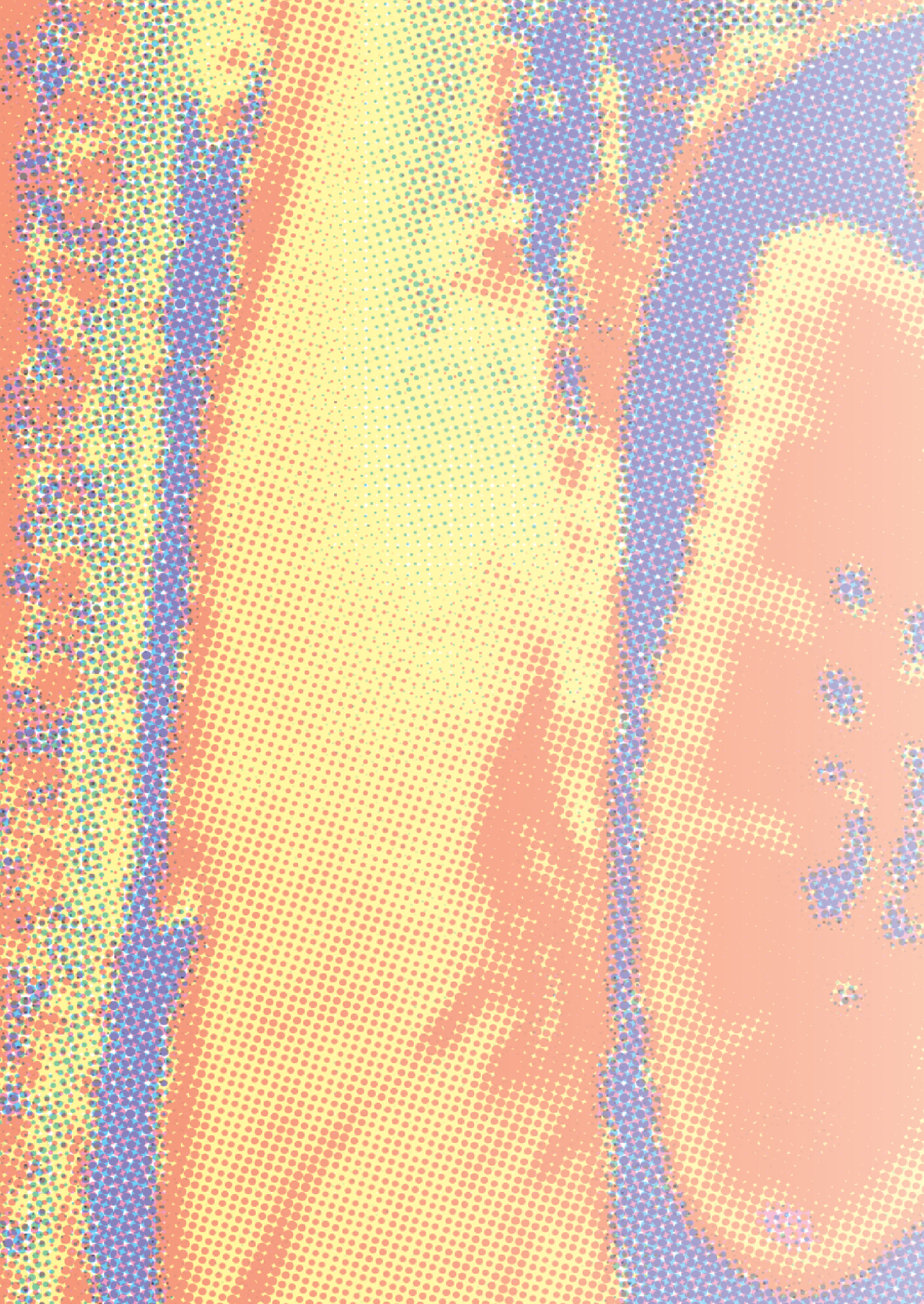

PART 2

Population-based imaging studies

7

Associations between Normal Range Albuminuria, Renal Function and Cardiovascular Function in a Population-Based Imaging Study

Dekkers IA, de Mutsert R, Jukema W, Rabelink TJ, de Roos A, Rosendaal FR, Lamb HJ, de Vries APJ.

Atherosclerosis. 2018 May;272:94-100.

ABSTRACT

Background and aims

In patients with impaired renal function and macroalbuminuria cardiovascular risk factors are highly prevalent, however whether this is also present in the general population is unclear. We investigated whether normal-range albuminuria and renal function are associated with cardiovascular function in the general population.

Methods

In this cross-sectional analysis of the NEO study, urinary albumin-creatinine ratio (UACR), estimated glomerular filtration rate (eGFR), and intima-media thickness was assessed in all participants (n=6,503), a random subset underwent MRI for pulse wave velocity (n=2,451) and/or cardiac imaging (n=1,138).

Results

Multiple linear regression analysis was performed while adjusting for sex, age, smoking, mean arterial blood pressure, total body fat, and fasting glucose. After adjustment, albuminuria and renal function were positively associated with LV mass index (UACR, 0.941g/m² [95% CI 0.21,1.67] *P*=0.012; eGFR, 0.748 g/m² [95% CI 0.15,1.35] *P*=0.015), and LV cardiac index (UACR, 0.056 L/min/m² [95% CI 0.00,0.11] *p*=0.038; eGFR, 0.080 L/min/m² [95% CI 0.03,0.13] *P*=0.001). Albuminuria showed a weak association with arterial thickness (UACR, 0.003 mm [95% CI 0.00,0.01] *P*=0.015) and arterial stiffness (UACR, 0.073 m/s [95% CI 0.01,0.13] *P*=0.036), but not with renal function. No associations were observed for LV ejection fraction and LV diastolic function.

Conclusion

Normal-range albuminuria was positively associated with LV mass index, LV cardiac index, arterial thickness and arterial stiffness. Our findings support the hypothesis that even within normal range, albuminuria is a marker of cardiovascular health.

INTRODUCTION

Chronic kidney disease (CKD), characterized by renal insufficiency and macroalbuminuria, is associated with a substantial risk of cardiovascular morbidity and mortality (1,2). The exact mechanism underlying the observed excess of cardiovascular disease in chronic kidney disease is unknown, and increasing evidence suggests that this relationship goes beyond indirect associations by hypertension (3,4). Macroalbuminuria is commonly used as a marker of kidney disease progression. Also microalbuminuria (5) and higher levels of albuminuria within 'normal range' are associated with a higher risk of cardiovascular events (6,7). In non-diabetic patients, microalbuminuria is considered to reflect endothelial damage via degradation of the endothelial glycocalyx (8). This endothelial glycocalyx degradation could be the biological pathway that explains the continuous relationship between urinary albumin excretion and cardiovascular risk. In this case, cardiac remodeling in advanced renal disease could be preceded by subclinical cardiovascular changes as a consequence of microalbuminuria. However, to what extent normal range albuminuria is related to cardiovascular function in the general population remains unclear. Better understanding of the relationship between albuminuria and cardiac remodeling, requires knowledge of associations in the general population. However, the majority of population-based studies thus far have focused on either the presence of hypertension (9,10). Moreover, these studies lacked functional data, such as LV systolic/diastolic function and arterial stiffness. The aim of this study is to investigate the association between normal range albuminuria, renal function, and cardiovascular imaging parameters in the general population. We hypothesize that also albuminuria within normal range is a marker of cardiovascular function in the middle-aged general population. By improving insight into cardiac remodeling mechanisms in the population at large, preventative strategies might eventually become feasible to reduce cardiovascular risk in CKD patients.

MATERIAL AND METHODS

Study population and study design

The Netherlands Epidemiology of Obesity (NEO) study is a population-based, prospective cohort study designed to investigate pathways that lead to obesity-related diseases (11). Men and women living in the greater area of Leiden (the Netherlands) were invited to participate in the study if they were aged between 45 and 65 years and had a self-reported body mass index (BMI) of ≥27 kg/m^2. In addition, all inhabitants from one municipality (Leiderdorp) were invited to participate irrespective of their BMI, allowing for a reference distribution of BMI. Participants with potential contraindications for MRI (i.e. metallic devices, or claustrophobia) were excluded for additional imaging. Of all MRI eligible

participants approximately 30% were randomly selected to undergo arterial stiffness measurement, and a second random subset of approximately 50% had additional cardiovascular magnetic resonance imaging as well. All procedures followed in this study were in accordance with the ethical standards of the responsible committee on human experimentation (institutional and national) and with the Helsinki Declaration of 1975, as revised in 2000 (12). The Medical Ethical Committee of the Leiden University Medical Center (LUMC) approved the design of the study and all participants gave their written informed consent.

Data collection

Participants were invited to a baseline visit at the NEO study center of the LUMC after an overnight fasting period. Prior to this study visit, participants collected their urine over 24 h and completed a general questionnaire at home to report demographic, lifestyle and clinical information. The participants were asked to bring all medication they were using to the study visit. At the baseline visit all participants underwent physical examination including anthropometry and blood pressure measurement. Height was measured with a vertically fixed, calibrated tape measure. Body weight and percent body fat were measured by the Tanita bio impedance balance (TBF-310, Tanita International Division, UK) without shoes and one kilogram was subtracted to correct for the weight of clothing. BMI was calculated by dividing the weight in kilograms by the height in meters squared. Brachial blood pressure was measured in a seated position on the right arm using a validated automatic oscillometric device (OMRON, Model M10-IT, Omron Health Care Inc, IL, USA). Blood pressure was measured three times with 5 min rest between consecutive measurements. The mean systolic, diastolic and mean arterial (|(2 x diastolic blood pressure) + systolic blood pressure] / 3) blood pressure was calculated.

Laboratory measurements

Fasting blood samples were drawn from the antecubital vein after 5 min rest of the participant, and were used to determine serum concentrations of glucose, insulin, triglycerides, creatinine, total cholesterol HDL, and LDL. Serum creatinine (mg/dl) was used to calculate the estimated GFR according to the Chronic Kidney Disease Epidemiology Collaboration (CKD-EPI) formula (13). For the measurement of albuminuria, the urinary albumin creatinine ratio (UACR) was derived from a first morning void. Normal range albuminuria was defined as UACR of <3 mg/mmol (<30 mg/g), microalbuminuria (moderately increased albuminuria) as UACR of 3-30 mg/mmol (30-300 mg/g), and macroalbuminuria (severely increased albuminuria) as UACR >30 mg/mmol (>300 mg/g) (14). All laboratory analyses were performed in the central clinical chemistry laboratory of the LUMC (11).

Carotid intima-media thickness

Carotid intima-media thickness (cIMT) was assessed by ultrasonography of the far wall of the left and right common carotid arteries along a 15 mm section 10 mm proximal of the bifurcation, using a 7.5–10 MHz linear-array transducer in B-mode setting (Art. Lab version 2.1, Esaote, Maastricht, The Netherlands).

Pulse wave velocity and cardiovascular imaging using MRI

Magnetic resonance imaging was performed on a 1.5 Tesla whole-body MR scanner (Philips Medical Systems, Best, the Netherlands). Through-plane flow measurements of the ascending, proximal descending, mid-descending, and distal descending aorta were acquired using multislice, one-directional in-plane velocity-encoded MRI with velocity sensitivity of 150 cm/s. Aortic PWV was calculated by dividing the aortic path length between the measurement sites (Δx) by the transit time between the arrival of the systolic wave front at these sites (Δt), and it is expressed in meters per second (15).

The entire heart was imaged in short-axis orientation using electrocardiographically gated breath-hold balanced steady-state free precession (repetition time 3.4 ms, echo time 1.7 ms; flip angle 35°; slice thickness 10 mm; slice gap 0 mm; field of view 400 x 400 mm; matrix size 256 x 256). LV mass determined by the sum of myocardial area times slice thickness multiplied by the myocardial gravity (1.05 g/mL), and LV mass index was calculated by dividing LV mass by body surface area (BSA). LV hypertrophy was defined as LV mass index >84.1 g/m² for men and >76.4 g/m² for women. LV cardiac output was calculated by multiplying stroke volume by heart rate, and LV cardiac index by dividing LV cardiac output by body surface area (BSA). LV ejection fraction by dividing stroke volume by the end-diastolic volume multiplied by 100%. An electrocardiographically gated gradient-echo sequence with velocity encoding was used to measure blood flow across the mitral valve (repetition time 6.5 ms, echo time 1 ms; flip angle 20°; section thickness 8 mm, field of view 350 x 350 mm; matrix size 256 x 256 mm; velocity encoding gradient 150 cm/s). Subsequent wave form analysis of mitral inflow pattern was performed, resulting in the quantification of early (E) and atrial (A) peak filling velocity, E/A ratio, and the E deceleration peak (16). Image post processing was performed with in-house developed software (MASS and FLOW, Medis, Leiden, the Netherlands) with consensus between two experienced radiologists. Imaging analysis of the cIMT, PWV and cardiac MRI group are visualized in **Figure 1 b**.

Statistical analysis

In the NEO study individuals with a BMI of 27 kg/m^2 or higher were oversampled. First, inhabitants of Leiden and its surroundings between 45 and 65 years of age and with a self-reported BMI of 27 kg/m² or higher were invited to participate in the NEO study. In addition, we included a reference population. To that extent, all inhabitants between 45

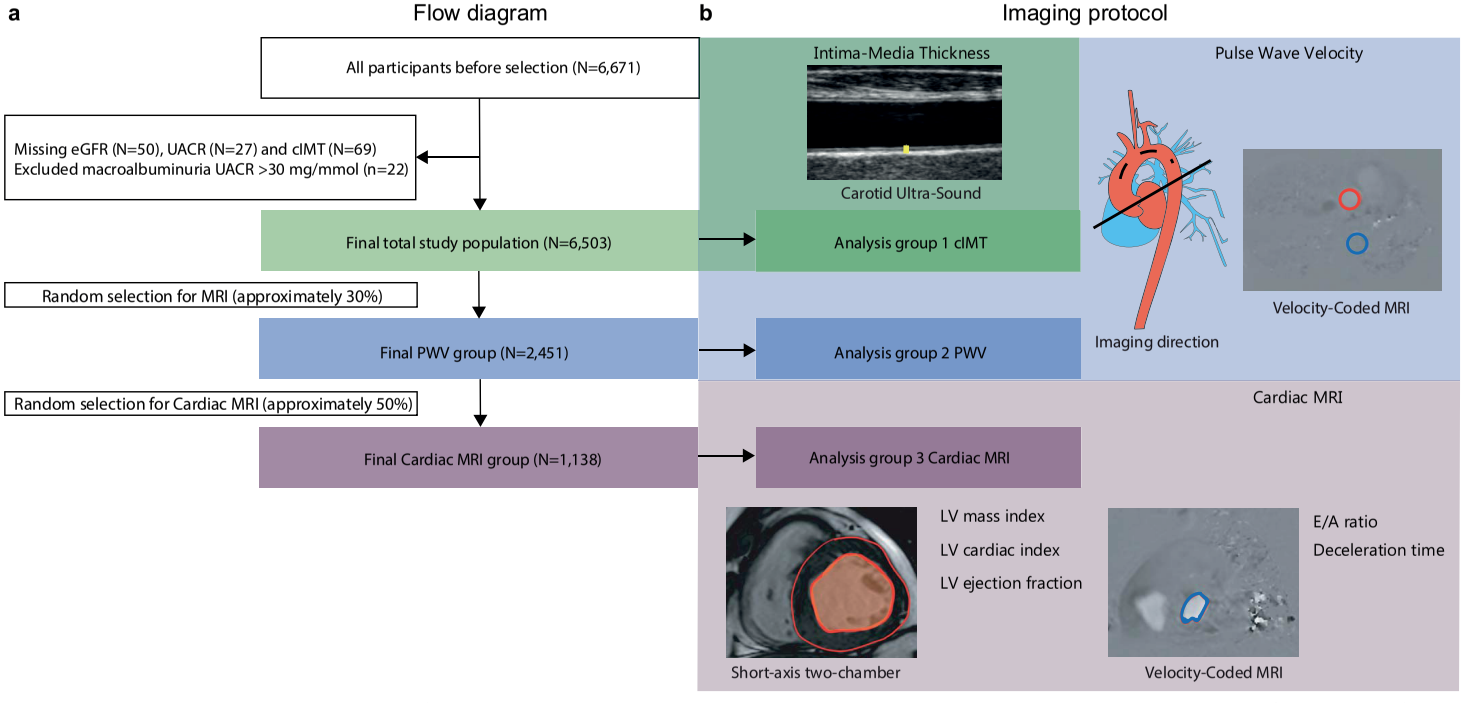

Figure. 1. Flow diagram and imaging protocol for the total population, and PWV and Cardiac MRI analysis subgroups. (**a**) Shows the study flow diagram for the final carotid Intima-Media Thickness (total population), pulse wave velocity subgroup (PWV), and Cardiac MRI subgroup. (**b**) Overview of the imaging protocol per analysis group; for the cIMT group this consisted of carotid ultrasound for the measurement of the intima-media thickness (yellow bar in the B-mode ultrasound image of the common carotid artery), for the PWV group this consisted of velocity-encoded MRI of the ascending aorta (red contour) and descending aorta (blue contour) with an imaging direction similar to the anatomical drawing of the aorta, for the cardiac MRI group this consisted of a short-axis two-chamber images of heart for the assessment of LV mass index (LV myocardial area contours in red) and volumetric derived LV systolic function (LV volume shaded in red), and velocity-encoded MRI of the mitral valve for the assessment of LV diastolic function (mitral valve contour in blue).

and 65 years living in one municipality, Leiderdorp, were asked to participate irrespective of their BMI. This resulted in an additional sample of 1,671 participants with a BMI distribution that was similar to the BMI distribution of the general Dutch population (17). If inference is made on the general population, the overrepresentation of overweight and obese participants in the NEO study may introduce bias, because of the skewed BMI distribution in the NEO population. Weighting towards the BMI distribution of the general population may solve this problem (18). Using the BMI distribution of the reference population, we calculated weight factors for the NEO population, resulting in a higher weight factor for participants with a lower BMI (19). Use of sampling weights yield results which apply to a population-based study without oversampling of individuals with a high BMI (20). UACR was log-2 transformed to account for the skewed distribution of the data, and because after log-2 transformation the regression coefficient (β) can be interpreted as a two-fold increase in UACR. Multiple linear regression was performed with UACR or eGFR as the exposure and cardiovascular imaging parameters as the outcome. Regression coefficients with corresponding 95% confidence intervals (CI) were calculated and reflect the change in cardiovascular outcome variable per two-fold increase in UACR or per 10 ml/min/1.73m² change in eGFR. Analyses were adjusted for sex, age, smoking, blood pressure, total body fat, and fasting glucose. Sensitivity analyses were performed by excluding participants with hypertension (blood pressure ≥140/90mmHg or on antihypertensive treatment) or highest quintile of eGFR, indicating supra-normal renal function (hyperfiltration). Analyses were performed using STATA (Statacorp, College Station, Texas, USA, version 12.0) and results are presented according to the STROBE guidelines (21).

RESULTS

Baseline characteristics

The total NEO study population consisted of 6,671 participants. After consecutive exclusion of participants with missing data on carotid ultrasound (n=69), urinary albumin creatinine ratio (n=27), eGFR (n=50), or with macroalbuminuria (UACR >30mg/mmol) (n=22), the final cIMT group consisted of 6,503 participants. Of these participants, a random subset (approximately 30%) underwent PWV measurement, resulting in the final PWV group of 2,451 participants. Of the participants who underwent PWV measurement, a second random subset of approximately 50% was selected for additional cardiac MRI, resulting in a final cardiac MRI group of 1,308 participants (**Fig. 1 a**). Mean (SD) age was 55.7 (6.0) years, median UACR was 0.45 mg/mmol (25th, 75th percentile; 0.30, 0.70), and mean eGFR was 86.3 (12.3) ml/min/1.73 m² in the total group. Microalbuminuria (UACR 3-30 mg/mmol or 30 mg/g) was present in 2.0% of the total group, and 0.2% of the participants had a moderately impaired renal function (eGFR <60 ml/min/1.73m²). Self-reported

history of CVD (defined as myocardial infarction, angina, congestive heart failure, stroke and peripheral vascular disease) was present in 6% of the total group. Participant characteristics of the total group are provided in **Table 1**. Participant characteristics of the PWV and cardiac MRI group were not different from the total group and excluded participants were not different from the included population (data not shown). An overview of the cardiovascular imaging parameters is presented in **Table 2**.

Table 1. Characteristics of the total study population (n =6,503)

Characteristic	Total population
Age (years)	55.7 (6.0)
Sex (% men)	44
Ethnicity (% whites)	95
Medical history	
Cardiovascular disease (% yes)*	6
Hypertension (BP ≥140/90 mmHg) (%)	34
Diabetes (Fasting glucose >8.0 mmol/L) (%)	3
Hypertriglyceridemia (Fasting triglyceride ≥2.3 mmol/L) (%)	8
Anthropometrics	
Total body fat (%) in men	30.0 (6.1)
Total body fat (%) in women	36.9 (6.5)
Body mass index (kg/m²)	26.3 (4.4)
Normal weight (%)	42
Overweight (%)	42
Obese (%)	16
Smoking	
Never (%)	39
Former (%)	46
Current (%)	16
Blood pressure	
Systolic blood pressure (mmHg)	130.2 (17.0)
Diastolic blood pressure (mmHg)	83.2 (10.3)
Mean arterial pressure (mmHg)	98.9 (11.9)
Use of medication	
Antihypertensives (%)	23
Glucose lowering medication (%)	3
Lipid lowering medication (%)	11
Statins (%)	11
Beta blockers (%)	11
Calcium channel blockers (%)	3
ACE inhibitors (%)	14

Table 1. Characteristics of the total study population (n =6,503) (continued)

Characteristic	Total population
Diuretics (%)	8
Fasting serum measurements	
Glucose (mmol/L)	5.5 (1.0)
Insulin (mU/L)	9.7 (8.1)
Triglyceride (mmol/L)	1.2 (0.8)
HDL cholesterol (mmol/L)	1.6 (0.5)
LDL cholesterol (mmol/L)	3.5 (1.0)
Total cholesterol (mmol/L)	5.7 (1.1)
Renal parameters	
Creatinine (umol/L)	76.4 (14.0)
estimated glomerular filtration rate (ml/min/1.73 m²)	86.3 (12.3)
Urinary albumin excretion (mg/L)	3.62 (2.99, 4.79)
Urinary albumin-creatinine ratio (mg/mmol)	0.44 (0.30, 0.70)

Results were weighted toward the BMI distribution of the general population. Data are shown as percentage, mean (SD) or median (25^{th}, 75^{th} percentile). Normal Weight BMI<25 kg/m², Overweight BMI 25-30 kg/m², and Obese BMI>30kg/m². ACE; angiotensin-converting-enzyme, BP; blood pressure, HDL; High-density-lipoprotein, LDL; Low-density-lipoprotein. Cardiovascular disease*; myocardial infarction, angina, congestive heart failure, stroke, and peripheral vascular disease.

Table 2. Mean (SD) of different cardiovascular imaging parameters measured

Outcome parameter	n	Mean (SD)
Arterial thickness	6,503	
carotid Intima-Media Thickness (mm)		0.6 (0.1)
Arterial stiffness	2,451	
Pulse Wave Velocity total (m/s)		6.6 (1.3)
Cardiovascular magnetic resonance	1,138	
Dimensions		
LV mass (g)		99.8 (26.1)
LV mass index ; LV mass/BSA (g/m²)		51.1 (10.2)
Systolic function		
LV Ejection Fraction (%)		63.7 (5.9)
LV Cardiac Output (L/min)		6.2 (1.4)
LV Cardiac Index; LVCO/BSA (L/min/m²)		3.2 (0.6)
Diastolic function		
E/A ratio		1.3 (0.5)
E deceleration peak ($ml/s^2 * 10^{-3}$)		-3.5 (1.1)

Results were weighted toward the BMI distribution of the general population. Data are shown as mean (SD). BSA; body surface area, E/A ratio; ratio of early peak filling rate and atrial peak filling rate, LV, left ventricular; LVCO, left ventricular cardiac output, UACR; urinary albumin creatinine ratio. LV hypertrophy; LV mass index > 84.1 g/m² for men and >76.4 g/m² for women.

Table 3. Differences (with 95% confidence intervals) in cardiovascular imaging parameters per two-fold increase in UACR

Imaging parameter	Log2-UACR (mg/mmol)			
	n	β	95% CI	*P*
carotid Intima-Media Thickness (mm)	6,503			
Crude		0.006	0.00, 0.01	<0.001
Adjusted		0.003	0.00, 0.01	0.036
Pulse Wave Velocity (m/s)	2,541			
Crude		0.246	0.18, 0.31	<0.001
Adjusted		0.073	0.01, 0.13	0.015
Cardiovascular magnetic resonance	1,138			
LV mass index (g/m²)				
Crude		-0.126	-0.93, 0.68	0.760
Adjusted		0.941	0.21, 1.67	0.012
LV Ejection Fraction (%)				
Crude		0.350	-0.04, 0.74	0.082
Adjusted		0.074	-0.36, 0.51	0.741
LV Cardiac Index (L/min/m²)				
Crude		0.020	-0.03, 0.07	0.445
Adjusted		0.056	0.00, 0.11	0.038
E/A ratio				
Crude		-0.057	-0.10, -0.01	0.008
Adjusted		-0.031	-0.06, -0.00	0.055
E deceleration peak ($ml/s^{2*}10^{-3}$)				
Crude		0.175	0.10, 0.25	<0.001
Adjusted		0.038	-0.03, 0.11	0.286

Results were weighted toward the BMI distribution of the general population. Crude and adjusted analysis (sex, age, smoking, mean arterial blood pressure, total body fat and fasting glucose) with linear regression coefficients and 95% confidence intervals are shown. Regression coefficients reflect the change in cardiovascular outcome variable with a 2-fold increase in UACR. E/A ratio, ratio of early peak filling rate and atrial peak filling rate; UACR, urinary albumin creatinine ratio.

Associations between albuminuria and cardiovascular imaging parameters

The crude and adjusted regression coefficients between UACR (per two-fold change) and cardiovascular parameters are shown in **Table 3**. In unadjusted analysis, albuminuria was associated with an increase of 0.006 mm (95% CI 0.00, 0.01) in arterial thickness (cIMT), which after adjustment changed to 0.003 mm (95% CI -0.00, 0.01). In crude analysis, per to two-fold increase in UACR arterial stiffness (PWV) was associated with an increase of 0.246 m/s (95% CI 0.18, 0.31), which diminished after adjustment. UACR was not associated with LV mass index in crude analysis (β -0.126 [95% CI -0.93, 0.68]), however UACR did relate to LV mass index after adjustment for sex, and this association attenuated after further adjustment for remaining confounding variables (β 0.941 [95% CI 0.21, 1.67]). This means that per two-fold

Table 4. Differences (with 95% confidence intervals) in cardiovascular imaging parameters associated per 10 ml/min/1.73m² higher eGFR

Imaging parameters	eGFR (10 ml/min/1.73m²)			
	n	β	95% CI	*P*
carotid Intima Media Thickness (mm)	6,503			
Crude		-0.004	-0.01, -0.00	0.002
Adjusted		0.002	-0.00, 0.00	0.137
Pulse Wave Velocity (m/s)	2,541			
Crude		-0.149	-0.21, -0.09	<0.001
Adjusted		-0.005	-0.06, 0.05	0.856
Cardiovascular magnetic resonance	1,138			
LV mass index (g/m²)				
Crude		0.969	0.26, 1.67	0.007
Adjusted		0.748	0.15, 1.35	0.015
LV ejection fraction (%)				
Crude		-0.374	-0.79, 0.04	0.075
Adjusted		-0.294	-0.72, 0.13	0.177
LV cardiac index (L/min/m²)				
Crude		0.078	0.03, 0.13	0.001
Adjusted		0.080	0.03, 0.13	0.001
E/A ratio				
Crude		0.07	0.03, 0.11	0.001
Adjusted		0.01	-0.02, 0.05	0.449
E deceleration peak ($ml/s^{2}*10^{-3}$)				
Crude		-0.133	-0.20, -0.06	<0.001
Adjusted		-0.040	-0.11, 0.03	0.257

Results were weighted toward the BMI distribution of the general population. Crude and adjusted analysis (sex, age, smoking, mean arterial blood pressure, total body fat and fasting glucose) with linear regression coefficients and 95% confidence intervals are shown. Regression coefficients reflect the change in cardiovascular outcome variable per 10ml/min/1.73m² increase in eGFR. E/A ratio, ratio of early peak filling rate and atrial peak filling rate; eGFR, estimated Glomerular Filtration Rate according to CKD-EPI.

increase in UACR, LV mass index is associated with an increase of 0.941 g/m^2. UACR was not related to LV ejection fraction in both unadjusted and adjusted analysis. UACR was not related to LV cardiac index in the unadjusted analysis, but after adjustment UACR did relate to LV cardiac index (β 0.056 L/min/m² [95% CI 0.00, 0.11]). In unadjusted analyses UACR was minimally associated with E deceleration peak (β 0.175 [95% CI 0.10, 0.25]), which diminished in adjusted analyses. Results from sensitivity analyses evaluating the associations between albuminuria and LV mass index without participants with hypertension (blood pressure ≥140/90 mmHg or on antihypertensive treatment) are presented in **Supplemental Table 1**.

Associations between renal function and cardiovascular imaging parameters

Unadjusted and adjusted regression coefficients between renal function (per 10 ml/min/1.73m^2 higher eGFR) and cardiovascular parameters are shown in **Table 4**. In crude analysis, renal function was associated with a decrease of -0.004 mm (95% CI -0.01, -0.00) in arterial thickness (cIMT) and with a decrease of -0.149 m/s (95% CI -0.21, -0.09) for arterial stiffness (PWV). These associations diminished after adjusting for confounding variables. In crude analysis, renal function was associated with LV mass index (β 0.969 [95% CI 0.26, 1.67]) and after adjustment for confounding variables per 10 ml/min/1.73m^2 higher eGFR LV mass index increased with 0.748 g/m² (95% CI 0.15, 1.35). Renal function was not associated with LV ejection fraction in both crude (β -0.374 [95% CI -0.79, 0.04]) and adjusted analysis (β -0.294 [95% CI -0.72, 0.13]). In crude analysis renal function was associated with LV cardiac index (β 0.08 [95% CI 0.03, 0.13]), which remained the same in adjusted analysis. In crude analysis, higher renal function was associated with an increase in E/A ratio (β 0.07 [95% CI 0.03, 0.11]) and negatively associated with E deceleration peak (β -0.133 [95% CI -0.20, -0.06]). These associations diminished after adjusting for confounding variables. Results from sensitivity analyses in the cardiac MRI group evaluating the associations between renal function and LV mass index after exclusion of participants with hypertension (blood pressure ≥140/90 mmHg or on antihypertensive treatment), and after exclusion of individuals in the highest quintile of eGFR (eGFR ≥97.1 ml/min/1.73m²) are presented in **Supplemental Table 1** and **Supplemental Table 2**.

DISCUSSION

In this large cross-sectional study of the middle-aged general population, we found that normal range albuminuria and renal function were positively associated with LV mass index and LV cardiac index. Weak positive associations were found between normal range albuminuria, arterial thickness, and arterial stiffness, and no associations were observed for LV ejection fraction and diastolic function.

We found that normal range albuminuria was independently associated with LV mass index even after adjustment of various confounders, such as mean arterial blood pressure and serum glucose. Also, subsequent sensitivity analyses excluding all participants with hypertension and/or using antihypertensives did not materially change our findings (**Supplemental Table 1**). Previous cardiovascular magnetic resonance based studies evaluating the relationship between normo- to microalbuminuria and LV mass in non-CKD populations were performed solely in hypertensive individuals (9,10), limiting conclusions on whether found associations were independent of blood pressure. Our findings are supported by the improved cardiac function and decrease in LV mass index after renal transplantation (22,23). Also, elevated circulating levels of endothelial glycocalyx

degrading enzymes, such as syndecan-1 and thrombomodulin, have shown to normalize after kidney transplantation, indicating improved systemic endothelial function (24).

The observed weak positive association between eGFR and LV mass index in our study is contra-intuitive compared to the inverse relationship in the CKD population (25). Previous population-based studies that evaluated renal function measured by cystatin C, rather than eGFR, also found a positive relationship with a concentric LV hypertrophy phenotype (3,4,26). However, this may be confounded by the association of cystatin C as the endogenous cathepsin inhibitor with a role in adipose tissue or cardiac remodeling (27). We thus hypothesized this finding to be an effect of the cross-sectional design including relatively early renal hyperfiltrating in obese subjects (28). However, exclusion of individuals within the highest eGFR quintile did not change the observed associations, and can thus not be clearly attributed to glomerular hyperfiltration (**Supplemental Table 2**). Other explanations are the presence of an U-shaped association or overestimation of renal function given that the CKD-EPI formula is not validated for an eGFR >90 ml/min/1.73m² (29).

In our study normal range albuminuria and renal function showed a moderately positive association with LV cardiac index, but not with LV ejection fraction. LV cardiac index is corrected for body surface area and heart rate in contrast to LV ejection fraction, which does not take this into account and has a relatively larger variance compared to LV cardiac index, making it less sensitive measure of LV systolic function. In the present study no associations were demonstrated between normal range albuminuria, renal function and LV diastolic function. These observations suggest that the association between normal range albuminuria and LV systolic function is a more linked to physiological endothelial function than LV diastolic function.

Vascular lipoprotein deposition and atherosclerosis have also been linked to loss of endothelial glycocalyx, which might explain the accelerated vascular aging in CKD ultimately leading to systemic arteriosclerosis (30, 31). Moreover, increased arterial stiffness reflecting impaired elastic vessel properties has been observed in the early stages of CKD, suggesting that arterial remodeling occurs early in the disease process (32). Older studies using tonometry observed associations between microalbuminuria, renal function, and arterial stiffness (33, 34). In the present study we elaborated on these findings by observed weak associations between normal-range albuminuria, arterial thickness, and arterial stiffness in the general population.

Strengths of our study are the extensive cardiovascular imaging protocol, and the large sample size based on a random subset of the general population without contra-indications for MRI. Moreover, previous studies have mainly used echocardiography rather than cardiovascular magnetic resonance, which is considered the gold standard for the assessment of LV mass, volume, and function (35). Also arterial stiffness assessed by MRI is considered a superior technique regarding accuracy and precision compared

to conventional tonometry (36, 37). Inaccurate measurement of the pressure wave path length by tonometry can lead to substantial measurement error in PWV of up to 30% (38,39). The use of MRI-based PWV measurements enabled us to detect weak associations between normal-range albuminuria and arterial stiffness in a relatively healthy sample of the general population. The quantitative nature of cardiovascular magnetic resonance makes this technique very suitable for the detection of early changes in cardiovascular morphology and functioning in large population based analyses.

There are several limitations that need to be considered. The observational cross-sectional nature of our study precludes causal inference. We thus cannot exclude that observed associations result from residual confounding or reverse causation (e.g. decreased renal perfusion and/or arterial remodeling due to lower cardiac output). Prospective analyses with repeated measurements over time are needed to determine the direction of the observed associations between normal range albuminuria, renal function and cardiovascular health. Furthermore, it should be recognized that residual confounding by hypertension cannot be eliminated since blood pressures levels were based on office measurements rather than 24-hours ambulatory or home blood pressure monitoring. Although the present study is based on a study population with oversampling of obesity, we adjusted for this by weighting all participants towards the BMI distribution of participants from the Leiderdorp municipality whose BMI distribution was similar to that of the general Dutch population. The results of the present study therefore apply to a population-based study without oversampling of individuals with a high BMI. Another important limitation is the use of estimated GFR, although the CKD-EPI formula has proven to be more accurate and precise than the MDRD formula, it has not been validated above 90 ml/min/1.73m² and might underestimate hyperfiltration in obesity (29). Gold standard exogenous clearance measurements are seldom used in epidemiological research due to invasiveness, time and high-cost, and Cystatin C derived equations lack an international standardized calibrator.

In conclusion, normal-range albuminuria was positively associated with LV mass index, LV cardiac index, arterial thickness and arterial stiffness in the middle-aged general population. Our findings support the hypothesis that normal range albuminuria is a marker of cardiovascular health, even before adverse changes in the setting of advanced kidney disease or cardiovascular disease occur.

Acknowledgements

We express our gratitude to all individuals who participate in the Netherlands Epidemiology of Obesity (NEO) study. We are grateful to all participating general practitioners for inviting eligible participants. We furthermore thank all research nurses for collecting the data, I. de Jonge, MSc, Leiden University Medical Center, for all data management of the NEO study, R.C.A. Rippe, PhD, Leiden University, for statistical input and guidance, and

R.L. Widya, MD PhD, J. Amersfoort, MSc, E. Ghariq, MD, M.F. Rodrigues, MD, and R.P.B. Tonino, all Leiden University Medical Center, for their help in MR data collection.

REFERENCES

1. Weiner DE, Tighiouart H, Stark PC, Amin MG, MacLeod B, Griffith JL, et al. Kidney disease as a risk factor for recurrent cardiovascular disease and mortality. Am J Kidney Dis. 2004;44(2):198-206.
2. Go AS, Chertow GM, Fan D, McCulloch CE, Hsu CY. Chronic kidney disease and the risks of death, cardiovascular events, and hospitalization. N Engl J Med. 2004;351(13):1296-305.
3. Ix JH, Shlipak MG, Chertow GM, Ali S, Schiller NB, Whooley MA. Cystatin C, left ventricular hypertrophy, and diastolic dysfunction: data from the Heart and Soul Study. J Card Fail. 2006;12(8):601-7.
4. Agarwal S, Thohan V, Shlipak MG, Lima J, Bluemke DA, Siscovick D, et al. Association between Cystatin C and MRI Measures of Left Ventricular Structure and Function: Multi-Ethnic Study of Atherosclerosis. Int J Nephrol. 2011;2011:15(3)868.
5. Hillege HL, Fidler V, Diercks GF, van Gilst WH, de Zeeuw D, van Veldhuisen DJ, et al. Urinary albumin excretion predicts cardiovascular and noncardiovascular mortality in general population. Circulation. 2002;106(14):1777-82.
6. Arnlov J, Evans JC, Meigs JB, Wang TJ, Fox CS, Levy D, et al. Low-grade albuminuria and incidence of cardiovascular disease events in nonhypertensive and nondiabetic individuals: the Framingham Heart Study. Circulation. 2005;112(7):969-75.
7. Ruggenenti P, Remuzzi G. Time to abandon microalbuminuria? Kidney international. 2006;70(7):1214-22.
8. Rabelink TJ, de Zeeuw D. The glycocalyx--linking albuminuria with renal and cardiovascular disease. Nat Rev Nephrol. 2015;11(11):667-76.
9. de Beus E, Meijs MF, Bots ML, Visseren FL, Blankestijn PJ. Presence of albuminuria predicts LV mass in patients with chronic systemic arterial hypertension. Eur J Clin Invest. 2015.
10. Tsioufis C, Stefanadis C, Toutouza M, Kallikazaros I, Toutouzas K, Tousoulis D, et al. Microalbuminuria is associated with unfavourable cardiac geometric adaptations in essential hypertensive subjects. J Hum Hypertens. 2002;16(4):249-54.
11. de Mutsert R, den Heijer M, Rabelink TJ, Smit JW, Romijn JA, Jukema JW, et al. The Netherlands Epidemiology of Obesity (NEO) study: study design and data collection. Eur J Epidemiol. 2013;28(6):513-23.
12. Adopted by the 18th WMA General Assembly H, Finland, June 1964; amended by the 29th WMA General Assembly, Tokyo, Japan, October 1975; 35th WMA General Assembly, Venice, Italy, October 1983; 41st WMA General Assembly, Hong Kong, September 1989; 48th WMA General Assembly, Somerset West, Republic of South Africa, October 1996, and the 52nd WMA General Assembly, Edinburgh, Scotland, October 2000. World Medical Association Declaration of Helsinki: Ethical Principles for Medical Research Involving Human Subjects. Bulletin of the World Health Organization. 2000;79(4):373-4.
13. Levey AS, Bosch JP, Lewis JB, Greene T, Rogers N, Roth D. A more accurate method to estimate glomerular filtration rate from serum creatinine: a new prediction equation. Modification of Diet in Renal Disease Study Group. Ann Intern Med. 1999;130(6):461-70.

14. KDIGO. 2012 clinical practice guideline for the evaluation and management of chronic kidney disease. Kidney Int Suppl. 2013;3(1):1-150.

15. Widya RL, de Mutsert R, Westenberg JJM, Gast KB, den Heijer M, le Cessie S, et al. Is Hepatic Triglyceride Content Associated with Aortic Pulse Wave Velocity and Carotid Intima-Media Thickness? The Netherlands Epidemiology of Obesity Study. Radiology. 2017;285(1):73-82.

16. Widya RL, de Mutsert R, den Heijer M, le Cessie S, Rosendaal FR, Jukema JW, et al. Association between Hepatic Triglyceride Content and Left Ventricular Diastolic Function in a Population-based Cohort: The Netherlands Epidemiology of Obesity Study. Radiology. 2016;279(2):443-50.

17. Ministry of Health WaS. Hoeveel mensen hebben overgewicht? [How many people are overweight?]. 2013.

18. Korn EL, Graubard BI. Epidemiologic studies utilizing surveys: accounting for the sampling design. Am J Public Health. 1991;81(9):1166-73.

19. Dekkers IA, de Mutsert R, de Vries AP, Rosendaal FR, Cannegieter SC, Jukema JW, et al. Determinants of Impaired Renal and Vascular Function are associated with higher Levels of Procoagulant Factors in the General Population. Journal of Thrombosis and Haemostasis. 2017.

20. Lumley T. Analysis of complex survey samples [Web page]. http://www.jstatsoft.org/v09/i08/paper. [

21. von Elm E, Altman DG, Egger M, Pocock SJ, Gotzsche PC, Vandenbroucke JP. The Strengthening the Reporting of Observational Studies in Epidemiology (STROBE) statement: guidelines for reporting observational studies. PLoS medicine. 2007;4(10):e296.

22. Kensinger C, Hernandez A, Bian A, Fairchild M, Chen G, Lipworth L, et al. Longitudinal assessment of cardiac morphology and function following kidney transplantation. Clin Transplant. 2017;31(1).

23. Wali RK, Wang GS, Gottlieb SS, Bellumkonda L, Hansalia R, Ramos E, et al. Effect of kidney transplantation on left ventricular systolic dysfunction and congestive heart failure in patients with end-stage renal disease. J Am Coll Cardiol. 2005;45(7):1051-60.

24. Dane MJ, Khairoun M, Lee DH, van den Berg BM, Eskens BJ, Boels MG, et al. Association of kidney function with changes in the endothelial surface layer. Clin J Am Soc Nephrol. 2014;9(4):698-704.

25. Afshinnia F, Spitalewitz S, Chou SY, Gunsburg DZ, Chadow HL. Left ventricular geometry and renal function in hypertensive patients with diastolic heart failure. Am J Kidney Dis. 2007;49(2):227-36.

26. Patel PC, Ayers CR, Murphy SA, Peshock R, Khera A, de Lemos JA, et al. Association of cystatin C with left ventricular structure and function: the Dallas Heart Study. Circ Heart Fail. 2009;2(2):98-104.

27. de Vries AP, Rabelink TJ. A possible role of cystatin C in adipose tissue homeostasis may impact kidney function estimation in metabolic syndrome. Nephrol Dial Transplant. 2013;28(7):1628-30.

28. D'Agati VD, Chagnac A, de Vries AP, Levi M, Porrini E, Herman-Edelstein M, et al. Obesity-related glomerulopathy: clinical and pathologic characteristics and pathogenesis. Nat Rev Nephrol. 2016;12(8):453-71.

29. Levey AS, Stevens LA, Schmid CH, Zhang YL, Castro AF, 3rd, Feldman HI, et al. A new equation to estimate glomerular filtration rate. Ann Intern Med. 2009;150(9):604-12.

30. van den Berg BM, Spaan JA, Rolf TM, Vink H. Atherogenic region and diet diminish glycocalyx dimension and increase intima-to-media ratios at murine carotid artery bifurcation. Am J Physiol Heart Circ Physiol. 2006;290(2):H915-20.

31. van den Berg BM, Spaan JA, Vink H. Impaired glycocalyx barrier properties contribute to enhanced intimal low-density lipoprotein accumulation at the carotid artery bifurcation in mice. Pflugers Archiv : European journal of physiology. 2009;457(6):1199-206.

32. Amann K. Media calcification and intima calcification are distinct entities in chronic kidney disease. Clin J Am Soc Nephrol. 2008;3(6):1599-605.

33. Sonoda H, Takase H, Dohi Y, Kimura G. Factors associated with brachial-ankle pulse wave velocity in the general population. J Hum Hypertens. 2012;26(12):701-5.

34. Kim BJ, Lee HA, Kim NH, Kim MW, Kim BS, Kang JH. The association of albuminuria, arterial stiffness, and blood pressure status in nondiabetic, nonhypertensive individuals. J Hypertens. 2011;29(11):2091-8.

35. Attili AK, Schuster A, Nagel E, Reiber JH, van der Geest RJ. Quantification in cardiac MRI: advances in image acquisition and processing. Int J Cardiovasc Imaging. 2010;26 Suppl 1:27-40.

36. Westenberg JJ, van Poelgeest EP, Steendijk P, Grotenhuis HB, Jukema J, de Roos A. Bramwell-Hill modeling for local aortic pulse wave velocity estimation: a validation study with velocity-encoded cardiovascular magnetic resonance and invasive pressure assessment. J Cardiovasc Magn Reson. 2012;14(1):2.

37. Suever JD, Oshinski J, Rojas-Campos E, Huneycutt D, Cardarelli F, Stillman AE, et al. Reproducibility of pulse wave velocity measurements with phase contrast magnetic resonance and applanation tonometry. Int J Cardiovasc Imaging. 2012;28(5):1141-6.

38. Wentland AL, Grist TM, Wieben O. Review of MRI-based measurements of pulse wave velocity: a biomarker of arterial stiffness. Cardiovasc Diagn Ther. 2014;4(2):193-206.

39. Salvi P, Magnani E, Valbusa F, Agnoletti D, Alecu C, Joly L, et al. Comparative study of methodologies for pulse wave velocity estimation. J Hum Hypertens. 2008;22(10):669-77.

Supplemental Table 1. Sensitivity analysis: relationship between UACR, eGFR and LV mass index after exclusion of participants with hypertension (BP>140/90 mmHg) or using antihypertensives (n=491)

LV mass index (g/m²)	Log2-UACR (mg/mmol)			eGFR (10 ml/min/1.73m²)		
	β	95% CI	*P*	β	95% CI	*P*
Crude	-0.685	-2.11, 0.74	0.346	0.880	-0.24, 2.00	0.124
Model 1	1.043	-0.23, 2.32	0.108	0.862	-0.07, 1.80	0.070
Model 2	1.048	-0.22, 2.32	0.106	0.866	-0.70, 1.80	0.070
Model 3	0.987	-0.30, 2.28	0.134	0.747	-0.15, 1.64	0.102
Model 4	0.827	-0.50, 2.15	0.220	0.681	-0.22, 1.58	0.137
Model 5	0.859	-0.53, 2.24	0.224	0.689	-0.20, 1.58	0.130

Results were weighted toward the BMI distribution of the general population.
Crude and adjusted analysis with linear regression coefficients and 95% confidence intervals are shown:
Model 1: adjusted for age and sex,
Model 2: Model 1 + mean arterial blood pressure,
Model 3: Model 2 + smoking
Model 4: Model 3+ Total body fat,
Model 5: Model 4 + fasting glucose.
Regression coefficients reflect the change in cardiovascular outcome variable with a 2-fold increase in UACR. eGFR, estimated Glomerular Filtration Rate according to CKD-EPI; MAP, mean arterial pressure; LV, left ventricular; UACR, urinary albumin creatinine ratio.

Supplemental Table 2. Sensitivity analysis cardiac MRI group: relationship between eGFR and LV mass index after exclusion of highest quintile of eGFR (≥97.1 ml/min/1.73m²) (n=893)

LV mass index (g/m²)	eGFR (10 ml/min/1.73m²)		
	β	95% CI	*P*
Crude	1.771	0.70, 2.84	0.001
Model 1	1.127	0.23, 2.02	0.014
Model 2	0.976	0.07, 1.88	0.034
Model 3	0.890	-0.01, 1.79	0.052
Model 4	0.852	-0.03, 1.73	0.059
Model 5	0.857	-0.03, 1.74	0.057

Results were weighted toward the BMI distribution of the general population. Crude and adjusted analysis with linear regression coefficients and 95% confidence intervals are shown:
Model 1: adjusted for age and sex,
Model 2: Model 1 + mean arterial blood pressure,
Model 3: Model 2 + smoking
Model 4: Model 3+ Total body fat,
Model 5: Model 4 + fasting glucose.
Regression coefficients reflect the change in cardiovascular outcome variable per 10 ml/min/1.73m² change in eGFR. eGFR, estimated Glomerular Filtration Rate according to CKD-EPI; LV, left ventricular.

8

Determinants of Impaired Renal and Vascular Function are associated with higher Levels of Procoagulant Factors in the General Population

Dekkers IA, de Mutsert R, de Vries APJ, Rosendaal FR, Cannegieter SC, Rabelink TJ, Lamb HJ, Lijfering WM.

J Thromb Haemost. 2018 Mar;16(3):519-528

ABSTRACT

Background

Impaired renal and vascular function have been associated with venous thrombosis, but the mechanism is unclear.

Objectives

We investigated whether estimated glomerular filtration rate (eGFR), urinary albumin-creatinine ratio (UACR), and pulse wave velocity (PWV) are associated with a procoagulant state.

Methods

In this cross-sectional analysis of the NEO Study, eGFR, UACR, fibrinogen, and coagulation factors (F)VIII, FIX, and FXI were determined in all participants (n=6,536), and PWV was assessed in a random subset (n=2,433). eGFR, UACR and PWV were analysed continuously and per percentile; per 6 categories for eGFR (>50th[reference] to <1st) and UACR (<50th[reference], to >99th), and per 4 categories (<50th[reference] to >95th percentile) for PWV. Linear regression was used and adjusted for age, sex, total body fat, smoking, education, ethnicity, total cholesterol, CRP, and vitamin K antagonists use (FIX).

Results

Mean age was 55.6 years, mean eGFR 86.0 ± 12 ml/1.73m² and median UACR 0.4 mg/mmol (25th,75th percentile 0.3;0.7). All coagulation factors showed a procoagulant shift with lower renal function and albuminuria. For example, FVIII was 22 IU/dL (95% CI 13, 32) higher in the eGFR <1st percentile compared with >50th percentile, and FVIII was 12 IU/dL (95% CI 3, 22) higher in the UACR >99th percentile compared with <50th percentile. PWV was positively associated with coagulation factors FIX and FXI in continuous analysis, per m/s difference in PWV, FIX was 2.0 IU/dL (95% CI 0.70, 3.2) higher.

Conclusions

Impaired renal and vascular function was associated with higher levels of coagulation factors, underlining the role of renal function and vascular function in the development of venous thrombosis.

INTRODUCTION

Venous thrombosis plays a major role in the morbidity and mortality of patients with advanced renal disease (1). Previous studies have shown that impaired renal function and the presence of microalbuminuria in patients with Chronic Kidney Disease (CKD) are associated with an increased risk of venous thrombosis (2, 3). To illustrate, individuals with an estimated glomerular filtration rate (eGFR) <60 ml/min/1.73m² have a 2-3-fold increased risk of venous thrombosis compared with individuals with normal renal function (4, 5). Moreover, impaired renal function is associated with higher levels of coagulation factors including fibrinogen, factors (F)VII, FVIII, FIX, FXI, and von Willebrand factor (6). This supports the hypothesis that the increased risk of venous thrombosis in CKD could be induced by elevated coagulation factors levels due to generalized endothelial damage (6).

Previous studies have focused on either the increased risk of venous thrombosis, or the presence of CKD in relation to coagulation factors (5). However, it remains unclear whether impaired vascular function is associated with higher levels of coagulation factors in the general population. Moreover, the few studies thus far evaluating associations between renal function, albuminuria and coagulation did not account for inflammation as a potential confounder (7, 8). Atherosclerosis measured by intima-media thickness has been suggested as a possible risk factor of VTE (9), and atherosclerosis has been associated with a procoagulant state (10). Arterial stiffness assessed by pulse wave velocity (PWV) is a functional and more robust marker for early atherosclerosis than intima-media thickness (11, 12), and has been linked with endothelial shear stress (13). Moreover, recent insights showed that arterial stiffness is regulated by hemodynamic and mechanosensitive properties of endothelial cells reflecting systemic vascular function (14, 15). Thus far, the association between vascular function (i.e. endothelial dysfunction, and arterial stiffness) and haemostasis in the general population remains elusive.

We hypothesize that impaired renal function and impaired vascular function is associated with hypercoagulability, evidenced by a procoagulant shift in coagulation factors which could ultimately lead to venous thrombosis, (**Fig. 1**).

MATERIAL AND METHODS

Study population and study design

The Netherlands Epidemiology of Obesity (NEO) study is a population-based, prospective cohort study in 6,671 individuals aged 45–65 years (16). Recruitment of participants started in September 2008 and was completed at the end of September 2012. Men and women living in the greater area of Leiden (in the West of the Netherlands) were invited by letters sent by GPs and municipalities and by local advertisements. They were invited

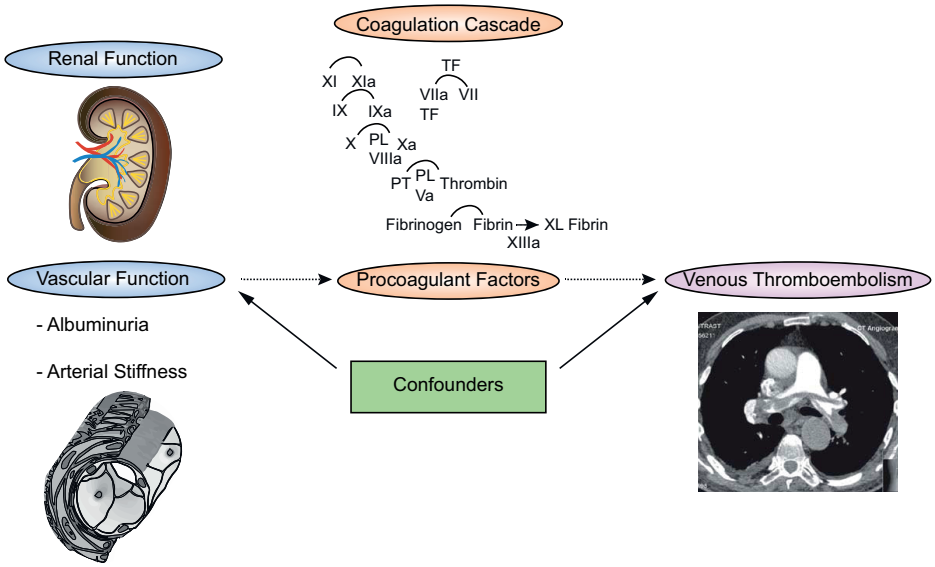

Figure 1. Hypothesis pathway of presumed effects of renal and vascular function (albuminuria and arterial stiffness) on prothrombotic coagulation factors and the subsequent development of venous thromboembolic events.

to respond if they were aged between 45 and 65 years and had a self-reported body mass index (BMI) of 27 kg/m^2 or higher. In addition, all inhabitants aged between 45 and 65 years from one municipality (Leiderdorp) were invited to participate irrespective of their BMI, allowing for a reference distribution of BMI. Exclusion criteria were missing data on eGFR, urinary albumin excretion, fibrinogen or FVIII, FIX, or FXI. All participants were screened for potential contraindications for MR imaging (metallic devices, claustrophobia or a body circumference of ≥1.70 m) at the NEO study center, and approximately 30% of the of the participants eligible for MR imaging were randomly selected to undergo MRI imaging. Participants with missing PWV measurements due to technical failures, were excluded for further analysis. The Medical Ethical Committee of the Leiden University Medical Center (LUMC) approved the design of the study and all participants gave their written informed consent.

Data collection

Participants were invited to a baseline visit at the NEO study center of the LUMC after an overnight fast. Prior to this study visit, participants collected their urine over 24 h and completed a general questionnaire at home to report demographic, lifestyle and clinical information. The participants were asked to bring all medication they were using to the study visit. At the baseline visit all participants underwent physical examination including anthropometry and blood pressure. Height was measured using a calibrated tape

measure and body weight and percentage of total body fat (TBF) were measured using the Tanita bio impedance balance (TBF-310, Tanita International Division, UK). Weight in kilograms was divided by height is meters squared to calculate BMI. Fasting blood samples were drawn from the antecubital vein after 5 min rest of the participant. Subsequently, fasting glucose, triglyceride, low- and high-density lipoprotein concentrations, C-reactive protein (CRP), serum creatinine, were measured with standard methods in the central clinical chemistry laboratory of the LUMC (16). Serum creatinine (mg/dl) was used to calculate estimated Glomerular Filtration Rate (eGFR) using the Chronic Kidney Disease Epidemiology Collaboration (CKD-EPI) formula (17). Blood samples for coagulation factor measurements were drawn into tubes containing 0.106M trisodium citrate (Sarstedt, Nümbrecht, Germany). Plasma was obtained by centrifugation at 2500g for 10 min at room temperature and stored in aliquots at -80°C until testing. Fibrinogen activity was measured according to the method of Clauss. Activity of FVIII, FIX, and FXI were measured with a mechanical clot detection method on an ACL TOP 700 analyzer (Werfen, Barcelona, Spain). All assays were performed by laboratory technicians who were unaware of the status of the samples. Urinary albumin was measured in early morning single urine void using an immunoturbidimetric assay and creatinine using a Jaffe kinetic compensated method between September 1st, 2008 until November 30th, 2010 and an enzymatic assay (IDMS calibrated against SRM 967) since December 1st, 2010 until the end of the inclusion period. Because urinary creatinine concentrations are not affected by pseudochromogens they are exchangeable using either a Jaffe or an enzymatic method. Normal renal function was defined as eGFR>90 ml/min/1.73m², mildly to moderately reduced renal function as eGFR 45-90 ml/min/1.73m², and moderately to severely reduced renal function as eGFR <45 ml/min/1.73m² (18). Normal range albuminuria was defined as UACR <3 mg/mmol (30-300 mg/g), microalbuminuria (also referred to as moderately increased albuminuria) as UACR of 3-30 mg/mmol (30-300 mg/g), and albuminuria (also referred to as macroalbuminuria or severely increased albuminuria) as UACR >30 mg/mmol (18).

Assessment of arterial stiffness

For the assessment of arterial stiffness, pulse wave velocity (PWV) was determined on a 1.5 Tesla (T) whole-body magnetic resonance imaging (MRI) scanner (Gyroscan ACS/NT15, Philips, Best, The Netherlands) using multislice, two one-directional in-plane velocity-encoded MRI. PWV was calculated by the ratio of the distance along the aortic center line (Δx) and the transit-time of the propagating systolic pulse wave between two measurement sites (Δt) (proximal aorta and distal aorta summed) (19). An overview of the assessment of PWV is given in **Figure 2**.

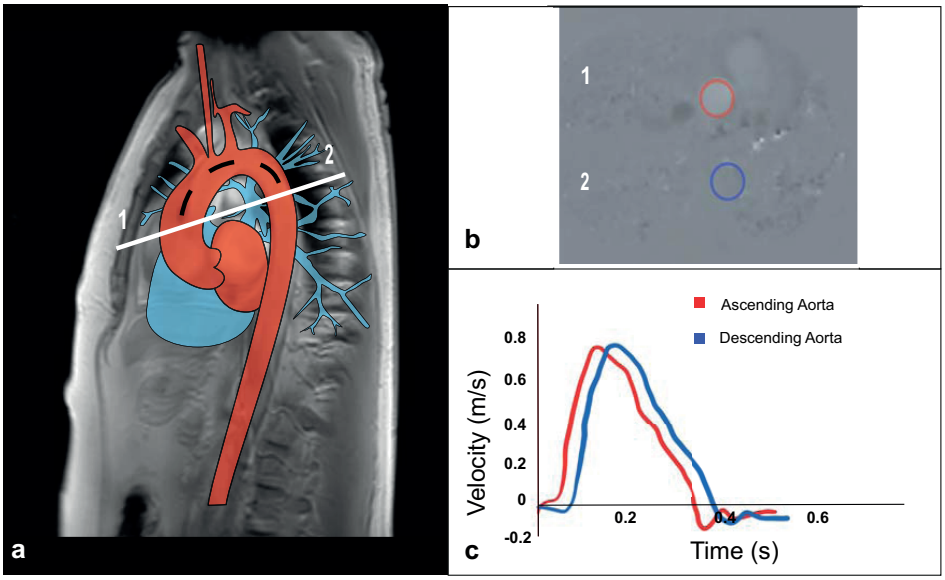

Figure 2. Assessment of arterial stiffness using MRI (a) MRI scout view of the thoracic aorta with anatomical drawing indicating proximal (1 ascending aorta) and distal (2 descending aorta) used for the planning of the velocity-encoded MRI planes. (b) Phase image of measurement site 1 and 2. (c) Derived velocity wave curves forms from measurement site 1 and 2.

Statistical analysis

In the NEO study individuals with a BMI of 27 kg/m² or higher were oversampled. First, inhabitants of Leiden and its surroundings between 45 and 65 years of age and with a self-reported BMI of 27 kg/m² or higher were invited to participate in the NEO study. In addition, we included a reference population. To that extent, all inhabitants between 45 and 65 years living in one municipality, Leiderdorp, were asked to participate irrespective of their BMI. This resulted in an additional sample of 1671 participants with a BMI distribution that was similar to the BMI distribution of the general Dutch population (20). If inference is made on the general population, the overrepresentation of overweight and obese participants in the NEO study may introduce bias, because of the skewed BMI distribution in the NEO population. Weighting towards the BMI distribution of the general population may solve this problem (21). Using the BMI distribution of the reference population, we calculated weight factors for the NEO population, resulting in a higher weight factor for participants with a lower BMI (**supplemental Table 3**). Use of sampling weights yield results which apply to a population-based study without oversampling of individuals with a high BMI (22). **Supplementary Figure 1** shows that the use of the weight factors results in a BMI distribution that is similar to that of the general population. Baseline characteristics of the weighted study population are expressed as mean (SD), median (25^{th} and 75^{th} percentile) or as percentage. Determinants were eGFR (CKD-

EPI), urinary albumin-creatinine ratio (UACR), and pulse wave velocity (PWV). Outcome variables were fibrinogen, FVIII, FIX, and FXI. UACR was log-2 transformed since this variable has a right-skewed distribution. Both renal function and albuminuria were grouped into six categories based on percentiles (>50th [reference], 10th to 50th, 5th to 10th, 2.5th to 5th, 1st to 2.5th, and <1st percentile for eGFR) and (<50th [reference], 50th to 90th, 90th to 95th, 95th to 97.5th, 97.5th to 99th, and >99th percentile for albuminuria). Because of the smaller sample size, pulse wave velocity was grouped into four instead of six categories based on percentiles (<50th [reference], 50th to 90th, 90th to 95th, >95th percentile). The use of percentile groups allows for the evaluation of wide ranges of values, particularly for abnormal levels. We calculated age- and sex-adjusted mean differences with 95% confidence intervals (CIs) in levels of hemostatic factors for the defined categories, compared with the reference using linear regression. Multiple linear regression was used to calculate the difference with 95% CIs in levels of hemostatic factors for every 10 ml/min/1.73m² change in eGFR, per two-fold change in albuminuria, and per ml/min change in PWV. Crude analyses were adjusted for age, sex, smoking (current, former, never), total body fat, CRP, total cholesterol, use of vitamin K antagonists (for factor IX only), ethnicity, and education. In order to correct for dyslipidaemia we only added total cholesterol to the regression analysis and not other measures of dyslipidemia in order to diminish the chance of an overfit statistical model. Additionally, we performed an analysis for clinical cut-off points for renal function (mildly to moderately reduced renal function [eGFR 45-90 ml/min/1.73m²], and moderately to severely reduced renal function [eGFR <45 ml/min/1.73m²]) and albuminuria (UACR >3 mg/mmol). Because gender and age specific cut-off points for vascular dysfunction based on PWV measured by MRI are yet to be defined, we investigated associations of PWV with the clotting factors over the whole range of PWV as a continuous variable and in percentiles. First degree linear spline modelling was used for exploring non-linear associations between renal function, vascular function and coagulation factors. Piecewise linear function was used, meaning that the adjusted regression models were composed of linear segments based on equally spaced knots (quintiles) (23). Analyses were performed using STATA (Statacorp, College Station, Texas, USA, version 12.0).

RESULTS

Baseline characteristics

The total NEO study population consisted of 6,671 participants. After consecutive exclusion of participants with missing data on renal function (n=50), albuminuria (n=27), coagulation factors (n=57) or fibrinogen (n=1) the final study population consisted of 6536 participants with a mean age of 55.6 ± 6 years. Mean eGFR was 86.0 ± 12.4 ml/

min/1.73m², normal eGFR (>90 ml/min/1.73m²) was present in 42%, mildly to moderately reduced renal function (eGFR 45-90 ml/min/1.73m²) in 57%, and moderately to severely reduced renal function (<45 ml/min/1.73m²) in 0.3% of the participants. Median UACR was 0.4 mg/mmol (25th, 75th percentile; 0.3; 0.7) and median UAE was 3.6 mg/L (25th, 75th percentile; 3.0, 4.8). Microalbuminuria was present in 2.0% and albuminuria in 0.4% of the participants, 4% of the participants had diabetes. ACE inhibitors or angiotensin-II antagonists were used by 14% of the participants. Baseline characteristics of the included study population are presented in **Table 1**. Approximately 30% of the participants who were eligible for additional MRI, were randomly selected to undergo PWV measurement (n=2,576). Participants with missing PWV measurements due to technical failures (n=143), were excluded for further analysis. The complete subgroup of participants with available PWV measurements consisted of 2,433 individuals, and was not statistically different from participants without PWV measurements (data not shown).

Associations of determinants of vascular function with coagulation factors

Adjusted mean differences of renal function, albuminuria, and arterial stiffness percentiles, and coagulant factors are provided in **Tables 2-5**. Crude mean differences and linear regression coefficients are provided in the **Supplemental Table 1 and 2**.

Compared with participants with an eGFR >50th percentile, the adjusted mean coagulation factor levels in participants with an eGFR <1st percentile were 33.3 (95% CI 13.0, 53.5) mg/dL for fibrinogen, 22 (95% CI 13, 32) IU/dL for FVIII, 16 (95% CI 7, 24) IU/dL for FIX and 4 (95% CI -5, 14) IU/dL for FXI. Similar results were found when clinical cut-off points were used to categorize renal function instead of percentiles. Participants with moderately to severely decreased kidney function (eGFR <45 ml/min/1.73m²) compared to participants with normal renal function (eGFR >90 mL/min; Table 5), had adjusted mean differences of 44.5 (95% CI 9.5, 79.4) mg/dL for fibrinogen, 43 (95% CI 22, 64) IU/dL for FVIII, 25 (95% CI 5, 46) IU/dL for FIX, and 2 (95% CI -1, 5) IU/dL for FXI.

For albuminuria the adjusted mean coagulation factor levels in participants with an UACR >99th percentile were 12.3 (95% CI -2.6, 27.10 mg/dL for fibrinogen, 12 (95% CI 3, 22) IU/dL for FVIII, 9 (95% CI 3, 14) IU/dL for FIX, and 4 (95% CI 0, 9) IU/dL for FXI compared with participants with an UACR <50th percentile. When using clinical cut-off points to categorize albuminuria instead of percentiles, participants with micro- and/or macroalbuminuria (UACR >3 mg/mmol) had as compared with participants with normal range albuminuria (UACR <3 mg/mmol) (**Table 5**), adjusted mean differences of 5.9 (95% CI -3.8, 15.3) mg/dL for fibrinogen, 2 (95% CI -6, 9) IU/dL for FVIII, 3 (95% CI -1, 6) IU/dL for FIX, and 2 (95% CI -1, 5) IU/dL for FXI.

Table 1. Characteristics of the study population (n=6,536)

Characteristic	
Demographic/anthropometric	
Age (y)	55.6 (6)
Sex (% men)	48
Ethnicity (% white)	95
Education (% higher)	46
BMI (kg/m^2)	26 (4)
Tobacco smoking (% never)	38
Comorbidity	
Hypertension (% yes)	34
Diabetes* (% yes)	4
Cardiovascular disease† (% yes)	6
Thromboembolic event‡ (% yes)	0.2
Medication use	
Antihypertensives (% yes)	24
Glucose lowering medication (% yes)	2.7
Vitamin K antagonist (% yes)	1.3
Lipid lowering drug (% yes)	11
ACE/Angiotensin-II antagonists (% yes)	14
Blood pressure	
Systolic (mmHg)	130 (17)
Diastolic (mmHg)	83 (10)
Mean arterial pressure (mmHg)	99 (12)
Biomarkers	
Serum creatinine (umol/L)	77.4 (15)
eGFR CKD-epi (ml/min/1.73m^2)	86.0 (12.4)
UAE (mg/l)	3.6 (3.0; 4.8)
UACR (mg/mmol)	0.4 (0.3; 0.7)
Total cholesterol (mmol/L)	5.7 (1.1)
Triglycerides (mmol/L)	1.2 (0.8)
High-density lipoprotein (mmol/L)	1.6 (0.5)
Low- density lipoprotein (mmol/L)	3.6 (1.0)
Fasting glucose (mmol/l)	5.4 (1.0)
C-Reactive Protein (mg/L)	1.9 (2.8)
Arterial Stiffness	
Pulse wave velocity§ (m/s)	6.6 (1.3)
Coagulation factors	
Fibrinogen (g/L)	290 (56)
Factor VIII (IU/dL)	122 (33)
Factor IX (IU/dL)	115 (21)
Factor XI (IU/dL)	116 (19)

Results were weighted toward the BMI distribution of the general population (n=6,536). Results are expressed as %, means (standard deviation) or medians (25th, 75th percentile). Diabetes*; raised fasting plasma glucose concentrations (≥5.56 mmol/L) or on drug treatment to lower glucose concentrations. Cardiovascular disease†; myocardial infarction, angina pectoris, congestive heart failure, Thromboembolic event‡; pulmonary embolism, deep venous thrombosis. eGFR, estimated glomerular filtration rate according to the CKD-EPI formula; UAE, urinary albumin excretion; UACR, urinary albumin-creatinine ratio. Pulse wave velocity§; assed in n=2,433

Table 2. Regression between eGFR percentiles and coagulant factors

	Adjusted* mean difference (95% CI) compared with >50th percentile (eGFR >87.3mL/min/1.73m²)				
Coagulation Factor	50th-10th Percentile (eGFR ranges, 69.4-87.3 mL/min/1.73m²)	5th-10th Percentile (eGFR ranges, 65.3-69.4 mL/min/1.73m²)	2.5th-5th Percentile (eGFR ranges, 60.5-65.3 mL/min/1.73m²)	1th-2.5th Percentile (eGFR ranges, 55.3-60.5 mL/min/1.73m²)	<1st Percentile (eGFR <55.3 mL/min/1.73m²)
Fibrinogen (g/L)	-0.4 (-3.7, 3.0)	-5.3 (-11.1, 0.5)	-1.1 (-12.0, 9.8)	0.9 (-11.4, 13.1)	33.3 (13.0, 53.5)
Factor VIII (IU/dL)	3 (0, 5)	3 (-2, 7)	11 (3, 19)	9 (-1, 20)	22 (13, 32)
Factor IX (IU/dL)†	1 (-1, 2)	5 (2, 8)	4 (1, 8)	5 (0, 10)	16 (7, 24)
Factor XI (IU/dL)	0 (-1, 2)	2 (-1, 5)	-1 (-5, 3)	4 (-3, 10)	4 (-5, 14)

Results were weighted toward the BMI distribution of the general population (n=6,536). *Adjusted for; sex, age, smoking, total body fat, CRP, total cholesterol, ethnicity and education. †Vitamin K antagonist users were excluded from the analysis. Corresponding linear regression coefficients, 95% Confidence Intervals.

Table 3. Regression between UACR percentiles and coagulant factors

	Adjusted* mean difference (95% CI) compared with <50th percentile (UACR <0.49 mg/mmol)				
Coagulation Factor	50th-90th Percentile (UACR ranges, 0.49-1.11 mg/mmol)	90th-95th Percentile (UACR ranges, 1.11-1.64 mg/mmol)	95th-97.5th Percentile (UACR ranges, 1.64-2.96 mg/mmol)	97.5th-99th Percentile (UACR ranges, 2.96-6.21 mg/mmol)	>99th Percentile (UACR >6.21 mg/mmol)
Fibrinogen (g/L)	1.3 (-2.4, 5.0)	2.1 (-4.7, 8.9)	5.5 (-5.1, 16.1)	0.8 (-11.1, 12.7)	12.3 (-2.6, 27.1)
Factor VIII (IU/dL)	-4 (-6, -1)	-5 (-10, 0)	-3 (-10, 4)	-8 (-18, 1)	12 (3, 22)
Factor IX (IU/dL)†	0 (-2, 1)	1 (-2, 4)	0 (-4, 4)	-2 (-5, 2)	9 (3, 14)
Factor XI (IU/dL)	1 (-1, 2)	-2 (-5, 1)	-2 (-6, 2)	1 (-3, 5)	4 (0, 9)

Results were weighted toward the BMI distribution of the general population (n=6,536). *Adjusted for; sex, age, smoking, total body fat, CRP, total cholesterol, ethnicity and education. †Vitamin K antagonist users were excluded from the analysis. Corresponding linear regression coefficients, 95% Confidence Intervals.

Table 4. Regression between PWV percentiles and coagulant factors

	Adjusted* mean difference (95% CI) compared with <50th percentile (PWV <6.31 m/s)		
Coagulation Factor	50th-90th Percentile (PWV ranges, 6.31-8.32 m/s)	90th-95th Percentile (PWV ranges, 8.31-9.14 m/s)	>95th Percentile (PWV >9.14 m/s)
Fibrinogen (g/L)	1.4 (-4.6, 7.4)	-6.8 (-15.7, 2.1)	11.4 (-2.6, 25.4)
Factor VIII (IU/dL)	0 (-4, 4)	1 (-6, 8)	-1 (-9, 8)
Factor IX (IU/dL) †	3 (1, 5)	9 (5, 13)	7 (-1, 15)
Factor XI (IU/dL)	3 (0, 5)	3 (-1, 8)	4 (-2, 10)

Results were weighted toward the BMI distribution of the general population (n=2,433). *Adjusted for; sex, age, smoking, total body fat, CRP, total cholesterol, ethnicity and education. †Vitamin K antagonist users were excluded from the analysis. Corresponding linear regression coefficients, 95% Confidence Intervals.

Table 5. Regression between clinical stages of eGFR, UACR and coagulant factors

	Adjusted* mean difference (95% CI) compared with normal kidney function (eGFR >90ml/min/1.73m²; 42.3%)		Adjusted* mean difference (95% CI) compared with normal UACR (<3 mg/mmol; 97.6%)
Coagulation Factor	eGFR 45-90 ml/ min/1.73m² (n=57.5%)	eGFR <45 ml/min/1.73m² (n=0.26%)	UACR >3 mg/mmol (n=0.24%)
Fibrinogen (g/L)	-1.4 (-4.8, 1.9)	44.5 (9.5, 79.4)	5.9 (-3.6, 15.3)
Factor VIII (IU/dL)	5 (3, 7)	43 (22, 64)	2 (-6, 9)
Factor IX (IU/dL) †	2 (0, 3)	25 (5, 46)	3 (-1, 6)
Factor XI (IU/dL)	0 (-1, 2)	21 (4, 38)	2 (-1, 5)

Results were weighted toward the BMI distribution of the general population (n=6,536). *Adjusted for; sex, age, smoking, total body fat, CRP, total cholesterol, ethnicity and education. †Vitamin K antagonist users were excluded from the analysis. Corresponding linear regression coefficients, 95% Confidence Intervals.

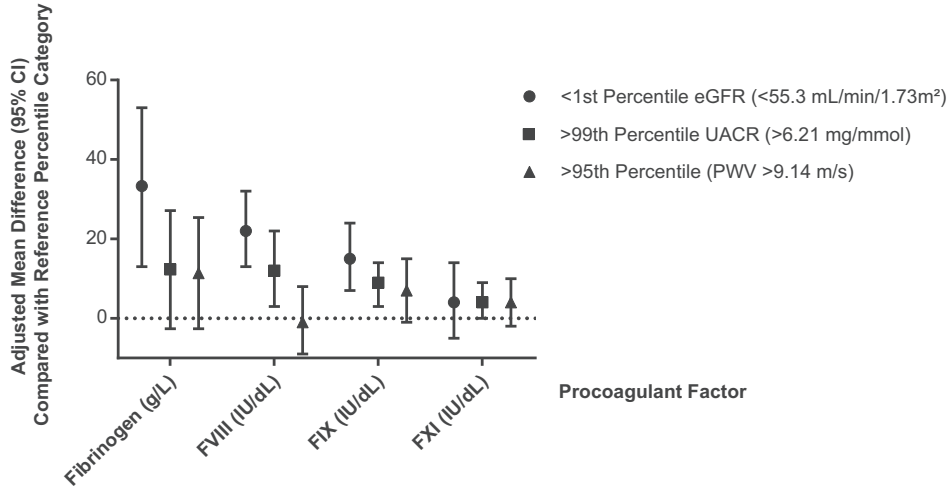

Figure 3. Overview of the adjusted mean factor levels of the <1st percentile eGFR, >99th percentile UACR and >95th percentile PWV compared with the reference percentile category. Results were weighted toward the BMI distribution of the general population (n=6,536) Adjusted for; sex, age, smoking, total body fat, CRP, total cholesterol, ethnicity and education Corresponding linear regression coefficients, 95% Confidence Intervals. The reference percentile category for eGFR was >50th percentile for eGFR, <50th percentile for UACR and PWV. Vitamin K antagonist users were excluded from the analysis of FIX.

For arterial stiffness the adjusted mean coagulation factor levels of participants with PWV >95th percentile were 11.4 (95% CI -2.6, 25.4) mg/dL for fibrinogen, -1 (95% CI -9, 8) IU/dL for FVIII, 7 (95% CI -1, 15) for FIX and 4 (95% CI -2, 10) for FXI compared with participants with PWV <50th percentile. An overview of the adjusted mean factor levels of the <1st percentile eGFR, >99th percentile UACR and >95th percentile PWV compared with the reference percentile category (>50th percentile for eGFR and <50th percentile

for UACR and PWV) is visualized in **Figure 3**. Spline models showing the association between eGFR, UACR, PWV and coagulation factors fibrinogen, FVIII, FIX, and FXI, suggest an inverse relationship between renal function and coagulation factors, and a positive relationship between vascular function and coagulation factors (except for fibrinogen). Results of spline models are visualized in **Supplementary Figure 2**.

DISCUSSION

In this large population-based cross-sectional study, coagulation factors showed a procoagulant shift with all three determinants of lower vascular function, and found associations were most pronounced for factor VIII (for eGFR and UACR) and factor IX (for PWV).

We found that the adjusted mean coagulation factor levels for participants with an eGFR <60 ml/min/1.73m² were significantly higher for fibrinogen, FVIII, FIX, and FXI compared to participants with normal renal function (eGFR >90 mL/min), while controlling for various confounding factors including CRP. These findings are supported by results based on linear spline models except for the relationship between PWV and fibrinogen for which we have no biological explanation. Our study adds novel information to the previous population-based multi-ethnic MESA study that observed that a decline in renal function was associated with both coagulation factors (fibrinogen and FVIII), and an increase in inflammatory markers (such as CRP and IL-6) in participants without cardiovascular disease or chronic kidney disease (7, 24). However, previous observations were limited by the use of coagulation factors that are also acute phase reactant proteins, meaning that previous findings could have been solely a reflection of the association of endothelial dysfunction with inflammation.

In the context of CKD, markers of endothelial dysfunction have been associated with a hypercoagulable state, and raised levels of FVIII and von Willebrand factor with an increased thrombo-embolic risk (6, 25). This is supported by the observed normalization of endothelial dysfunction and hypercoagulability after renal transplantation (26, 27), suggesting a causal relationship between renal vascular function and hypercoagulability (28). We observed that higher levels of albuminuria associate with higher levels of coagulation factors. For the >99th UACR percentile (>6.21 mg/mmol) these findings were most pronounced for FVIII and fibrinogen. FVIII is of particular interest, since it is synthesized by vascular, glomerular, and tubular endothelium, as well as the sinusoidal cells of the liver. FVIII could therefore be considered both as a marker of endothelial dysfunction, and a risk factor for venous thrombosis (25). The found link between higher levels of albuminuria and a procoagulant state in this study, might be explained by endothelial regulation of vascular homeostasis, which could become dysfunctional due to sustained inflammatory endothelial activation (29). Two other studies evaluating the association

between UACR and venous thromboembolism, however did not observe such an association (30, 31). In the present study, the differences in adjusted mean coagulation factor levels for the highest / lowest percentile compared with the reference category was also most pronounced for eGFR, rather than for albuminuria or arterial stiffness.

In the current study we found a positive association between increased arterial stiffness and higher levels of FIX and FXI in continuous analysis, however this association was not convincingly present when the analyses were based on percentile cut-offs of arterial stiffness. Arterial stiffness is a reflection of the elastic properties of a vessel (i.e. compliance and ability to contract and dilate), which is mainly determined by the intima-media and can respond to mechanical changes through the production vasoactive molecules, extracellular matrix, and extracellular matrix-degrading proteases (15). Previous basic science studies have shown that mechanical injury to vasculature can result in increased procoagulant state (32), however further studies are needed to verify whether a true association exists between arterial stiffness and the coagulation system.

Strengths of our study are the large sample size with extensive phenotyping, including data on four different coagulation factors and data on three different measures of vascular function. Both albuminuria and arterial stiffness can be considered to reflect systemic vascular injury; albuminuria may potentially serve as a surrogate marker of systemic endothelial dysfunction (33), and arterial stiffness as a marker of intima-medial calcification (11, 34). Arterial stiffness was assessed in a large random subgroup using MRI, which is highly superior compared to conventional tonometry (19), and has not been studied in relation to coagulation thus far.

This study also has a number of limitations that need to be considered. The observed associations appeared to be the strongest in individuals with the lowest renal and vascular function. It must be noted that these individuals represented only 1% of the total population, because this is a population-based analysis without any prior selection criteria for chronic kidney disease. Therefore, our findings are representative for the general population rather than CKD patients. The results from the spline models also suggest an inverse relation between renal function and increased levels of procoagulant factors. Although our results are based on a population-based study, we cannot completely exclude the influence of other potentially clinically relevant conditions that would affect renal and vascular function in relation to coagulation factor levels. Another limitation was the use of estimated GFR rather than (invasive) gold standard exogenous clearance measurements. Although the CKD-EPI formula has proven to be more accurate and precise than the older MDRD formula, it has not been validated above 90 ml/min/1.73m² (35). Furthermore, in the present study overall markers of hypercoagulability or natural coagulation inhibitors such as d-dimer and antithrombin were unfortunately not measured and could not be taken into account in the analyses. Our findings support the hypothesis that vascular function is a marker of hypercoagulability, however the cross-sectional observational

nature of our study precludes a causal interpretation. The exact mechanism explaining why CKD is associated with an increased risk of venous thrombosis remains unclear. Recently, potential novel pathways for the regulation of haemostasis and thrombosis in kidney disease have been described suggesting that a subclinical inflammatory state initiates glomerular injury via altered expression of coagulation factors, rather than impaired renal function or vascular damage initiating procoagulant changes (28). This has been supported by various laboratory findings and preclinical studies showing that renal cell-specific expression and activity of coagulation proteases, and its associated regulators and receptors tend to alter during renal disease processes (28). Future analysis with repeated measurements could contribute to the assessment of the direction of the observed associations between vascular function and coagulation factors.

In summary, in this middle-aged sample of the general population impaired renal and vascular function (i.e. albuminuria and arterial stiffness) was associated with higher levels of coagulation factors. These findings support the hypothesis that impaired renal and vascular function plays a role in the etiology of venous thrombosis.

REFERENCES

1. Kerlin BA, Smoyer WE, Tsai J, Boulet SL. Healthcare burden of venous thromboembolism in childhood chronic renal diseases. Pediatr Nephrol. 2015; 30: 829-37.
2. Wattanakit K, Cushman M, Stehman-Breen C, Heckbert SR, Folsom AR. Chronic kidney disease increases risk for venous thromboembolism. JASN. 2008; 19: 135-40.
3. Mahmoodi BK, Gansevoort RT, Veeger NJ, Matthews AG, Navis G, Hillege HL, van der Meer J. Microalbuminuria and risk of venous thromboembolism. JAMA. 2009; 301: 1790-7.
4. Ocak G, Verduijn M, Vossen CY, et al. Chronic kidney disease stages 1-3 increase the risk of venous thrombosis. J Thromb Haemost. 2010;8:2428-35.
5. Mahmoodi BK, Gansevoort RT, Naess IA, et al. Association of mild to moderate chronic kidney disease with venous thromboembolism: pooled analysis of five prospective general population cohorts. Circulation. 2012; 126: 1964-71.
6. Ocak G, Vossen CY, Lijfering WM, et al. Role of hemostatic factors on the risk of venous thrombosis in people with impaired kidney function. Circulation. 2014; 129: 683-91.
7. Hiramoto JS, Katz R, Peralta CA, et al. Inflammation and coagulation markers and kidney function decline: the Multi-Ethnic Study of Atherosclerosis (MESA). Am J Kidney Dis. 2012; 60: 225-32.
8. Keller C, Katz R, Cushman M, et al. Association of kidney function with inflammatory and procoagulant markers in a diverse cohort: a cross-sectional analysis from the Multi-Ethnic Study of Atherosclerosis (MESA). BMC Nephrol. 2008; 9: 9.
9. Prandoni P, Bilora F, Marchiori A, et alA. An association between atherosclerosis and venous thrombosis. N Engl J Med. 2003; 348: 1435-41.
10. Borissoff JI, Spronk HM, ten Cate H. The hemostatic system as a modulator of atherosclerosis. N Engl J Med. 2011; 364: 1746-60.
11. Whitlock MC, Hundley WG. Noninvasive Imaging of Flow and Vascular Function in Disease of the Aorta. JACC Cardiovasc Imaging. 2015; 8: 1094-106.
12. van Popele NM, Grobbee DE, Bots ML, et al. Association between arterial stiffness and atherosclerosis. Stroke. 2001; 32: 454-60.
13. Duivenvoorden R, Vanbavel E, de Groot E, et al. Endothelial shear stress: a critical determinant of arterial remodeling and arterial stiffness in humans–a carotid 3.0-T MRI study. Circ Cardiovasc Imaging. 2010; 3: 578-85.
14. Davies PF. Hemodynamic shear stress and the endothelium in cardiovascular pathophysiology. Nat Clin Pract Cardiovasc Med. 2009; 6: 16-26.
15. Collins C, Osborne LD, Guilluy C, et al. Haemodynamic and extracellular matrix cues regulate the mechanical phenotype and stiffness of aortic endothelial cells. Nat Commun. 2014; 5: 3984.
16. de Mutsert R, den Heijer M, Rabelink TJ, et al. The Netherlands Epidemiology of Obesity (NEO) study: study design and data collection. Eur J Epidemiol. 2013; 28: 513-23.

17. Levey AS, Bosch JP, Lewis JB, Greene T, Rogers N, Roth D. A more accurate method to estimate glomerular filtration rate from serum creatinine: a new prediction equation. Modification of Diet in Renal Disease Study Group. Ann Intern Med. 1999; 130: 461-70.

18. KDIGO. 2012 Clinical practice guideline for the evaluation and management of chronic kidney disease. Kidney Int Suppl. 2013; 3: 1-150.

19. Grotenhuis HB, Westenberg JJ, Steendijk P, van der Geest RJ, Ottenkamp J, Bax JJ, Jukema JW, de Roos A. Validation and reproducibility of aortic pulse wave velocity as assessed with velocity-encoded MRI. J Magn Reson Imaging. 2009; 30: 521-6.

20. Hoeveel mensen hebben overgewicht? [How many people are overweight]. Ministry of Health WaS, ed.: NdMG, the Netherlands. 2013.

21. Korn EL, Graubard BI. Epidemiologic studies utilizing surveys: accounting for the sampling design. Am J Public Health. 1991; 81: 1166-73.

22. Lumley T. Analysis of complex survey samples [Web page]. http://www.jstatsoft.org/v09/i08/paper. Accessed April 29, 2017.

23. Gould W. Linear splines and piecewise linear functions. Stata Technical Bulletin. 1993; 15: 13-7.

24. Dubin R, Cushman M, Folsom AR, et al. Kidney function and multiple hemostatic markers: cross sectional associations in the multi-ethnic study of atherosclerosis. BMC Nephrol. 2011; 12: 3.

25. Kyrle PA, Minar E, Hirschl M, et al. High plasma levels of factor VIII and the risk of recurrent venous thromboembolism. N Engl J Med. 2000; 343: 457-62.

26. Ghisdal L, Broeders N, Wissing KM, et al. Thrombophilic factors in Stage V chronic kidney disease patients are largely corrected by renal transplantation. Nephrol, Dial, Transplant. 2011; 26: 2700-5.

27. Keven K, Elmaci S, Sengul S, et al. Soluble endothelial cell protein C receptor and thrombomodulin levels after renal transplantation. Int Urol Nephrol. 2010; 42: 1093-8.

28. Madhusudhan T, Kerlin BA, Isermann B. The emerging role of coagulation proteases in kidney disease. Nat Rev Nephrol. 2016; 12: 94-109.

29. Rabelink TJ, de Zeeuw D. The glycocalyx--linking albuminuria with renal and cardiovascular disease. Nat Rev Nephrol. 2015; 11: 667-76.

30. Cheung KL, Zakai NA, Folsom AR, et al. Measures of Kidney Disease and the Risk of Venous Thromboembolism in the REGARDS (Reasons for Geographic and Racial Differences in Stroke) Study. Am J Kidney Dis. 2017. 70 (2):182-190.

31. Folsom AR, Lutsey PL, Astor BC, et al. Chronic kidney disease and venous thromboembolism: a prospective study. Nephrol, Dial, Transplant. 2010; 25: 3296-301.

32. Chiu JJ, Chien S. Effects of disturbed flow on vascular endothelium: pathophysiological basis and clinical perspectives. Physiol Rev. 2011; 91: 327-87.

33. Boor P. Biomarkers: Albuminuria - a marker of systemic microvascular function. Nat Rev Nephrol. 2016; 12: 449-50.

34. Dhaun N, Webb DJ. Targeting Blood Vessel Stiffness to Protect Kidney Function. Clin J Am Soc Nephro. 2015; 10: 2107-9.

35. Levey AS, Stevens LA, Schmid CH, et al. A new equation to estimate glomerular filtration rate. Ann Intern Med. 2009; 150: 604-12.

Supplemental Table 1. Regression between PWV, eGFR, UACR and coagulant factors

Coagulation Factor	Per 10 ml/min/1.73m² lower eGFR (n=6,536)	Per 2-fold higher UACR (mg/mmol) (n=6,536)	Per m/s higher PWV (n=2,433)
Fibrinogen (g/L)			
Crude	1.1 (-0.6, 2.7)	5.4 (3.7, 7.2)	2.3 (0.5, 4.0)
Adjusted	0.4 (-1.0, 1.9)	2.0 (0.6, 3.3)	0.6 (-1.9, 3.1)
Factor VIII (IU/dL)			
Crude	3.1 (2.2, 4.1)	0.4 (-0.6, 1.3)	1.4 (0.3, 2.4)
Adjusted	2.3 (1.3, 3.3)	-0.9 (-1.9, 0.1)	0.4 (-1.2, 1.9)
Factor IX (IU/dL)*			
Crude	1.1 (0.5, 1.7)	0.8 (0.2, 1.4)	1.9 (1.3, 2,5)
Adjusted	1.0 (0.4, 1.6)	0.3 (-0.2, 0.8)	2.0 (0.7, 3.2)
Factor XI (IU/dL)			
Crude	0.8 (0.1, 1.4)	1.0 (0.5, 1.6)	0.7 (0.1, 1.3)
Adjusted	0.5 (-0.1, 1.1)	-0.1 (-0.6, 0.5)	1.1 (0.1, 2.0)

Results were weighted toward the BMI distribution of the general population. *Vitamin K antagonist users were excluded from the analysis. Adjusted for; sex, age, smoking, total body fat, CRP, total cholesterol, ethnicity and education. Corresponding linear regression coefficients, 95% Confidence Intervals. Regression coefficients reflect the difference in coagulant factor per 10 ml/min/1.73m^2 eGFR, per 2-fold difference in UACR and per m/s difference in PWV.

Supplemental Table 2. Regression between eGFR, UACR and PWV percentiles and coagulant factors

	Crude and adjusted# mean difference (95% CI) compared with >50th percentile (eGFR >87.3mL/min/1.73m²)				
Coagulation Factor	50th-10th Percentile (eGFR ranges, 69.4-87.3 mL/min/1.73m²)	5th-10th Percentile (eGFR ranges, 65.3-69.4 mL/min/1.73m²)	2.5th-5th Percentile (eGFR ranges, 60.5-65.3 mL/min/1.73m²)	1th-2.5th Percentile (eGFR ranges, 55.3-60.5 mL/min/1.73m²)	<1st Percentile (eGFR <55.3 mL/min/1.73m²)
Fibrinogen (g/L)					
Crude	-2.7 (-6.4, 1.9)	-6.2 (-13.9, 1.6)	8.3 (-4.4, 21.0)	10.1 (-5.2, 25.4)	56.8 (31.1, 82.5)
Adjusted*	-0.4 (-3.7, 3.0)	-5.3 (-11.1, 0.5)	-1.1 (-12.0, 9.8)	0.9 (-11.4, 13.1)	33.3 (13.0, 53.5)
Factor VIII (IU/dL)					
Crude	4 (1, 6)	6 (0, 11)	15 (7, 23)	13 (3, 23)	31 (22, 40)
Adjusted*	3 (0, 5)	3 (-2, 7)	11 (3, 19)	9 (-1, 20)	22 (13, 32)
Factor IX (IU/dL)†					
Crude	0 (-1, 2)	4 (1, 8)	7 (2, 11)	6 (0, 12)	20 (10, 30)
Adjusted*	1 (-1, 2)	5 (2, 8)	4 (1, 8)	5 (-0, 10)	15 (7, 24)
Factor XI (IU/dL)					
Crude	1 (-1, 2)	3 (0, 6)	1 (-4, 6)	5 (-2, 12)	7 (-3, 18)
Adjusted*	0 (-1, 2)	2 (-1, 5)	-1 (-5, 3)	4 (-3, 10)	4 (-5, 14)

	Crude and adjusted# mean difference (95% CI) compared with <50th percentile (UACR <0.49 mg/mmol)				
Coagulation Factor	50th-90th Percentile (UACR ranges, 0.49-1.11 mg/mmol)	90th-95th Percentile (UACR ranges, 1.11-1.64 mg/mmol)	95th-97.5th Percentile (UACR ranges, 1.64-2.96 mg/mmol)	97.5th-99th Percentile (UACR ranges, 2.96-6.21 mg/mmol)	>99th Percentile UACR >6.21 mg/mmol)
Fibrinogen (g/L)					
Crude	6.4 (2.2, 10.6)	17.4 (7.8, 27.0)	24.1 (9.8, 38.5)	14.3 (-0.4, 29.0)	37.7 (16.8, 58.6)
Adjusted*	1.3 (-2.4, 5.0)	2.1 (-4.7, 8.9)	5.5 (-5.1, 16.1)	0.8 (-11.1, 12.7)	12.3 (-2.6, 27.1)
Factor VIII (IU/dL)					
Crude	-1 (-4, 1)	1 (-4, 6)	2 (-5, 9)	0 (-11, 11)	18 (8, 28)
Adjusted*	-4 (-6, -1)	-5 (-10, 0)	-3 (-10, 4)	-8 (-18, 1)	12 (3, 22)
Factor IX (IU/dL)†					
Crude	0 (-2, 1)	3 (0, 6)	4 (-1, 9)	2 (-3, 8)	17 (10, 25)
Adjusted*	0 (-2, 1)	1 (-2, 4)	0 (-4, 4)	-2 (-5, 2)	9 (3, 14)
Factor XI (IU/dL)					
Crude	4 (2, 5)	2 (-2, 5)	2 (-2, 7)	3 (-2, 7)	6 (2, 11)
Adjusted*	1 (-1, 2)	-2 (-5, 1)	-2 (-6, 2)	1 (-3, 5)	4 (0, 9)

	Crude and adjusted# mean difference (95% CI) compared with <50th percentile (PWV <6.31 m/s)		
oagulation Factor	50th-90th Percentile (PWV ranges, 6.31-8.32 m/s)	90th-95th Percentile (PWV ranges, 8.32-9.14 m/s)	>95th Percentile (PWV >9.14 m/s)
Fibrinogen (g/L)			
Crude	12.5 (5.6, 19.4)	2.7 (-7.7, 13.1)	16.8 (2.4, 31.1)
Adjusted*	1.4 (-4.6, 7.4)	-6.8 (-15.7, 2.1)	11.4 (-2.6, 25.4)
Factor VIII (IU/dL)			
Crude	4 (0, 8)	5 (-2, 12)	5 (-4, 14)
Adjusted*	0 (-4, 4)	1 (-6, 8)	-1 (-9, 8)
Factor IX (IU/dL)†			
Crude	6 (4, 9)	12 (7, 17)	7 (-1, 15)
Adjusted*	3 (1, 5)	9 (5, 13)	7 (-1, 15)
Factor XI (IU/dL)			
Crude	4 (2, 6)	6 (1, 11)	4 (-2, 10)
Adjusted*	3 (0, 5)	3 (-1, 8)	4 (-2, 10)

Results were weighted toward the BMI distribution of the general population (n=6,536). †Vitamin K antagonist users were excluded from the analysis *Adjusted for; sex, age, smoking, total body fat, CRP, total cholesterol, ethnicity and education. Corresponding linear regression coefficients, 95% Confidence Intervals

Supplemental Table 3. Weight factors for the different BMI categories of the NEO population, as used in the statistical analyses.

BMI categories (kg/m²)	Weight factor
>=30	1
29-30	1.304461
28-29	1.472934
27-28	2.458912
26-27	4.445434
25-26	8.668198
<25	10.26279

Weight factors were calculated using the BMI distribution of the reference (Leiderdorp) population (n=1,671), whose BMI distribution was similar to the BMI distribution of the general Dutch population (20). All results were based on weighted analyses. Consequently, the results apply to a population-based study without oversampling of individuals with a BMI ≥ 27 kg/m^2.

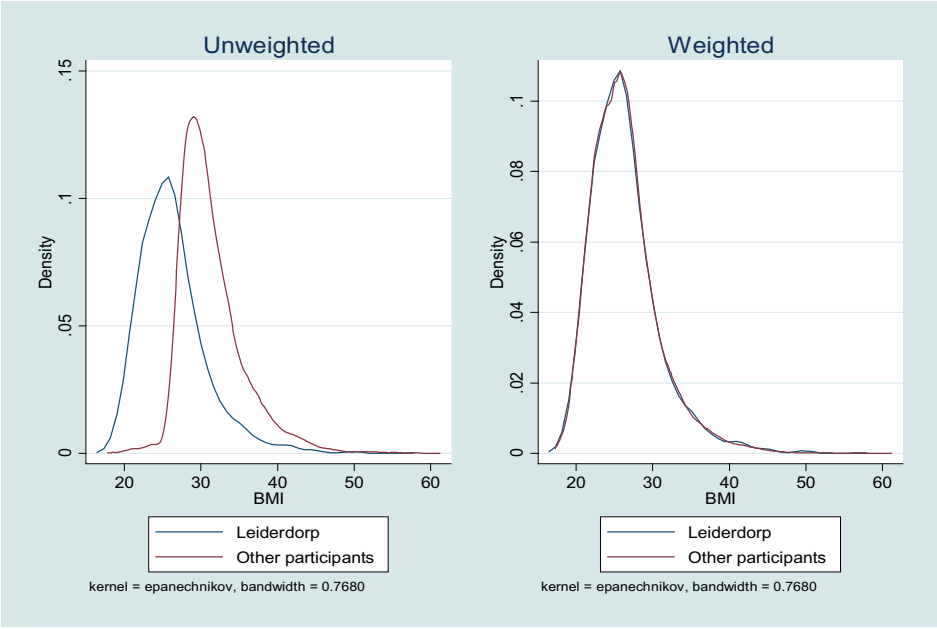

Supplemental Figure 1. Distribution of BMI in the Leiden population (blue) and in the total NEO population (red) before weighting (left) and after weighting (right). The unweighted and weighted density plots show that weighting corrects for oversampling of participants with a BMI >27 kg/m^2, and that the BMI distribution in the NEO population after weighting is similar to the BMI distribution of the general population.

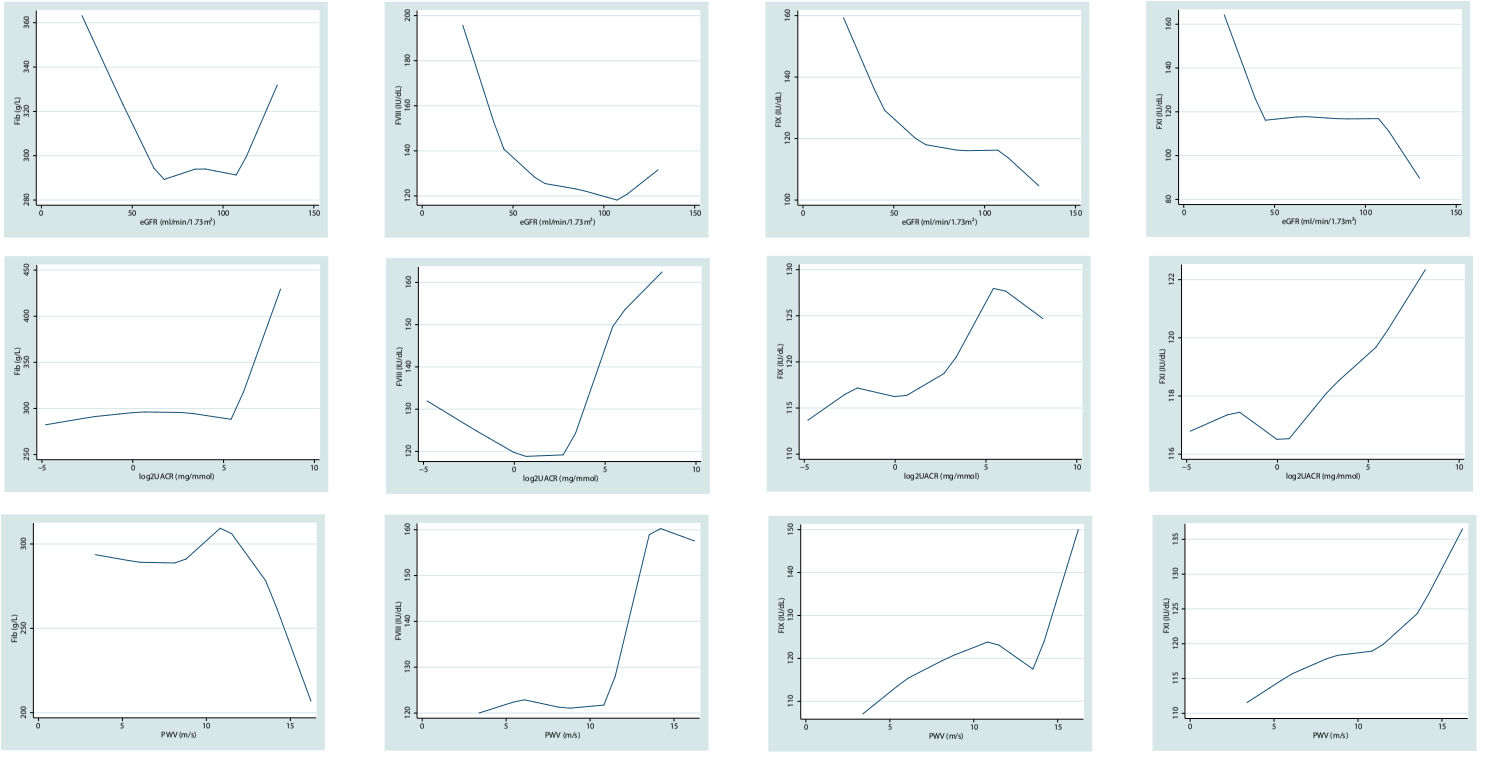

Supplemental Figure 2. Spline models showing the association between eGFR (upper row), UACR (middle row), PWV (lower row), and coagulation factors fibrinogen, FVIII, FIX, and FXI.

9

The separate contributions of visceral fat and liver fat to CKD-related renal outcomes

Dekkers IA, de Vries APJ, Smit RAJ, Rosendaal FR, Rabelink TJ, Lamb HJ, de Mutsert R.

J Ren Nutr. 2019 Oct 25. pii: S1051-2276(19)30323-1.

ABSTRACT

Objective

To investigate the separate contributions of liver fat and visceral fat on microalbuminuria and impaired renal function. Second, to examine whether NAFLD is causally related to microalbuminuria and/or impaired renal function.

Methods

In this cross-sectional analysis of the NEO study associations between visceral adipose tissue (VAT), hepatic triglyceride content (HTGC) and risk of microalbuminuria and renal function were studied using logistic regression. Mendelian randomization using GWAS meta-analysis data was performed to estimate the causal effect of NAFLD (*PNPLA3, LYPLAL1, NCAN, GCKR* from) on eGFR (N_{max}118,460), micro-albuminuria (N_{max}54,116), and impaired renal function (N_{max}118,147).

Results

2,023 participants (mean age 55.5 ± 6.0 years, 53% women) were included of which 29% had fatty liver and 2.0% CKD stage ≥3. In joint models, VAT was associated with a two-fold increased risk of microalbuminuria which was mainly driven by the association in women (total population: per SD=55.4 cm^2 OR=2.02, 95% CI 1.18, 3.47; women: OR=2.83, 95% CI 1.44, 5.56), but HTGC was not (total population: per SD=7.9% OR=1.20, 95% CI 0.85, 1.70). No associations were found for VAT and HTGC with eGFR (VAT: per SD=55.4 cm^2 OR=1.25, 95% CI 0.83, 1.87; HTGC: per SD=7.9% OR=0.65, 95% CI 0.42, 0.99). No causal effect of NAFLD on microalbuminuria or impaired renal function was found.

Conclusions

In observational analyses, visceral fat was associated with microalbuminuria in women (but not in men). Liver fat was not associated with microalbuminuria or renal function, which was supported by Mendelian randomization analyses. These findings suggest that visceral fat might be more important than liver fat in the etiology of microalbuminuria.

INTRODUCTION

Non-alcoholic Fatty Liver Disease (NAFLD) and Chronic Kidney Disease (CKD) have shared pathophysiological mechanisms and increasing evidence suggests that NAFLD is an important risk factor for CKD (1,2). As decline in renal function often only occurs late in the disease course of CKD, microalbuminuria is of particular interest as an early subclinical marker of endothelial dysfunction, especially in obese individuals who are known to show hyperfiltration in the early phases of CKD (3). Besides liver fat, also total body fat and visceral fat have been implicated as risk factors for microalbuminuria (4), and endothelial dysfunction (5). It has been postulated that excess visceral fat via increased levels of adipokines and free fatty acids lead to systemic inflammation, and ultimately renal detoriation (6,7). However, the separate contribution of liver fat on the associations with microalbuminuria and impaired renal function remains unclear as previous studies did not take visceral fat or total body fat into account (8). Furthermore, it has been shown that visceral fat is more strongly associated with cardiometabolic risk factors than liver fat, however associations with microalbuminuria or renal function were not evaluated (9). Previous studies have been limited by the use of ultrasonography or computed tomography for the assessment of the presence of hepatic steatosis rather than direct quantification of hepatic triglyceride content (HTGC) using proton magnetic resonance spectroscopy, which is considered to be the gold standard technique for non-invasive measurement liver fat (10). In addition, recent methods such as Mendelian randomization, which offers the ability to infer a causal relationship between a risk factor and a certain disease by using genetic markers as a proxy for a modifiable risk factor (11), have not yet been applied to study the associations between liver fat and CKD-related renal outcomes such as microalbuminuria, and impaired renal function. Our aim was to study the separate contributions of liver fat and visceral fat to microalbuminuria in the general population, and whether NAFLD has a causal effect on microalbuminuria and impaired renal function (**Fig. 1**).

METHODS

Study population and study design

The present study is a cross-sectional analysis of baseline measurements of the Netherlands epidemiology of obesity (NEO) study, a population-based, prospective cohort study in 6671 men and women between 45 and 65 years at baseline (12). Men and women living in the greater area of Leiden (in the west of the Netherlands) were invited to participate in the study if they were aged between 45 and 65 years and had a self-reported body mass index (BMI) of ≥27 kg/m^2. In addition, all inhabitants from one municipality

(Leiderdorp) were invited to participate irrespective of their BMI, allowing for a reference distribution of BMI. Participants were invited to a baseline visit at the NEO study center after an overnight fast. Prior to this study visit, participants collected a morning spot of urine and completed a general questionnaire at home to report demographic, lifestyle, and clinical information. At the baseline visit, all participants underwent an extensive physical examination including anthropometry and blood sampling. Participants with potential contraindications for magnetic resonance imaging (MRI) (i.e. metallic devices, or claustrophobia) were excluded for additional imaging. Approximately 35% of the participants without potential MRI contraindications were randomly selected for assessment of abdominal visceral adipose tissue (VAT) and hepatic triglyceride content (HTGC) using MRI. Inclusion criteria were a successful measurement of VAT and HTGC. Exclusion criteria were alcohol consumption of ≥10 units per day, and missing data on urine and serum measurements, total body fat, smoking, and education. The Medical Ethical Committee of the Leiden University Medical Center (LUMC) approved the design of the study and all participants gave their written informed consent. The study was performed according to the ethical standards of the Helsinki Declaration of 1975, as revised in 2013.

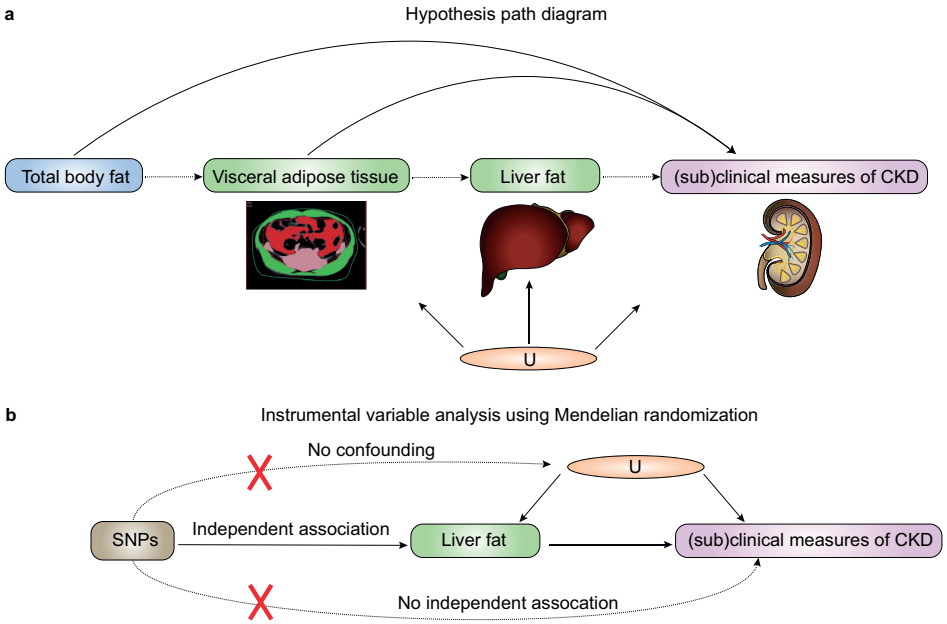

Figure 1. (a) Hypothesis path diagram. Assessed presumed effects of visceral adipose tissue and liver fat on (sub)clinical measures of CKD, and influences of confounders that are either known or unknown (U). (b) Instrumental variable analysis using Mendelian randomization. Assessed presumed effects of the instrumental variable (brown; single nucleotide polymorphism (SNP) genetic variants for non-alcoholic fatty liver disease (NAFLD)) on the exposure (green; liver fat); the instrumental variable does not associate with confounders that are either known or unknown (U).

Data collection

The participants were asked to bring all medication they were using to the study visit. All use of medication in the month preceding the study visit was recorded by research nurses. On the questionnaire, participants reported ethnicity by self-identification, tobacco smoking, highest level of education, and alcohol consumption using a food frequency questionnaire (in grams/day). In women, we grouped use of contraceptives and hormone replacement therapy into current, past and never (reference) use of estrogens. Menopausal state was categorized in pre- and postmenopausal state (reference) according to information on oophorectomy, hysterectomy and self-reported state of menopause in the questionnaire. Body weight and percent total body fat (TBF) were assessed using the Tanita bio impedance balance (TBF-310, Tanita International Division, UK).

Laboratory measurements

Fasting blood samples were drawn from the antecubital vein after 5 min rest of the participant. Serum creatinine (mg/dl) was used to calculate the estimated GFR according to the Chronic Kidney Disease Epidemiology Collaboration (CKD-EPI) formula (13). Urinary albumin-creatinine ratio (UACR) was derived from a first morning void. Microalbuminuria was defined as UACR ≥2.5 mg/mmol in men and ≥3.5 mg/mmol in women. All laboratory analyses were performed in the central clinical chemistry laboratory of the LUMC.

Magnetic resonance imaging and spectroscopy

Magnetic resonance Imaging (MRI) was performed on a 1.5 Tesla MRI scanner (Philips Medical Systems, Best, the Netherlands). Visceral fat was imaged using three transverse turbo spin echo slices at the level of the fifth lumbar vertebra (repetition time 300 ms; echo time 20 ms; flip angle 90°; slice thickness 10 mm, slice gap 2 mm). VAT was quantified by converting the number of pixels to square cm for all three slides using in-house-developed software (MASS, Medis, Leiden, the Netherlands), and the mean VAT areas of the three slides was calculated and used in the analyses. Cross-sectional images at the level of the fifth lumbar vertebra are highly correlated to total volumes and thus validly represent total VAT (14,15). Hepatic triglyceride content (HTGC) was quantified by proton magnetic resonance spectroscopy (^{1}H-MRS) of the liver using the point-resolved spectroscopy sequence (16). An 8 ml voxel was positioned in the right lobe of the liver, avoiding gross vascular structures and adipose tissue depots. Spectra were obtained with an echo time of 26 ms and a repetition time of 3,000 ms, and 64 averages were collected with water suppression. Data points were collected using a 1,000 Hz spectral line. Without changing any parameters, spectra without water suppression, with a repetition time of 10 seconds, and with four averages were obtained as an internal reference. Spectral data were fitted using Java-based magnetic resonance user interface software (jMRUI version 2.2, Leuven, Belgium; http://www.jmrui.eu) (17,18). HTGC relative to water was calculated

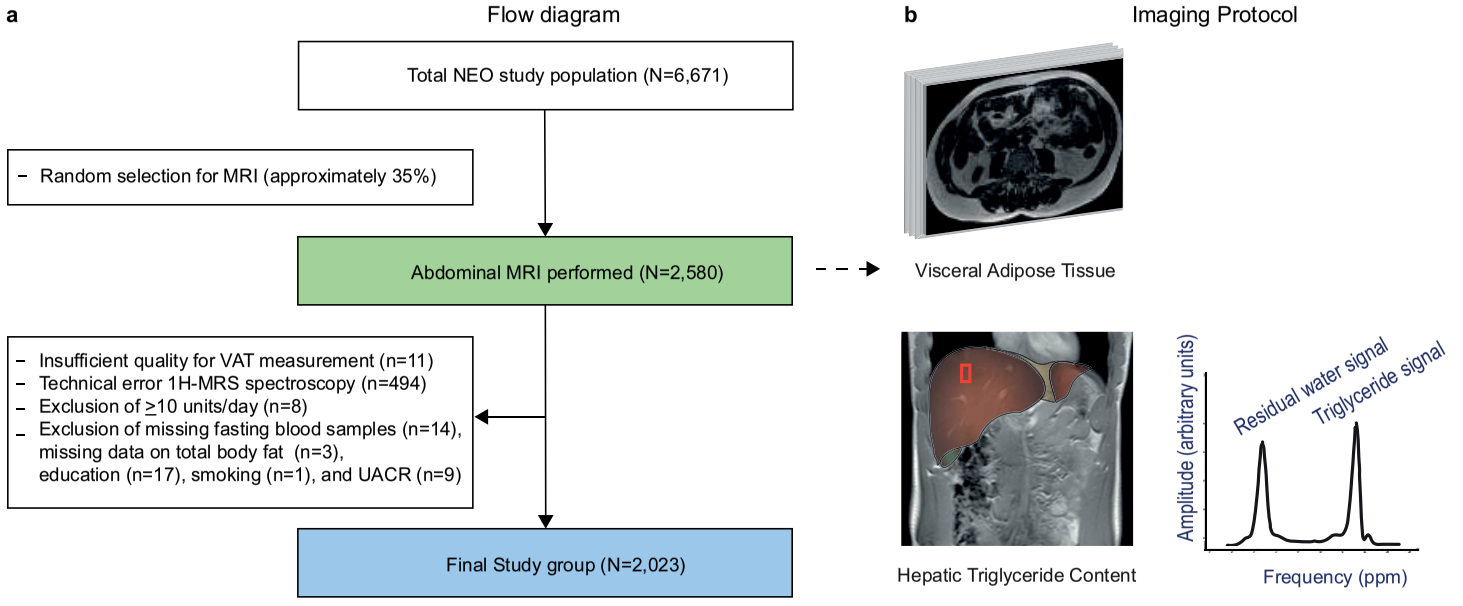

Figure 2. Flow diagram and imaging protocol of the study. (a) Shows the flow diagram of the total Netherlands Epidemiology of Obesity study population. (b) Overview of the imaging protocol consisting of measurement of visceral adipose tissue (upper row: area in red) and hepatic triglyceride content (lower row: right panel, ^{1}H-MRS voxel in red placed in right liver lobe; left panel, obtained liver spectrum with metabolite frequency relative to water frequency in parts per million).

as (signal amplitude of triglyceride [arbitrary unit]) / (signal amplitude of water [arbitrary unit]) x 100%. A short overview of the imaging protocol is visualized in **Figure 2b**.

Statistical analyses

In the NEO study individuals with a BMI of 27 kg/m^2 or higher were oversampled. First, inhabitants of Leiden and its surroundings between 45 and 65 years of age and with a self-reported BMI of 27 kg/m² or higher were invited to participate in the NEO study. In addition, we included a reference population. To that extent, all inhabitants between 45 and 65 years living in one municipality, Leiderdorp, were asked to participate irrespective of their BMI. This resulted in an additional sample of 1,671 participants with a BMI distribution that was similar to the BMI distribution of the general Dutch population (19). If inference is made on the general population, the overrepresentation of overweight and obese participants in the NEO study may introduce bias, because of the skewed BMI distribution in the NEO population. Weighting towards the BMI distribution of the general population may solve this problem (20). Using the BMI distribution of the reference population, we calculated weight factors for the NEO study, resulting in a higher weight factor for participants with a lower BMI (21). Use of sampling weights yields results that apply to a population-based study without oversampling of individuals with a high BMI (22). Data are presented as mean (SD), median (25th, 75th percentiles) or as percentage, and stratified by fatty liver, defined as a HTGC as 5.56% (10). We calculated population-based Z-scores and standardized the values of visceral fat and liver fat to a mean of zero with a SD of one. Population-based Z-scores are a widely used method for analyzing anthropometric data, as the calculated Z-scores are likely to be normally distributed and thus allow for the use of analysis methods that assume normality such as regression (23). With linear regression analysis we examined associations between visceral fat and liver fat (determinants), and eGFR and UACR (outcome variables). Because of skewed distributions we used the natural logarithm of UACR in the regression analyses. For interpretation of the results, we back-transformed the regression coefficients towards percentages increase: (exp(beta) – 1)*100 with 95% confidence intervals per standard deviation of VAT and HTGC. In addition, we performed logistic regression analyses and calculated odds ratios (ORs) with 95% confidence intervals of microalbuminuria or impaired renal function (<60 ml/min/1.73m²). Crude associations were adjusted for age, sex, ethnicity, education, tobacco smoking, alcohol consumption, fasting state during MRI, and in women additionally for current use of estrogens and menopausal state. Since abdominal fat is strongly related with total body fat, for the study of specific effects of abdominal fat it is important to adjust the associations for total body fat (24). Therefore, all models were additionally adjusted for total body fat. To examine the separate contributions of VAT and HTGC we performed joint models and simultaneously included VAT and HTGC into the models. To investigate whether associations were different between men and women, we repeated all analyses

separately for men and women. The above mentioned analyses were performed with STATA Statistical Software (Statacorp, College Station, Texas, USA), version 12.0.

Selection of genetic instruments and Mendelian randomization approach

Genetic instrumental variables for NAFLD were selected from the largest GWAS meta-analysis on computed tomography (CT) measured hepatic steatosis in individuals of European ancestry to date (25). Of the 46 variants showing suggestive statistical evidence of association with CT hepatic steatosis, four were also significantly associated with histological evidence for NAFLD. These four variants were selected as genetic proxies for NAFLD, and were each located in the following genes *PNPLA3* (rs738409), *LYPLAL1* (rs12137855), *NCAN* (rs2228603), and *GCKR* (rs780094). These variants explained 2.4, 0.2, 0.8, and 0.2 of the variation in CT hepatic steatosis, respectively (25). We subsequently extracted information on the association between these variants and (sub)clinical measures of CKD from summary-level datasets from published European-descent GWAS meta-analyses on eGFR (sex- and age-adjusted residuals of eGFR based on serum creatinine, in up to 118,460 non-diabetic individuals) (26), microalbuminuria (defined as UACR ≥2.5 mg/mmol in men and ≥3.5 mg/mmol in women, using sex-specific residuals, in up to 54,116 individuals) (27), and impaired renal function (defined as eGFR <60 ml min^{-1} per 1.73 m^2, in up to 118,147 individuals, analyses adjusted for sex and age) (26). Specifically, we extracted per-allele beta estimates as well as accompanying standard errors for the four instruments from datasets publicly available on the CKDgen consortium website (http://ckdgen.imbi.uni-freiburg.de/). The studies contributing to these GWAS meta-analyses had also adjusted for study-specific covariates including study center, principal components of ancestry, and family-based studies accounted for relatedness. While we could not precisely determine the sample overlap between the GWAS on NAFLD and those on microalbuminuria and impaired renal function, this may have been up to 13% for CKD, 14% for eGFR, and 18% for microalbuminuria, all with respect to the larger dataset.

Subsequently, to estimate the causal effect of NAFLD on (sub)clinical measures of CKD, we performed an inverse-variance weighted (IVW) linear regression of SNP-outcome associations on SNP-exposure associations, with the intercept constrained to zero (28). The SNP-exposure estimates were defined as the per-allele regression coefficient for presence of histological evidence for non-alcoholic steatohepatitis (log-odds) (25). We rescaled the causal effect estimates such that they represent effect on the outcome per doubling of the odds for histologically proven NAFLD in the population, by multiplying the causal effect estimate from the IVW-regression by 0.693 (i.e. $\log_e 2$). As *GCKR* likely has pleiotropic effects on glucose metabolism, we also calculated the causal effect estimates without excluding *GCKR* as a sensitivity analysis. Mendelian Randomization analyses were performed in R version 3.4.3, Vienna, Austria. 2016] using the TwoSample MR R-package.

Table 1. Characteristics of participants stratified by liver fat (n=2,023)

Characteristic	HTGC≤5.56 (71%)	HTGC>5.56 (29%)
Age (years)	55 (5)	57 (7)
Sex (% women)	59	38
Menopausal state (% postmenopausal)	54	72
Ethnicity (% white)	96	96
Current smoker (%)	15	12
Former smoker (%)	42	54
Body mass index (kg/m²)		
men	25.6 (2.4)	28.2 (4.3)
women	24.4 (3.3)	28.8 (6.3)
Waist circumference (cm)		
men	94.3 (7.6)	102.5 (12.2)
women	82.9 (9.4)	95.8 (15.5)
Total body fat (%)		
men	22.8 (4.0)	27.4 (6.7)
women	34.8 (5.4)	41.2 (7.0)
Visceral adipose tissue (cm²)		
men	95.1 (39.9)	144.3 (71.7)
women	55.4 (28.8)	109.1 (65.8)
Hepatic triglyceride content (%)		
men	2.4 (1.54, 3.51)	11.0 (7.23, 17.11)
women	1.5 (1.02, 2.40)	11.0 (7.07, 19.00)
Alcohol consumption (g/d)	12.8 (11.4)	18.4 (23.4)
Hypertension (%)	31	47
Cardiovascular disease (%)	4	6
Type 2 diabetes (%)	2	11
Glucose lowering therapy (%)	1	5
Antihypertensives (%)	15	31
ACE inhibitors/Angiotensin-II antagonists (%)	8	19
Statins (%)	6	15
Current use of sex hormones* (%)	11	2
Serum creatinine (µmol/L)	76.6 (12.8)	78.7 (17.0)
eGFR CKD-epi (mL/min/1.73m²)	86.1 (10.8)	86.6 (14.8)
eGFR >90 mL/min/1.73m²	42	43
eGFR 60-90 mL/min/1.73m²	56	56
eGFR <60 mL/min/1.73m²	2	1
UAE (mg/L)	3.55 (2.99, 4.52)	3.78 (2.99, 5.11)
UACR(mmol/mg)	0.43 (0.30, 0.66)	0.42 (0.28, 0.66)
Microalbuminuria (%)	1	3

Results were based on analyses weighted toward the BMI distribution of the general population (n=2,023; 1,052 men, 971 women). Continuous variables are expressed as %, means (standard deviation) or medians (25^{th}, 75^{th} percentile). Sex hormone use by woman*; contraceptive pill or hormone replacement therapy. Microalbuminuria was defined as UACR ≥2.5 mg/mmol for men and ≥3.5 mg/mmol for woman. ACE, angiotensin-converting-enzyme; eGFR, estimated Glomerular Filtration Rate according to the CKD-epi formula; HTGC, hepatic triglyceride content; UAE, urinary albumin excretion; UACR, urinary albumin creatinine ratio.

Table 2. Differences in UACR with 95% confidence intervals and eGFR per SD of visceral fat and liver fat

	Percent difference (95% CI) UACR		
Determinant	**Total population**	**Men**	**Women**
VAT (SD=55.4cm^2)			
Crude	-4 (-8, 0)	3 (-2, 8)	7 (0, 15)
Multivariate	1 (-3, 6)	0 (-4, 5)	4 (-3, 11)
+ TBF	5 (-1, 12)	2 (-5, 8)	13 (1, 27)
+ HTGC	5 (-1, 12)	1 (-6, 8)	14 (1, 28)
HTGC (SD=7.9%)			
Crude	0 (-4, 4)	3 (-3, 8)	3 (-3, 9)
Multivariate	1 (-3, 5)	2 (-3, 7)	1 (-5, 7)
+ TBF	3 (-2, 7)	2 (-3, 8)	2 (-4, 9)
+ VAT	2 (-3, 6)	2 (-3, 8)	0 (-7, 6)
	Difference (95% CI) per ml/min/1.73m² lower eGFR		
Determinant	**Total population**	**Men**	**Women**
VAT (SD=55.4cm^2)			
Crude	0.52 (-0.12, 1.17)	0.33 (-0.58, 1.24)	1.25 (0.12, 2.39)
Multivariate	0.17 (-0.56, 0.90)	0.18 (-0.76, -1.12)	0.30 (-0.89, 1.49)
+ TBF	0.30 (-0.65, 1.24)	0.76 (-0.39, 1.92)	-0.12 (-1.79, 1.55)
+ HTGC	0.52 (-0.46, 1.50)	0.99 (-0.18, 2.15)	0.06 (-1.67, 1.79)
HTGC (SD=7.9%)			
Crude	-0.19 (-0.79, 0.41)	-0.65 (-1.41, 0.10)	0.25 (-0.64, 1.14)
Multivariate	-0.42 (-1.03, 0.19)	-0.72 (-1.48, 0.04)	-0.11 (-1.03, 0.81)
+ TBF	-0.49 (-1.14, 0.16)	-0.65 (-1.46, 0.15)	-0.29 (-1.26, 0.68)
+ VAT	-0.60 (-1.29, 0.09)	-0.84 (-1.69, 0.01)	-0.31 (-1.31, 0.70)

Results were based on analyses weighted toward the BMI distribution of the general population (n=2,023; 1,052 men, 971 women). Results were derived from beta coefficients (β) with 95% confidence intervals from linear regression analyses and are expressed as percentages increase or decrease in UACR (mg/mmol) or as difference in lower eGFR (ml/min/1.73m²) per standard deviation in visceral adipose tissue (VAT) or hepatic triglyceride content (HTGC). Multivariate analysis was adjusted for age, sex, ethnicity, education, tobacco smoking, alcohol consumption, fasting state during ^{1}H-MRS, and in women additionally adjusted for current use of estrogens and menopausal state.

RESULTS

Baseline characteristics

Of the 6,671 included participants, 2,580 participants without potential contraindications for MRI were randomly selected to undergo abdominal imaging. In 11 participants, the images were of insufficient quality for the quantification of VAT. In another 494 participants, ^{1}H-MRS of the liver was not available owing to technical errors, exceeded scan time, or claustrophobia. In addition, we excluded 8 participants who reported to consume more than 10 units of alcohol per day. Finally, we consecutively excluded participants with missing fasting blood samples (n=14), and missing data for total body fat

Table 3. Odds ratio's with 95% confidence intervals for risk of microalbuminuria and impaired renal function per SD change in visceral fat and liver fat

	OR (95% CI) for microalbuminuria		
Determinant	**Total population**	**Men**	**Women**
VAT (SD=55.4cm^2)			
Crude	1.54 (1.19, 1.99)	1.76 (1.32, 2.34)	1.87 (1.31, 2.65)
Multivariate	1.75 (1.34, 2.30)	1.66 (1.19, 2.33)	1.92 (1.19, 3.09)
+ TBF	2.16 (1.29, 3.61)	1.71 (0.95, 3.08)	3.03 (1.51, 6.08)
+ HTGC	2.02 (1.18, 3.47)	1.65 (0.88, 3.09)	2.83 (1.44, 5.56)
HTGC (SD=7.9%)			
Crude	1.34 (1.05, 1.72)	1.46 (1.06, 2.01)	1.30 (0.94, 1.81)
Multivariate	1.36 (1.05, 1.76)	1.36 (0.96, 1.93)	1.32 (0.98, 1.77)
+ TBF	1.34 (1.02, 1.77)	1.26 (0.83, 1.93)	1.35 (0.96, 1.89)
+ VAT	1.20 (0.85, 1.70)	1.17 (0.69, 1.98)	1.13 (0.76, 1.69)
	OR (95% CI) for impaired renal function		
Determinant	**Total population**	**Men**	**Women**
VAT (SD=55.4cm^2			
Crude	1.02 (0.75, 1.37)	0.80 (0.40, 1.59)	1.52 (1.09, 2.13)
Multivariate	1.00 (0.64, 1.56)	0.69 (0.32, 1.49)	1.40 (0.84, 2.34)
+ TBF	1.10 (0.75, 1.63)	1.10 (0.63, 1.90)	1.35 (0.74, 2.47)
+ HTGC	1.25 (0.83, 1.87)	1.24 (0.64, 2.38)	1.56 (0.86, 2.84)
HTGC (SD=7.9%)			
Crude	0.74 (0.52, 1.05)	0.28 (0.11, 0.73)	0.99 (0.77, 1.27)
Multivariate	0.71 (0.45, 1.12)	0.23 (0.06, 0.88)	0.92 (0.64, 1.32)
+ TBF	0.70 (0.47, 1.04)	0.39 (0.17, 0.89)	0.83 (0.58, 1.19)
+ VAT	0.65 (0.42, 0.99)	0.36 (0.14, 0.94)	0.74 (0.50, 1.09)

Results were based on analyses weighted toward the BMI distribution of the general population (n=2,023; 1,052 men, 971 women). Results were derived from logistic regression analyses and ORs with 95% confidence intervals are expressed per standard deviation in visceral adipose tissue (VAT) or hepatic triglyceride content (HTGC). Multivariate analysis was adjusted for age, sex, ethnicity, education, tobacco smoking, alcohol consumption, fasting state during ^{1}H-MRS, and in women additionally adjusted for current use of estrogens and menopausal state. Microalbuminuria was defined as UACR ≥2.5 mg/mmol for men and ≥3.5 mg/mmol for woman. Impaired renal function was defined as eGFR <60 ml/min/1.73m².

(n=3), smoking (n=1), UACR (n=9) and education (n=17) (see flow diagram, **Fig 2a**). After these exclusions, 2,023 participants (1,052 men and 971 women) were included in the present analysis with a mean (SD) age of 55.5 (6.0) years (range 44-66 years) and 53% were women. For the total population, mean BMI was 25.9 (4.0) kg/m^2, and mean eGFR was 86.2 (12.2) ml/min/1.73m². Microalbuminuria was present in 1.9% (UACR ≥2.5 mg/mmol in men and ≥3.5 mg/mmol in women) and 0.1% of the total study sample had UACR levels ≥25 mg/mmol in men and ≥35 mg/mmol in women. 1.5% of the total study population had both diabetes and microalbuminuria. Mildly to moderately impaired renal function (eGFR ≤60 ml/min/1.73m^2) was present in 2.0% of the study population. The baseline

Table 4. Per-allele effect of genetic instruments for NAFLD, and inverse-variance weighted Mendelian randomization estimators, on renal function, microalbuminuria, and impaired renal function

Outcome	Locus	SNP	Effect allele	OR for NAFLD	Effect estimate (95% CI)	*P*
$eGFR_{crea}$ (log-transformed)	PNPLA3	rs738409	G	3.24	-0.0016 (-0.0038, 0.0006)	0.14
	LYPLAL1	rs12137855	C	1.21	-0.0004 (-0.0026, 0.0018)	0.71
	NCAN	rs2228603	T	1.9	-0.0020 (-0.0055, 0.0015)	0.27
	GCKR	rs780094	T	1.18	0.0063 (0.0045, 0.0081)	**$4.8x10^{-12}$**
N_{max} 118,460		Causal effect estimator			-0.0004 (-0.005, 0.004)	0.87
Micro-albuminuria (odds ratio)	PNPLA3	rs738409	G	3.24	0.97 (0.93, 1.02)	0.31
	LYPLAL1	rs12137855	C	1.21	0.97 (0.93, 1.02)	0.29
	NCAN	rs2228603	T	1.9	1.05 (0.97, 1.14)	0.23
	GCKR	rs780094	T	1.18	1.09 (1.04, 1.13)	**$4.9x10^{-05}$**
N_{max} 54,116		Causal effect estimator			1.00 (0.93, 1.07)	0.97
Impaired renal function (odds ratio)	PNPLA3	rs738409	G	3.24	1.03 (0.99, 1.07)	0.13
	LYPLAL1	rs12137855	C	1.21	0.99 (0.97, 1.05)	0.57
	NCAN	rs2228603	T	1.9	1.01 (0.95, 1.07)	0.73
	GCKR	rs780094	T	1.18	0.98 (0.95, 1.01)	0.20
N_{max} 118,147		Causal effect estimator			1.01 (0.99, 1.03)	0.21

NAFLD denotes non-alcoholic fatty liver disease; eGFRcrea, estimated glomerular filtration rate based on serum creatinine, using sex-and age-adjusted residuals of logarithm; CKD, chronic kidney disease. Data presented as per-allele effect on outcome for odds-for-NAFLD (i.e. histological evidence of NAFLD) increasing allele. Per-allele effect on biopsy-proven NAFLD (odds ratio) as observed by Speliotes et al (23).
The causal effect estimates were calculated using inverse-variance weighted regression of SNP-outcome on SNP-exposure estimates, with the intercept constrained to zero, and can be interpreted as the change in the outcome (or odds ratio for CKD and microalbuminuria) per doubling in the odds of NAFLD in the population.

characteristics of these participants are shown in Table 1, and flow diagram and scan protocol are shown in **Figure 2**.

Associations between visceral fat, liver fat, microalbuminuria and impaired renal function

Results of linear regression analyses showing the differences in UACR and eGFR per SD in visceral fat and liver fat are provided in **Table 2**. In crude analysis, no associations were found for both VAT (per SD=55.4cm^2, -4 percent difference, 95% CI -8, 0) and HTGC (per SD=7.9%, 0 percent difference, 95% CI -4, 4) with UACR in the total population. After adjustment for confounding factors including HTGC, the association for VAT and UACR was +5 percent difference per SD in VAT (95% CI -1, 12). The associations between HTGC and UACR was 2 percent difference in adjusted analysis per SD in HTGC (95% CI -3, 6). In the sex-stratified adjusted analysis, VAT was associated with UACR in women only (per SD 14 percent difference, 95% CI 1, 28).

Regarding renal function, in crude analysis VAT was significantly associated with lower eGFR in women (per SD 1.25 ml/min/1.73m^2, 95% CI 0.12, 2.39), but not in men (per SD 0.33 ml/min/1.73m^2, 95% CI -0.58, 1.24). No associations were found between HTGC and renal function for both men (per SD -0.65 ml/min/1.73m^2, 95% CI-1.41, 0.10) and women (per SD 0.25 ml/min/1.73m^2, 95% CI -0.64, 1.14) in unadjusted analyses. In adjusted analyses, neither VAT (per SD 0.52 ml/min/1.73m^2, 95% CI -0.46, 1.50) nor HTGC (per SD -0.60 ml/min/1.73m^2, 95% CI -1.29, 0.09) were associated with renal function (**Table 2**).

Results of logistic regression analyses for the associations between visceral fat and liver fat with the risk of microalbuminuria and impaired renal function are provided in **Table 3**. In crude analysis, per SD change in VAT the OR for microalbuminuria was 1.54 (95% CI 1.19, 1.99) and 1.34 (95% CI 1.05, 1.72) per SD in HTGC. In adjusted models, VAT was associated with a two-fold increased risk of microalbuminuria (OR=2.02, 95% CI 1.18, 3.47), whereas for HTGC the OR of microalbuminuria per SD change was 1.20 (95% CI 0.85, 1.70). In sex-stratified analysis, VAT was associated with microalbuminuria in women (OR=2.83, 95% CI 1.44, 5.56), but not in men, and HTGC was not associated with microalbuminuria in either sex (**Table 3**). For renal function, no associations were found for both VAT and HTGC with the risk of impaired renal function in crude analysis and adjusted analysis. In sex-stratified adjusted models, per SD in HTGC the OR of impaired renal function was 0.36 (95% CI 0.14, 0.94) in men, and 0.74 (95% CI 0.50, 1.09) in women.

Mendelian randomization analyses

Using publicly available data of four genetic instruments for histological evidence of NAFLD, only the lead variant for GCKR (rs780094) showed statistically significant per-allele effects on impaired renal function and presence of microalbuminuria (**Table 4**). However, combining the genetic instruments, we did not observe any evidence of a causal effect of histologically proven NAFLD on any of the CKD-related renal outcomes (**Table 4**), also after excluding the instrument for *GCKR* (data not shown).

DISCUSSION

In our observational analyses, visceral fat was associated with microalbuminuria in women (but not in men), although an association with impaired renal function was not found. Liver fat was not associated with microalbuminuria or renal function in either sex, which was supported by our Mendelian randomization analyses showing no evidence for a causal relationship between liver fat and microalbuminuria or impaired renal function.

Our findings suggest that visceral fat is more important in the etiology of microalbuminuria than liver fat and supports the hypothesis that microalbuminuria might be a manifestation of visceral adiposity (4). Possible mechanisms linking visceral adiposity to

microalbuminuria and renal dysfunction, include higher levels of adipokines, leptin, and resistin (29,30). In addition, the free fatty acid flux of visceral fat and liver fat possibly predisposes to insulin resistance and microalbuminuria (31). The combined Framingham Offspring and MDCT cohort previously investigated the association of SAT/VAT on prevalent CKD, found that neither VAT nor SAT (assessed by computed tomography) was independently associated with CKD, using eGFR based on the creatinine-based MDRD equation (32). However, in a subsequent study VAT was associated with microalbuminuria in men, whereas SAT was more associated with microalbuminuria in women (33). In our study, the association between VAT and microalbuminuria was mainly driven by the association in women, suggesting a possible sex difference in the association of visceral fat with microalbuminuria. This is supported by previous research showing stronger relations between visceral fat and cardiometabolic outcomes in women than in men (34–36). Although, the underlying pathophysiology of this difference is still not yet fully understood and merits further study, the smaller amount of visceral fat depot in women, and the influence of sex hormones on the regulation of adipose tissue distribution and function, are likely involved (37). In men the results for VAT and microalbuminuria were not statistically significant, and might be due to the lack statistical power considering the limited amount of participants with microalbuminuria. This indicates the need for larger studies to further elucidate the association between VAT and microalbuminuria in men.

Although our study supports the link between visceral fat and microalbuminuria, our study did not show any associations between VAT or liver fat with renal function, which could be explained by the limited number of participants with an eGFR below 60 ml/min/1.73m^2 in our sample. Furthermore, it can be argued whether the use of ACE inhibitors/Angiotensin-II antagonists may confound the results, additional adjustment for ACE inhibitors/Angiotensin-II antagonists did not markedly change the results (**Supplementary Table 1**).

In our Mendelian randomization analysis only the lead variant for *GCKR* showed evidence for causal effects of NAFLD on impaired renal function and presence of microalbuminuria. However, the lead variant for *GCKR* is also known to be involved in glucose metabolism, and diabetic nephropathy (38). Our results thus do not support the hypothesis that liver fat by itself is causally related to CKD-related renal outcomes. In contrast, a recent meta-analysis estimated that NAFLD is associated with a nearly 40% increase in the long-term risk of incident CKD (8), albeit none of the included studies adjusted for VAT nor used gold standard techniques such as ^{1}H-MRS for the measurement of ectopic lipids. A recent small (n=400) Chinese study evaluating the association between liver fat measured by ^{1}H-MRS however, did show that NAFLD was independently associated with CKD after adjustment for VAT (39). We were not able to perform a Mendelian randomization analysis for VAT, since the most recent GWAS meta-analysis on VAT was unable to identify genome-wide significant VAT-specific SNPs (40). Future large-scale GWAS studies

are needed to identify the genetic variants of VAT before investigating the causal relationship between visceral fat and CKD.

Besides combining observational research with Mendelian randomization analysis, one of the major strengths of the present study is the use of magnetic resonance spectroscopy for the measurement of hepatic triglyceride content in over two thousand individuals, which is considered the gold standard technique for the non-invasive measurement of liver fat (41). Previous studies showed that the presence of NAFLD was associated with an increased risk of CKD were limited by the relatively small sample size of biopsy proven NAFLD and by the suboptimal sensitivity of ultrasound and/or liver enzyme elevations for the detection of NAFLD in population-based studies (8). Moreover, these studies did not take VAT into account, and anthropometric indices such as BMI and WC poorly predict the volumes of internal body fat compartments, which could lead to underestimation of associations with chronic disease risks (42).

There are several limitations that need to be considered. First, as we use data of a population-based cohort, our study consists of relatively healthy participants and the prevalence of microalbuminuria and moderately to severely impaired renal function is very low. Because of these low numbers we decided not to make a distinction between microalbuminuria and macroalbuminuria (UACR levels ≥25 mg/mmol in men and ≥35 mg/mmol in women) as macroalbuminuria was virtually absent in the study sample. Another limitation is the use of first morning urine void samples rather than 24-h urine collection in the present study. However, previous studies have shown that albuminuria measures derived from first morning voids are a reliable alternative to 24-h urine albumin excretion and UACR is more reliable than urinary albumin excretion for the assessment of microalbuminuria in spot urine samples (43). Furthermore, although the CKD-EPI formula has proven to be more accurate and precise for estimating renal function than the older MDRD formula, it has not been validated ≥90 ml/min/1.73m² (13). Also the error of eGFR in the normal to high range of renal function is quite substantial (44). These limitations of eGFR could also be the explanation for the found contradictory association between HTGC and lower risk of impaired renal function in men. In this study visceral fat and liver fat were quantified at 1.5T using conventional non-water-saturated T1 weighted images and ^{1}H-MRS respectively. However use of advanced multiecho techniques that generate fat-only MR images, and use of high field strength MRI scanners might have improved measurement accuracy and precision (45). Moreover, recent technical advances have also enabled non-invasive quantification of renal sinus fat volume, pararenal fat, and intra-renal triglyceride content (46,47), which are other potentially important ectopic fat compartments related to the kidney (e.g. fatty kidney) (48). Especially pararenal fat is of great interest considering this is an location that in adults consists mainly of dormant brown adipose tissue which could be potentially reactivated into active brown adipose, a potential strategy for combatting obesity and metabolic disease including

obesity-related renal disease (49). In addition, future studies are needed investigating the potential mechanisms underlying the association between visceral fat and microalbuminuria. Adipocyte-derived hormones and cytokines leading to low-grade inflammatory state may play a role in this.

In conclusion, in observational analyses visceral fat was associated with microalbuminuria in women (but not in men), although an association with impaired renal function was not found. Liver fat was not associated with microalbuminuria or renal function in either sex, which was supported by our Mendelian randomization analyses showing no evidence for a causal relationship between liver fat and microalbuminuria or impaired renal function. Future Mendelian randomization studies are needed to investigate the causality between visceral fat and CKD.

Practical applications

Our study indicates that visceral fat might be more important in the etiology of obesity-related renal disease rather than liver fat. In addition, Mendelian randomization analysis did not support a causal relation between liver fat and renal outcomes, suggesting that liver fat plays a less important role in the risk of CKD than previously suspected. The findings with regard to visceral fat, support the importance of body composition assessment in renal disease.

REFERENCES

1. Targher G, Byrne CD. Non-alcoholic fatty liver disease: an emerging driving force in chronic kidney disease. Nat Rev Nephrol. 2017;13(5):297–310.
2. Armstrong MJ, Adams LA, Canbay A, Syn W-K. Extrahepatic complications of nonalcoholic fatty liver disease. Hepatology. 2014;59(3):1174–1197.
3. Palatini P. Glomerular hyperfiltration: a marker of early renal damage in pre-diabetes and pre-hypertension. Nephrol Dial Transplant. 2012;27(5):1708–1714.
4. Foster MC, Hwang S-J, Massaro JM, et al. Association of subcutaneous and visceral adiposity with albuminuria: the Framingham Heart Study. Obesity. 2011;19(6):1284–1289.
5. Romero-Corral A, Sert-Kuniyoshi FH, Sierra-Johnson J, et al. Modest Visceral Fat Gain Causes Endothelial Dysfunction in Healthy Humans. J Am Coll Cardiol. 2010;56(8):662–666.
6. Fontana L, Eagon JC, Trujillo ME, Scherer PE, Klein S. Visceral fat adipokine secretion is associated with systemic inflammation in obese humans. Diabetes. American Diabetes Association; 2007;56(4):1010–1013.
7. Van Gaal LF, Mertens IL, De Block CE. Mechanisms linking obesity with cardiovascular disease. Nature. 2006;444(7121):875–880.
8. Mantovani A, Zaza G, Byrne CD, et al. Nonalcoholic fatty liver disease increases risk of incident chronic kidney disease: A systematic review and meta-analysis. Metabolism. 2018;79:64–76.
9. Liu J, Fox CS, Hickson D, Bidulescu A, Carr JJ, Taylor HA. Fatty liver, abdominal visceral fat, and cardiometabolic risk factors: the Jackson Heart Study. Arterioscler Thromb Vasc Biol. 2011;31(11):2715–2722.
10. Szczepaniak LS, Nurenberg P, Leonard D, et al. Magnetic resonance spectroscopy to measure hepatic triglyceride content: prevalence of hepatic steatosis in the general population. Am J Physiol Metab. 2005;288(2):E462–E468.
11. Davey Smith G, Ebrahim S. 'Mendelian randomization': can genetic epidemiology contribute to understanding environmental determinants of disease?*. Int J Epidemiol. 2003;32(1):1–22.
12. de Mutsert R, den Heijer M, Rabelink TJ, et al. The Netherlands Epidemiology of Obesity (NEO) study: study design and data collection. Eur J Epidemiol. 2013;28(6):513–523.
13. Levey AS, Stevens LA, Schmid CH, et al. A new equation to estimate glomerular filtration rate. Ann Intern Med. 2009;150(9):604–612.
14. Schweitzer L, Geisler C, Pourhassan M, et al. What is the best reference site for a single MRI slice to assess whole-body skeletal muscle and adipose tissue volumes in healthy adults? Am J Clin Nutr. 2015;102(1):58–65.
15. Han TS, Kelly IE, Walsh K, Greene RM, Lean ME. Relationship between volumes and areas from single transverse scans of intra-abdominal fat measured by magnetic resonance imaging. Int J Obes Relat Metab Disord. 1997;21(12):1161–1166.
16. Bottomley PA. Spatial localization in NMR spectroscopy in vivo. Ann N Y Acad Sci. 1987;508:333–348.

17. Naressi A, Couturier C, Devos JM, et al. Java-based graphical user interface for the MRUI quantitation package. 2001;12(2–3):141–152.

18. Stefan D, Cesare F Di, Andrasescu A, et al. Quantitation of magnetic resonance spectroscopy signals: the jMRUI software package. Meas Sci Technol. 2009;20(10):104035.

19. Ministerie van, V W S [Dutch Ministry of Health, Welfare and S. Hoeveel Mensen Hebben Overgewicht? [How many people are overweight?]. 2013.

20. Korn EL, Graubard BI. Epidemiologic studies utilizing surveys: accounting for the sampling design. Am J Public Health. 1991;81(9):1166–1173.

21. Dekkers IA, de Mutsert R, de Vries APJ, et al. Determinants of impaired renal and vascular function are associated with elevated levels of procoagulant factors in the general population. J Thromb Haemost. 2018;16(3):519–528.

22. Lumley T. Analysis of Complex Survey Samples. J Stat Softw. 2004;9(8):1–19http://www.jstatsoft.org/v09/i08/. Accessed March 9, 2019.

23. Gorstein J, Sullivan K, Yip R, et al. Issues in the assessment of nutritional status using anthropometry. Bull World Health Organ. 1994;72(2):273-83.

24. Seidell JC, Bouchard C. Visceral fat in relation to health: is it a major culprit or simply an innocent bystander? Int J Obes Relat Metab Disord. 1997;21(8):626–631.

25. Speliotes EK, Yerges-Armstrong LM, Wu J, et al. Genome-wide association analysis identifies variants associated with nonalcoholic fatty liver disease that have distinct effects on metabolic traits. PLoS Genet. 2011;7(3):e1001324.

26. Pattaro C, Teumer A, Gorski M, et al. Genetic associations at 53 loci highlight cell types and biological pathways relevant for kidney function. Nat Commun. 2016;7:10023.

27. Teumer A, Tin A, Sorice R, et al. Genome-wide Association Studies Identify Genetic Loci Associated With Albuminuria in Diabetes. Diabetes. 2016;65(3):803–817.

28. Burgess S, Butterworth A, Thompson SG. Mendelian randomization analysis with multiple genetic variants using summarized data. Genet Epidemiol. 2013;37(7):658–665.

29. Wajchenberg BL. Subcutaneous and Visceral Adipose Tissue: Their Relation to the Metabolic Syndrome. Endocr Rev. 2000;21(6):697–738.

30. Guerre-Millo M. Adipose tissue hormones. J Endocrinol Invest. 2002;25:855–861.

31. Votruba SB, Jensen MD. Regional Fat Deposition as a Factor in FFA Metabolism. Annu Rev Nutr. 2007;27(1):149–163.

32. Young JA, Hwang S-J, Sarnak MJ, et al. Association of Visceral and Subcutaneous Adiposity with Kidney Function. Clin J Am Soc Nephrol. 2008;3:1786–1791.

33. Teumer A, Tin A, Sorice R, et al. Genome-wide Association Studies Identify Genetic Loci Associated With Albuminuria in Diabetes. Diabetes. 2016;65(3):803–817.

34. de Mutsert R, Gast K, Widya R, et al. Associations of Abdominal Subcutaneous and Visceral Fat with Insulin Resistance and Secretion Differ Between Men and Women: The Netherlands Epidemiology of Obesity Study. Metab Syndr Relat Disord. 2018;16(1):54–63.

35. Hanley AJG, Wagenknecht LE, Norris JM, et al. Insulin resistance, beta cell dysfunction and visceral adiposity as predictors of incident diabetes: the Insulin Resistance Atherosclerosis Study (IRAS) Family study. Diabetologia. 2009;52(10):2079–2086.

36. Foster MC, Hwang S-J, Massaro JM, et al. Association of Subcutaneous and Visceral Adiposity With Albuminuria: The Framingham Heart Study. Obesity. 2011;19(6):1284–1289.

37. Geer EB, Shen W. Gender differences in insulin resistance, body composition, and energy balance. Gend Med. 2009;6:60–75.

38. Bonetti S, Trombetta M, Boselli ML, et al. Variants of GCKR affect both β-cell and kidney function in patients with newly diagnosed type 2 diabetes: the Verona newly diagnosed type 2 diabetes study 2. Diabetes Care. American Diabetes Association; 2011;34(5):1205–1210.

39. Pan L-L, Zhang H-J, Huang Z-F, et al. Intrahepatic triglyceride content is independently associated with chronic kidney disease in obese adults: A cross-sectional study. Metabolism. 2015;64(9):1077–1085.

40. Chu AY, Deng X, Fisher VA, et al. Multiethnic genome-wide meta-analysis of ectopic fat depots identifies loci associated with adipocyte development and differentiation. Nat Genet. 2017;49(1):125–130.

41. Bohte AE, van Werven JR, Bipat S, Stoker J. The diagnostic accuracy of US, CT, MRI and 1H-MRS for the evaluation of hepatic steatosis compared with liver biopsy: a meta-analysis. Eur Radiol. 2011;21(1):87–97.

42. Neamat-Allah J, Wald D, Hüsing A, et al. Validation of Anthropometric Indices of Adiposity against Whole-Body Magnetic Resonance Imaging – A Study within the German European Prospective Investigation into Cancer and Nutrition (EPIC) Cohorts. PLoS One. 2014;9(3):e91586.

43. Witte EC, Lambers Heerspink HJ, de Zeeuw D, Bakker SJL, de Jong PE, Gansevoort R. First Morning Voids Are More Reliable Than Spot Urine Samples to Assess Microalbuminuria. J Am Soc Nephrol. 2009;20(2):436–443.

44. Porrini E, Ruggenenti P, Luis-Lima S, et al. Estimated GFR: time for a critical appraisal. Nat Rev Nephrol. 2019;15(3):177–190.

45. Zhou A, Murillo H, Peng Q. Impact of partial volume effects on visceral adipose tissue quantification using MRI. J Magn Reson Imaging. 2011;34(6):1452–1457.

46. Jonker JT, de Heer P, Engelse MA, et al. Metabolic imaging of fatty kidney in diabesity: validation and dietary intervention. Nephrol Dial Transplant. 2018;33(2):224–230.

47. Dekkers IA, de Heer P, Bizino MB, de Vries APJ, Lamb HJ. 1 H-MRS for the assessment of renal triglyceride content in humans at 3T: A primer and reproducibility study. J Magn Reson Imaging. Wiley-Blackwell; 2018;48(2):507–513.

48. de Vries APJ, Ruggenenti P, Ruan XZ, et al. Fatty kidney: emerging role of ectopic lipid in obesity-related renal disease. Lancet Diabetes Endocrinol. 2014;2(5):417–426.

49. Jespersen N, Feizi A, Andersen E, et al. Heterogeneity in the perirenal region of humans suggests presence of dormant brown adipose tissue that contains brown fat precursor cells. Mol Metab. 2019;24:30–43.

Supplemental Table 1. Differences in UACR with 95% confidence intervals and eGFR per SD of visceral fat and liver fat with additional adjustment for ACE inhibitors / Angiotensin-II antagonists.

	Percent difference (95% CI) UACR		
Determinant	**Total population**	**Men**	**Women**
VAT (SD=55.4cm^2)			
Crude	-4 (-7, 0)	3 (-2, 8)	7 (0, 15)
Multivariate	1 (-3, 5)	0 (-5, 4)	3 (-4, 11)
+ TBF	4 (-1, 11)	1 (-5, 8)	13 (1, 26)
+ HTGC	4 (-1, 11)	1 (-6, 8)	13 (1, 28)
HTGC (SD=7.9%)			
Crude	0 (-4, 4)	3 (-3, 8)	3 (-3, 9)
Multivariate	1 (-3, 5)	1 (-4, 6)	1 (-5, 7)
+ TBF	2 (-2, 7)	2 (-3, 8)	2 (-4, 9)
+ VAT	1 (-3, 6)	2 (-3, 8)	0 (-7, 6)
	Difference (95% CI) per ml/min/1.73m² lower eGFR		
Determinant	**Total population**	**Men**	**Women**
VAT (SD=55.4cm^2			
Crude	0.52 (-0.12, 1.17)	0.33 (-0.58, 1.24)	1.25 (0.12, 2.39)
Multivariate	0.26 (-0.49, 1.00)	0.23 (-0.74, -1.20)	0.43 (-0.79, 1.66)
+ TBF	0.37 (-0.59, 1.32)	0.78 (-0.37, 1.93)	0.04 (-1.68, 1.75)
+ HTGC	0.58 (-0.40, 1.56)	1.00 (-0.17, 2.17)	0.19 (-1.57, 1.95)
HTGC (SD=7.9%)			
Crude	-0.19 (-0.79, 0.41)	-0.65 (-1.41, 0.10)	0.25 (-0.64, 1.14)
Multivariate	-0.37 (-0.99, 0.25)	-0.69 (-1.47, 0.09)	0.04 (-0.99, 0.90)
+ TBF	-0.46 (-1.11, 0.21)	-0.64 (-1.45, 0.17)	-0.23 (-1.23, 0.76)
+ VAT	-0.57 (-1.27, 0.13)	-0.83 (-1.68, 0.02)	-0.27 (-1.30, 0.76)

Results were based on analyses weighted toward the BMI distribution of the general population (n=2,023; 1,052 men, 971 women). Results were derived from beta coefficients (β) with 95% confidence intervals from linear regression analyses and are expressed as percentages increase or decrease in UACR (mg/mmol) or as difference in lower eGFR (ml/min/1.73m²) per standard deviation in visceral adipose tissue (VAT) or hepatic triglyceride content (HTGC). Multivariate analysis was adjusted for age, sex, ethnicity, education, tobacco smoking, alcohol consumption, fasting state during ^{1}H-MRS, ACE inhibitors/angiotensin-II antagonists and in women additionally adjusted for current use of estrogens and menopausal state.

10

Obesity, Brain Volume and White Matter Microstructure by MRI: A Cross-sectional Study of the UK Biobank.

Dekkers IA, Jansen PR, Lamb HJ.

Radiology. 2019 Jun;291(3):763-771.

ABSTRACT

Background

Obesity has been associated with increased risk of accelerated cognitive decline, and dementia, suggesting underlying neurobiological changes.

Purpose

To investigate the associations between obesity and brain structure (overall and regional brain volumes, and white matter microstructure) assessed by MRI in a sample of the general population.

Materials and methods

Between March 2014 and January 2018, 12,087 participants (53% women; mean age 62 years; range 45-76 years) of the prospective observational UK Biobank study underwent 3T multiparametric (3D T1-weighted, diffusion tensor imaging [DTI]) brain imaging. Total body fat percentage (TBF) was assessed by body impedance. Volumetric measures included brain volume, grey matter volume, white matter volume, volumes of subcortical grey matter structures, and regional cortical volumes. Global and tract-specific microstructure was assessed by fractional anisotropy (FA) and mean diffusivity (MD) using DTI. Linear regression was performed using TBF as determinant and brain measures as outcome variables, and effect estimates are expressed as standardized beta's.

Results

Mean BMI was 26.6 ± 4.4 kg/m^2, mean TBF in men was 24.4 ± 5.5% and 35.5 ± 6.5% in women. In men, TBF was negatively associated with all subcortical grey matter volumes (thalamus, caudate nucleus, putamen, globus pallidus, hippocampus, nucleus accumbens) except amygdala volume. In women, TBF was solely negatively associated with globus pallidus volume. In females and males TBF was positively associated with global FA (females|males: 0.05|0.07 SD change in global FA per SD change in TBF, P<0.001). TBF was negatively associated with global MD in females (-0.07 SD change in global MD per SD change in TBF, P<0.001).

Conclusions

Our findings provide evidence that obesity is associated with smaller subcortical grey matter volumes. In addition, obesity was associated with higher coherence but lower magnitude of white matter microstructure suggesting differential influences of obesity on the geometric organisation of white matter microstructure.

INTRODUCTION

The disease burden of obesity has increased substantially over the last decades, making excess body weight and associated metabolic disorders one of the most challenging public health problems to date (1). The global obesity pandemic has not only led to a greater incidence of cardiovascular disease and type 2 diabetes (2), but has also coincided with a rise in brain diseases, such as accelerated cognitive decline (3), and dementia (4). The metabolic syndrome has been proposed as the shared common component of these different diseases associated with obesity, as it leads to low-grade systemic inflammation affecting various organs, including the liver, pancreas, adipose tissues, and brain via complex intermediate pathways (5).

In obesity, inflammatory responses in the central nervous system (CNS) with subtle glial cell activation, commonly referred to as neuro-inflammation without peripheral immune cells, have been described in different structures, such as the hypothalamus (6). These observations have been supported by preclinical animal studies relating high-fat and high-sugar diet to neuro-inflammatory changes in the brain (7), and post-mortem studies showing higher concentrations of Alzheimer's disease associated hippocampal markers (amyloid beta and tau) in elderly obese patients compared to non-obese patients (8).

Possible detrimental influences of obesity on brain structure can be assessed on a large scale in population-based imaging studies. High field three-dimensional MRI-based volumetric brain metrics allow for the assessment of volumetric differences in regional brain volumes, and diffusion tensor imaging (DTI) for the assessment of global and tract-specific white matter integrity by fractional anisotropy (FA; directional coherence of water molecule diffusion) and mean diffusivity (MD; magnitude of water molecule diffusion) (9). Previous imaging studies in obesity have linked body-mass index (BMI) to lower grey matter volume and white matter integrity (10,11), and to the presence of hypothalamic gliosis in insulin resistance (12). However, structural brain differences in regions that have been implicated to play a role in the regulation of eating behavior (e.g. food-reward circuitry) have also been described in human obesity (13). Studies performed thus far have focused on solely BMI as a measure of obesity and were limited by small sample sizes. Total body fat (TBF) percentage assessed by bio-impedance is a more accurate measure of obesity compared to indirect measurements, such as BMI and waist-hip-ratio (WHR) which may introduce misclassification and bias when estimating the effects of obesity (14).

We hypothesize that TBF is negatively associated with brain volume and microstructural integrity, which could be due to underlying systemic inflammation. Alternatively, lower volume of brain regions or decreased microstructural integrity of tracts involved in the neuronal regulation of the food-reward circuitry might also be associated with obesity.

In this study, we investigated the associations between obesity and brain architecture (overall and regional brain volumes, and white matter microstructure) assessed by MRI in a large study sample of the general population.

MATERIAL AND METHODS

The protocol for this prospective observational study was approved by the National Research Ethics Service Committee reference 11/NW/0382). Written informed consent was obtained from all participants.

Study population and study design

The UK Biobank Study (www.ukbiobank.ac.uk) is a large population-based cohort including 503,325 individuals between the age of 45 to 69 years (15). The participants were recruited across the United Kingdom for participation in the UK Biobank over a 5-year period beginning in 2006, of which a consecutive subset of participants underwent additional magnetic resonance imaging (MRI) and were included in our study (starting March 2014 until the data release of January 2018). Data collection included extensive baseline data based on questionnaires, anthropometric assessments, biological samples, genetics and imaging data. This research has been conducted using the UK Biobank Resource under Application Number 20666. Questionnaire-based data was used for ethnicity, smoking (never, former, current), frequency of alcohol use, socio-economic status according to the Townsend deprivation index (TDI), self-reported history of diabetes and cardiovascular disease (myocardial infarction, angina pectoris, stroke, and hypertension) diagnosed by doctor, and self-reported medication use for high cholesterol, hypertension or diabetes.

Measures of obesity

Anthropometric measurements were obtained by trained research clinic staff. Weight was measured using the Tanita BC 418 body composition analyzer (Tanita Corporation, Arlington Heights, IL), and height was measured using the wall-mounted SECA 240 height measure (SECA, Hamburg, Germany). BMI was calculated as weight divided by squared height (kg/m^2) and WHR as waist circumference divided by hip circumference. Total body fat (TBF) percentage was estimated with the body composition analyzer using electrical impedance. Healthy weight was defined as BMI between 18 to 25 kg/m^2, overweight as BMI between ≥25 and 30 kg/m², and obesity was defined as BMI ≥30 kg/m².

Brain MRI

All brain imaging data were obtained using a 3T MRI scanner (Siemens Skyra, Siemens Healthcare, Erlangen, Germany) with a standard 32-channel RF receive head coil. Prepro-

cessing was done using FSL (the FMRIB Software Library) packages, version 5.0. Imaging acquisition, processing and imaging analysis for brain volumes and DTI measures of white matter tracts were conducted by the coordinating UK Biobank research team as part of the imaging processing and quality-control pipeline, referred to as FBP (FMRIB's Biobank Pipeline), version 1.0 (16).

Volumetric measures

T1-weighted imaging was performed using a 3D MPRAGE sequence (voxel 1.0 x 1.0 x 1.0 mm, matrix 208 x 256 x 256, IT/RT=880/2000 ms). T1-weighted data were first segmented using FAST (version 4.1, FMRIB's Automated Segmentation Tool), to extract grey matter, white matter, and cerebrospinal fluid (CSF). Subcortical structures were extracted using FIRST (version 5.0, FMRIB's Integrated Registration and Segmentation Tool). Intracranial volume was based on the sum of grey matter, white matter and CSF volumes. We calculated the mean of both hemispheres for each of the bilateral subcortical structures. In addition, to obtain cerebral cortical regional volumes according to the Desikan–Killiany atlas, field-of-view reduced T1-weighted volumes were used to segmented the cortex using default parameters in FreeSurfer, version 5.3 (17). An overview of derived volumetric metrics is given in supplemental figure 1a and supplemental table 1, and an overview of all 49 cortical regions is provided in supplemental table 2 and 3.

Diffusion-tensor imaging

An echo-planar imaging (EPI), single-shot Stejskal-Tanner pulse sequence with TE=92ms was applied to obtain 36 slices (voxel 2.0 x 2.0 x 2.0mm, matrix 104 x 104 x 72) in 50 distinct diffusion-weighted directions (b=1000 and b=2000 s/mm^2). Eigenvectors, eigenvalues and FA were calculated by feeding the b=1000 s/mm^2 shell into the DTI fitting tool DTIFIT (version 2.0, the FSL diffusion tensor fitting program), creating FA and mean diffusivity (MD) outputs. Weighted tract-averaged FA and MD values were acquired for association and commissural fibers, and projection fibers. Global measures of FA and MD were calculated by averaging the diffusion metrics over all white matter tracts of both hemispheres per individual. An overview of derived DTI metrices is given in supplemental figure 1b.

Statistical analysis

Baseline characteristics are expressed as percentage or mean (SD), inter-quartile range (IQR) and range. Multiple linear regression was used to calculate standardized beta coefficients (β), representing the change in SDs in the outcome measure (brain imaging phenotypes) per SD TBF. Complete case analysis was performed, and a one-way multivariate analysis of variance (MANCOVA) was conducted to assess whether one or more mean differences were present between BMI levels (healthy weight, overweight and obese), specific regional brain regional volumes and white matter tracts. Analyses were adjusted

for age, ethnicity, TDI, assessment center (baseline visit and imaging visit), smoking, alcohol frequency, diabetes, and cardiovascular disease. Interaction for sex was evaluated by adding an interaction term TBF × sex. Since sex effects were highly significant for each brain imaging outcome measure ($P<0.001$), sex main effects were also included in the models resulting in separate intercepts for men and women (i.e. respectively β male and β female) (18). Volumetric measures were additionally adjusted for intra-cranial volume, while DTI measures were adjusted for brain volume because of potential confounding of partial volume effects. All statistical analyses were corrected for multiple testing using False Discovery Rate (FDR) (19). Based on the total number of all statistical tests over 13 global and subcortical brain volumes, 49 cortical regional volumes and 19 white matter metrics for FA and MD, the defined *P*-value significance threshold was set to pFDR = 0.023 (Benjamini-Hochberg, at $\alpha=0.05$). Uncorrected *P*-values below this threshold were considered statistically significant (uncorrected *P*-values are presented). All effect size estimates were reported as standardized effect estimates (β) to provide comparable, unit-independent measures of effect for different determinants and outcomes. Analyses were performed in R, using package MANCOVA.RM (version 3.3.1, R Foundation for Statistical Computing, Vienna, Austria).

RESULTS

Baseline characteristics

In the UK Biobank 22,059 participants out of 502,616 individuals participating in the full cohort underwent brain imaging, of which 14,515 participants had fully segmented T1-weighted brain MRI scans with derived volumetric outcome measures and 12,857 participants had both volumetric and quantified DTI outcome measures available at the data release of 30th January 2018 (22). After exclusion of participants with missing data regarding covariates used in the regression models (n=656) and outliers (n=114), the final population consisted of 12,087 individuals (**Fig. 1**). Mean age was 62 ± 7.3 years (range 45-76 years) and 53% were women. An overview of the baseline characteristics is provided in **Table 1**.

General associations of obesity and sex with brain structure

General overall MANCOVA was performed prior to conducting multiple linear regression analysis to assess the presence of multivariate of obesity on brain structure. MANCOVA showed that mean differences between BMI levels (healthy weight, overweight, and obese) and brain MRI outcome measures including both global and subcortical brain volumes (Pillai's Trace=0.063, F=20, df=36, $P<0.001$) and specific cortical regions (Pillai's Trace=0.088, F=7, df=147, $P<0.001$) were present. For white matter integrity, MANCOVA

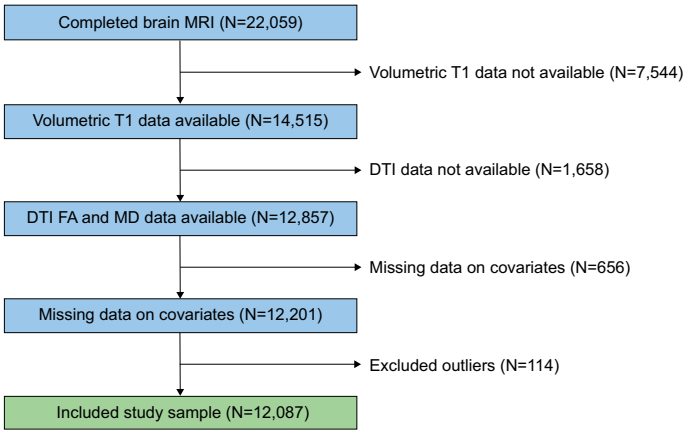

Figure 1. Flow diagram of UK Biobank study. DTI; Diffusion tensor imaging; FA, fractional anisotropy; MD, mean diffusivity.

showed that mean differences between categorical BMI levels and specific white matter tracts were present for both FA based (Pillai's Trace=0.061, F=15, df=45, *P*<0.001) as well as for MD based metrics (Pillai's Trace=0.056, F=14, df=45, *P*<0.001). Tests for TBF × sex interaction were highly significant (*P*<0.001) in the MANCOVA models for global and subcortical brain volumes, cortical regional volumes, and for both FA and MD based metrics. Therefore, all subsequent analyses were performed reporting slopes for males and females.

Total body fat and brain volumetric imaging data

An overview of means and SDs of all global and subcortical grey matter structures are presented in **Table 2** for men and women separately. Means and SDs of regional cortical volumes in the whole study sample and in men and women separately are presented in Supplemental Table 2. TBF was negatively associated with almost all subcortical grey matter volumes except for amygdala volume in men, while in women only globus pallidus volume (-0.06 change in SD [95% CI -0.09, -0.03] per SD change in TBF) was significantly associated with TBF in the adjusted analysis (**Table 3, Figure 2**). Of the subcortical volumes that were associated with TBF in men, the association between TBF and globus pallidus volume was most pronounced (β:-0.13 [95% CI -0.17, -0.10] per SD change in TBF), which was significantly larger than the association between TBF and globus pallidus volume in women (difference between men and women: *P*=0.001). To illustrate, per SD increase in TBF the globus pallidus volume was 27.2 mm^3 smaller in men (mean globus pallidus volume in men: 1857 ± 209 mm^3). In women, this was associated with 11.2 mm^3 smaller volumes (mean globus pallidus volume in women: 1706 ± 187 mm^3).

Positive associations were found for TBF and overall brain volume (0.04 change in SD [95% CI 0.02, 0.06] per SD change in TBF), grey matter volume (0.03 change in SD [95%

Table 1. Characteristics of the included participants of the UK Biobank

Characteristic	Study sample (n=12,087) % or mean ± SD
Age (years)	62.0 ± 7.3
Sex (% women)	53
Ethnicity (% whites)	97
Townsend deprivation index	-2.0 ± 2.6
Smoking, Former (%)	33
Smoking, Current (%)	6
Alcohol, ≥3 drinks per week (%)	13
Diabetes diagnosed by doctor (%)	3
CVD diagnosed by doctor (%)*	21
Use of statines (%)	24
Use of antihypertensives (%)	10
Use of insulin (%)	0.2
Body mass index (kg/m²)	26.6 ± 4.4
Men	27.2 ± 4.0
Women	26.1 ± 4.7
Waist-hip-ratio	0.86 ± 0.08
Men	0.92 ± 0.06
Women	0.81 ± 0.06
Total body fat (%)	30.3 ± 8.2
Men	24.4 ± 5.5
Women	35.5 ± 6.5
Healthy weight (%)	39
Men	29
Women	48
Overweight weight (%)	43
Men	52
Women	35
Obese (%)	18
Men	19
Women	17

Data are shown as percentage, or mean ± standard deviation (SD). Healthy weight was defined as BMI 18-25 kg/m², overweight as BMI ≥25-30 kg/m², and obese as BMI≥30kg/m². CVD, cardiovascular disease was defined as myocardial infarction, angina pectoris, stroke and hypertension diagnosed by doctor.

CI 0.010, 0.05] per SD change in TBF) and white matter volume (0.05 change in SD [95% CI 0.02, 0.07] per SD change in TBF) in women. In men, a positive association was found with white matter volume, but this was not significant after multiple testing correction (*P*=0.050). Analysis of cortical regional volumes found 21 out of 49 tested regions to be significantly associated with TBF in females of which all but two showed a positive

Table 2. Distributions of different MRI outcome measures for females and males separately

MRI outcome measures	Females (n=6,381)	Males (n=5,706)
Volume	Mean (SD)	Mean (SD)
Brain volume (mm^3)	$1.11 \cdot 10^6$ ($8.87 \cdot 10^4$)	$1.23 \cdot 10^6$ ($1.00 \cdot 10^5$)
Grey matter (mm^3)	$5.94 \cdot 10^5$ ($4.75 \cdot 10^4$)	$6.41 \cdot 10^5$ ($5.27 \cdot 10^4$)
White matter (mm^3)	$5.17 \cdot 10^5$ ($4.71 \cdot 10^4$)	$5.88 \cdot 10^5$ ($5.44 \cdot 10^4$)
Brain stem (mm^3)	$2.17 \cdot 10^4$ ($2.24 \cdot 10^3$)	$1.17 \cdot 10^6$ ($1.11 \cdot 10^5$)
CSF (mm^3)	$2.92 \cdot 10^4$ ($1.25 \cdot 10^4$)	$6.16 \cdot 10^5$ ($5.53 \cdot 10^4$)
Thalamus (mm^3)	$7.41 \cdot 10^3$ ($6.24 \cdot 10^2$)	$5.50 \cdot 10^5$ ($6.18 \cdot 10^4$)
Caudate nucleus (mm^3)	$3.35 \cdot 10^3$ ($3.75 \cdot 10^2$)	$3.62 \cdot 10^3$ ($4.17 \cdot 10^2$)
Putamen (mm^3)	$4.61 \cdot 10^3$ ($4.72 \cdot 10^2$)	$5.08 \cdot 10^3$ ($5.53 \cdot 10^2$)
Pallidus (mm^3)	$1.71 \cdot 10^3$ ($1.87 \cdot 10^2$)	$1.86 \cdot 10^3$ ($2.09 \cdot 10^2$)
Hippocampus (mm^3)	$3.77 \cdot 10^3$ ($3.78 \cdot 10^2$)	$3.98 \cdot 10^3$ ($4.56 \cdot 10^2$)
Amygdala (mm^3)	$1.20 \cdot 10^3$ ($1.89 \cdot 10^2$)	$1.34 \cdot 10^3$ ($2.25 \cdot 10^2$)
Accumbens (mm^3)	$4.43 \cdot 10^2$ ($9.48 \cdot 10^1$)	$4.73 \cdot 10^2$ ($1.08 \cdot 10^2$)
Subcortical (mm^3)	$2.25 \cdot 10^4$ ($1.71 \cdot 10^3$)	$2.43 \cdot 10^4$ ($2.01 \cdot 10^3$)
DTI tract – Fractional anisotropy		
Mean Global FA	$4.49 \cdot 10^{-1}$ ($1.35 \cdot 10^{-2}$)	$4.53 \cdot 10^{-1}$ ($1.38 \cdot 10^{-2}$)
Mean FA of Commissural fibers	1.04 ($3.81 \cdot 10^{-2}$)	1.05 ($4.04 \cdot 10^{-2}$)
Mean FA of Association fibers	$3.21 \cdot 10^{-1}$ ($1.19 \cdot 10^{-2}$)	$3.24 \cdot 10^{-1}$ ($1.23 \cdot 10^{-2}$)
Mean FA of Projection fibers	$4.45 \cdot 10^{-1}$ ($1.28 \cdot 10^{-2}$)	$4.51 \cdot 10^{-1}$ ($1.30 \cdot 10^{-2}$)
DTI tract – Mean diffusivity		
Mean Global MD	$8.11 \cdot 10^{-4}$ ($2.25 \cdot 10^{-5}$)	$8.14 \cdot 10^{-4}$ ($2.35 \cdot 10^{-5}$)
Mean MD of Commissural fibers	$1.73 \cdot 10^{-3}$ ($6.62 \cdot 10^{-5}$)	$1.74 \cdot 10^{-3}$ ($6.95 \cdot 10^{-5}$)
Mean MD of Association fibers	$6.02 \cdot 10^{-4}$ ($1.93 \cdot 10^{-5}$)	$6.05 \cdot 10^{-4}$ ($1.99 \cdot 10^{-5}$)
Mean MD of Projection fibers	$8.02 \cdot 10^{-4}$ ($2.21 \cdot 10^{-5}$)	$8.05 \cdot 10^{-4}$ ($2.31 \cdot 10^{-5}$)

CSF, cerebral spinal fluid; FA, fractional anisotropy; MD, mean diffusivity.

association between TBF and specific cortical regional volume (Supplemental table 3). Negative associations were found for temporal fusiform anterior cortex and ventral striatum in women. In men, 19 out of 49 regions were found to be associated with TBF of which the majority was negatively associated. Six cortical regional volumes were significantly associated with TBF in both males and females (temporal fusiform anterior cortex, ventral striatum, percuneous cortex, occipital pole, and cuneal cortex). Sensitivity analysis in healthy weight individuals (BMI 18–25 kg/m²) showed similar associations for global volumes, subcortical grey matter volumes, and cortical regional volumes after adjustment and multiple comparisons correction (Supplemental table 4). An example of T1-weighted brain MRI scans of two UK biobank participants with low and high body fat percentage respectively is given in **Figure 3**.

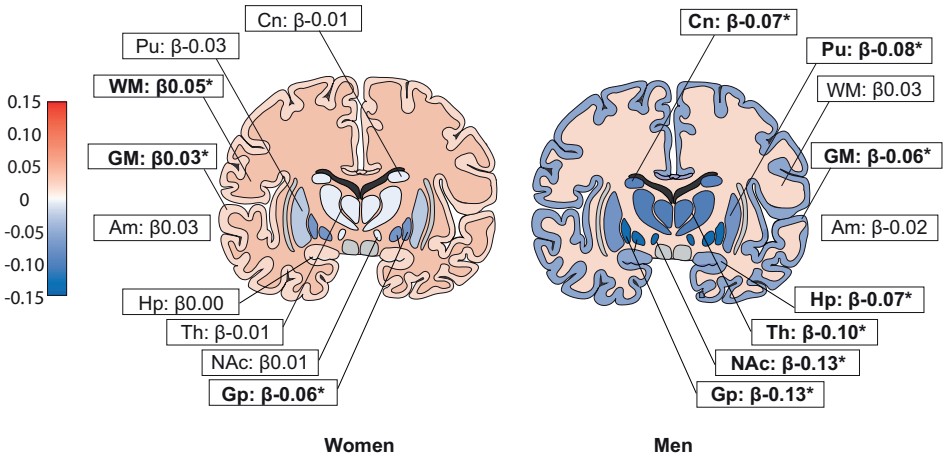

Figure 2. Overview of observed standardized regression coefficients (β) for the associations between total body fat and specific brain regions for men and women. Standardized regression coefficients reflect the SD change in regional brain volume per SD (=6.5% in women and 5.5% in men) change in total body fat. Example of interpretation, in men per SD increase in TBF globus pallidus volume was 27.2 mm^3 lower, and in women per SD increase in TBF globus pallidus volume was 11.2 mm^3 lower. *Significant after FDR correction (threshold pFDR=0.023). Results were adjusted for age, ethnicity, Townsend deprivation index, assessment center (baseline visit and imaging visit), smoking, alcohol use, diabetes, cardiovascular disease, and intra-cranial volume. Am, amygdala; Cn, caudate nucleus; GM, grey matter; Gp, globus pallidus; Hp, hippocampus; NAc, nucleus accumbens; Pu, putamen; Th, thalamus; WM, white matter.

Total body fat and white matter integrity

An overview of means and SDs of global FA and MD for the whole study sample and for men and women separately, is presented in table 2 and means of SDs of tract-specific FA and MD are presented in supplemental table 2. After adjustment for potential confounding variables, TBF was positively associated with global FA in both men (0.07 change in SD [95% CI 0.03, 0.11] per SD change in TBF) and women (0.05 change in SD [95% 0.02, 0.08] per SD change in TBF) (**Table 4, Figure 4**). TBF was not associated with FA of commissural fibers in either men or women. Significant positive associations were found for FA of the majority of both association and projection fibers in men and women. In women, TBF was negatively associated with global MD (-0.07 change in SD [95% CI -0.10,-0.05] per SD change in TBF). However, in men the association between TBF and global MD did not reach statistical significance (*P*=0.09). Negative associations with TBF were found for commissural fibers, association fibers, and projection fibers in men and women. Sensitivity analyses in healthy weight individuals (BMI 18–25 kg/m^2) only showed similar associations compared to the whole study sample for global FA and MD, and tract-specific DTI measures (Supplemental Table 4).

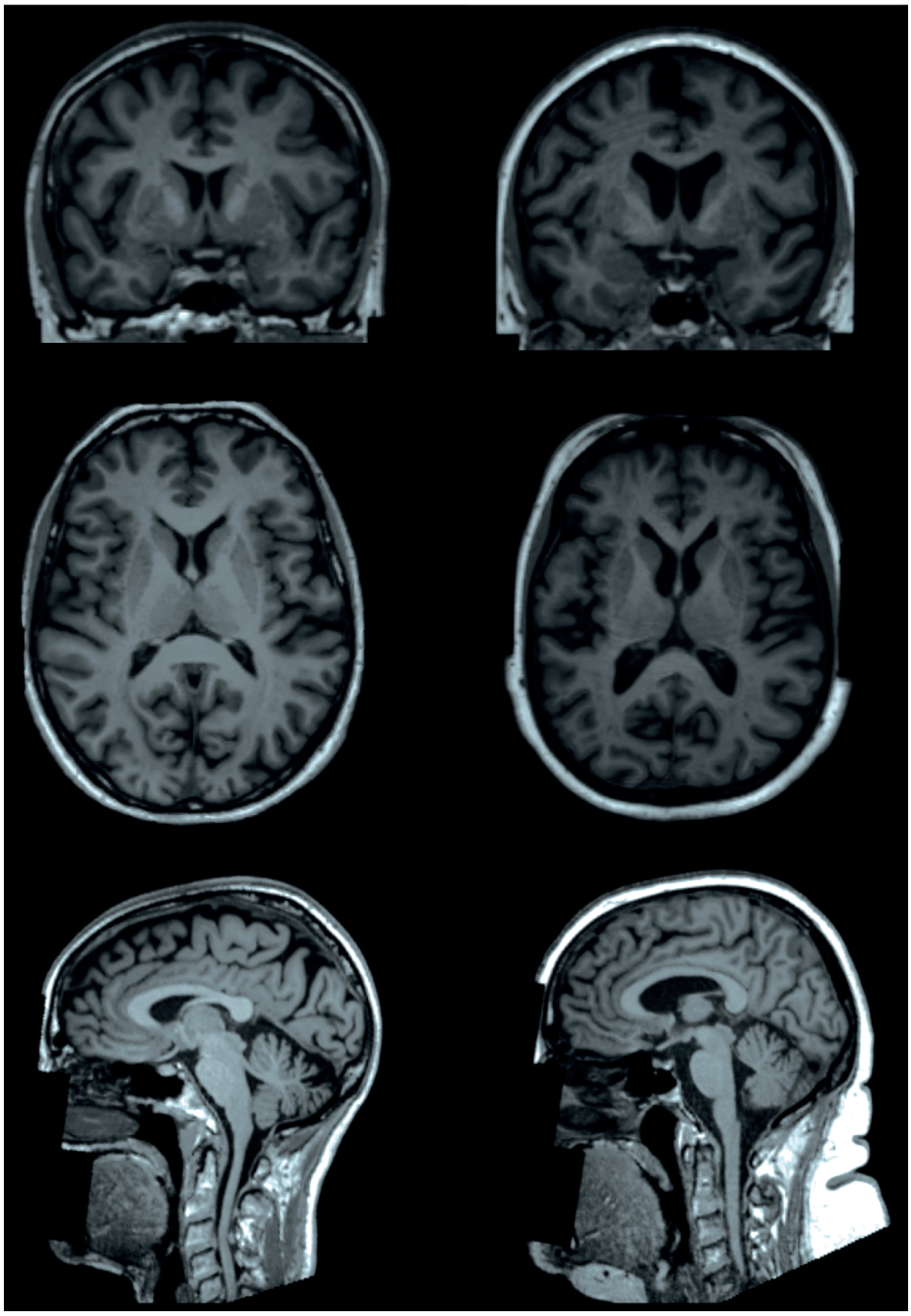

Figure 3. Example of T1-weighted brain MRI scans (coronal, axial and sagittal plane) of two UK biobank participants (both female and 65 years old), one with a body fat percentage of 13% (left) and one with a body fat percentage of 49% (right) showing lower volumes of subcortical gray matter structures in the individual with higher total body fat percentage.

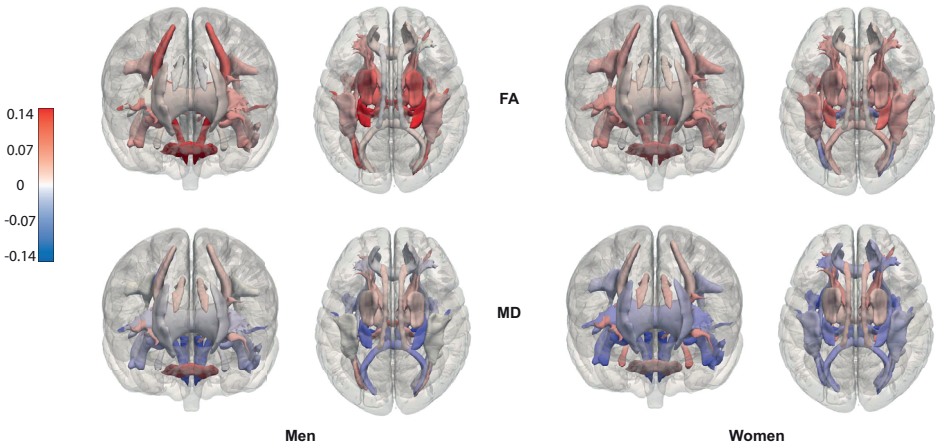

Figure 4. Overview of observed standardized regression coefficients (β) for the associations between total body fat and FA (upper) and MD (lower) based DTI tracts for men and women. Standardized regression coefficients reflect the SD change in FA and MD respectively per SD (=6.5% in women and 5.5% in men) change in total body fat.

DISCUSSION

Using large-scale multiparametric imaging data from 12,087 individuals from the UK Biobank study, we examined whether obesity was associated with brain morphology and microstructural integrity. In our study, we showed that sex-differences are present with regard to negative associations of TBF with regional subcortical grey matter volumes, including the globus pallidus and caudate nucleus, which have been associated with the reward circuitry of food-related stimuli (20). Our effect estimates are provided as standardized beta's meaning that, for example, per SD increase in TBF resulted in 0.13 SD lower globus pallidus volume (corresponding to 27.2 mm^3) in men, and 0.06 SD lower globus pallidus volume (corresponding to 11.2 mm^3) per SD increase in TBF in women. A possible explanation of previously described associations between obesity and lower grey matter volume (21) could be based on potential adverse effects of low grade systemic inflammation in obesity preferentially affecting grey matter volume over white matter volume (22). This has been supported by previous findings from the Framingham Heart study showing that several inflammatory biomarkers linked to obesity have also been associated with lower brain volume (23), and preclinical evidence linking high fat diet to neuroinflammatory changes and neurodegeneration (24). In addition, insulin resistance has been implicated as a possible pathway of cognitive impairment and neuroimaging findings in type 2 diabetes and Alzheimer's disease (25).

Aside from obesity influencing brain structure, a reverse direction of associations could be also possible via a neuronal influence on body weight regulation and eating behavior. Lower grey matter volume of mainly frontal and limbic brain areas in obesity suggest that

Table 2. Multiple linear regression results for total body fat and brain volumes

a. Global volumes	Brain volume	Grey matter	White matter	Brain stem	CSF			
Adjusted TBF (female; SD 6.6%)†	**0.04; 0.02,0.06; *P*=0.001**	**0.03; 0.01,0.05; *P*=0.02**	**0.05; 0.02,0.07; *P*=<0.001***	-0.01; -0.04,0.02; *P*=0.36	-0.02; -0.05,0.00; *P*=0.07			
Adjusted TBF (male; SD 5.5%)†	-0.01; -0.04,0.02; *P*=0.52	**-0.06; -0.09,-0.03; *P*<0.001***	0.03; 0.00,0.06; *P*=0.050	**-0.10; -0.13,-0.06; *P*<0.001***	**0.07; 0.04,0.11; *P*<0.001***			
b. Subcortical GM volumes	All	Thalamus	Caudate nucleus	Putamen	Globus Pallidus	Hippocampus	Amygdala	Nucleus accumbens
Adjusted TBF (female; SD 6.6%)†	-0.01; -0.04,0.02; *P*=0.23	-0.01; -0.03,0.02; *P*=0.55	-0.01; -0.04,0.02 *P*=0.38	**-0.03; -0.05,0.00; *P*=0.03**	**-0.06; -0.09,-0.03; *P*<0.001***	0.00; -0.03,0.03; *P*=0.93	0.03; 0.00,0.06; *P*=0.06	0.01; -0.02,0.03; *P*=0.69
Adjusted TBF (male; SD 5.5%)†	**-0.11; -0.14,-0.07; *P*<0.001***	**-0.10; -0.13,-0.06; *P*<0.001***	**-0.07; -0.11,-0.03; *P*<0.001***	**-0.08; -0.11,-0.04; *P*<0.001***	**-0.13; -0.17,-0.10; *P*<0.001***	**-0.07; -0.11,-0.04; *P*<0.001***	-0.02; -0.06,0.02; *P*=0.38	**-0.13; -0.17,-0.10; *P*<0.001***

Whole study sample n=12,087; females n=6,381, males n=5,706. Standardized regression coefficients (β), with corresponding 95% confidence intervals and uncorrected P-values are shown. Standardized regression coefficients reflect the SD change in regional brain volume per SD (=6.5% in women and 5.5% in men) change in TBF. *Significant after FDR correction (threshold pFDR=0.023). Adjusted model includes: age, ethnicity, TDI, assessment center (baseline visit and imaging visit), smoking, alcohol use, diabetes, cardiovascular disease, and intra-cranial volume. CSF, cerebral spinal fluid; TBF, total body fat; TDI, Townsend deprivation index. †P for interaction of TBF and sex, in adjusted model <0.001. TBF (female) (per SD=6.5%)†, TBF (male) (per SD=5.5%)†

Table 3. Multiple linear regression results for total body fat and global and tract specific FA

Mean FA of DTI tracts	Global FA	Commissural fibers	Assocation fibers	Projection fibers
Adjusted TBF (female; SD 6.6%)†	**0.05; 0.02,0.08; *P*=0.001***	0.02; -0.01,0.04; *P*=0.11	0.03; 0.00,0.06; *P*=0.027	**0.07; 0.04,0.10; *P*<0.001***
Adjusted TBF (male; SD 5.5%)†	**0.07; 0.03,0.11; *P*=<0.001***	0.01; -0.03,0.05; *P*=0.51	**0.05; 0.01,0.08; *P*=0.009***	**0.11; 0.07,0.14; *P*<0.001***
Mean MD of DTI tracts	Global MD	Commissural fibers	Assocation fibers	Projection fibers
Adjusted TBF (female; SD 6.6%)†	**-0.07; -0.10,-0.05; *P*<0.001***	**-0.05; -0.08,-0.02; *P*=0.001***	**-0.07; -0.10,-0.04; *P*<0.001***	**-0.07; -0.10,-0.04; *P*<0.001***
Adjusted TBF (male; SD 5.5%)†	-0.03; -0.07,0.01; *P*=0.09	**-0.05; -0.09,-0.01; *P*=0.01***	-0.04; -0.08,-0.00; *P*=0.03	-0.01; -0.04,0.03; *P*=0.07

Whole study sample n=12,087; females n=6,381, males n=5,706. Standardized regression coefficients (β), with corresponding 95% confidence intervals and uncorrected *P*-values are shown. Standardized regression coefficients reflect the SD change in regional brain volume per SD (=6.5% in women and 5.5% in men) change in TBF. *Significant after FDR correction (threshold pFDR=0.023). Adjusted model includes: age, ethnicity, TDI, assessment center (baseline visit and imaging visit), smoking, alcohol use, diabetes, cardiovascular disease, and intra-cranial volume. FA, fractional anisotropy; MD, mean diffusivity; TBF, total body fat; TDI, Townsend deprivation index. †P for interaction of TBF and sex, in adjusted model <0.001. TBF (female) (per SD=6.6%)†, TBF (male) (per SD=5.5%)†

regulation of eating behavior could be influenced by altered inhibitory control via lower grey matter volume in these areas and affected signaling pathways of the cortico-limbic tract (26). Altered inhibitory control in obesity shares clinical overlap and vulnerability with substance addiction (20), which has been supported by functional imaging showing lower levels of striatal dopamine receptors in obesity (similar to addiction) (27), and different brain responses to food-related stimuli in obese individuals compared to non-obese individuals (28). In our study no associations were found for TBF and amygdala volume, which had also not shown differences in brain responses to food stimuli between obese and non-obese individuals in functional imaging studies (28).

Lower microstructural integrity of several white matter tracts, such as callosal and limbic tracts have been described previously (29). In contrast, we found that increases in total body fat percentages were linked to higher levels of white matter microstructure assessed by FA. In addition, negative associations were found between body fat and MD. This means that body fat percentage, as a measure of general obesity, was associated with higher coherence and with a lower magnitude of water diffusion. This suggests that associations between obesity and white matter microstructural integrity are opposite to previously described findings in ageing (9).

Our findings are *not* consistent with previous studies that showed negative associations between high BMI and FA (30). The reason for this is unknown. However differences may

be methodological (e.g. voxel based approach, higher scan resolution). Prior studies compared healthy weight versus obese individuals whereas our study evaluated total body fat percentage as a continuous variable. However, previous reported significant differences in DTI metrics in obesity might also stem from false-positive findings as the lower statistical power of these studies (sample sizes ranging between 15 to 499 individuals (30)) increases the likelihood of overestimating effect sizes, leading to a lower reproducibility of results (31).

It has been suggested that obese men are more susceptible to mild cognitive impairment than obese women (32), which has been supported by previous observations indicating greater brain atrophy in obese men compared to obese women (10). In our study, we found significant interaction between TBF and sex, and stronger negative associations between volumes of subcortical grey matter structures for total body fat in men compared to women. A possible explanation for these findings might be a relative protective effect of estrogen on the metabolic syndrome (33). Sex-differences for associations between TBF and DTI were less pronounced but also present for effect estimates of global and tract specific measures showing the same directions in males and females but different strengths of associations.

Our study has some limitations. Although growing evidence indicates that obesity adversely affects the CNS and cognitive functioning, our observational cross-sectional design precludes causal inference. Additionally, our study solely focused on brain architecture as we did not assess associations with cognitive functioning. Since laboratory measurements (e.g. HbA1c, serum glucose etc.) were not available at the time of our study and questionnaire data on physical exercise and medication use were only available for a limited subset, these were not taken into account in our analysis and could be a source of possible residual confounding. In addition to these limitations, we note that although multiple associations were shown to be significant, the observed effect estimates are small. The large sample size of the study enabled us to detect these subtle associations between obesity measures and brain structure. These modest associations may be expected given that our study was performed in the general population, which also included non-obese individuals.

More research is needed to assess changes in brain architecture in obesity over time, and metabolic influences such as insulin-resistance (25) and metabolic responses to fasting/exercise and eating/resting conditions (34). Further research is needed to investigate to what extent a greater amount of visceral adipose tissue (via a low grade systemic metabolic inflammation) leads to detrimental effects on brain structure and cognitive functioning above and beyond measures of general obesity (35). In addition, more functional brain imaging studies (e.g. nuclear metabolic studies, and arterial spin labelling) are warranted, as altered brain metabolism and cerebral hypoperfusion have been

hypothesized as possible underlying pathophysiological pathways of the adverse effects of obesity on cognitive functioning.

Our findings provide further evidence that obesity is associated with smaller subcortical grey matter volumes. In addition, obesity was associated with higher coherence but lower magnitude of white matter microstructure in our study, which provides insights into the potential influences of obesity on the geometric organization of white matter microstructure. Future research is needed to evaluate whether stringent weight reduction and treatment of obesity related metabolic disorders also benefit the potential neurological consequences of obesity.

REFERENCES

1. GBD 2015 Obesity Collaborators, Afshin A, Forouzanfar MH, et al. Health Effects of Overweight and Obesity in 195 Countries over 25 Years. N Engl J Med. 2017;377(1):13–27.
2. The Emerging Risk Factors Collaboration, Wormser D, Kaptoge S, et al. Separate and combined associations of body-mass index and abdominal adiposity with cardiovascular disease: collaborative analysis of 58 prospective studies. Lancet. 2011;377(9771):1085–1095.
3. Gunstad J, Paul RH, Cohen RA, Tate DF, Spitznagel MB, Gordon E. Elevated body mass index is associated with executive dysfunction in otherwise healthy adults. Compr Psychiatry. 2007;48(1):57–61.
4. Whitmer RA, Gunderson EP, Barrett-Connor E, Quesenberry CP, Yaffe K. Obesity in middle age and future risk of dementia: a 27 year longitudinal population based study. BMJ. 2005;330(7504):1360.
5. Lumeng CN, Saltiel AR. Inflammatory links between obesity and metabolic disease. J Clin Invest. 2011;121(6):2111–2117.
6. Parimisetty A, Dorsemans A-C, Awada R, Ravanan P, Diotel N, Lefebvre d'Hellencourt C. Secret talk between adipose tissue and central nervous system via secreted factors—an emerging frontier in the neurodegenerative research. J Neuroinflammation. 2016;13(1):67.
7. Guillemot-Legris O, Muccioli GG. Obesity-Induced Neuroinflammation: Beyond the Hypothalamus. Trends Neurosci. 2017;40(4):237–253.
8. Mrak RE. Alzheimer-type neuropathological changes in morbidly obese elderly individuals. Clin Neuropathol. 2009;28(1):40–45.
9. Cox SR, Ritchie SJ, Tucker-Drob EM, et al. ARTICLE Ageing and brain white matter structure in 3,513 UK Biobank participants. 2016.
10. Taki Y, Kinomura S, Sato K, et al. Relationship Between Body Mass Index and Gray Matter Volume in 1,428 Healthy Individuals. Obesity. 2008;16(1):119–124.
11. Raji CA, Ho AJ, Parikshak NN, et al. Brain structure and obesity. Hum Brain Mapp. 2009;31(3).
12. Schur EA, Melhorn SJ, Oh S-K, et al. Radiologic evidence that hypothalamic gliosis is associated with obesity and insulin resistance in humans. Obesity. 2015;23(11):2142–2148.
13. Pannacciulli N, Del Parigi A, Chen K, Le DSNT, Reiman EM, Tataranni PA. Brain abnormalities in human obesity: A voxel-based morphometric study. Neuroimage. 2006;31(4):1419–1425.
14. Rothman KJ. BMI-related errors in the measurement of obesity. Int J Obes. 2008;32(S3):S56–S59.
15. Sudlow C, Gallacher J, Allen N, et al. UK Biobank: An Open Access Resource for Identifying the Causes of a Wide Range of Complex Diseases of Middle and Old Age. PLOS Med. 2015;12(3):e1001779.
16. Alfaro-Almagro F, Jenkinson M, Bangerter NK, et al. Image processing and Quality Control for the first 10,000 brain imaging datasets from UK Biobank. Neuroimage. 2018;166:400–424.
17. Ritchie SJ, Cox SR, Shen X, et al. Sex Differences in the Adult Human Brain: Evidence from 5216 UK Biobank Participants. Cereb Cortex. Oxford University Press; 2018;28(8):2959–2975.
18. Kawut SM, Lima JAC, Graham Barr R, et al. Sex and Race Differences in Right Ventricular Structure and Function: The MESA-Right Ventricle Study.

19. Benjamini Y, Hochberg Y. Controlling the False Discovery Rate: A Practical and Powerful Approach to Multiple Testing. J. R. Stat. Soc. Ser. B. 1995. p. 289–300.

20. Volkow ND, Wise RA, Baler R. The dopamine motive system: implications for drug and food addiction. Nat Rev Neurosci. 2017;18(12):741–752.

21. Medic N, Ziauddeen H, Ersche KD, et al. Increased body mass index is associated with specific regional alterations in brain structure. Int J Obes. 2016;40(7):1177–1182.

22. Vachharajani V, Granger DN. Adipose tissue: A motor for the inflammation associated with obesity. IUBMB Life. 2009;61(4):424–430.

23. Jefferson AL, Massaro JM, Wolf PA, et al. Inflammatory biomarkers are associated with total brain volume: The Framingham Heart Study. Neurology. 2007;68(13):1032–1038.

24. Granholm A-C, Bimonte-Nelson HA, Moore AB, Nelson ME, Freeman LR, Sambamurti K. Effects of a Saturated Fat and High Cholesterol Diet on Memory and Hippocampal Morphology in the Middle-Aged Rat. J Alzheimer's Dis. 2008;14(2):133–145.

25. Arnold SE, Arvanitakis Z, Macauley-Rambach SL, et al. Brain insulin resistance in type 2 diabetes and Alzheimer disease: concepts and conundrums. Nat Rev Neurol. 2018;14(3):168–181.

26. Yokum S, Ng J, Stice E. Relation of regional gray and white matter volumes to current BMI and future increases in BMI: a prospective MRI study. Int J Obes. 2012;36(5):656–664.

27. Volkow ND, Wang G-J, Fowler JS, Telang F. Overlapping neuronal circuits in addiction and obesity: evidence of systems pathology. Philos Trans R Soc B Biol Sci. 2008;363(1507):3191–3200.

28. Ziauddeen H, Farooqi IS, Fletcher PC. Obesity and the brain: how convincing is the addiction model? Nat Rev Neurosci. 2012;13(4):279–286.

29. Xu J, Li Y, Lin H, Sinha R, Potenza MN. Body mass index correlates negatively with white matter integrity in the fornix and corpus callosum: A diffusion tensor imaging study. Hum Brain Mapp. 2013;34(5):1044–1052.

30. Kullmann S, Schweizer F, Veit R, Fritsche A, Preissl H. Compromised white matter integrity in obesity. Obes Rev. 2015;16(4):273–281.

31. Button KS, Ioannidis JPA, Mokrysz C, et al. Power failure: why small sample size undermines the reliability of neuroscience. Nat Rev Neurosci. 2013;14(5):365–376.

32. Elias MF, Elias PK, Sullivan LM, Wolf PA, D'Agostino RB. Obesity, diabetes and cognitive deficit: The Framingham Heart Study. Neurobiol Aging. 2005;26(1):11–16.

33. Mauvais-Jarvis F. Sex differences in metabolic homeostasis, diabetes, and obesity. Biol Sex Differ. BioMed Central; 2015;6:14.

34. Mattson MP, Moehl K, Ghena N, Schmaedick M, Cheng A. Intermittent metabolic switching, neuroplasticity and brain health. Nat Rev Neurosci. 2018;19(2):63–80.

35. Klöting N, Blüher M. Adipocyte dysfunction, inflammation and metabolic syndrome. Rev Endocr Metab Disord. 2014;15(4):277–287.

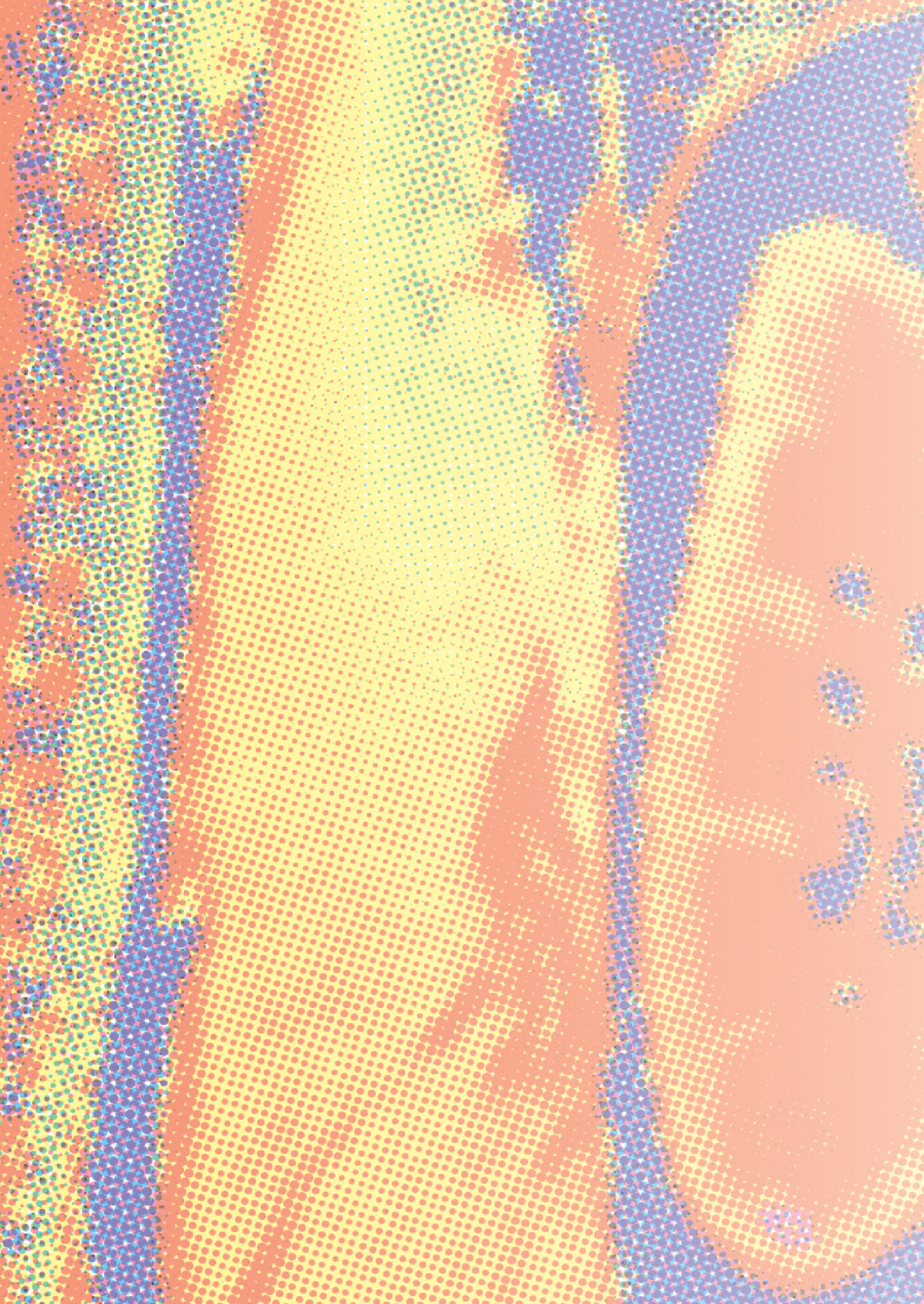

APPENDIX

Contrast media safety

11

Gadolinium retention after administration of contrast agents based on linear chelators and the recommendations of the European Medicines Agency

Dekkers IA, Roos R, van der Molen AJ.

Eur Radiol. 2018 Apr;28(4):1579-1584.

ABSTRACT

The Pharmacovigilance Risk Assessment Committee (PRAC) of the European Medicines Agency (EMA) earlier this year recommended to suspend some marketing authorisations for Gadolinium Containing Contrast Agents (GCCAs) based on linear chelators due to the potential risk of gadolinium retention in the human body. These recommendations have recently been re-evaluated by EMA's Committee for Medicinal Products for Human Use (CHMP), and confirmed the final opinion of the European Medicines Agency. This editorial provides an overview of the available GCCAs and summarises the recent evidence of gadolinium retention. Moreover, a critical appraisal of the strengths and limitations of the scientific evidence currently available on gadolinium retention is given.

INTRODUCTION

The Pharmacovigilance Risk Assessment Committee (PRAC) of the European Medicines Agency (EMA) earlier this year recommended suspending some marketing authorisations for gadolinium-containing contrast agents (GCCAs) based on linear chelators due to the potential risk of gadolinium retention in the human body (1). The recommendations made by the PRAC were based on the evaluation of recent research findings indicating gadolinium retention in the brain, which can be measured as increased signal intensities on T1-weighted sequences of unenhanced MRI scans. The PRAC has re-evaluated its recommendations based on questions by the marketing authorisation holders, which has subsequently been confirmed by the Committee for Medicinal Products for Human Use (CHMP). The CHMP is a regulatory organ within the EMA with a central role in the authorisation of medicines inside the European Union (EU). On 21 July 2017, the EMA published its final opinion to suspend and/or restrict some of the marketing authorisations of four GCCAs based on linear chelators from the European market (2). These four agents based on linear chelators are gadobenate dimeglumine (MultiHance), gadodiamide (Omniscan), gadopentetate dimeglumine (Magnevist) and gadoversetamide (OptiMark). This is not the first time that linear gadolinium agents are under investigation by the EMA. In 2007, exposure to high doses of gadolinium were for the first time linked to the development of nephrogenic systemic fibrosis (NSF) in patients with severe renal insufficiency. In this period, the EMA gave a serious warning (e.g. 'Black Box' warning) regarding the relationship between NSF and linear chelators; however, the scientific evidence at that time was considered insufficient to proceed with a ban from the European market. However, how strong is the scientific evidence for the current recommendations and what are the implications for radiology practice in the EU?

Physical chemistry of gadolinium-containing contrast agents (GCCAs)

GCCAs can be classified into four different groups based on the type of ligand (linear or macrocyclic) and charge (ionic or non-ionic; **Table 1**). Gadolinium is a heavy metal from the lanthanide group with strong paramagnetic properties (shortening of the proton T1 relaxation time), which is chelated by binding to a strong ligand. In the linear chelates the gadolinium ion is bound to an open-chain ligand, while in the macrocyclic chelates the gadolinium ion is bound inside a cubic chemical structure. These differences in the chemical structure of the ligands explain the difference in thermodynamic and kinetic stability, whereby the non-ionic linear chelates are the least stable and the ionic macrocyclic chelates are the most stable (3). The free gadolinium ion is mostly hydrated in biological systems, and this $Gd(H2O)8^{3+}$ ion is toxic because of its chemical similarities to Ca^{2+}, which is an important factor for proper functioning of many processes in the human body such as contraction of the heart muscle and smooth muscle cells, and

nerve transmission. Gd^{3+} can compete with Ca^{2+} due to its similarity in ion radius, and could thereby disturb physiological processes. In unstable chelates, the gadolinium ion could, partly depending on the local environment (acidic pH), become detached from the ligand by transmetallation (exchange with other ions present in the local environment, such as Fe^{3+}, Cu^{2+}, or Zn^{2+} ions) and the Gd^{3+} ion could then precipitate locally as a salt (gadolinium hydroxide, gadolinium carbonate or gadolinium phosphate) or bind to other macromolecules, such as proteins, peptides or metalloenzymes (4).

Table 1. Current arsenal of linear and macrocyclic GCCAs

Linear	Macrocyclic
Ionic	Ionic
Magnevist (gadopentetate dimeglumine - Bayer) Magnevision (gadopentetate dimeglumine – B.E. Imaging)	Dotarem (gadoterate meglumine - Guerbet) Clariscan (gadoterate meglumine – GE) Dotagraf (gadoterate meglumine - Bayer) Dotagita (gadoterate meglumine - Agfa) Cyclolux (gadoterate meglumine - Sanochemia)
MultiHance (gadobenate dimeglumine - Bracco)	
Primovist (gadoxetate disodium - Bayer)	
Non-ionic	Non-ionic
Omniscan (gadodiamide – GE)	ProHance (gadoteridol - Bracco)
OptiMARK (gadoversetamide - Guerbet)	Gadovist (gadobutrol - Bayer)

Classification of available gadolinium based contrast agents (GBCA's) in four different groups based on the type of ligand (linear or macrocyclic) and charge (ionic or non-ionic), with corresponding brand name and manufacturer.

Evidence for gadolinium retention

In 2014, Kanda et al. described a positive correlation between previous exposure to GCCAs based on linear chelators and increased signal intensity in basal ganglia on subsequent unenhanced T1-weighted MRI sequences in 35 patients (5). This increase in signal intensity was not found in the control group, which consisted of patients who underwent multiple MRI scans without the addition of a contrast agent. These findings were soon replicated by multiple independent research groups in different countries. To date, a total of 19 studies have been performed that investigated whether repeated exposure to GCCAs causes increased signal intensity in the brain. Thus far, 15 out of 19 studies found a positive correlation between the number of administrations of a linear chelate and the measured signal intensity in the basal ganglia. At this moment, the association has not been demonstrated for the macrocyclic chelates (6, 7). The four contrast agents that the EMA has recommended suspending and/or restricting marketing authorisations are all based on linear chelators (**Table 2**). Furthermore, small post-mortem studies showed the presence of miniscule amounts of gadolinium in brain tissue in patients who received GCCAs in the past (8, 9, 10). The recent post-mortem study by Murata et al. found that gadolinium deposition in normal brain and bone tissue occurs with both agents based

Table 2. Physiochemical characteristics based on summary of manufacturer product characteristics of currently available GCCAs

Name	Brand name	Ligand	Structure	Ionicity	Osmolality (mOsm/kg) at 37 °C	Viscosity (mPa's) at 37 °C	T1 Relaxivity in full blood 1.5T (L/mmols)	T2 Relaxivity in full blood 1.5T (L/mmols)	Thermo-dynamic stability (pH 14) (Log K_{therm})	Conditional stability (pH 7.4) (Log K_{cond})	Excess ligand (mmol/l)	Renal Excretion ($T^1/_2$ in hours) pH1	EMA
Gadopentetate	Magnevist	DTPA	Linear	Ionic	1960	2.9	4.3	4.4	22.5	18.4	1	1.6	**Suspend**
Gadopentetate	Magnevision	DTPA	Linear	Ionic	1960	2.9	4.2	4.3	NA*	NA*	NA*	NA*	**Suspend**
Gadobenate	MultiHance	BOPTA	Linear	Ionic	1970	5.3	6.7	8.9	22.6	18.4	0	1.2-2	**Restrict**
Gadoxetate	Primovist	EOB-DTPA	Linear	Ionic	688	1.2	7.3	9.2	23.5	18.7	1.3	1.6	Maintain
Gadodiamide	Omniscan	DTPA-BMA	Linear	Non-ionic	789	1.4	4.6	6.9	16.9	14.9	25	1.3	**Suspend**
Gadoverseta-mide	OptiMARK	DTPA-BMEA	Linear	Non-ionic	1110	2.0	5.2	6.0	16.6	15.0	50	1.7	**Suspend**
Gadoterate	Dotarem	DOTA	Macrocyclic	Ionic	1350	2.0	4.2	6.7	25.8	19.0	0	1.6	Maintain
Gadoterate	Clariscan	DOTA	Macrocyclic	Ionic	1350	2.1	3.1	3.6	NA*	NA*	NA*	1.6	Maintain
Gadoterate	Dotagraf	DOTA	Macrocyclic	Ionic	1350	1.8	3.4	4.27	NA*	NA*	NA*	1.6	Maintain
Gadoterate	Cyclolux	DOTA	Macrocyclic	Ionic	1350	1.8	3.4	4.27	NA*	NA*	NA*	1.6	Maintain
Gadoteridol	ProHance	HP-DO3A	Macrocyclic	Non-ionic	630	1.3	4.4	5.5	23.8	17.1	0.5	1.6	Maintain
Gadobutrol	Gadovist	BT-DO3A	Macrocyclic	Non-ionic	1603	4.9	5.3	5.4	21.8	14.8	1	1.5	Maintain

NA*: not available based on publicly available summary of product characteristics

on macrocyclic (only nonionic, i.e. gadobutrol and gadoteridol) and linear chelators in patients with normal renal function (10). Gadolinium retention in bone and skin had already been described by histology studies (11, 12), and very recent data based on autopsy studies suggest that gadolinium can accumulate in other organs as well, such as the liver and kidney (13, 14).

Methodological limitations of current studies

The studies performed thus far have several important limitations that need to be considered when interpreting these data. All studies have an observational retrospective design, which makes these studies vulnerable to different forms of bias and confounding. The retrospective data collection introduces uncertainty about the number of administered doses and included patients could have received different types of contrast agents rather than solely linear or macrocyclic, which could lead to misclassification bias. Furthermore, only few studies have sufficiently corrected for potential confounders that could distort the association between gadolinium exposure and an increased signal intensity in the brain. Examples of such potential confounders are age, gender and follow-up time. Control groups were also not always included in the analyses and if present were often limited to small sample sizes and comprised different patient populations compared to the exposed group. Besides the above-mentioned methodological drawbacks, there are also significant limitations to the use of increased signal intensity as a primary outcome measure. The increased signal intensity in the brain on MRI scans is not always reliable and comparable due to different field strengths (1.5 Tesla and 3.0 Tesla), and the use of different T1-weighted sequences or sequence parameters. Moreover, the proton T1 relaxivity also depends on the molecular weight of the molecule to which the Gd-ions or Gd-contrast media molecules are attached (either soluble macromolecules or insoluble cell components), the water residence time of the coordinated water molecules, and, for some GCCAs, the presence of albumin (15, 16). It is therefore unclear to what extent the increased signal intensity in the brain truly reflects higher gadolinium concentrations (17). Each of the GCCAs possibly has a different level of administered doses before signal changes can be observed on MR images. It could be that for agents based on macrocyclic chelators this level involves such a substantially high number of administrations, which hardly occurs in individual patients and is therefore difficult to investigate.

Thus far, five post-mortem studies, all using inductively coupled plasma mass spectroscopy, have measured levels of elemental Gd in different brain areas with possibly intact blood-brain barriers (8, 10, 17-19). Overall, data are limited to 31 patients exposed to either linear or macrocyclic-based GCCAs compared to 28 controls. Only one study (n=13) has assessed the possible distribution of Gd compounds in brain tissues, and the possible presence of histological changes (18). To summarise, these studies found that Gd deposition has been observed in all 31 patients exposed to either linear or macrocyclic

GCCAs, even after one single exposure, compared to controls. Second, calculation of normalised Gd deposition ratios (Gd deposited in 1 g of tissue per millimole of GCCA administered) did not show significant differences between linear and macrocyclic GCCAs. In contrast to the imaging-based studies, the post-mortem study of Murata et al. suggests that gadolinium retention is not solely limited to agents based on linear chelators (8). This suggests that extension of the suspension of marketing authorisations to certain GCCAs based on macrocyclic chelators cannot be completely excluded if more evidence becomes available. However, the current number of patients studied in tissue analysis is too small to draw any conclusions on differences among the various GCCAs tested, and does not allow for differentiation between the various forms of gadolinium (e.g. chelated Gd, Gd-associated macromolecules) as different GCCAs with various cumulative doses and with heterogeneous sampling times have been studied.

The association between gadolinium accumulation and the occurrence of physical symptoms or neurotoxic damage has not been demonstrated yet. Thus far, two studies aimed to assess the possible influence of gadolinium accumulation and clinical symptoms (20, 21). The study by Welk et al. involving 99,739 patients with one or more Gd-enhanced MRI and 146,818 control patients with only non-enhanced MRIs did not find a significant association with parkinsonism (20). A very recent retrospective cohort study involving nearly 20 years of longitudinal data in 23 multiple sclerosis patients and 23 healthy age- and sex-matched controls found a possible association between Gd exposure and cognitive impairment (verbal fluency) (21). However, it should be noted that these findings need to be interpreted with caution since retrospective studies are highly susceptible to 'confounding by indication'. Patients requiring contrast administration in general tend to be more ill than patients in whom contrast administration is not needed, which biases the assessment of the effect of contrast media and clinical outcome. To test the association between Gd and clinical symptoms, one would ideally do a prospective study with clinical symptoms as the study outcome, whereby the patients are randomised for receiving contrast agents or not. However, a prospective study on rare clinical outcomes is impracticable since very large sample sizes are needed and are, furthermore, unethical. Previous animal studies evaluating side effects of lanthanum carbonate, which is a rare metal of the same lanthanide family as gadolinium, have related this agent to reduced learning behaviour in rats at lower concentrations than now found in humans for gadolinium (22). However, no direct neurotoxicity endpoints were evaluated (23), and adverse effects on learning behaviour in both humans and animals have not yet been described for gadolinium. Nevertheless, caution is needed regarding patient safety and unknown long-term effects. In this view, the advice of the PRAC is understandable and probably a safe decision considering the availability of several different classes of GCCAs (**Table 1**). Additionally, as radiologists it is advisable to keep in mind that for every diagnostic

examination, especially when using contrast agents or radiation, a clear clinical indication should be present, and to keep the contrast agent dose as low as reasonably possible.

Implications

Following the PRAC's March 2017 recommendation, some of the marketing authorisation holders concerned by this referral procedure have requested a re-examination. Upon receipt of the grounds for their requests, the PRAC has completed a re-examination, which was published on 7 July 2017. An additional assessment was performed by the CHMP, which was unfavourable for the four linear contrast agents regarding quality, safety and efficacy requirements and risk-benefit analysis. The GCCAs that fulfil an important diagnostic need in patients with few alternatives such as the hepatobiliary specific linear agent gadoxetic acid and a formulation of gadopentetic acid used for MR arthrography, were excluded from the PRAC investigation and will thus maintain their marketing authorisation. In line with contrast agents fulfilling specific diagnostic needs, the use of gadobenic acid has been restricted to liver MRI scans. The reactions to the statement in the field have been diverse. For example, the Committee of Contrast Media and Drugs of the American College of Radiology previously noted finding the statement of the PRAC premature and are not in favour of the suspension of marketing authorisations of these agents for the US market based on the current available data (24). In May 2017 the US Food and Drug Administration (FDA) announced a safety update regarding the evaluation of the risk of Gd accumulation associated with repeated administration of GCCAs. The FDA concluded that although GCCAs may be associated with some Gd retention in the brain and other organs, no adverse health effects from Gd retention have been identified. Previous recommendations of the FDA regarding the use of GCCAs remain thus unchanged (25).

International research cooperation

Since gadolinium retention in the body (in the brain but also in bone, skin and liver) is a rare phenomenon, multiple centers in Europe are collaborating to achieve international cooperation on this topic. The European Gadolinium Retention Evaluation Consortium (E-GREC), founded in 2016, is a collaboration of academic clinical researchers and basic researchers from the contrast agent manufacturers (26). Additionally, the consortium has close connections to researchers in the USA. E-GREC will initially focus on acquiring resources to fund future scientific projects and will focus on guidelines to improve the quality of the preclinical and clinical research on gadolinium retention.

REFERENCES

1. PRAC concludes assessment of gadolinium agents used in body scans and recommends regulatory actions, including suspension for some marketing authorisations. Pharmacovigilance Risk Assessment Committee 2017;EMA/157486/2017.
2. EMA's final opinion confirms restrictions on use of linear gadolinium agents in body scans. European Medicines Agency 2017;EMA/457616/2017.
3. Sherry AD, Caravan P, Lenkinski RE. Primer on gadolinium chemistry. J Magn Reson Imaging. 2009;30:1240–1248
4. Idee JM, Port M, Raynal I, Schaefer M, Le Greneur S, Corot C. Clinical and biological consequences of transmetallation induced by contrast agents for magnetic resonance imaging: a review. Fundam Clin Pharmacol 2006;20:563–576
5. Kanda T, Ishii K, Kawaguchi H, Kitajima K, Takenaka D. High signal intensity in the dentate nucleus and globus pallidus on unenhanced T1-weighted MR images: relationship with increasing cumulative dose of a gadolinium-based contrast material. Radiology 2014;270:834–841
6. Radbruch A, Weberling LD, Kieslich PJ et al. Gadolinium retention in the dentate nucleus and globus pallidus is dependent on the class of contrast agent. Radiology 2015;275:783–791
7. Olchowy C, Cebulski K, Lasecki M et al. The presence of the gadolinium-based contrast agent depositions in the brain and symptoms of gadolinium neurotoxicity - A systematic review. PLoS One 2017;12:e0171704
8. Kanda T, Fukusato T, Matsuda M et al. Gadolinium-based Contrast Agent Accumulates in the Brain Even in Subjects without Severe Renal Dysfunction: Evaluation of Autopsy Brain Specimens with Inductively Coupled Plasma Mass Spectroscopy. Radiology 2015;276:228–232
9. Kanda T, Oba H, Toyoda K, Kitajima K, Furui S. Brain gadolinium deposition after administration of gadolinium-based contrast agents. Jpn J Radiol 2016;34:3–9
10. Murata N, Gonzalez-Cuyar LF, Murata K et al. Macrocyclic and Other Non-Group 1 Gadolinium Contrast Agents Deposit Low Levels of Gadolinium in Brain and Bone Tissue: Preliminary Results From 9 Patients With Normal Renal Function. Invest Radiol 2016;51:447–453
11. Darrah TH, Prutsman-Pfeiffer JJ, Poreda RJ, Ellen Campbell M, Hauschka PV, Hannigan RE. Incorporation of excess gadolinium into human bone from medical contrast agents. Metallomics 2009;1:479–488
12. van der Meij N, Keur I, van Lienden KP, Scheepstra CG, Bos JD. Nephrogenic systemic fibrosis possibly caused by gadolinium-containing contrast agent. Ned Tijdschr Geneeskd 2007;151:2898–2903
13. McDonald J, Jentoft M, Paolini M et al. Deposition of Gadolinium in the Organs, Tissue, and Bone of Patients who Underwent Multiple Gadodiamide-Enhanced MR Exams. Mayo Clinic, Rochester, MN, 2017;ASNR O-259
14. McDonald RJ, McDonald JS, Dai D et al. Comparison of gadolinium concentrations within multiple rat organs after intravenous administration of linear versus macrocyclic gadolinium chelates. Radiology 2017;161594

15. Frenzel T, Apte C, Jost G, Schöckel L, Lohrke J, Pietsch H. Quantification and assessment of the chemical form of residual gadolinium in the brain after repeated administration of gadolinium-based contrast agents: comparative study in rats. Invest Radiol 2017;52:396–404

16. Idée J-M, Fretellier N, Robic C, Corot C. The role of gadolinium chelates in the mechanism of nephrogenic systemic fibrosis: a critical update. Critical reviews in toxicology 2014;44:895–913

17. Roberts DR, Welsh CA, LeBel DP 2nd, Davis WC. Distribution map of gadolinium deposition within the cerebellum following GBCA administration. Neurology 2017;88:1206–1208

18. McDonald RJ, McDonald JS, Kallmes DF et al. Intracranial Gadolinium Deposition after Contrast-enhanced MR Imaging. Radiology 2015;275:772–782

19. McDonald JS, McDonald RJ, Jentoft ME et al. Intracranial Gadolinium Deposition Following Gadodiamide-Enhanced Magnetic Resonance Imaging in Pediatric Patients: A Case Control Study. JAMA Pediatr. Eur Radiol 2017;28:1579–1584 1583

20. Welk B, McArthur E, Morrow SA et al Association Between Gadolinium Contrast Exposure and the Risk of Parkinsonism. JAMA 2016;316:96–98

21. Forslin Y, Shams S, Hashim F et al. Retention of Gadolinium-Based Contrast Agents in Multiple Sclerosis: Retrospective Analysis of an 18-Year Longitudinal Study. AJNR Am J Neuroradiol. 2017 Jul;38(7):1311-1316.

22. Feng L, Xiao H, He X et al. Neurotoxicological consequence of long-term exposure to lanthanum. Toxicol Lett 2006;165:112–120

23. Damment SJ, De Broe ME, D'Haese PC, Bramall N, Cox AG, McLeod CW Incredulous effects of lanthanum? Toxicol Lett 2007;168:186–189

24. ACR Response to the European PRAC Recommendations. 2017 American College of Radiology

25. FDA identifies no harmful effects to date with brain retention of gadolinium-based contrast agents for MRIs. 2017 Food and Drug Administration

26. Quattrocchi CC, van der Molen AJ. Gadolinium Retention in the Body and Brain: Is It Time for an International Joint Research Effort? Radiology 2017;282:12–16

12

General discussion and summary

Nederlandse samenvatting

List of publications

List of scientific oral presentations

Curriculum vitae

Dankwoord

GENERAL DISCUSSION AND SUMMARY

The aim of this thesis was to evaluate quantitative MRI techniques in reno-cardiovascular health, and to study the links between obesity and reno-cardiovascular health using quantitative MRI metrics. Furthermore, we aimed to address novel insights on the safety of contrast media with regard to the use of gadolinium. The **general introduction (Chapter 1)** of this thesis introduces the concept of quantitative MRI, its application in epidemiological research, reno-cardiovascular health, and in obesity. In addition, the general introduction addresses the safety of gadolinium as an MRI contrast agent. Following the general introduction a **review** of the clinical application and technical considerations of quantitative MRI using T1 and T2(*) mapping in cardiac and renal imaging was provided in **Chapter 2**. **Part 1** of this thesis **(Chapter 3-6)** focuses on the reproducibility and clinical validity of T1 mapping and proton magnetic resonance spectroscopy (^{1}H-MRS) in renal imaging. **Part 2 (Chapter 7-10)**, describes different studies evaluating the association between obesity and reno-cardiovascular function which was analyzed in population-based imaging studies using different quantitative MRI metrics. The **appendix (Chapter 11)**, provides an overview of the safety profile of gadolinium containing contrast agents, and reflection on the recent EMA recommendations.

PART 1. REPRODUCIBILITY AND CLINICAL VALIDATION STUDIES

The reproducibility and clinical validation of novel quantitative MRI metrics in renal imaging was studied.

In **Chapter 3** we evaluated the intra- and inter-examination reproducibility of native T1 mapping for renal tissue characterization in 15 healthy volunteers and in 11 diabetic nephropathy patients. Overall mean T1 values of healthy volunteers were 1418±73 ms for renal cortex and 1886±86 ms for medulla, and in diabetic nephropathy patients this was 1445±81 ms for renal cortex and 1840±79 ms for medulla. We found that intra- and inter-examination reproducibility of renal native T1 mapping showed good-strong ICCs (0.83-0.89) for renal cortex and medulla in both healthy volunteers and diabetic nephropathy patients, indicating that renal native T1 mapping is a reproducible technique that could be used for renal tissue characterization.

In **Chapter 4** the consensus-based technical recommendations on renal T1 and T2 mapping were described. The consensus-based recommendations were developed using the Delphi method, which was initiated by the European Cooperation in Science and Technology Action PARENCHIMA CA16103. The Delphi panel consisted of a multidisciplinary group of experts in the field of renal T1 and T2 mapping. In total 36 consensus-based

recommendations on hardware, patient preparation, acquisition, analysis and reporting were formulated.

Chapter 5 describes the reproducibility of renal metabolic imaging for the quantification of renal triglyceride content using ^{1}H-MRS in 23 healthy volunteers and 15 diabetic nephropathy patients. Renal steatosis (fatty kidney) is a potential biomarker for obesity-related renal disease; however, noninvasive assessment of renal fat content is technically challenging due to the low-signal to noise ratio of renal triglyceride content, and motion of the kidneys with the respiratory cycle. We demonstrated that renal metabolic imaging using ^{1}H-MRS is a reproducible albeit technically challenging method for the non-invasive measurement of renal triglyceride content. In **Chapter 6** we presented a prospective clinical trial evaluating the effect of glycemic control on renal triglyceride content measured by ^{1}H-MRS in patients with type 2 diabetes. In this study we found that twenty-six weeks of glycemic control resulted in lower RTGC, in particular for liraglutide. However, larger clinical studies are needed to assess whether these changes reflect a true effect of glycemic control on renal steatosis.

PART 2. POPULATION-BASED IMAGING STUDIES

Different quantitative MRI metrics were used to study the association between obesity and reno-cardiovascular health in population-based imaging studies, namely the Netherlands Epidemiology of Obesity (NEO) study, and the UK Biobank.

In **Chapter 7** we studied the associations between normal range albuminuria, renal function and cardiovascular function assessed via MRI in 6,503 participants of the NEO study. We found that normal-range albuminuria was positively associated with LV mass index, LV cardiac index, arterial thickness and arterial stiffness. Our findings support the hypothesis that even within normal range, albuminuria is a marker of cardiovascular health.

In **Chapter 8** we investigated whether determinants of impaired renal function and vascular function, assessed by urinary albumin-creatinine ratio and MRI-based pulse wave velocity, were associated with elevated levels of procoagulant factors in the NEO study. This study showed that impaired renal and vascular function was associated with higher levels of coagulation factors, underlining the role of renal function and vascular function in the development of venous thrombosis.

Chapter 9 describes the separate contributions of visceral fat and liver fat measured by MRI, on chronic kidney disease related outcomes in the NEO study. In observational analyses, visceral fat was associated with microalbuminuria in women (but not in men). Liver fat was not associated with microalbuminuria or renal function, which was sup-

ported by Mendelian randomization analyses. These findings suggest that visceral fat might be more important than liver fat in the etiology of microalbuminuria.

In **Chapter 10** we investigated whether total body fat was associated with different quantitative MRI metrics on brain morphology and white matter microstructure in 12,053 participants of the imaging cohort of the UK biobank. In this study total body fat percentage was negatively associated with subcortical grey matter volumes in men and with globus pallidus volume in women. With regard to white matter microstructure, positive associations were found for total body fat and global fractional anisotropy, and negative associations for global mean diffusivity. This study provides further evidence that obesity is associated with smaller subcortical grey matter volumes. In addition, obesity was associated with higher coherence but lower magnitude of white matter microstructure suggesting that obesity has potentially differential influences on the geometric organization of white matter microstructure.

APPENDIX. CONTRAST MEDIA SAFETY

In the last recent years, important new insights have been made with regard to safety profile of gadolinium containing contrast agents, particularly in relation to renal function.

In **Chapter 11** we provided an overview of the safety profile of gadolinium containing contrast agents based on the respective physiochemical characteristics. In addition, this chapter reflects on the EMA recommendations regarding the suspension of marketing authorization of four linear gadolinium agents. It should be noted however, that the available scientific evidence for gadolinium retention has several important methodological limitations, and its clinical relevance remains unclear.

CONSIDERATIONS

There are several important methodological considerations that need to be taken into account when interpreting the results of this thesis.

First, the reproducibility studies presented in **Chapter 3** and **Chapter 5** on renal T1 mapping and ^{1}H-MRS had a limited sample size and were mainly performed in young healthy volunteers, which limits the possibility to assess to what extent quantitative renal MRI metrics were associated with clinical parameters such as glomerular filtration rate, and albuminuria. Other limitations of our reproducibility studies were lack of comparison with other field strengths (e.g. 1.5T versus 3T), and different MR vendors. With regard to renal spectroscopy, although this thesis shows that renal ^{1}H-MRS is feasible, it

remains technically challenging due to limited maximum size of the spectroscopy voxel, close proximity of renal sinus fat and perirenal fat, and the necessity of many signal averages for sufficient signal-to-noise ratio due to the very low lipid levels in the kidney. We applied the use of water-fat-acquisition to improve voxel planning, and pencil beam navigation for respiratory triggering, however motion artefacts remain an important issue in the spectral quality requiring careful analysis of the acquired averages.

In **Chapter 6** we described an exploratory study that evaluated the potential effect of glycemic control on renal triglyceride content. Considering, renal ^{1}H-MRS involves triglyceride concentrations that are substantially lower than in the liver, adequate water suppression and shimming are especially of great importance to ensure sufficient spectral quality. Because of these, we had a substantial amount of renal spectra that did not meet the quality criteria and were excluded from the analysis, limiting the sample size of the study needed to detect differences between the two study arms. Moreover, the initial MAGNA VICTORIA study was not powered for renal outcomes, but were pre-defined secondary outcomes.

In contrast to renal spectroscopy, renal T1 and T2 mapping are more robust renal imaging sequences and of increasing interest in the MR research community (1).

In **Chapter 4** we presented consensus-based technical recommendations for renal T1 and T2 mapping. This was the first initiative to define technical recommendations on renal T1 and T2 mapping, and may serve as a guideline that can be implemented by other research groups and facilitate pooling of data across study sites. However, it should be noted that these recommendations are bound by the limited number of experts that participated in this consensus formation process, and continues to be an ongoing process as renal relaxometry is currently confined to a limited number of dedicated research groups.

Part 2 of this thesis involves cross-sectional studies of the NEO study and UK Biobank, that evaluated the association between obesity and reno-cardiovascular function using different quantitative MRI metrics. The cross-sectional design of these studies limits our abilities to distinguish cause and effect, and it cannot be excluded that the determinants preceded the study outcomes.

In addition, there are specific considerations with regard to observational epidemiological studies of obesity (2), see **Fig.1**. Regarding measurement error, in **Chapter 9** we used direct measurements of obesity, which minimizes concerns related to proxy measures, such as body mass index which was used in **Chapter 10**. In addition, we used concordant measurement and analysis of visceral fat and liver fat in **Chapter 9** which allows for studying the specific contributions of these fat compartments and their associations with CKD-related outcomes. A general limitation with regard to measurement error in this thesis, is the use of manual and/or visual assessment of MR images, which is time intensive, observer-dependent, and may compromise reproducibility in settings where

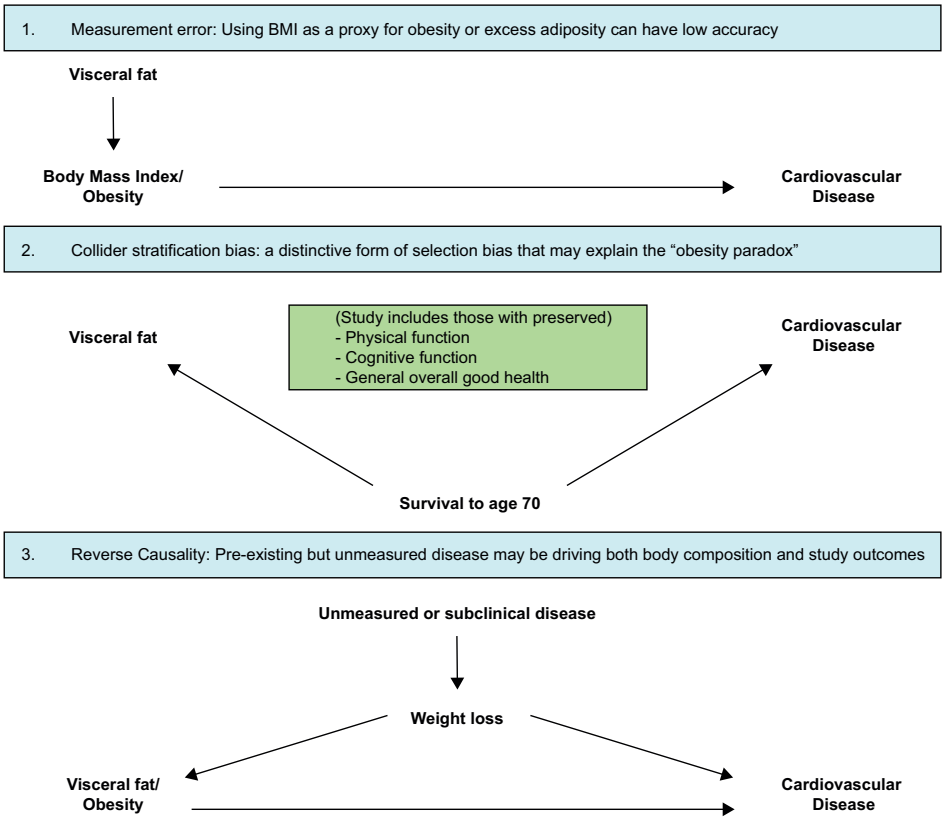

Figure 1. Overview of potential biases in observational studies of obesity (2).

raters change over time. Another form of bias that needs to be considered is collider stratification bias and healthy volunteer bias. Healthy volunteer bias emerges from the fact that to participate in a population-based study at middle age, one tends to be in a better physical state and have a better cognitive function and individuals who decide to participate in a clinical study are in general more concerned about their health and tend to have a healthy lifestyle. A previous study comparing life style characteristics and health outcomes of the UK Biobank participants to the general population, found evidence of a 'healthy volunteer' selection bias however valid assessment of exposure-disease relationships may be widely generalizable and does not require participants to be representative of the population at large (2). Also in **Chapter 7, 8 and 9** the prevalence of microalbuminuria in the NEO study was substantially lower than in the general Dutch population (3). Finally, with regard to reversed causation, a pre-existing but unmeasured clinical outcome may be driving both body composition and study outcomes, see **Fig.1**. The issue of reverse causation can be addressed by using genetic variants as instrumental variables for the tested exposure (e.g. the alleles of this exposure–associated genetic

variant are randomly allocated and not subject to reverse causation) as in Mendelian randomization (4). Our observational analyses in **Chapter 9** suggested that liver fat by itself is not related to microalbuminuria or impaired renal function. For this reason, we performed a subsequent Mendelian randomization analysis which found that only the lead variant for GCKR (rs780094) showed evidence for causal effects of NAFLD on impaired renal function and microalbuminuria. Considering this lead variant for GCKR is also known to be involved in glucose-metabolism and diabetic nephropathy (5), this finding does not fulfill of the core assumptions of Mendelian randomization, namely (i.e., it is independent of the outcome given the exposure).

CLINICAL IMPLICATIONS

There are several ways how the findings described in this thesis can contribute to improved clinical care of patients. The prevalence of renal disease are expected to rise in the upcoming years, and go accompanied by increasing health care costs and societal costs. For this reason, there is an increasing clinical demand for earlier diagnosis and evaluation of treatment response, for which renal MRI biomarkers show great promise considering their non-invasiveness and versatility.

The reproducibility studies renal T1 mapping and ^{1}H-MRS in **part 1** of this thesis are the first steps in the evaluation on potential clinical usefulness of renal imaging biomarkers. The technical recommendations on renal T1 and T2 mapping via harmonization of imaging protocols aims to facilitate direct comparison of renal MRI biomarkers between different imaging sites which is needed in order to qualify as a clinical biomarker. Finally, in part one we performed an exploratory study using renal triglyceride content as a biomarker. Although we were unable to demonstrate that renal triglycerides significantly change after 26 weeks of glycemic control, the novelty of this study lies in the feasibility of applying MR spectroscopy for renal metabolic imaging in a clinical setting.

In **part 2** of this thesis we performed different population-based imaging studies on obesity and reno-cardiovascular function. Obesity is related to various negative health outcomes including insulin resistance, diabetes and cardiovascular disease, and the disease burden-related to obesity is expected to further increase in the next decades. The focus of obesity research is therefore on early detection of pathologic changes and prevention. Population-based studies, such as described in this thesis, contribute to unraveling the preclinical disease markers or prevention of disease progression. Addressed topics in this thesis are; albuminuria within normal range as a marker of cardiovascular health, renal and vascular function in relation to procoagulant factors, visceral fat and liver fat in relation to CKD-related outcomes, and total body fat percentage with brain morphology and white matter integrity. Although longitudinal evaluations are needed to

determine whether a certain biomarker indicates early disease, the findings in this thesis may serve as a basis for further research.

FUTURE PERSPECTIVES

In the coming years, quantitative imaging will take a prominent place in clinical diagnostic radiology. In cardiovascular imaging the use of quantitative measures on cardiac function is considered part of standard clinical imaging protocols and reporting, and other fields of diagnostic radiology are expected to follow and increasingly use quantitative metrics such as in renal imaging. With regard to renal quantitative MRI, it is expected that the interest in renal MRI will continue to grow as evidenced by (inter) national research networks such as, PARENCHIMA, and the UK Renal Imaging Network (UKRIN), and ongoing larger studies evaluating the evidence of the clinical utility of renal MRI biomarkers. In contrast to renal T1 and T2 mapping, renal spectroscopy is still at its infancy and to achieve broader implementation body MR spectroscopy protocols from MR vendors are needed. With regard to the use of MRI in epidemiological studies, we expect that imaging will play an increasingly important role. Initiatives like the UK biobank are expected to acquire larger samples of MRI biomarkers than ever before of up to 100,000 individuals, allowing for an integrative approach which combines imaging biomarkers with e.g. genomics, proteomics, and metabolomics. The transition towards quantitative imaging will coincide with more complex image sequences and increasingly large datasets, requiring advanced computational resources and data-storage infrastructure. To illustrate, the application of 4D (3D+T) flow in clinical care involves datasets of >25,000 sampling points, which are registered over 30 phases during one average cardiac cycle leading to a dataset of up to 750,000 data points to define intra-cardiac flow patterns in a single patient [Cardiovascular imaging group, CVIG]. Considering the expected further demand for radiological assessments, as well as the rising complexity of clinical scan protocols, automated measurements of quantitative imaging biomarkers are needed in order to use these effectively in clinical care. This requires the use of new techniques such as machine learning and artificial intelligence using deep learning methods such as artificial neural networks. Dealing with these increasing technical demands will be one of the main hurdles in adopting quantitative imaging for clinical care. With regard to clinical care, the transition of qualitative image interpretation to quantitative image analyses provides radiologists new tools that can contribute to earlier and more accurate diagnosis, and enable treatment-monitoring, which adds a new dimension to the clinical value of radiological examinations.

CONCLUSIONS

This thesis evaluates the application of quantitative MRI in reno-cardiovascular health and studies the links between obesity and reno-cardiovascular health using quantitative MRI metrics. This thesis shows that native renal T1 mapping and ^{1}H-MRS are both reproducible techniques that can be used as quantitative MRI metrics in renal imaging for the assessment of renal tissue characterization and renal triglyceride content respectively. In addition, this thesis provides expert-based consensus recommendations on the acquisition and reporting of renal T1 and T2 mapping, which contributes to the valorization of renal quantitative MRI. Moreover, we demonstrated the use of quantitative MRI metrics in four different population-based imaging studies on reno-cardiovascular health and obesity. Quantitative MRI is the ideal technique for studying obesity in a holistic approach, assessing inter-organ relation and multi-organ impact of obesity in a single scan session. MRI enables not only the assessment of body fat distribution but also the structural and/or functional consequences of obesity on different organs such as heart, liver, kidney and brain during the same visit. In addition, this thesis contemplated contrast media safety in relation to the use of gadolinium. Finally, it is expected that quantitative MRI will play an increasingly important role in both research settings and clinical care. As such, the use of quantitative MRI will add a new dimension to the practice of clinical radiology.

REFERENCES

1. Mendichovszky I, Pullens P, Dekkers IA, et al. Technical recommendations for clinical translation of renal MRI: a consensus project of the Cooperation in Science and Technology Action PARENCHIMA. MAGMA. 2020 Feb;33(1):131-140
2. Anderson CA, Mongraw-Chaffin M. Central Obesity in Older Adults: What Should Be the Priority? J Am Heart Assoc. 2018 Aug 21;7(16):e010119.
3. Fry A, Littlejohns TJ, Sudlow C, Doherty N, Adamska L, Sprosen T, Collins R, Allen NE. Comparison of sociodemographic and health-related characteristics of UK Biobank participants with those of the general population. 2017 Jun 21;186(9):1026-34.
4. De Zeeuw D, Hillege HL, De Jong PE. The kidney, a cardiovascular risk marker, and a new target for therapy. Kidney international. 2005 Sep 1;68:S25-9.
5. Sekula P, Fabiola Del Greco M, Pattaro C, Köttgen A. Mendelian randomization as an approach to assess causality using observational data. J Am Soc Nephrol. 2016 Nov 1;27(11):3253-65.
6. Bonetti S, Trombetta M, Boselli ML, et al. Variants of GCKR affect both β-cell and kidney function in patients with newly diagnosed type 2 diabetes: the Verona newly diagnosed type 2 diabetes study 2. Diabetes Care. 2011;34(5):1205-1210.

NEDERLANDSE SAMENVATTING

Het doel van het onderzoek, zoals beschreven in dit proefschrift, was het verkennen van de toepassing van kwantitatieve magnetische kernspinresonantie (magnetic resonance imaging, MRI) in reno-cardiovasculaire beeldvorming. Daarnaast was het doel om door middel van kwantitatieve MRI maten de link tussen obesitas en reno-cardiovasculaire functie te bestuderen. De **algemene inleiding (Hoofdstuk 1)** van dit proefschrift geeft achtergrondinformatie over het concept kwantitatieve MRI, en de toepassing hiervan in epidemiologisch onderzoek op het gebied van obesitas en reno-cardiovasculaire functie. Daarnaast worden verschillende aspecten van de veiligheid van gadoliniumhoudende contrastmiddelen toegelicht. Aansluitend op de algemene inleiding wordt in **Hoofdstuk 2** een **overzicht** gegeven van de klinische toepassing en de technische overwegingen van kwantitatieve MRI door middel van T1 en T2(*) mapping in cardiale en renale beeldvorming.

Deel 1 (Hoofdstuk 3-6) van dit proefschrift is gefocust op de reproduceerbaarheid en klinische validatie van T1 mapping en proton-magnetische resonantiespectroscopie (^{1}H-MRS) van de nier. **Deel 2 (Hoofdstuk 7-10)** beschrijft meerdere populatiestudies die met behulp van verschillende kwantitatieve MRI-maten de associaties tussen obesitas en reno-cardiovasculaire functie in kaart brengen. In de **appendix (Hoofdstuk 11)** worden tenslotte de recente ontwikkelingen op het gebied van de veiligheid van gadoliniumhoudende contrastmiddelen besproken.

DEEL 1. REPRODUCEERBAARHEID EN KLINISCHE VALIDATIESTUDIES

Door middel van MRI is het mogelijk om de morfologie van de nier met hoge resolutie in beeld te brengen en de weefselcompositie van de nier te kwantificeren. Voor de klinische toepassing hiervan is naast een goede beeldkwaliteit ook een hoge reproduceerbaarheid noodzakelijk.

In **Hoofdstuk 3** hebben wij de intra- en inter-reproduceerbaarheid van natieve T1 mapping van de nier onderzocht bij 15 gezonde vrijwilligers en 11 patiënten met diabetische nefropathie. De gemiddelde T1 waarden van de gezonde vrijwilligers waren 1418±73 ms in de nierschors en 1886±86 ms in het merg. Bij patiënten met diabetische nefropathie was dit 1445±81 ms in de nierschors en 1840±79 ms in het merg. De intra-class correlatiecoëfficiënten voor nierschors en merg kwamen overeen met een goede tot sterke intra- en inter-reproduceerbaarheid (0.83-0.89) bij zowel gezonde vrijwilligers als patiënten met diabetische nefropathie. Deze bevindingen tonen aan dat T1 mapping van de nier een reproduceerbare techniek is voor weefselkarakterisatie van de nier.

In **Hoofdstuk 4** wordt een Delphi-studie beschreven, waarbij expert-consensus aanbevelingen voor het scanprotocol van T1 en T2 mapping van de nier zijn geformuleerd. Dit is het eerste initiatief om technische aanbevelingen te formuleren met betrekking tot de acquisitie en beeldanalyse van T1 en T2 mapping van de nier met als doel om scanprotocollen tussen verschillende centra te harmoniseren.

Hoofdstuk 5 beschrijft de reproduceerbaarheid van ^{1}H-MRS voor het kwantificeren van triglyceriden in de nier bij 23 gezonde vrijwilligers en 15 patiënten met diabetische nefropathie. Steatose van de nier of 'fatty kidney' is een potentiële biomarker voor obesitas-gerelateerde nierziekten, echter het non-invasief meten van vet in de nier blijft een technische uitdaging door de lage signaal-ruisverhouding en beweging van de nier tijdens de ademhaling. Wij hebben aangetoond dat ^{1}H-MRS van de nier, alhoewel technisch uitdagend, een reproduceerbare methode is voor het meten van triglyceriden in de nier. Gezonde vrijwilligers hadden een mediaan van 0.12% [0.08, 0.22; 25ste percentiel, 75ste percentiel] triglyceriden in de nier vergeleken met 0.20% [0.13, 0.22] bij patiënten met diabetische nefropathie.

In **Hoofdstuk 6** worden de resultaten beschreven van een experimenteel onderzoek, waarbij patiënten met type 2 diabetes mellitus zijn gerandomiseerd in een behandelarm met liraglutide of placebo toegevoegd aan standaard glucoregulatie. Bij aanvang van de studie en na 26 weken follow-up werd met behulp van ^{1}H-MRS de hoeveelheid triglyceriden in de nier gemeten. In deze studie maten wij na 26 weken glucoregulatie een afname van de hoeveelheid triglyceriden in de nier, met name voor liraglutide, echter in hoeverre deze bevindingen berusten op een daadwerkelijk effect van glucoregulatie op steatose van de nier is vooralsnog niet geheel duidelijk.

DEEL 2. POPULATIEONDERZOEK MET BEHULP VAN BEELDVORMING

Binnen populatiestudies kan kwantitatieve MRI een bijdrage leveren aan het bestuderen van de associaties tussen obesitas en reno-cardiovasculaire gezondheid. Voorbeelden van dergelijke populatiestudies die gebruik maken van gekwantificeerde MRI maten, zijn de Nederlandse Epidemiologie van Obesitas (NEO) studie en de UK Biobank.

In **Hoofdstuk 7** hebben wij de associaties onderzocht tussen normal range albuminurie, nierfunctie en cardiovasculaire functie, waarbij we gebruik hebben gemaakt van MRI gekwantificeerde hartfunctiemetingen bij 6.503 deelnemers van de NEO studie. In deze studie hebben wij gevonden dat normal-range albuminurie een positieve associatie had met de linker ventrikel massa-index, de linker ventrikel cardiac-index, de vaatwanddikte en de vaatstijfheid. Onze bevindingen ondersteunen de hypothese dat ook albuminurie binnen de range van het normale een marker is van cardiovasculaire gezondheid.

In **Hoofdstuk 8** hebben wij in de NEO studie onderzocht of determinanten van verminderde nierfunctie en vaatfunctie (op basis van albumine-creatine ratio in de urine en MRI pulse-wave velocity) waren geassocieerd met hogere stollingswaarden in het bloed. Uit deze studie is gebleken dat zowel verminderde nierfunctie als -vaatfunctie waren geassocieerd met hogere stollingswaarden in het bloed, wat de mogelijke rol van de nierfunctie en de vaatfunctie bij het ontwikkelen van veneuze trombose verder ondersteunt.

Hoofdstuk 9 beschrijft de onafhankelijke bijdrage van visceraal vet en levervet op verscheidene uitkomstmaten gerelateerd aan chronische nierschade in de NEO studie. Uit de observationele analyses is gebleken dat visceraal vet geassocieerd is met microalbuminurie, maar niet met levervet. Resultaten van de aanvullende Mendeliaanse randomisatie analyses leverden geen ondersteunend bewijs voor de hypothese dat levervet causaal is gerelateerd aan micro-albuminurie of een verminderde nierfunctie.

In **Hoofdstuk 10** hebben wij onderzocht of het totale lichaamsvetpercentage geassocieerd is met verschillende kwantitatieve MRI maten van de hersenen, inclusief de microstructuur van de witte stof. Deze studie bij 12.053 deelnemers van de UK Biobank liet zien dat het totale lichaamsvetpercentage negatief geassocieerd is met subcorticale grijze stof volumes in mannen en met globus pallidus volume in vrouwen. Ten aanzien van de witte stof microstructuur, vonden wij positieve verbanden tussen lichaamsvetpercentage en globale fractionele anisotropie (fractional anisotropy), en negatieve verbanden voor globale gemiddelde diffusiviteit (mean diffusivity). Deze bevindingen ondersteunen de hypothese dat obesitas geassocieerd is met subcorticaal grijze stof volumes en witte stof microstructuur.

APPENDIX. DE VEILIGHEID VAN CONTRASTMIDDELEN

De afgelopen jaren zijn er belangrijke nieuwe ontwikkelingen geweest op het gebied van de veiligheid van gadoliniumhoudende contrastmiddelen. In **Hoofdstuk 11** geven wij een overzicht van het veiligheidsprofiel van gadoliniumhoudende contrastmiddelen en reflecteren wij op de aanbevelingen van de Europese Geneesmiddelen Autoriteit ten aanzien van vier gadoliniumhoudende contrastmiddelen. Hierbij moet echter wel worden opgemerkt dat het beschikbare wetenschappelijke bewijs voor gadoliniumstapeling aan meerdere belangrijke methodologische tekortkomingen onderhevig is en dat de klinische relevantie hiervan nog onduidelijk is.

CONCLUSIES

Dit proefschrift beschrijft de toepassing van kwantitatieve MRI van de nier en het hart voor het analyseren van verbanden tussen obesitas en reno-cardiovasculaire gezondheid. Dit proefschrift laat zien dat T1 mapping van de nier en ^{1}H-MRS beide reproduceerbare technieken zijn, die gebruikt kunnen worden voor respectievelijk weefselkarakterisatie van de nier en het meten van triglyceriden in de nier. Daarnaast is dit proefschrift voorzien van expert-consensus aanbevelingen ten aanzien van het scanprotocol voor nier T1 en T2 mapping, wat bijdraagt aan de kennisvalorisatie van kwantitatieve beeldvorming van de nier. Verder hebben wij in dit proefschrift laten zien hoe kwantitatieve MRI-maten in vier verschillende populatiestudies worden gebruikt voor het bestuderen van reno-cardiovasculaire gezondheid en obesitas. Kwantitatieve MRI is een ideale techniek om obesitas te bestuderen via een holistische benadering, waarbij de relatie tussen verschillende organen, zoals hart, lever, nier en hersenen, met behulp van een enkele scansessie kunnen worden gevisualiseerd en gekwantificeerd. Tenslotte beschrijft dit proefschrift meerdere veiligheidsaspecten van contrastmiddelen, in het bijzonder in relatie tot het gebruik van gadolinium. Het is de verwachting dat kwantitatieve MRI-technieken een toenemende rol zullen gaan spelen in zowel wetenschappelijke als klinische toepassingen, en zo een nieuwe dimensie zal geven aan de radiologie.

LIST OF PUBLICATIONS

Accepted / published peer-reviewed articles

1. **Dekkers IA**, Blijdorp K, Cransberg K, Pluijm SM, Pieters R, Neggers SJ, van den Heuvel-Eibrink MM. Long-term nephrotoxicity in adult survivors of childhood cancer. *Clin J Am Soc Nephrol*. 2013 Jun;8(6):922-9.
2. **Dekkers IA**, Blijdorp K, Pieters R, Cransberg K, Neggers SJ, van den Heuvel-Eibrink MM. Chronische nierinsufficiëntie na kinderkanker [Chronic renal insufficiency following childhood cancer]. *Ned Tijdschr Geneeskd*.2014;158:A6692.
3. Jonker JT, de Heer P, Engelse MA, van Rossenberg EH, Klessens CQF, Baelde HJ, Bajema IM, Koopmans SJ, Coelho PG, Streefland TCM, Webb AG, **Dekkers IA**, Rabelink TJ, Rensen PCN, Lamb HJ, de Vries APJ. Metabolic imaging of fatty kidney in diabesity: validation and dietary intervention. *Nephrol Dial Transplant*. 2018 Feb 1;33(2):224-230.
4. Jansen PR, Dremmen M, van den Berg A, **Dekkers IA**, Blanken LME, Muetzel RL, Bolhuis K, Mulder RM, Kocevska D, Jansen TA, de Wit MY, Neuteboom RF, Polderman TJC, Posthuma D, Jaddoe VWV, Verhulst FC, Tiemeier H, van der Lugt A, White TJH. Incidental Findings on Brain Imaging in the General Pediatric Population. *N Engl J Med*. 2017 Oct 19;377(16):1593-1595.
5. **Dekkers IA**, Roos R, van der Molen AJ. Gadolinium retention after administration of contrast agents based on linear chelators and the recommendations of the European Medicines Agency. *Eur Radiol. 2018* Apr;28(4):1579-1584.
6. Mark PB, **Dekkers I**, Blankestijn PJ, Leiner T, Roditi G. Letter on 'European dermatology forum S1-guideline on the diagnosis and treatment of sclerosing diseases of the skin, Part 2: Scleromyxedema, scleredema and nephrogenic systemic fibrosis'. *J Eur Acad Dermatol Venereol*. 2018 Feb;32(2):e84-e85.
7. **Dekkers IA**, de Mutsert R, de Vries APJ, Rosendaal FR, Cannegieter SC, Jukema JW, le Cessie S, Rabelink TJ, Lamb HJ, Lijfering WM. Determinants of impaired renal and vascular function are associated with elevated levels of procoagulant factors in the general population. *J Thromb Haemost*. 2018 Mar;16(3):519-528.
8. van der Molen AJ, Reimer P, **Dekkers IA**, Bongartz G, Bellin MF, Bertolotto M, Clement O, Heinz-Peer G, Stacul F, Webb JAW, Thomsen HS. Post-contrast acute kidney injury. Part 2: risk stratification, role of hydration and other prophylactic measures, patients taking metformin and chronic dialysis patients : Recommendations for updated ESUR Contrast Medium Safety Committee guidelines. *Eur Radiol*. 2018 Jul;28(7):2856-2869.
9. van der Molen AJ, Reimer P, **Dekkers IA**, Bongartz G, Bellin MF, Bertolotto M, Clement O, Heinz-Peer G, Stacul F, Webb JAW, Thomsen HS. Post-contrast acute kidney injury - Part 1: Definition, clinical features, incidence, role of contrast medium and risk factors : Recommendations for updated ESUR Contrast Medium Safety Committee guidelines. *Eur Radiol*. 2018 Jul;28(7):2845-2855.

10. **Dekkers IA**, de Heer P, Bizino MB, de Vries APJ, Lamb HJ. ^{1}H-MRS for the assessment of renal triglyceride content in humans at 3T: A primer and reproducibility study. *J Magn Reson Imaging*. 2018 Aug;48(2):507-513.
11. **Dekkers IA**, de Mutsert R, Rabelink TJ, Jukema JW, de Roos A, Rosendaal FR, Lamb HJ, de Vries APJ. Associations between normal range albuminuria, renal function and cardiovascular function in a population-based imaging study. *Atherosclerosis*. 2018 May;272:94-100.
12. **Dekkers IA**, Lamb HJ. Clinical application and technical considerations of T1 & T2(*) mapping in cardiac, liver, and renal imaging. *Br J Radiol*. 2018 Dec;91(1092):20170825.
13. **Dekkers IA**, van der Molen AJ. Propensity Score Matching as a Substitute for Randomized Controlled Trials on Acute Kidney Injury After Contrast Media Administration: A Systematic Review. *AJR Am J Roentgenol*. 2018 Oct;211(4):822-826.
14. **Dekkers IA**, Paiman EHM, de Vries APJ, Lamb HJ. Reproducibility of native T1 mapping for renal tissue characterization at 3T. *J Magn Reson Imaging*. 2019 Feb;49(2):588-596.
15. de Leeuw CA, Stringer S, **Dekkers IA**, Heskes T, Posthuma D. Conditional and interaction gene-set analysis reveals novel functional pathways for blood pressure. *Nat Commun*. 2018 Sep 14;9(1):3768.
16. **Dekkers IA**, de Mutsert R, Lamb HJ, Lijfering WM. Determinants of impaired renal and vascular function are associated with elevated levels of procoagulant factors in the general population: reply. *J Thromb Haemost*. 2018 Dec;16(12):2535-2536.
17. **Dekkers IA**, Jansen PR, Lamb HJ. Obesity, Brain Volume, and White Matter Microstructure at MRI: A Cross-sectional UK Biobank Study. *Radiology*. 2019 Jun;291(3):763-771.
18. **Dekkers IA**, Cleven A, Lamb HJ, Kroon HM. Primary Osteosarcoma of the Breast. *Radiographics*. 2019 May-Jun;39(3):626-629.
19. Xiao X, Wang Y, Gao Y, Xie Q, Zhou X, Lin L, **Dekkers IA**, Lamb HJ. Abdominal visceral adipose tissue is associated with unsuspected pulmonary embolism on routine CT scans in patients with gastrointestinal cancer. *Br J Radiol*. 2019 Dec;92(1104):20190526.
20. Paiman EHM, van Eyk HJ, Bizino MB, **Dekkers IA**, de Heer P, Smit JWA, Jazet IM, Lamb HJ. Phenotyping diabetic cardiomyopathy in Europeans and South Asians. *Cardiovasc Diabetol*. 2019 Oct 11;18(1):133.
21. Mendichovszky I, Pullens P, **Dekkers I**, Nery F, Bane O, Pohlmann A, de Boer A, Ljimani A, Odudu A, Buchanan C, Sharma K, Laustsen C, Harteveld A, Golay X, Pedrosa I, Alsop D, Fain S, Caroli A, Prasad P, Francis S, Sigmund E, Fernández-Seara M, Sourbron S. Technical recommendations for clinical translation of renal MRI: a consensus project of the Cooperation in Science and Technology Action PARENCHIMA. *MAGMA*. 2019 Oct 18;10.1007/s10334-019-00784-w.
22. **Dekkers IA**, de Vries APJ, Smit RAJ, Rosendaal FR, Rabelink TJ, Lamb HJ, de Mutsert R. The Separate Contributions of Visceral Fat and Liver Fat to Chronic Kidney Disease-Related Renal Outcomes. *J Ren Nutr*. 2019 Oct 25;S1051-2276(19)30323-1.

23. Ljimani A, Caroli A, Laustsen C, Francis S, Mendichovszky IA, Bane O, Nery F, Sharma K, Pohlmann A, **Dekkers IA**, Vallee JP, Derlin K, Notohamiprodjo M, Lim RP, Palmucci S, Serai SD, Periquito J, Wang ZJ, Froeling M, Thoeny HC, Prasad P, Schneider M, Niendorf T, Pullens P, Sourbron S, Sigmund EE. Consensus-based technical recommendations for clinical translation of renal diffusion-weighted MRI. *MAGMA*. 2019 Nov 1;10.1007/s10334-019-00790-y.
24. Bizino MB, Jazet IM, de Heer P, van Eyk HJ, **Dekkers IA**, Rensen PCN, Paiman EHM, Lamb HJ, Smit JW. Placebo-controlled randomised trial with liraglutide on magnetic resonance endpoints in individuals with type 2 diabetes: a pre-specified secondary study on ectopic fat accumulation. *Diabetologia*. 2020 Jan;63(1):65-74.
25. van Hout MJP, **Dekkers IA**, Westenberg JJM, Schalij MJ, Scholte AJHA, Lamb HJ. The impact of visceral and general obesity on vascular and left ventricular function and geometry: a cross-sectional magnetic resonance imaging study of the UK Biobank. *Eur Heart J Cardiovasc Imaging*. 2019 Nov 13;jez279.
26. **Dekkers IA**, de Boer A, Sharma K, Cox EF, Lamb HJ, Buckley DL, Bane O, Morris DM, Prasad PV, Semple SIK, Gillis KA, Hockings P, Buchanan C, Wolf M, Laustsen C, Leiner T, Haddock B, Hoogduin JM, Pullens P, Sourbron S, Francis S. Consensus-based technical recommendations for clinical translation of renal T1and T2 mapping MRI. *MAGMA*. 2019 Nov 22;10.1007/s10334-019-00797-5.
27. Bane O, Mendichovszky IA, Milani B, **Dekkers IA**, Deux JF, Eckerbom P, Grenier N, Hall ME, Inoue T, Laustsen C, Lerman LO, Liu C, Morrell G, Pedersen M, Pruijm M, Sadowski EA, Seeliger E, Sharma K, Thoeny H, Vermathen P, Wang ZJ, Serafin Z, Zhang JL, Francis ST, Sourbron S, Pohlmann A, Fain SB, Prasad PV. Consensus-based technical recommendations for clinical translation of renal BOLD MRI. *MAGMA*. 2019 Nov 25;10.1007/s10334-019-00802-x.
28. Lin L, **Dekkers IA**, Tao Q, Lamb HJ. Novel artificial neural network and linear regression based equation for estimating visceral adipose tissue volume. *Clin Nutr.* 2020 Feb 14:S0261-5614(20)30061-3.

INVITED ORAL PRESENTATIONS

1. Prevention of Contrast Nephropathy in Daily Practice. *Radiologen Dagen*, Rotterdam, the Netherlands. September 11, 2015.
2. Implementation of the new ESUR Guidelines for Prevention of PC-AKI. *European Society of Urogenital Radiology (ESUR)*, Barcelona, Spain. September 15, 2018.
3. Technical validation: Demonstrating accuracy, precision and quality assurance of renal MR biomarkers. Member Initiated Symposium. *International Society for Magnetic Resonance in Medicine (ISMRM)*, Montreal, Canada. May 13, 2019.
4. MRI for the non-expert: T1 and T2 mapping of the kidney. *3rd International Symposium on Functional Renal Imaging*, Nottingham, United Kingdom. October 15, 2019.

SCIENTIFIC ORAL PRESENTATIONS

1. Long-term nephrotoxicity in adult survivors of childhood cancer. **Dekkers IA**, Blijdorp K, Cransberg K, Pluijm SM, Pieters R, Neggers SJ, van den Heuvel-Eibrink MM. Oral presentation. *International Conference on Long-Term Complications of Treatment of Children and Adolescents for Cancer*, Memphis, USA. June 14, 2013.
2. Emergent Stenting of extracranial Internal Carotid Artery Occlusions in case of tandem lesions in Acute Ischemic Stroke - A Critical Appraisal of a Topic. **Dekkers IA**, van Walderveen MA. *Radiologen Dagen*, Rotterdam. September 11, 2015.
3. What is the Value of Propensity Scores in Contrast Induced - Acute Kidney Injury? **Dekkers IA**, van der Molen AJ. *European Society of Urogenital Radiology (ESUR)*, Bordeaux, France. September 18, 2016.
4. Associations between Renal Function, Urinary Albumin Excretion and Left Ventricular Mass and Function: A Population-based MR Imaging Study. **Dekkers IA**, de Mutsert R, Rabelink T, Jukema W, de Roos A, Rosendaal F, de Vries A, Lamb H. *Radiological Society of North America (RSNA)*, Chicago, USA. November 30, 2016.
5. Towards renal metabolic imaging of fatty kidney. **Dekkers IA**, de Heer P, Bizino MB, de Vries APJ, Lamb HJ. *European Congress of Radiology (ECR)*, Vienna, Austria. March 3, 2018.
6. Associations between liver fat, visceral fat and microalbuminuria in the general population. **Dekkers IA**, de Vries APJ, Rosendaal FR, Rabelink TJ, Lamb HJ, de Mutsert R. *European Congress of Radiology (ECR)*, Vienna, Austria. March 2, 2018.
7. The Impact of Visceral and General Obesity on LV Function and Geometry, and Vascular Function. Van Hout MJP, **Dekkers IA**, Westenberg JJM, Schalij MJ, Scholte AJHA, Lamb HJ. *European Society of Cardiovascular Radiology (ESCR)*, Antwerp, Belgium. October 26, 2019.

SCIENTIFIC POSTER PRESENTATIONS

1. Associations between liver fat, visceral fat and microalbuminuria in the general population. **Dekkers IA**, de Vries APJ, Rosendaal FR, Rabelink TJ, Lamb HJ, de Mutsert R. *Nederlands Epidemiologie Congres WEON*, de Bilt, the Netherlands. June 7-8, 2018.
2. Native T1-mapping for renal tissue characterisation. **Dekkers IA**, Paiman EHM, de Vries APJ, Lamb HJ. Electronic EPOS poster presentation. *European Congress of Radiology (ECR)*, Vienna, Austria. February 28-March 4, 2018.
3. Dutch guideline on contrast media, NSF & nephrotoxicity. **Dekkers IA**, van der Molen AJ, Geenen RWF, Dekker HM. Power pitch presenation. *International Society for Magnetic Resonance in Medicine (ISMRM)*. MRI safety, Utrecht, the Netherlands. September 20-22, 2019.
4. The effect of glycemic control on renal triglyceride content in patients with type 2 diabetes mellitus. **Dekkers IA**, de Heer P, Bizino MB, de Vries APJ, Lamb HJ. *3rd International Symposium on Functional Renal Imaging*. Nottingham, United Kingdom. 15-17 October, 2019.

PARTICIPATION IN SCIENTIFIC COMMITTEES

1. Working group member of the Guideline Safety Use of Contrast Media part 2, the Radiological Society of the Netherlands.
2. Working group member of the Guideline Safety Use of Contrast Media part 3, the Radiological Society of the Netherlands.
3. Co-chair of Technical Recommendations on Clinical Renal MRI: T1 and T2 mapping, COST Action PARENCHIMA (CA16103). https://www.renalmri.org/taskforce/15

CURRICULUM VITAE

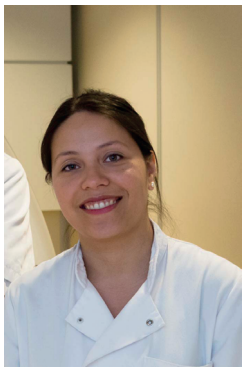

Ilona Alexandra Dekkers (1989, Rotterdam) grew up together with her twin sister Jacqueline in Capelle aan den IJssel (nearby Rotterdam), the Netherlands. After completing VWO at the Emmaus college in Rotterdam, she started medical school at the Erasmus University Medical Center (Erasmus MC) in Rotterdam in 2007. During medical school. Ilona became interested in clinical epidemiology and enrolled in a research master program at the Netherlands Institute of Health Sciences (NIHES). During her master's, she investigated the long-term effects of cancer treatment on renal function in adult survivors of childhood cancer at the Erasmus MC (supervisor: prof. dr. Marry van den Heuvel-Eibrink), combined with a research internship abroad studying the epigenetics of acute myeloid leukemia at the Johns Hopkins University, Baltimore, USA (supervisor: prof. dr. Robert Arceci). This resulted in a master's degree in Clinical Research in 2012 and registration as a clinical epidemiologist. After medical school, Ilona continued with her residency in radiology at the Leiden University Medical Center (LUMC) from May 2014 until January 2020. In 2015, Ilona started with her PhD project focused on the application of quantitative MRI in obesity and reno-cardiovascular function. This PhD project was conducted at the radiology department (supervisor: prof. dr. H.J. Lamb) in collaboration with the epidemiology and nephrology department of the LUMC, resulting in this thesis. Ilona currently works as a radiologist at the LUMC, where she will continue to combine her clinical work with scientific research in the field of cardiovascular imaging, epidemiology and translation to clinical care.

DANKWOORD

Hildo, dank voor de mogelijkheden die je mij hebt gegeven om mijzelf te ontwikkelen in de wetenschap. Jouw enthousiasme voor onderzoek heeft mij geïnspireerd om altijd nieuwsgierig te blijven, en ik kijk uit naar onze toekomstige onderzoeksprojecten.

Renée, dank voor de fijne begeleiding als copromotor en voor je input en adviezen over statistische analyses.

Aiko, ik wil je bedanken voor je kritische klinische blik en nefrologische input als copromotor.

Albert, dank voor het aannemen van de rol als secretaris bij mijn promotie. Nu je met pensioen bent weten we pas echt wat we moeten missen op de afdeling.

Maurice, Malou, Paul, Joe, Max en Ling, dank voor de prettige samenwerking afgelopen jaren.

Janey, dank voor de vele mooie jaren als collega en natuurlijk als paranimf.

Ik wil de AIOS en jonge klaren bedanken voor de fijne samenwerking van de afgelopen jaren en de gezellige uitjes buiten werk.

Alexandr, ik wil je bedanken voor de afgelopen jaren dat je mijn opleider bent geweest en je volle inzet voor de AIOS.

Sectie drie: Lucia, Lauran en Hildo, jullie hebben de afgelopen tijd een hechte groep van hoog niveau neergezet, en ik kijk er naar uit de sectie te mogen versterken.

Aart, de projecten over contrastmiddelen waren een leuke en leerzame ervaring, op naar het laatste deel van de richtlijntriologie.

Verder wil de rest van de Leidse radiologie staf bedanken voor de fijne tijd op de afdeling.

Nicole, Mery, Elvira, Femke, en de overige ‘independent women’, dank voor de fijne momenten die mijn studententijd kleur hebben gegeven.

Huub en Hanneke, dank voor de fijne schoonouders die jullie zijn.

Jacqueline, als tweelingzus ben je altijd aan mijn zijde en ik ben blij dat je nu ook bij mijn verdediging wederom aan mijn zijde staat. Raoul en jij zijn een mooi stel samen.

Mama en papa, veel dank voor jullie steun en hulp afgelopen jaren. Ik ben trots op jullie.

Philip, ik ben trots op jou en ik kijk uit naar onze mooie grote dag samen. Je bent mijn steun en toeverlaat.